

Development of CNS Penetrant Inhibitors of *Toxoplasma gondii* Cathepsin L

by

Jeffery D. Zwicker

A dissertation submitted in partial fulfillment
of the requirements for the degree of
Doctor of Philosophy
(Medicinal Chemistry)
in the University of Michigan
2018

Doctoral Committee:

Professor Vernon B. Carruthers, Co-Chair
Professor Scott D. Larsen, Co-Chair
Professor Henry I. Mosberg
Associate Professor Peter J. Scott

Jeffery D. Zwicker

zwickerj@umich.edu

ORCID iD: 0000-0002-3926-3647

© Jeffery D. Zwicker 2018

Dedication

To my family: DeAnna, Keelia, and Bella

Acknowledgements

First and foremost, I have to thank the two most important women in my life. My wife DeAnna and my daughter Keelia. These two beautiful and amazing women have stuck with me and been the greatest support to me through this time. These wonderful ladies have been my inspiration to push further and harder than I ever could have done alone. I love you both! Next, my parents Joe and Reggi have never faltered in their love and support for their children. My amazing upbringing coupled with their constant encouragement has shaped me into the person I am today. My brothers and sisters, Rachel, Renee, Mark, Angela, and Chris have always been encouraging and supportive. I am truly blessed to have such a huge supportive family. Thank you to my friends in Ann Arbor that provided some necessary relief and a recreation. From Thanksgiving climbing trips to happy-hour beers, these people have kept me in some level of sanity.

I want to thank my mentor Scott Larsen for giving me the perfect balance between guidance and autonomy to become the scientist I am today. He has truly been the model of what a PI should be. Likewise, my co-mentor Vern Carruthers for his constant support and guidance on the biological side of this project. I am grateful to have been fortunate enough to have such fantastic mentors. Thanks to the rest of the Larsen lab for the mentorship and friendships over these several years! The staff in the VMCC, Michael Wilson, Kim Hutchings, and Walajapet Rajeswaran have been a constant source of guidance and encouragement. Thanks to Brandt Huddle, Dylan Kahl, Janice Sindac, Helen Waldschmidt, Scott Barraza, Jake Hitchens, Rachel

Rowlands, and Shiyuan Zhang for the conversations, lunches, coffee, and everyday bantering. Thank you all for the last 5 years!

There were many talented people involved in this project. Thanks to Jake Hitchens, David Smith, Alfredo Guerra, and Nick Diaz for their huge contributions to the chemistry and biology of this project! Thanks to the other members of my committee Hank Mosberg and Peter Scott for always being supportive and helpful. Thanks to Hollis Showalter, Pil Lee, and Andy White for their advice on the project and guidance in group meetings. Thanks to the PK core, CSB, and CCG for their contributions to this research. Thanks to everyone else within the CoP and related departments for the excellent education and opportunities I have received here. This work couldn't have been done without you all!

Table of Contents

Dedication	ii
Acknowledgements	iii
List of Figures	ix
List of Tables	xii
List of Schemes	xiii
List of Abbreviations	xiv
Abstract	xvi
Chapter 1 Introduction	1
<i>Toxoplasma Gondii</i> : Historical Perspective	1
Parasite Phylogeny	3
Parasite Life Cycle	4
Toxoplasmosis In Humans	6
- Statistics and Epidemiology	6
Pathogenicity of <i>Toxoplasma gondii</i>	9
- Immunocompetent Patients	9
- Congenital Infection	10
- Immunocompromised Patients	11
- Diagnosis of Toxoplasmosis	12
Treatments and Prevention of Toxoplasmosis	13

- Current Treatments	13
Challenges in Identifying Novel Target for the Treatment of Chronic Toxoplasmosis	15
<i>Toxoplasma gondii</i> Cathepsin L (<i>TgCPL</i>) as a Potential New Target	16
- Discovery of <i>TgCPL</i>	16
- Proteases and Broader Classification	17
- Cathepsins and Their Classification	21
- Cysteine Proteases as Viable Antiparasitic and Clinical Targets	22
<i>Toxoplasma gondii</i> Cathepsin L Classification, Structure, and Localization	23
Genetic Validation of <i>TgCPL</i> as a Potential Target	24
Chemical Validation of <i>TgCPL</i> as a Potential Target	26
Chapter 2 The Development of Dipeptide Nitrile Inhibitors of <i>TgCPL</i>	28
Identification of New Lead Inhibitors of <i>TgCPL</i>	28
- Computational Evaluation of Literature Cathepsin L Inhibitors	28
Rational and Selection of AZ-12878478 / CCG: 232877 as Lead Dipeptide Nitrile	29
First Generation Dipeptide Nitrile Inhibitors of <i>TgCPL</i>	33
- General Synthesis of Dipeptide Nitriles	33
- Synthesis of Dimethyl-lysine Analog	34
- Synthesis of Trifluoroethylamines	35
- Synthesis of Fluoroleucine Dipeptide Nitrile	36
SAR Analysis	37
- Initial Set of Dipeptide Nitriles.	37
- SAR of Additional P3 Analogs	41
- SAR of P2 Analogs for Metabolic Stability and Selectivity	42
- SAR of Analogs Designed for Improved CNS Profile	44
Metabolic Stability and Pharmacokinetics.	45
Synthesis and SAR of P3-CBZ Peptide Probes	47
Vinyl Sulfone (VS) Inhibitors of <i>TgCPL</i>	49
- Synthesis of VS Analogs	49
- VS Trends and SAR	50
SAR of Additional Dipeptide Nitrile Inhibitors	52
Conclusions	56

Experimental Section	59
Chapter 3 The Identification and Optimization of Triazine Nitrile Inhibitors of <i>TgCPL</i>	124
Rationale	124
Identification of Triazine Nitriles via High-Throughput Screen	125
Scaffold Hop from Dipeptide to Triazine Nitrile	126
Synthesis of Triazine Nitriles	128
Results	129
- Docking of Triazine Lead with <i>TgCPL</i>	129
- SAR of P3 Vectors	131
- SAR Analysis of P2 Vectors	136
- P2 Vectors for Improved Metabolic Profile and Selectivity	139
Microsomal Stability and Pharmacokinetics	145
- MDR1/MDCK Permeability and Efflux	149
Conclusions	150
Experimental	151
Chapter 4 Design of Fluorescent Probes and <i>In Vitro</i> Activity	205
Dipeptides, Bradyzoite Viability, and Rationale	205
Synthesis of BODIPY-CO ₂ H	207
Synthesis of VS-BODIPY probe	208
Synthesis of Triazine Nitrile BODIPY Probe	209
Puncta Formation and Autophagy in CPL Deficient Bradyzoite Cysts	210
BODIPY labeling of <i>TgCPL</i> in bradyzoite cysts	213
Fluorescent Labeling Competition Assay	215
Bradyzoite Cyst viability assay	218
Conclusion	219
Experimental	221
Chapter 5 Future Directions	232
Overview of Objectives	232
Conformational restriction	233

-Variable binding modes and conformational restriction	233
-Example conformationally restricted analogs:	235
-Benzylic modification for improved solubility and restriction of binding mode	236
P3 heterocyclic and basic vectors	238
Bibliography	248

List of Figures

Figure 1. Morphology of intracellular <i>Toxoplasma gondii</i> tachyzoites.....	1
Figure 2. Phylogenetic tree of parasitic alveolates in the Apicomplexa phylum.....	3
Figure 3. <i>Toxoplasma gondii</i> infection cycle.....	4
Figure 4. SEM of a <i>T. gondii</i> bradyzoite cyst.....	5
Figure 5. Global distribution of <i>T. gondii</i> infection rates	8
Figure 6. Kinetics of the antibody (Ab) response.	12
Figure 7. Current drugs used for the treatment of toxoplasmosis.....	14
Figure 8. The catalytic mechanisms of different proteases.....	18
Figure 9. Diagram representing the peptide substrate	20
Figure 10. Cleavage mechanism and subsite nomenclature of cathepsin cysteine proteases.	22
Figure 11. Crystal structure of activated <i>Toxoplasma gondii</i> cathepsin L	23
Figure 12. Genetic validation of TgCPL as a target for chronic stage <i>T. gondii</i> infection	25
Figure 13. CPL activity is required for cyst viability <i>in vitro</i>	27
Figure 14. Literature lead cathepsin L inhibitors.....	29
Figure 15. Protease warheads	30
Figure 16. Ligplot diagram of 232877 in HsCPL.....	31
Figure 17. TgCPL and HsCPL active site comparison	31
Figure 18. Overlay of 232877 and 258070 in TgCPL	40
Figure 19. SMARTCyp prediction of the top three sites of metabolism	46

Figure 20. Vinyl sulfone inhibitors of <i>TgCPL</i>	50
Figure 21. Key compounds in the optimization of 2 for <i>TgCPL</i> potency, metabolic stability, and a CNS-penetrant profile.	58
Figure 22. Inhibitors of <i>Toxoplasma gondii</i> cathepsin L.....	124
Figure 23. Structural overlay and active sites of <i>TgCPL</i>	126
Figure 24. Scaffold hop from dipeptide nitrile to triazine nitrile.....	127
Figure 25. Covalent docking of 262962 into <i>TgCPL</i> and <i>HsCPL</i>	130
Figure 26. Potential flip of binding mode for triazine nitriles	135
Figure 27. Metabolic liabilities for 262962	138
Figure 28. Mouse liver microsome half-life of select inhibitors	145
Figure 29. Initial Pharmacokinetic studies.....	147
Figure 30. Additional pharmacokinetic studies	148
Figure 31. Bradyzoite viability assay results for dipeptide nitriles and vinyl sulfones	206
Figure 32. Puncta formation in lysosomal dysfunction	211
Figure 33. CytoID staining of bradyzoite cysts	212
Figure 34. BODIPY vinyl sulfone probe 263252 enters bradyzoite cyst and binds to <i>TgCPL</i> ..	213
Figure 35. Competition assay between labeled and unlabeled <i>TgCPL</i> vinyl sulfone inhibitors	216
Figure 36. Competition assay between BODIPY labeled (263473) and unlabeled (262962) <i>TgCPL</i> triazine nitrile inhibitors suggests they compete for the same target.	217
Figure 37. Bradyzoite viability assay results for triazine nitrile inhibitors of <i>TgCPL</i>	219
Figure 38. Select developed inhibitors of <i>Toxoplasma gondii</i> cathepsin L.....	232
Figure 39. Potential flip of binding mode.....	234

Figure 40. Possible conformational restrictions to keep the desired binding orientation of TgCPL inhibitors	235
Figure 41. Docking of 263251 in <i>TgCPL</i>	236
Figure 42. Modifications of benzylic position to impede rotation and improve solubility	237
Figure 43. Synthesized alternative cores and <i>TgCPL</i> inhibition.....	240
Figure 44. Alternative core scaffolds.....	241
Figure 45. Intramolecular stabilization of transition state	242
Figure 46. Example purification of mature <i>TgCPL</i>	245

List of Tables

Table 1. Comparison of calculated properties of lead inhibitors vs CNS and non-CNS drugs	28
Table 2. Cathepsin L inhibitory activity of initial P2 and P3 analogs.	38
Table 3. Inhibitory activity of additional aryl P3 substitution analogs.	41
Table 4. Inhibitory activity of additional aliphatic P2 analogs.	42
Table 5. Inhibitory activity of trifluoroethylamine and cyclopropyl-nitrile analogs.	44
Table 6. Metabolic stability of select analogs in mouse liver microsomes.	45
Table 7. <i>In Vivo</i> Exposure of Compound 258070 Following IP or IV Administration to Mice ^a	47
Table 8. P3 CBZ probes for rapid P2 analysis.	48
Table 9. Cathepsin L inhibitory activity of initial P2 and P3 analogs.	52
Table 10. Cathepsin L inhibitory activity of initial P2 and P3 analogs.	55
Table 11. SAR of P3 vectors.	131
Table 12. Screen of various P2 vectors.	136
Table 13. P2 Vectors for Improved Metabolic profile and Selectivity.	139
Table 14. MDR1 / MDCK Assay results.	149

List of Schemes

Scheme 1. General synthesis of dipeptide nitriles	33
Scheme 2. Synthesis of dimethyl-lysine analog	34
Scheme 3. Synthesis of trifluoroethylamines.....	35
Scheme 4. Synthesis of fluoroleucine dipeptide nitriles.....	36
Scheme 5. General synthesis of P3-CBZ P2 probes.....	48
Scheme 6. Synthesis of dipeptide vinyl sulfone inhibitors of <i>TgCPL</i>	49
Scheme 7. General synthesis for triazine nitrile inhibitors.....	128
Scheme 8. Alternative triazine nitrile synthetic scheme.....	128
Scheme 9. Synthesis of BODPIY-CO ₂ H	207
Scheme 10. Synthesis of BODIPY-tagged dipeptide vinyl-sulfone 263252	208
Scheme 11. Synthesis of BODIPY-tagged triazine nitrile probe 263473.....	209

List of Abbreviations

ADME - Absorption, distribution, metabolism, excretion

BBB – blood-brain barrier

CCG - Center for Chemical Genomics (University of Michigan)

CDC – Center for Disease Control and Prevention

CMPD- compound

CNMR - Carbon nuclear magnetic resonance spectroscopy

CNS – central nervous system

CPB – Cathepsin B

CPL – Cathepsin L

CPS – Cathepsin S

CYP - Cytochrome P450

DMSO - dimethyl sulfoxide

FPLC - Fast protein liquid chromatography

HNMR - Proton nuclear magnetic resonance spectroscopy

HPLC - High-performance liquid chromatography

*Hs*CPL – Human cathepsin L

IC₅₀ - half maximal inhibitory concentration

LC - liquid chromatography

MDCK - Madin-Darby canine kidney cells

MDR1 - Multidrug resistance protein 1

MLM - Mouse liver microsome

MS - Mass spectrometry

MW - Molecular weight

NMR - Nuclear magnetic resonance spectroscopy

Pgp - P-glycoprotein

PDB - protein data bank

SDS-PAGE - sodium dodecyl sulfate Polyacrylamide electrophoresis

SAR - Structure-activity relationship

SEM - Standard error of the mean

SD - Standard deviation

TgCPL – *Toxoplasma gondii* cathepsin L

TPSA Topological polar surface area

Abstract

Toxoplasma gondii chronically infects ~2 billion people worldwide. This neurotropic protozoan is the 2nd leading cause of death due to foodborne illness in the US, and has been designated as one of five Neglected Parasitic Infections targeted by the CDC for public health action. Currently, there is no efficacious *T. gondii* therapeutic capable of treating the chronic dormant-phase toxoplasmosis infection in the CNS. *T. gondii* cathepsin L (TgCPL) has been implicated as a viable target for treatment of the chronic stage infection. Confirmation that TgCPL inhibition can eliminate neuronal cysts in a mouse with chronic toxoplasmosis is a crucial step in demonstrating that TgCPL is a valid target in chronic toxoplasmosis. Initially, a series of TgCPL dipeptide nitrile inhibitors was developed, improving potency for the *T. gondii* enzyme from 2 μ M to as low as 115 nM. Although we successfully demonstrated that this compound class can penetrate the blood brain barrier, it also exhibits rapid clearance *in vivo*. A high throughput screen was then conducted and a triazine nitrile scaffold was selected based on literature precedent of this chemotype as inhibitors of human cathepsins and predicted BBB penetrant properties. Scaffold hopping to this chemotype resulted in an instantaneous gain of potency (TgCPL IC₅₀ = 34 nM), however reduced metabolic stability relative to the corresponding dipeptide. Analogs were then synthesized to optimize metabolic stability, CNS permeability, and selectivity over human isoforms. Overall, we improved potency against TgCPL to as low as 5 nM and identified features that can be exploited to gain selectivity vs HsCPL (10-fold), and significantly improved metabolic stability (up to t_{1/2} >60 min in MLM). Importantly, we achieved CNS penetrance (up to Brain /Plasma = 1.4) and demonstrated that treatment of

chronic stage *T. gondii* bradyzoite cysts with triazine nitrile inhibitors reduces parasite viability with efficacy equivalent to a *TgCPL* genetic knockout. This is the first example of a CNS penetrant, reversible *TgCPL* inhibitor showing efficacy in an *in vitro* model of the chronic stage parasite. Current endeavors are advancing toward *in vivo* proof-of-concept that pharmacological inhibition of *TgCPL* is an effective method of treating chronic *T. gondii* infection in the CNS.

Chapter 1 Introduction

Toxoplasma Gondii: Historical Perspective

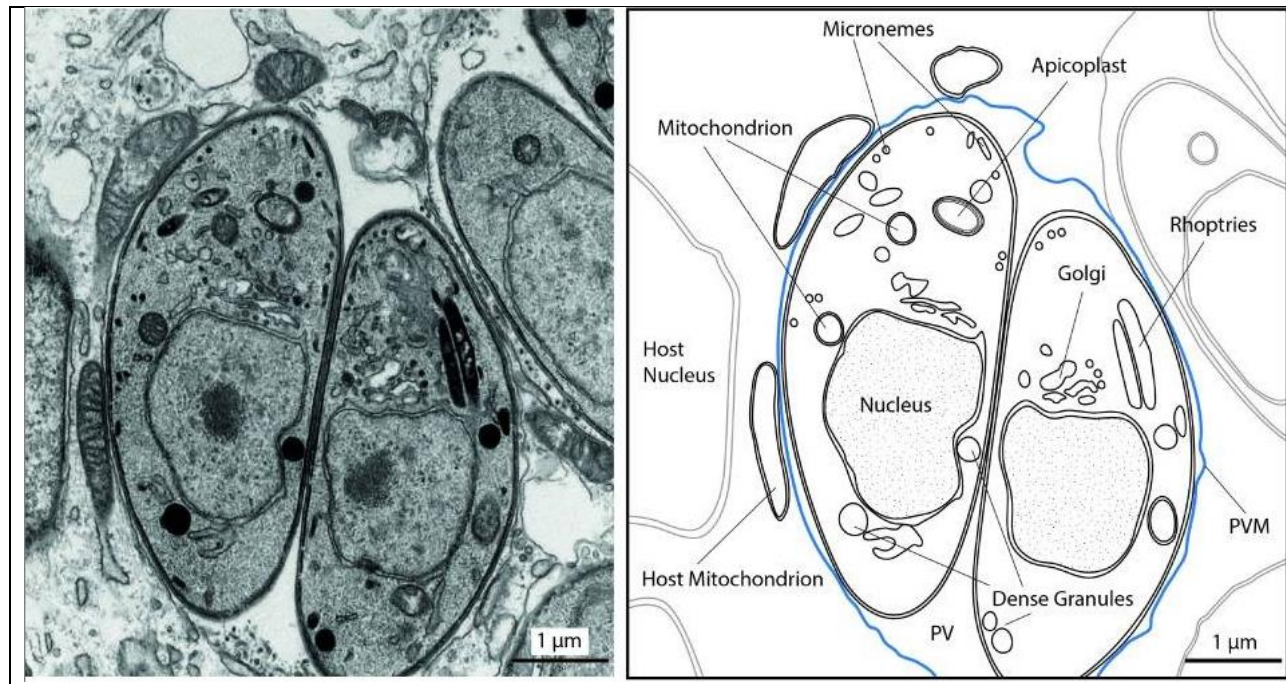


Figure 1. Morphology of intracellular *Toxoplasma gondii* tachyzoites.

(left) Transmission electron micrograph of the intracellular *Toxoplasma gondii* tachyzoite stage. (right) Outlines of some host and parasite organelles.¹

Toxoplasma gondii was first discovered in 1908 by Nicolle and Manceaux in the tissues of the North African comb rat, or Gundi (*Ctenodactylus gundi*). Around the same time in Brazil, Splendore also isolated the protozoan from rabbit tissues.²⁻⁴ Some historians additionally credit two other researchers with the discovery of *Toxoplasma*.⁵⁻⁶ In 1908, Samuel Taylor Darling observed what may have been *Toxoplasma* in a human muscle biopsy, but incorrectly identified it as *Sarcosporidia*.⁷ Alphonse Laveran may have also observed toxoplasma prior to Nicolle and Manceaux during his work describing *Plasmodium sp.* and the causative agent of malaria.⁸⁻⁹ As

the only member of the genus *Toxoplasma*, this parasite's name does not originate from its "toxic" or harmful nature. Nicolle and Manceaux conferred this name to the protozoan based on the parasites morphology (toxon = bow, plasma = shape) and the original infected host.¹⁰⁻¹¹ It wasn't until 1932 that this parasite was found to be an agent of infectious disease in humans when Wolf et al. reported a case of a congenitally infected infant and another case of toxoplasma encephalitis.¹² Over the course of the next 50 years, Toxoplasma-like infections were described in various animal species, including humans, and our understanding of human toxoplasmosis increased. It wasn't until the 1970's that the complex *T. gondii* life cycle and various routes of transmission were fully understood when Hutchinson et.al. reported the discovery of parasite oocysts in cat feces.¹³⁻¹⁶ *Toxoplasma gondii* became recognized as a severe and life-threatening organism after several cases of toxoplasmic encephalitis were reported around the same time. In the 1980s, once immunodeficiency syndrome (AIDS) became epidemic, *T. gondii* became widely recognized as a cause of morbidity and mortality in immunodeficient patients. This parasite continues to be a relevant disease in the modern era, especially in the case of immunodeficient patients and pregnant women. With an estimated two billion people chronically infected, *Toxoplasma gondii* remains one of the most pervasive infectious agents in the world.¹⁷⁻

Parasite Phylogeny

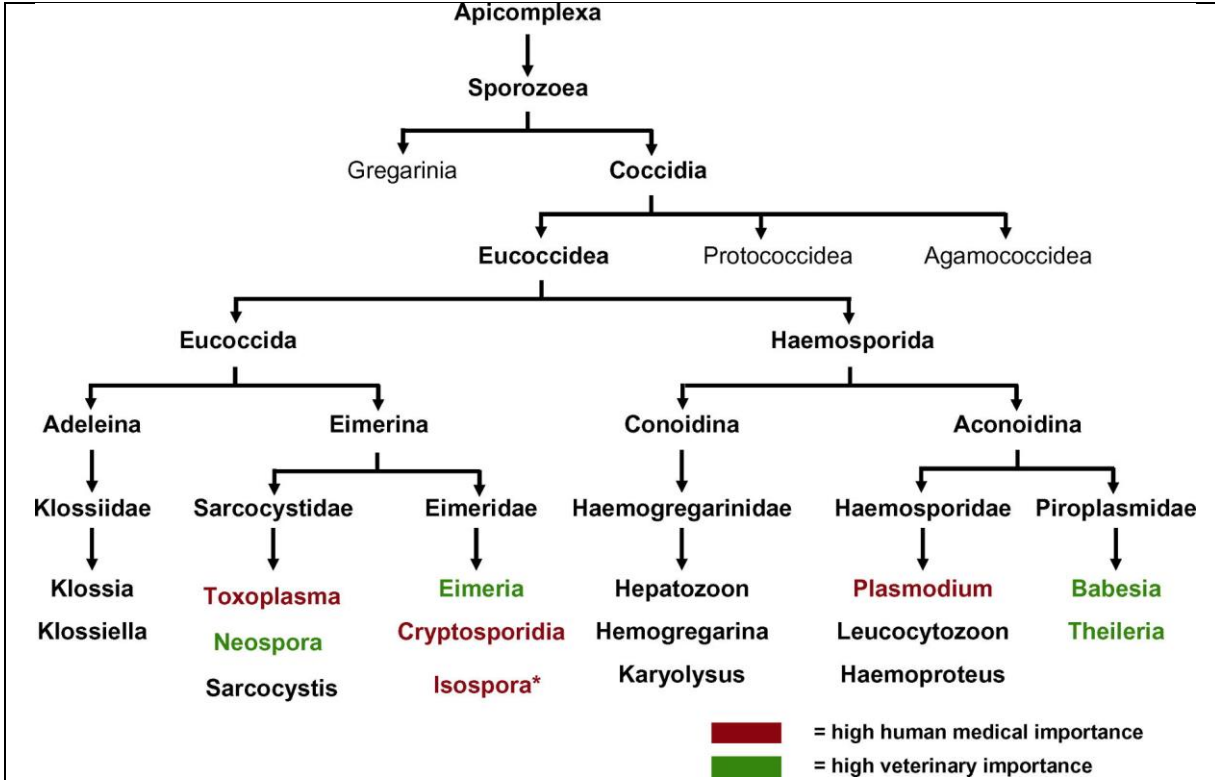


Figure 2. Phylogenetic tree of parasitic alveolates in the Apicomplexa phylum

Toxoplasma gondii is an obligate intracellular protozoan parasite that belongs to the Apicomplexa phylum, Conoidasida class, Eucoccidiorida order, Sarcocystidae family, Toxoplasmatinae subfamily, and is the only member of the genus *Toxoplasma* that has been described (Figure 2).¹⁹ All Apicomplexa are intracellular parasites that cause a variety of diseases in humans and animals. All the Apicomplexa (over 5000) are characterized by a complex organelle structure at the anterior region called the apical complex. This unique structure is used in host cell invasion and is what gives the phylum its name.²⁰ *Toxoplasma* is often used as a model system for Apicomplexa for its amenability to genetic manipulation, high efficiency of transfection, availability of cell markers, and the relative ease with which the parasite can be studied using microscopic techniques due to its size.²¹⁻²²

Parasite Life Cycle

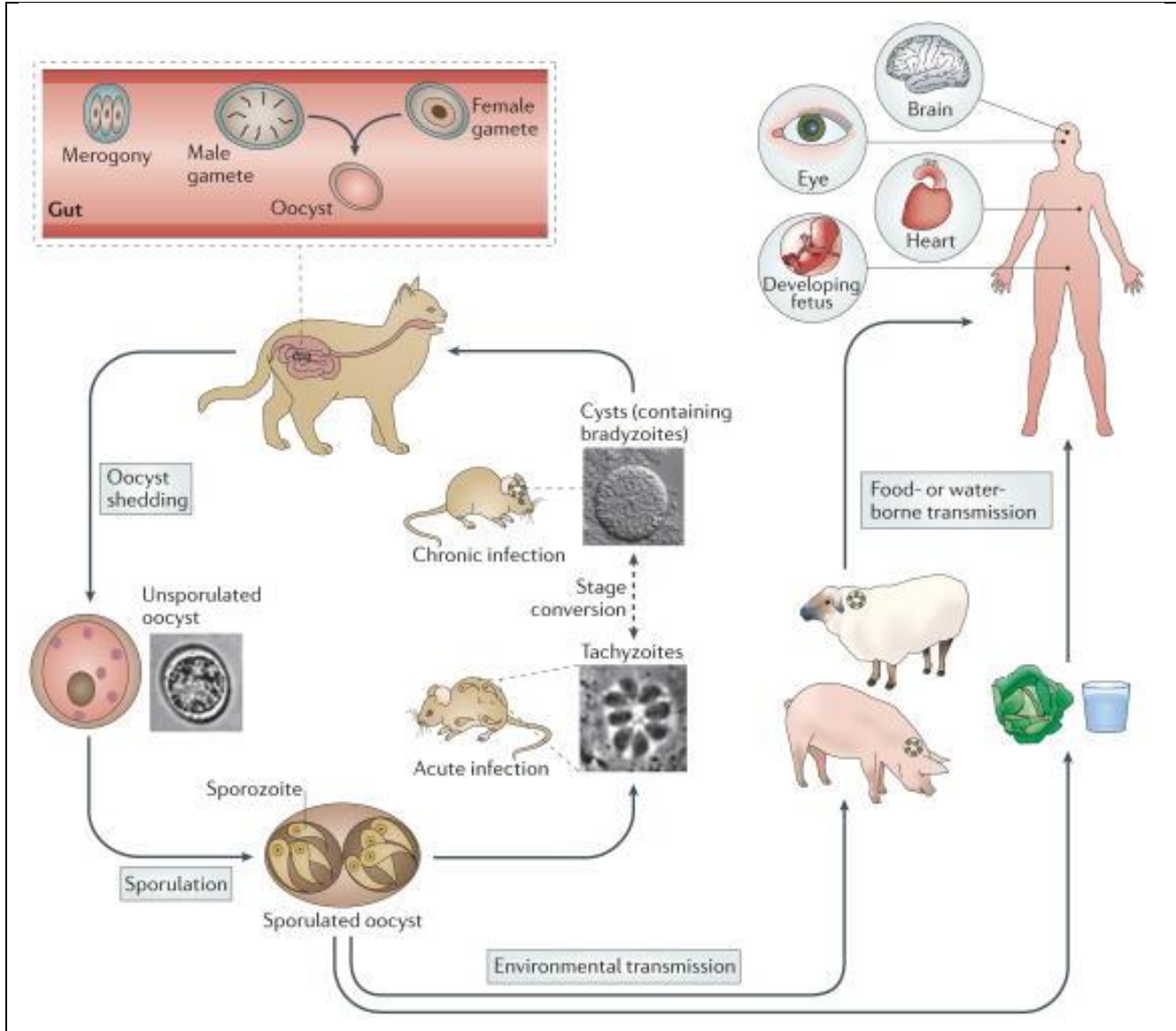


Figure 3. *Toxoplasma gondii* infection cycle
 Image derived from Hunter and Sibley (2012)²³

As is common for Apicomplexa, *T. gondii* exhibits a complex life cycle. The protozoan can adopt three distinct forms (oocyst, tachyzoite, and bradyzoite), and is capable of replicating both sexually and asexually. Felines are the parasite's definitive host in which sexual replication occurs. After a replication process known as merogony occurs in the feline gut, male and female gametes are formed within the host cell. These gametes then fuse into a diploid oocyst, which are

then shed from the feces of the cat into the environment.^{10, 24-25} These oocysts disseminate throughout the soil, water, and vegetation, where they can persist in nature for months in a cool dry environment.²⁶⁻²⁷ Ingestion of these spores, either from direct contact with cat feces or ingestion of oocyst-contaminated food, is a common route of infection for intermediate hosts. In the intermediate host, (shown in **Figure 3** as rodents) the parasite undergoes asexual replication. Upon initial infection, the oocysts convert into a rapidly multiplying trophozoite form known as tachyzoites (Greek: tachos = fast). At this stage, the tachyzoite permeates the intestinal epithelial cells and subsequently enters the blood stream, allowing the parasite to disseminate throughout the host body. They undergo rapid division, causing inflammation, tissue destruction and further spread the infection through the host.

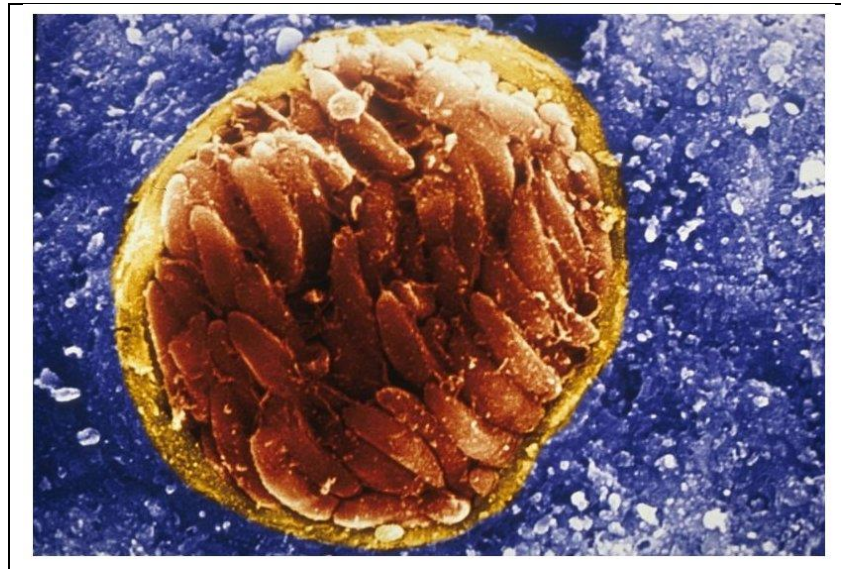


Figure 4. SEM of a *T. gondii* bradyzoite cyst
From the brain of an infected mouse. © David Ferguson

Approximately a week post-infection, the host immune response forces the parasite to transition into a persistent tissue cyst. This slow growing cyst form known as the bradyzoite

(**Figure 4**, Greek: brady = slowly), is predominant in areas of the host where the immune response is weak, such as muscle, brain, retina, and testes.²⁸⁻²⁹

The host immune response is key for the parasite life cycle for two reasons. First, in the absence of an immune response, the parasite would kill the host. Second, the pressure from the host immune system is what drives the tachyzoite to convert into the chronic bradyzoite form, where it can persist indefinitely, as the tissue cysts cannot be eliminated by the host immune system.³⁰ When a feline ingests a rodent or bird carrying *T. gondii* bradyzoites in its muscle and brain tissues, the parasite reconverts back into its tachyzoite form and the cycle of sexual reproduction continues. As this parasite is capable of infecting nearly all warm-blooded mammals, humans become infected and serve as an intermediate host through the consumption of undercooked meat containing bradyzoite cysts, or oocysts in contaminated water. While most symptoms of infection in humans are mild, toxoplasmosis can cause serious health issues if the host immune system is compromised.³¹

Toxoplasmosis In Humans

- Statistics and Epidemiology

Thanks to its multiple routes of infection and the ability to infect nearly all warm-blooded animals, *T. gondii* continues to be one of the most pervasive parasites in the world. It has been found throughout the animal kingdom and infection with this protozoan parasite is globally distributed amongst humans. Estimates suggest over 30% of the global human population is currently infected with human seroprevalence reaching as high as 90% in some countries.³²⁻³⁴ Roughly 60 million persons in the United States (15-20% of the population) are infected with

Toxoplasma, imposing a health care burden estimated in 2012 of \$3 billion annually due to the treatment and institutionalization of afflicted individuals.^{32, 35} Each year in the US, roughly 800,000 cases of *Toxoplasma* infection are reported annually, resulting in an estimated 4428 hospitalizations. This neurotropic protozoan is currently the second leading cause of death due to foodborne illness in the US (~327 deaths per year), and has been designated as one of five neglected parasitic infections targeted by the Center for Disease Control and Prevention for public health action.³⁶ In patients with AIDS, one to five percent will develop toxoplasmic encephalitis.³⁷ Furthermore, *T. gondii* is the most common cause of infectious necrotizing retinochoroiditis, which manifests in 1-20% of patients with acquired systemic infections. In the United States, ocular toxoplasmosis affects an estimated 21,000 people each year, eventually leading to loss of vision in approximately 4,800 individuals annually.³⁸ Significant differences are observed with *Toxoplasma* infection rates being higher in various geographic regions and in populations with lower socioeconomic status. One study found that *Toxoplasma* seroprevalence in the US was higher in the Northeast (29.2%) than in the South (22.8%), Midwest (20.5%), or West (17.5%) ($p < 0.05$).³⁹ Infection in humans primarily occurs through ingestion of undercooked contaminated meat, especially pork and lamb. As such, *T. gondii* also has significant veterinary importance as toxoplasmosis in sheep and goats results in neonatal infection and abortion.⁴⁰

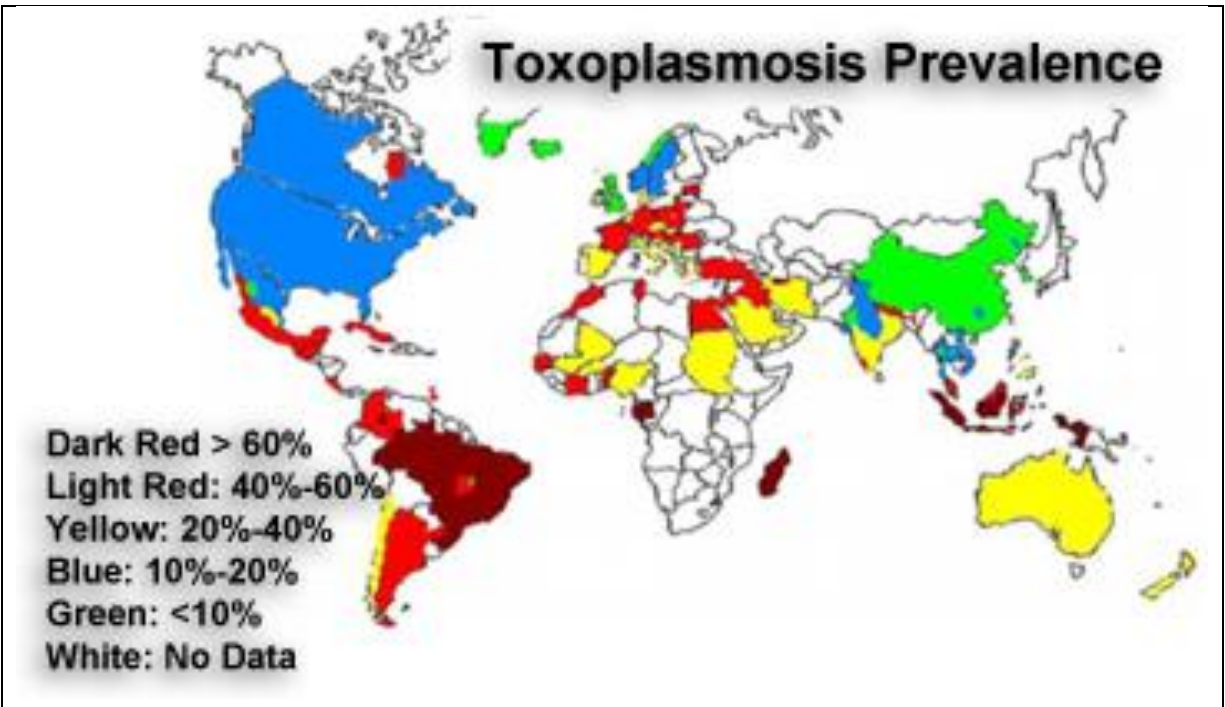


Figure 5. Global distribution of *T. gondii* infection rates
 From Pappas, G et. al. (2009)⁴¹

At the international level, climate, socioeconomic factors, and food preparation habits play important roles in parasite distribution. In cooler climates, such as North America, South East Asia, and Northern Europe, low seroprevalences are observed ranging between 10 to 30%. Increased seroprevalence (30 to 50%) are often found in countries of Central and Southern Europe and high prevalences are common in Latin America and tropical African countries (**Figure 5**).^{31, 42} In many populations where undercooked meat is commonly consumed, such as those in El Salvador and France, the seropositivity rate is as high as 75%. As much as 90% of adults in Paris have been found to be seropositive for *Toxoplasma* infections. In certain regions of Western Europe and Africa, approximately 50 to 78% of individuals with HIV tested seropositive for *T. gondii* infection. Approximately 37% of AIDS patients in France displayed evidence of toxoplasmic encephalitis at autopsy. In general, older individuals are more likely to

manifest evidence of reactivated *Toxoplasma gondii* infection and congenitally acquired retinochroiditis is more likely to occur in person's over 40 years old. [36]

Pathogenicity of *Toxoplasma gondii*

- Immunocompetent Patients

Most people (ca. 80%) who become infected with *Toxoplasma gondii* are asymptomatic. In some scenarios, patients will experience mild flu like symptoms including fever, myalgia, tender lymph nodes, and muscle aches. This initial disease state is caused by the rapidly replicating tachyzoite form. This stage typically lasts for a few weeks, at which point the host immune system drives that tachyzoites into their bradyzoite form and the parasite begins its latent infection. If the host maintains a healthy immune system this chronic infection generally presents few symptoms although a growing body of evidence suggests at this chronic stage infection may significantly contribute to a wide array of neuropsychiatric symptoms.⁴³⁻⁴⁶ Animal studies have shown that *T. gondii* infection can have an influence on host behavior, neuronal function, and mate choice. These studies demonstrated that rats that are chronically infected with brain cysts have altered risk taking behavior, and unconditioned fear responses.⁴⁷ Evolutionarily this makes sense, as this behavior leads to increased opportunities for the transmission of the parasite from a rodent host to the definitive feline host. *T. gondii* has also been shown to enhance the sexual attractiveness of infected male rats.⁴⁸ In humans, dozens of studies have linked chronic *T. gondii* infection to major mental illnesses including schizophrenia (odds ratio 2.7, $P < 0.000001$), bipolar depression (odds ratio 2.4, $P < 0.05$), and various other mood alterations.⁴⁹⁻⁵¹ *T. gondii* seropositive schizophrenic patients also have worse symptoms, require more treatment, and have longer hospital stays compared to seronegative schizophrenics.⁵²⁻⁵⁵ The genotype of the

infecting parasite strain also plays a role in the severity of the infection. For example, North America and Europe are correlated with strains resulting in low prevalence and infection severity. Strains from South America or Brazil often lead to more severe infections. For example, toxoplasmosis infection accounts for higher levels of visual impairment in Brazil and is the leading cause of blindness in South America.⁵⁶ There have been more recently reported cases of atypical strains, including one case in French Guiana, where *Toxoplasma* was shown to cause lethal infections in immunocompetent individuals.⁵⁷⁻⁵⁹

- **Congenital Infection**

If a woman has been infected prior to becoming pregnant, the unborn child is generally protected through the mother's developed immune system. However, some of the more severe outcomes of *Toxoplasma* infection are observed when a woman becomes infected for the first time while pregnant.⁶⁰ Post-primary infection, the mother vertically transmits the tachyzoites to her unborn baby. The frequency of this transmission and resulting severity to the child differs between the stages of pregnancy. During the beginning of gestation, the placenta serves as an efficient barrier against the parasite, limiting the transmission rate to 15-20%. This rate is increased to 30-50% during the second trimester and reaches rates as high as 60-70% during the third trimester of pregnancy.⁴¹ Conversely the severity of infection is inversely proportional to the transmission rate, the most severe symptoms resulting from infection during the first trimester. This has been shown to lead to symptoms such as miscarriage, encephalomyelitis, still born children, hydrocephalus, microcephaly, jaundice, convulsions, and more.⁶¹ For this reason, pregnant women are often counseled by physicians to avoid changing the cat litter box, in order to prevent contact with recently shed oocysts. Often, infants infected before birth often show no

symptoms at birth but develop them later in life with potential vision loss, mental disabilities, and seizures. Eye lesions due to congenital infection occur in 20-80% of infected persons by adulthood, however they manifest in less than 2% of persons infected after birth. In sheep and goats, congenital infections also are also responsible for a high percentage of spontaneous abortions.⁶²

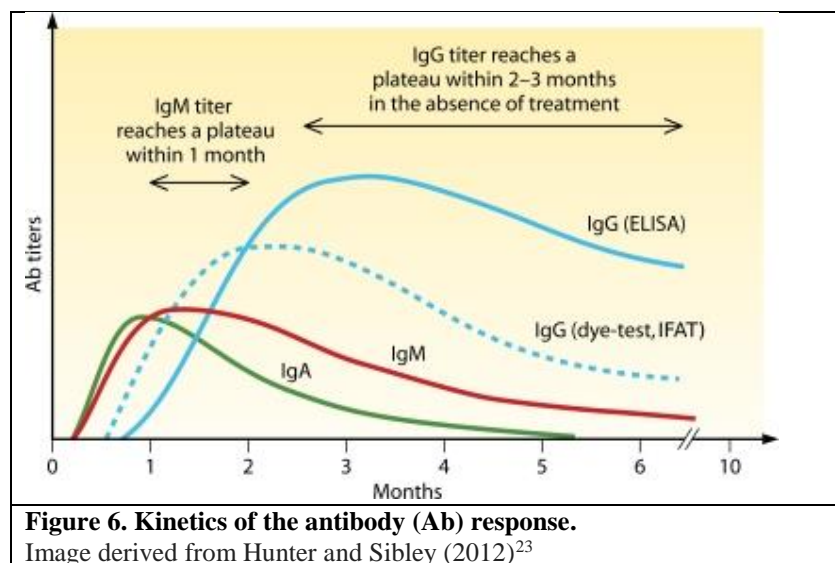
- **Immunocompromised Patients**

In its mammalian hosts, *T. gondii* exists in two principal forms, the tachyzoite and bradyzoite.²⁹ The initial disease state is caused by the rapidly replicating tachyzoite form. This stage typically lasts for a several days to weeks during which the parasite disseminates to peripheral sites including the central nervous system (CNS). *T. gondii* then transitions into a chronic bradyzoite cyst form within the CNS and muscle tissue to establish life-long infection. The host immune system is of critical importance to keep the *T. gondii* infection suppressed. A person infected with *Toxoplasma* may experience severe symptoms if their immune system becomes compromised due to reasons such as HIV infection, immunosuppressive therapies, and cancer chemotherapies. For example, *Toxoplasma* can reactivate in a patient infected with HIV and lead to severe symptoms including fever, confusion, headache, seizure, nausea, encephalitis, and death.⁶³ Immuno-depression results in the rupture of the bradyzoite cysts in the tissues, which convert back into tachyzoites causing inflammation. In the CNS, this results in severe encephalitis, which is fatal if left untreated. Patients with HIV who have not previously been infected with the parasite, are more likely to develop a severe primary *Toxoplasma* infection. Toxoplasmic encephalitis (TE) is an HIV-indicative event in 35% of patients and an AIDS-defining event in 75% of cases.⁶⁴ Individuals who progress towards marked immunodeficiency

are prone to several opportunistic infections, but TE is the most common cerebral opportunistic disease in many countries.⁶⁵⁻⁶⁷ Pulmonary or disseminated toxoplasmosis are characteristic of infections acquired from organ transplants where the organ was received from a *Toxoplasma*-seropositive donor.³¹ Serological screening of both donors and recipients should be performed to mitigate the potential risks of toxoplasmosis.⁶⁸ The reactivation of *T. gondii* in immunocompromised pregnant women who were infected prior to their pregnancy, can lead to congenital infection.

- Diagnosis of Toxoplasmosis

A variety of methods are used to diagnose toxoplasmosis. In general the diagnosis of toxoplasmosis is typically done by serological testing that measures immunoglobulin G (IgG) and immunoglobulin M (IgM) via automated or semi-automated immunoassays.⁶⁹⁻⁷⁰ This can determine if the patient has been infected; however, the difficulty lies in determining whether the infection is in its chronic or acute stage. High levels of IgM antibodies indicate an acute phase infection while IgG antibodies are indicative of a chronic infection (**Figure 6**).⁷¹



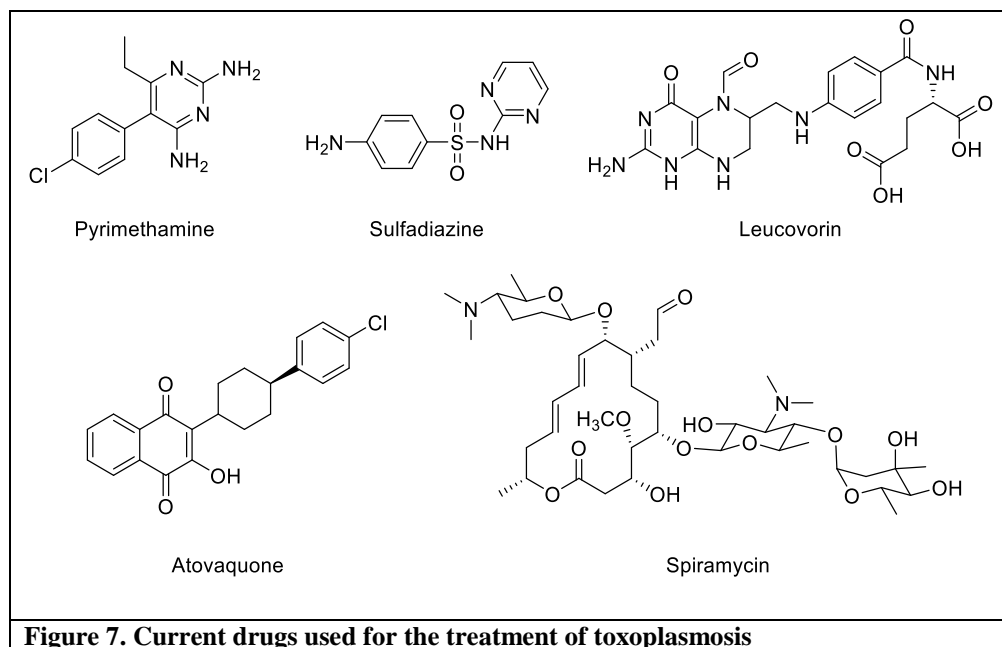
This is of particular importance to pregnant women. Parasites can be isolated from the blood or other bodily fluids such as the cerebral spinal fluid to verify an acute infection; however, this technique is not frequently used due to the time required and the difficulty of isolating the parasite. Although congenital infection can be determined by the presence of cysts in the placenta or in the tissues of the fetus, isolation of the *T. gondii* cysts is inadequate in determining if the infection is still active or latent. Therefore, the diagnosis still relies on serological testing as well. Molecular techniques such as PCR are capable of detecting parasite DNA in the amniotic fluid and may be used in cases of possible congenital transmission. If the *T. gondii* is determined to be in the early stages of infection, the diagnosis is followed up with early treatment to mitigate the risk of congenital infection. In the cases of ocular toxoplasmosis the diagnosis is made based on the appearance of lesions in the eye, disease symptoms, and serological testing.⁷²

Treatments and Prevention of Toxoplasmosis

- Current Treatments

In general, the treatment of toxoplasmosis in an immunocompetent patient is unnecessary. In immunocompromised patients, the standard treatment is a combination of pyrimethamine (inhibitor of the dihydrofolate reductase enzyme, **Figure 7**) given at 25-100 mg daily and a sulfonamide of the trisulfapyrimidine type given at 2-6 g daily, both for a month. The parasite synthesizes folates *de novo* and is unable to utilize dietary folates. This combination therapy blocks the biosynthesis of parasite folates (thus its nucleic acids) and consequently prevents synthesis of DNA and protein. Leucovorin (folinic acid) is used to decrease the toxic effects, such as bone marrow depression, caused by the pyrimethamine.⁷³ However, these combination therapies are often not tolerated and can cause symptoms such as nausea, insomnia, headache,

lightheadedness, and blood problems in some severe cases.



Clindamycin (Cleocin) can be used as an alternative treatment and has been shown to be effective at combating TE in AIDS patients.⁷⁴⁻⁷⁵ This lincosamide antibiotic functions via the inhibition of the 50s ribosomal subunit of bacteria, and thus targets the protozoan mitochondrion and a remnant non-photosynthetic chloroplast termed the apicoplast.⁷⁶⁻⁷⁷ Pyrimethamine combination therapies and Clindamycin only target efficiently proliferating tachyzoites during the acute phase of infection and is therefore ineffective against the bradyzoite cysts in the latent infection.⁷⁸ Atovaquone (an inhibitor of the mitochondrial electron transport system) has been shown to reduce the number of brain cysts in infected hamsters and can be used in patients unable to tolerate sulfonamides and clindamycin.⁷⁹⁻⁸³ The teratogenic effects of pyrimethamine prevent its use in infected pregnant women. For women still in the acute phase of infection, the recommended treatment is spiramycin if the fetus has not yet acquired the infection.⁸⁴⁻⁸⁶ Spiramycin localizes to the placenta and has been shown to reduce placental infection by 60%. Unfortunately, spiramycin has no effect on the infection if the fetus is already infected.

Additionally, it has teratogenic effects, and must be weighed against the risk of congenital infection. It is important to note that all of these treatment regimens have significant shortcomings including poor tolerance, allergic complications, and lack of efficacy against the chronic form of infection. The ability to preclude reactivation by reducing or eliminating the chronic *T. gondii* infection from at risk individuals remains a key unmet need. Currently, there is no efficacious *T. gondii* therapeutic capable of treating the chronic-phase infection. Given the limitations and current inadequacies of antiparasitic therapies, there is a serious need for the development of novel and alternative strategies for the treatment of chronic *T. gondii* infection.

Challenges in Identifying Novel Target for the Treatment of Chronic Toxoplasmosis

While the tachyzoite stage of *Toxoplasma* is used as a model system for Apicomplexans, it has been very difficult to identify new targets for the treatment of the chronic *T. gondii* infection due to several reasons. In the latent stage of infection, the bradyzoites grow very slowly in both culture and infected mice. This greatly impedes the workflow of researchers and dissuades many investigators. Clinically, this also precludes the use of many standard antiparasitics that target rapidly replicating parasites. Additionally, it is difficult to obtain the large quantities of the chronic *T. gondii* parasites needed for proteins analysis and drug discovery. Furthermore, many of the parasite strains fail to efficiently convert to the bradyzoite stage cysts in-vitro. Dr. Vern Carruthers and his lab have made substantial advancements in understanding mechanisms of chronic *T. gondii* infection, and optimized methods for culturing and harvesting chronic stage parasites.⁸⁷⁻⁹¹ The genetic tools for differentiation of competent strains they developed have led to the identification of a new target for chronic toxoplasmosis.⁹²

***Toxoplasma gondii* Cathepsin L (TgCPL) as a Potential New Target**

- Discovery of TgCPL

T. gondii has a complete endolysosomal system, including a lysosome-like vacuolar compartment (VAC).⁹³ While in the latent phase, *T. gondii* retains an active endocytic system in which the VAC receives and degrades material derived from the cytoplasm of infected host cells.⁹⁴⁻⁹⁵ Recent studies revealed a key role for proteolysis within the parasite VAC in the turnover of autophagosomes and persistence during neural infection.⁹⁶ *T. gondii* expresses five cysteine proteases. Two of these members are predominantly localized in the VAC. These have been termed *Toxoplasma gondii* cathepsin protease L (TgCPL; toxodb accession number TGME49_321530) and *Toxoplasma gondii* cathepsin protease B (TgCPB; TGME49_249670).⁹⁷ The remaining three belong to the cathepsin C class of proteases (TgCPC, TgCPC2, and TgCPC3), with the former two being expressed in the tachyzoite stage, and the latter in the sporozoite form. None of the TgCPC's have been detected in the bradyzoite stage.⁹⁸ Upregulated expression of TgCPL and TgCPB in chronically infected mice suggests an active role for VAC proteolysis in *Toxoplasma* persistence.⁹⁹ The maturation of TgCPB is dependent on TgCPL activity, thus ablating TgCPL effectively impairs both proteases⁹⁷ The disruption of these cysteine proteases (primarily TgCPL) impedes the digestive function of the VAC and shows a notable impact on the chronic infection, implicating TgCPL as a potential new target in the treatment of toxoplasmosis.

- **Proteases and Broader Classification**

Proteases are enzymes involved in protein catabolism through the catalytic hydrolysis of peptide bonds in macromolecules and oligomeric peptides. These enzymes, also known as peptide hydrolases, range from monomers as small as 10 kDa to large multimeric complexes of hundreds of kDa. These enzymes are found in nearly all biological systems, and genome sequencing projects have revealed that proteases comprise approximately 2% of all expressed genes.¹⁰⁰⁻¹⁰¹ They are classified by the clans and families they belong to as well as by the catalytic mechanism used in protein hydrolysis. The main types are serine proteases, metalloproteinases, aspartic acid proteases, threonine proteases, cysteine proteases and other ‘cryptic’ proteases may exist.¹⁰² The MEROPS database classifies these peptidase families by their catalytic type, the first character representing the catalytic type (ex. A, aspartic; C, cysteine; M, metallo; S, serine; etc...).

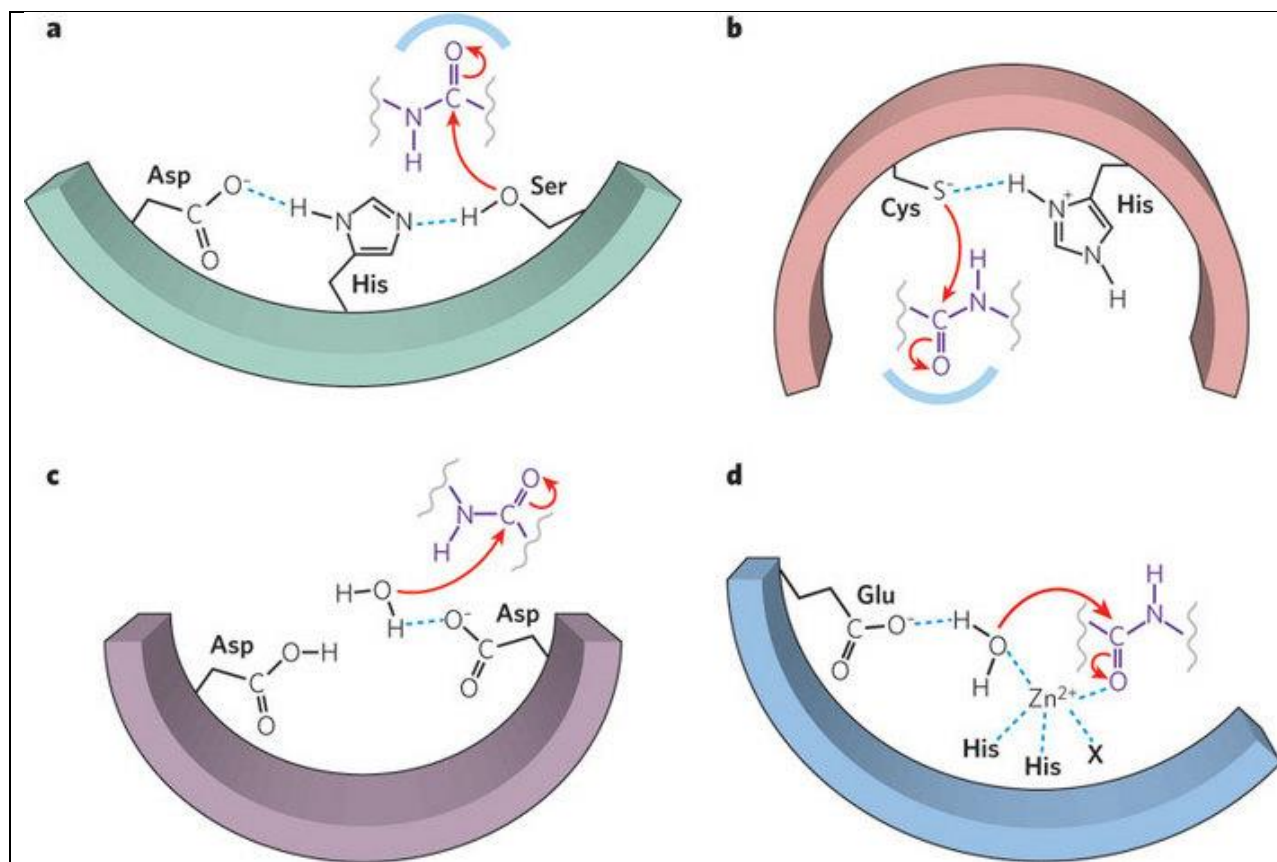


Figure 8. The catalytic mechanisms of different proteases

A) Serine proteases, B) Cysteine proteases, C) Aspartic proteases, D) Metalloproteinase. Hydrogen bonds are shown in blue dotted lines. The oxygen anion in (A), (B) and (C), and the thiolate in (D) are positioned to attack the amide carbonyl in peptides (red arrows).¹⁰³

Serine Protease: A serine protease active site consists of a catalytic triad comprised of 3 key amino acids, His 57, Ser 195 and Asp 102, with the serine acting as the nucleophile. While these amino acids are located distally from each other on the primary sequence of the peptide, protein folding is assembled in a manner that holds these residues in the catalytic site near each other (**Figure 8A**). In this catalytic triad the aspartic acid forms hydrogen bond with the histidine, increasing its ability to pull the proton from the serine residue. Lacking the hydrogen the Serine becomes a stronger nucleophile and readily attacks the carbonyl of the substrate amide bonds. Serine proteases are classified in 2 broad categories, chymotrypsin-like (trypsin-like) or subtilisin-like.¹⁰⁴ Some serine proteases have specificity that is determined by the amino acid

residues of the substrate. For example, chymotrypsin is a digestive enzyme found in pancreatic juice preferentially cleaves substrates where the P1 position is a large hydrophobic amino acid such as tyrosine, tryptophan, or phenylalanine. In humans, serine proteases are responsible for coordinating various physiological functions, including digestion, immune response, blood coagulation and reproduction.¹⁰⁵ They have also been found to play an active role in ECM remodeling.¹⁰⁶⁻¹⁰⁸

Cysteine Protease: Cysteine proteases function through a mechanism like that of the serine proteases, however the nucleophile used in catalysis is a cysteine thiol rather than a serine oxygen. Once the histidine pulls the hydrogen away from the cysteine thiol, the anion readily cleaves the substrate in a mechanism like that of the serine protease (**Figure 8B**). Cysteine proteases play crucial roles in virtually every aspect of physiology and development

Aspartic Protease: Aspartic proteases rely on a water molecule to catalyze the degradation of its substrate. (**Figure 8C**). The water is coordinated by 2 aspartic residues in the active site. In general, Aspartic proteases function optimally in low pH / acidic environment. For this reason, they are rarely reported to degrade extracellular proteins as the pH of extracellular space is generally neutral. Aspartic proteases are known to be involved in various biological functions such as blood pressure regulation (Renin), digestion (Pepsin), and HIV life cycle (HIV protease).

Metalloproteinase: A metalloproteinase is an enzyme that uses coordinated metal, most often zinc, for active site catalysis. In this scenario water is used as a nucleophilic agent to attack the carbonyl oxygen of the substrate through interactions with the coordinated zinc and a glutamate

residue in the active site as shown in **Figure 8D**. With over 50 different classification families, metalloproteases are the most diverse of the 4 main proteinase types. Matrix metalloproteinases (MMPs) are the main enzyme responsible for the degradation of extracellular matrix, and as such, are crucial in cell proliferation, morphogenesis, tissue remodeling and metastasis, migration (adhesion/dispersion), angiogenesis, apoptosis, and host defense.¹⁰⁹

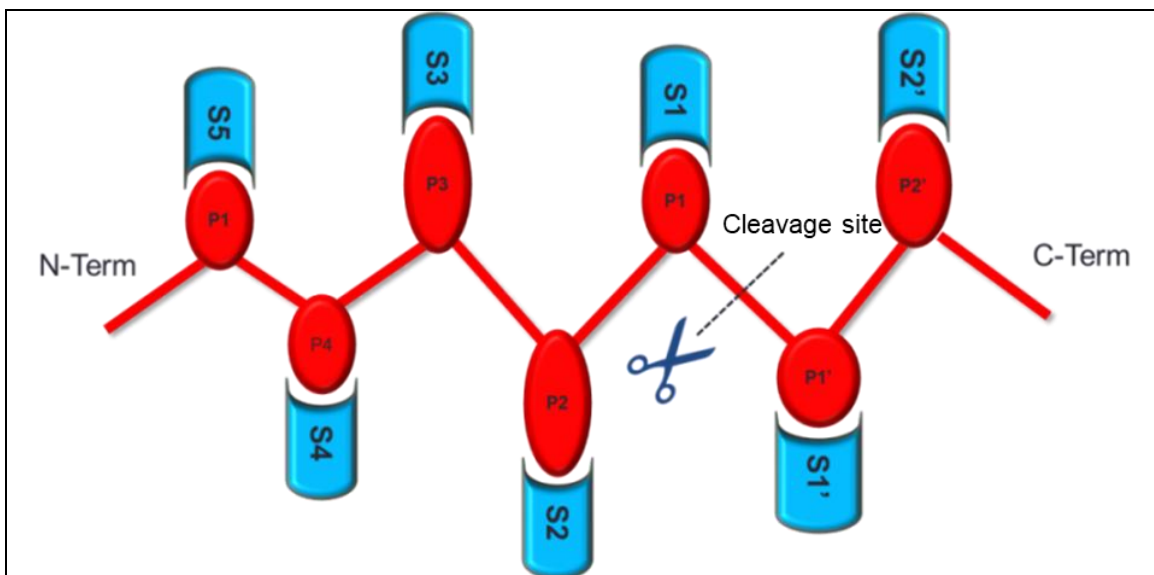


Figure 9. Diagram representing the peptide substrate
(Red) interaction with the active site pockets of a protease (Blue).

Each subsite pocket of the protease binds to a corresponding residue in the substrate sequence. Substrate amino acid residues are consecutively numbered outward from the cleavage site as $P_1'-P_2'-P_n'$ toward the C-terminus, and $P_1-P_2-P_n$ toward the N-terminus. The scissile bond is located between the P_1 and P_1' positions. Similarly, the subsites are named corresponding to the residue it binds ($S_1-S_1'-S_2-S_2'-S_n-S_n'$). Proteases that cleave protein substrates adjacent to the N- or C- terminus are termed exopeptidases, while those that cleave anywhere else in the substrate are termed endopeptidases.

- **Cathepsins and Their Classification**

Cathepsins are a group of proteolytic enzymes that are ubiquitous in the human body and nearly all living organisms. They were first discovered in 1929 as acid proteases distinct from pepsin in the gastric mucosa of pig and dog.¹¹⁰ Belonging to the papain super family of clan CA, cathepsin is derived from the Greek words, loosely meaning “to digest” (*kata* = "down" and *hepsein* = "boil"). In humans, the cathepsins are classified into various categories based on their structure, substrate specificities, and catalytic mechanisms. Cathepsins A, G are serine proteases, while cathepsins D, E are aspartate proteases. The remainder are lysosomal cysteine proteases, including the human isoforms B, C, F, H, K, L, O, S, V, X and W. Cathepsins function optimally in slightly acidic pH, corresponding to the lysosomal environment in which they are found. Cysteine cathepsins are generally considered to be intracellular enzymes that function in protein degradation and processing within lysosomes, late endosomes and vesicular compartments. The low pH in the lysosomes allows the protease to function optimally and protects the cysteine thiol from oxidation. More recently, cysteine cathepsins, namely B, K, and L, have been shown to have specific roles in bone remodeling and the degradation of ECM proteins.¹¹¹⁻¹¹²

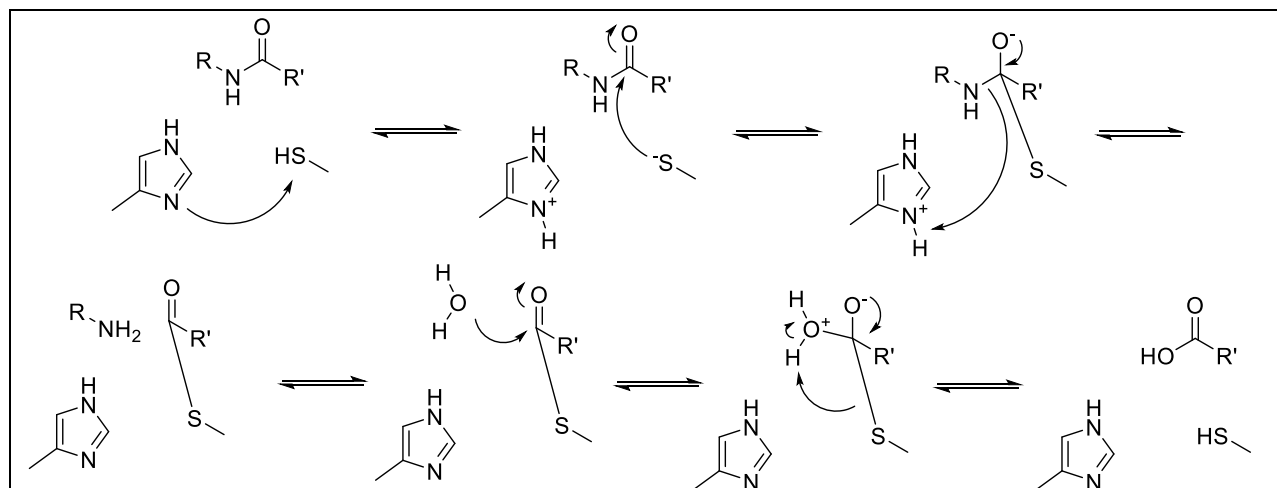


Figure 10. Cleavage mechanism and subsite nomenclature of cathepsin cysteine proteases.

The first step in the reaction mechanism, the active site thiol is deprotonated by an adjacent amino acid with a basic side chain, usually a histidine residue. The next step is nucleophilic attack by the deprotonated cysteine anion on the carbonyl of the substrate protein. The amine is then protonated and released from the complex, followed by the hydrolysis of the thioester to complete the catalytic cycle by releasing the carboxylic acid and restoring the enzyme free thiol.

- Cysteine Proteases as Viable Antiparasitic and Clinical Targets

Inhibition of vital cysteine proteases is an increasingly attractive approach for the treatment of various disease states caused by related protozoans such as *Trypanosoma cruzi*, *Plasmodium falciparum*, and others.^{102, 113-115} These parasitic organisms such as *Toxoplasma gondii* show a critical dependence on cysteine proteases for their survival.^{102, 116-117} Several protease inhibitors are showing promise in pre-clinical testing as agents against malaria and Chagas' disease.¹¹⁸ Further supporting the feasibility of protease inhibitor as drugs, many proteases are currently targeted for the treatment of various human disease states such as cancer, osteoporosis, diabetes, hypertension, myocardial infarction, acute lung injury, hepatitis C and AIDS. Several protease inhibitors are used clinically in antiretroviral therapies such as Darunavir targeting the HIV aspartyl protease, and Boceprevir and Telaprevir are used in the treatment of hepatitis C infections.¹¹⁹ Human cathepsin L is also being pursued as a target for cancer metastasis. Given the close homology to their parasitic counterparts, the vast libraries of inhibitors originally

developed against human isoforms, can provide a fruitful source of lead anti-parasitic compounds.¹²⁰ This offers an excellent starting position for utilizing a structure based medicinal chemistry approach in the development of small molecule inhibitors of *T. gondii* cathepsin L.

***Toxoplasma gondii* Cathepsin L Classification, Structure, and Localization**

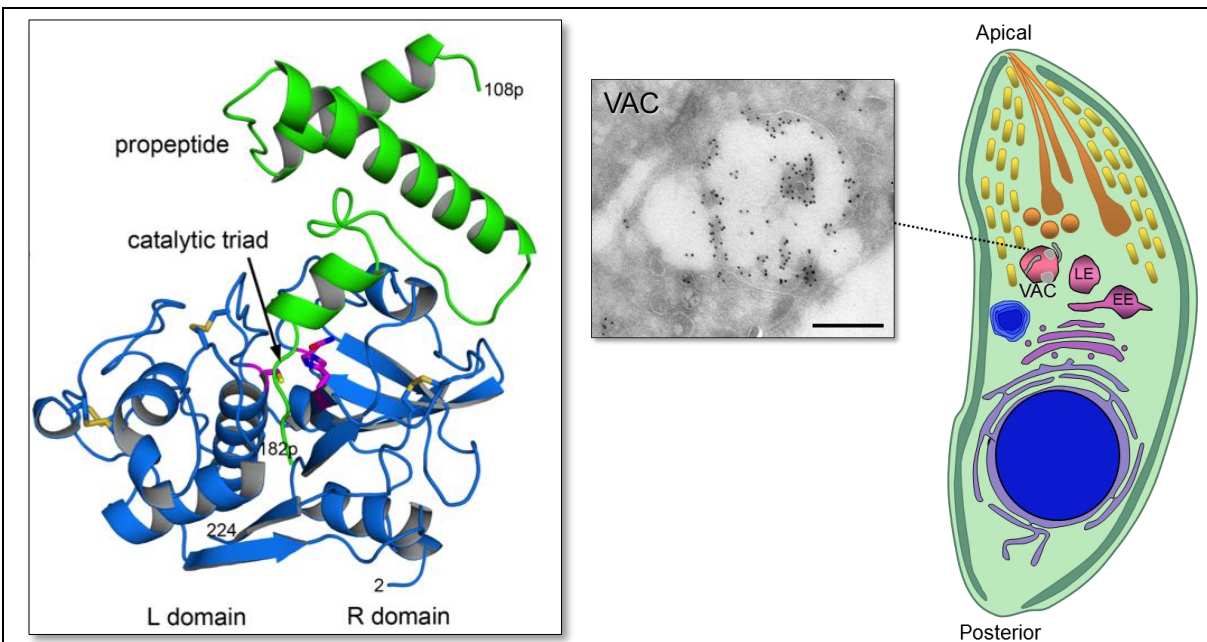


Figure 11. Crystal structure of activated *Toxoplasma gondii* cathepsin L
Derived from PDB: 3F75

TgCPL, also known as toxopain-2, is a cysteine hydrolase that is predominantly localized within the VAC (lysosome) of the *Toxoplasma* endolysosomal system in the apical region of the parasite. (Figure 11) *TgCPL* is a member of the C1 family, CA ‘papain-like’ clan of cysteine proteases. It is the only *Toxoplasma* cathepsin encoded on chromosome Ib and contains four exons. Like the rest of the members of the papain family of proteases, *TgCPL* retains the conserved cysteine, histidine, asparagine catalytic triad within its active site. *TgCPL* is 422 amino acids in length, with the C-terminal 75 residues comprising its inactivating pro-peptide tail. *TgCPL* is expressed as a zymogen and kept inactivated via its propeptide tail sterically

occluding the active site. As an endopeptidase/auto-maturase, TgCPL self-activates via the catalyzed cleavage of its propeptide tail once it reaches a low pH environment. The 30 kDa mature form functions optimally in a low pH environment (5.5 - 6.0) and preferentially cleaves P2 hydrophobic substrates. It is expressed in both the tachyzoite and bradyzoite stages of the *T. gondii* life cycle.

Genetic Validation of TgCPL as a Potential Target

The VAC-resident cathepsin protease L (*TgCPL*) is responsible for degrading host-derived proteins. Loss of *TgCPL* function in *T. gondii* results in compromised parasite replication and attenuated virulence during the acute tachyzoite infection, suggesting an important role for the *TgCPL* in pathogenesis. *TgCPL* is substantially upregulated in bradyzoites, implying a key role in this stage. Recent studies have shown it to be critical to parasite survival during the chronic phase of infection.^{96, 121} Genetic and chemical ablation of *TgCPL* severely compromises *T. gondii* chronic infection both in culture and infected mice (**Figure 12**).

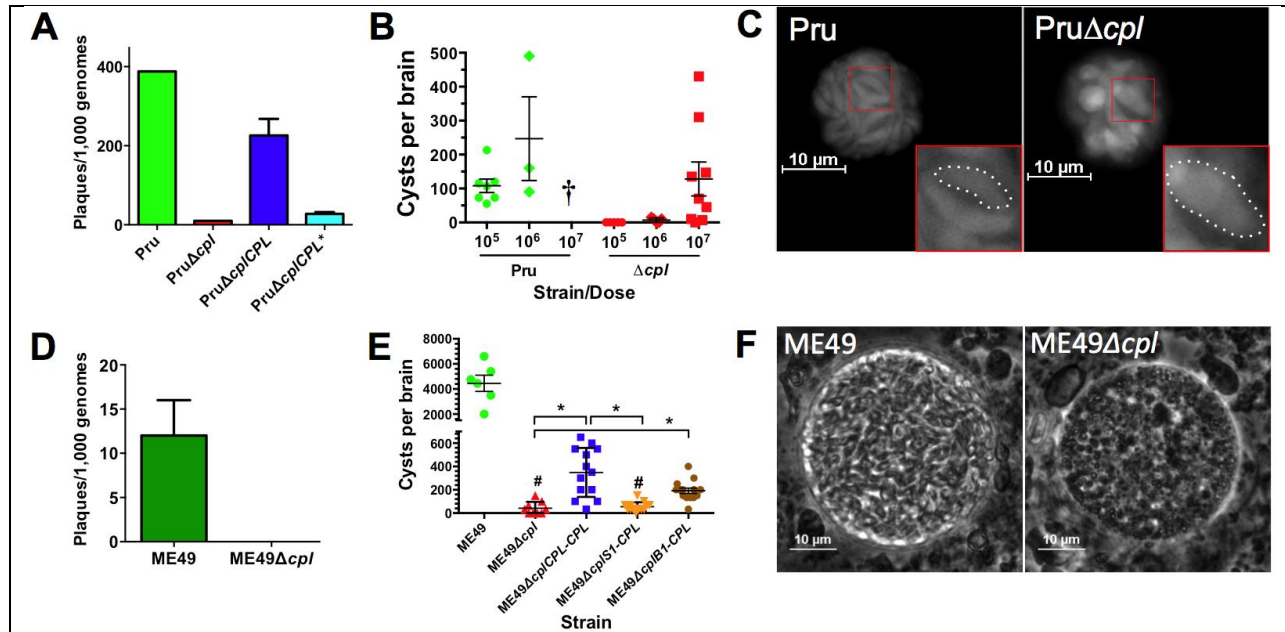


Figure 12. Genetic validation of *TgCPL* as a target for chronic stage *T. gondii* infection

(A) *TgCPL* deficient cysts are not viable *in vitro*. Parasites were stage converted to the chronic form for 2-wk before assessing viability using qPCR to measure total parasites and plaque assay to measure viable parasites. (B) Mice infected with *TgCPL*-deficient parasites have markedly fewer cysts. C57BL/6 mice were infected for 4-wk with the indicated dose, brain homogenates were blinded, and cysts were enumerated by GFP fluorescence microscopy. (†=no mice survived initial infection). (C) *PruΔcpl* cysts contain deformed bradyzoites. Shown are representative cysts from mice infected with 10^5 *Pru* or 10^7 *PruΔcpl*. Inset shows enlargement of two (*Pru*) or one (*PruΔcpl*) bradyzoite. (D) Independent confirmation that *TgCPL* deficient cysts are highly compromised. A second strain of the parasite termed ME49 strain was used to create ME49Δ*cpl*. Viability was assessed as in A. (E) Cyst burden depends on expression of *TgCPL* during the chronic phase. CBA/J mice were infected for 4-wk with 500 tachyzoites of each strain. Brain cysts were enumerated by phase contrast microscopy. Note the discontinuous y-axis. # indicates residual cysts appear degenerate. *, $p < 0.05$ student's t-test. (F) Residual ME49Δ*cpl* cysts are degenerate. Phase contrast images of ME49 and ME49Δ*cpl* cysts observed within mouse brain homogenates. (Results courtesy of Vern Carruthers lab)

The Carruthers lab utilized a genetically amenable, cyst-forming strain (*Prugnium* (*PruΔku80*; *Pru* hereafter)) to create *TgCPL*-deficient parasites (*PruΔku80Δcpl*; *PruΔcpl* hereafter).^{92, 96} They also created parasite strains that re-express active *TgCPL* (*PruΔcplCPL*) or inactive *TgCPL* (*PruΔcplCPL**) due to alanine substitution of the catalytic cysteine residue. A *T. gondii* mutant strain lacking *TgCPL* loses viability within 2 weeks of differentiating to the chronic stage in *in vitro* cultures (**Fig. 12A**), indicating that *TgCPL* is essential for survival of chronic stage parasites. Similar loss of parasite viability was seen in infected mice (data not shown). Restoring expression of an active allele of *TgCPL* rescues viability in an independently

created *TgCPL* deficient strain, but expression of a catalytically inactive allele fails to preclude death, underscoring the requirement for active *TgCPL*. Mouse infection showed that chronic stage cysts were readily detected in mice infected with 10^5 and 10^6 wild-type Pru tachyzoites, but few or no cysts were seen with *TgCPL*-deficient Pru Δ cpl at these doses (**Fig. 12B**). Pru Δ cpl cysts were observed in 10^7 infected mice, but these cysts were highly abnormal, with bloated and often misshapen bradyzoites (**Fig. 12C**). CRISPR-Cas9 genetic technology was used to create *TgCPL* deficient parasites in a second cyst forming strain called ME49. These efforts independently validated a crucial role for *TgCPL* for chronic stage viability (**Fig. 12D-F**), with >99% loss of *TgCPL*-deficient parasites after differentiation in culture and in mice. Using strains that express *TgCPL* in a stage-specific manner, this analysis also established that *TgCPL* expression, specifically during the chronic infection, is required for normal cysts (**Fig. 12E**). Taken together, these findings show that *TgCPL* activity is required for chronic *T. gondii* infection.

Chemical Validation of *TgCPL* as a Potential Target

Having genetically established a role for *TgCPL* in chronic *T. gondii* infection, the Carruthers lab moved to assess vulnerability of *TgCPL* to small molecule inhibition in the Pru strain, which expresses cytosolic GFP after differentiation to bradyzoite cysts. Cysts exposed in culture to a validated, irreversible *TgCPL* inhibitor termed LHVS lost cytosolic GFP fluorescence (**Fig. 13A**) and became degenerate similar to *TgCPL*-deficient cysts.¹²¹ A novel qPCR/plaque assay to directly assess cyst viability was used to measure the number of viable bradyzoites capable of forming plaques on a host cell monolayer and the total number of bradyzoites based on qPCR. Consistent with LHVS efficacy, no viable bradyzoites were detected

after a 3-wk treatment (**Fig. 13B**). These results provide *in vitro* proof-of-concept that *TgCPL* is a viable target for the treatment of chronic stage toxoplasmosis.

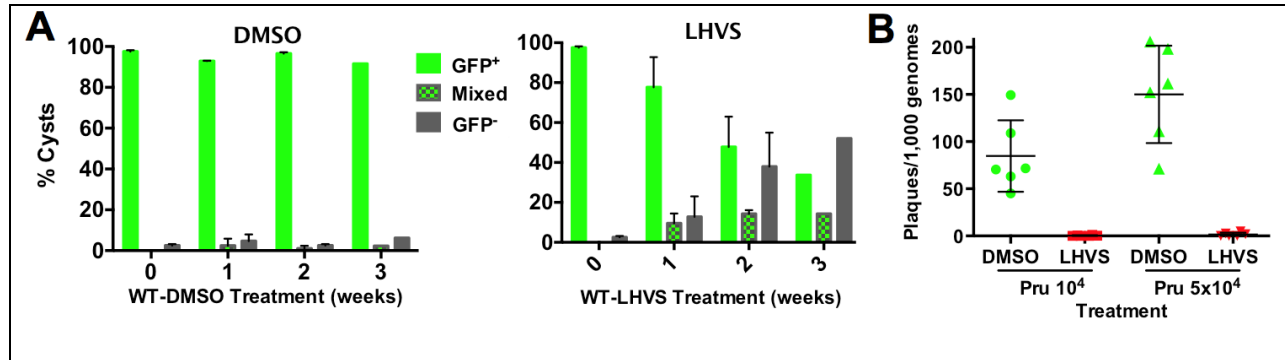


Figure 13. CPL activity is required for cyst viability *in vitro*

(A) *TgCPL* inhibitor treatment kills cysts based on GFP signal. Pru (WT) cysts were differentiated in culture for 1-wk prior to treatment with solvent control (DMSO, left panel) or LHVS (right panel), fixed, viewed and enumerated for GFP by fluorescence microscopy. n=2 independent experiments. (B) CPL inhibitor treatment kills bradyzoites based on qPCR/plaquing. Parasites were inoculated into HFF cells, differentiated for 1-wk then treated with solvent (0.1% DMSO) or inhibitor (1 μ M LHVS) for 3-wk

Mouse gene knockout studies have shown that cathepsin L is dispensable in higher mammals. This is likely due to the functional redundancy with other cathepsin proteases.¹²² Humans express a total of 11 Cathepsins proteases while *Toxoplasma gondii* only expresses five. As mentioned previously, only two of these, *TgCPL* and *TgCPB*, are expressed during the latent infection, leaving the parasite much more susceptible to cathepsin inhibition. This concept however, remains invalidated in an *in vivo* model of toxoplasmosis. LHVS does not cross the blood-brain barrier, precluding its use as an *in vivo* proof-of-concept treatment in infected mice. Fortunately, a crystal structure of *TgCPL* is available from our previous work, thus aiding rationale selection of candidate inhibitors from the literature as lead compounds.¹²¹ The next crucial step and the objective of this study is to identify and optimize CNS penetrable, lead compounds as a prelude to proof-of-concept studies in chronically infected animals.

Chapter 2 The Development of Dipeptide Nitrile Inhibitors of *TgCPL*

Identification of New Lead Inhibitors of *TgCPL*

- Computational Evaluation of Literature Cathepsin L Inhibitors

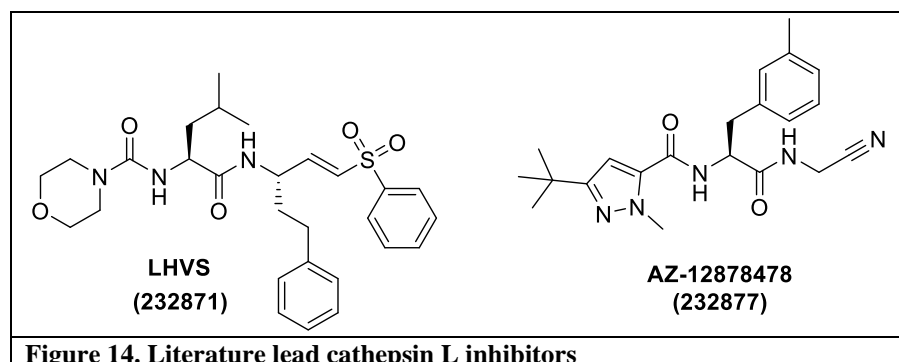
An enormous amount of drug discovery and development has been done in regard to both human and parasitic cathepsins isoforms, and extensive mechanistic and structural information is available.¹²³⁻¹³⁰ Given the close homology between the human and parasitic isoforms of cathepsin L, we considered the vast libraries of inhibitors already developed against human isoforms to be a promising source of lead anti-parasitic compounds.¹²⁰ To identify a better potential lead compound than LHVS, we conducted a broad literature search of structurally diverse cathepsin L inhibitors emphasizing physicochemical properties predictive of CNS permeability, selectivity over other human cathepsins, and potency ($IC_{50} < 1 \mu M$).

Table 1. Comparison of calculated properties of lead inhibitors vs CNS and non-CNS drugs

Compound	MW	SlogP	tPSA	HBA	HBD	RotB
CNS drug	288 ± 88	2.8 ± 1.4	46 ± 26	2.6 ± 1.3	1.0 ± 0.9	4.0 ± 2.6
non-CNS drug	383 ± 210	2.1 ± 2.9	98 ± 84	4.8 ± 4.1	2.8 ± 3.3	6.2 ± 5.5
LHVS	527.69	3.6	104.8	5	2	14
AZ-12878478	381.48	2.4	99.8	4	2	10

Calculated using The Molecular Operating Environment (MOE), version 2008.10, Chemical Computing Group Inc., Montreal, Quebec, Canada.¹³¹ Mean values and standard deviations derived from 198 approved CNS drugs and 1015 approved non-CNS drugs (DrugBank).

Rational and Selection of AZ-12878478 / CCG: 232877 as Lead Dipeptide Nitrile

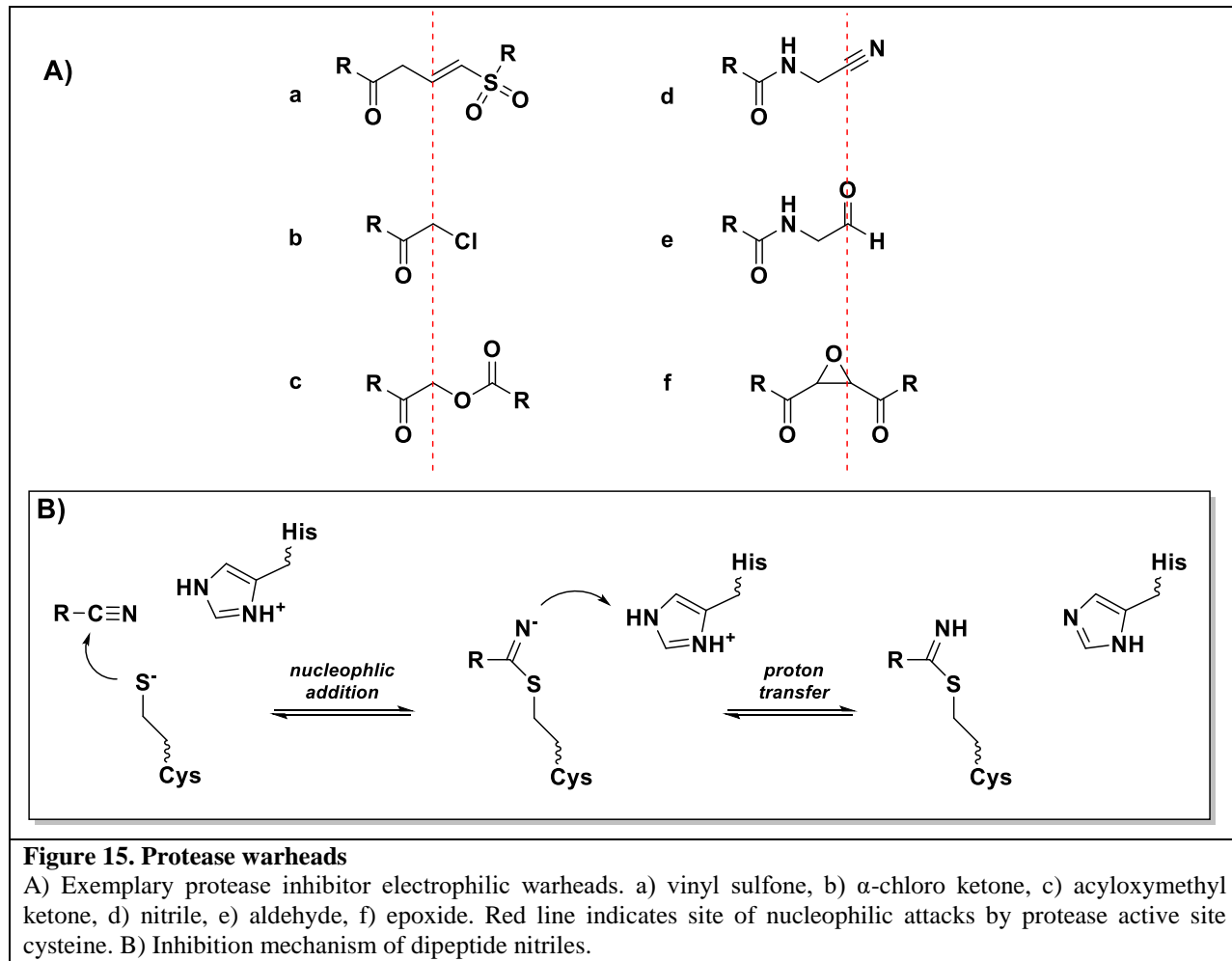


We ultimately selected our initial lead compound **232877** (Figure 14) based on its calculated properties: molecular weight (MW), topological polar surface area (tPSA), numbers of hydrogen bond acceptors and donors (HBA, HBD), and rotatable bonds (RotB), which are collectively closer to marketed CNS drugs vs non-CNS drugs than are those of LHVS and most other literature leads we considered (Table 1)¹³². In addition, we considered the ease with which we could expect to improve predicted BBB access by further lowering the tPSA.

As the first ever SAR campaign targeting *TgCPL*, we elected to use a dipeptide nitrile scaffold as our lead, based on the extensive amount of dipeptide-type cathepsin inhibitors previously developed for related human isoforms.¹³³⁻¹³⁵ We believed the use of dipeptide probes would enable rapid elucidation of the pharmacophore necessary for the selective inhibition of *TgCPL* due to their synthetic accessibility and ease of diversity introduction.

Another key rationale for selecting **232877** as our lead was the aminoacetonitrile “warhead”. The majority of small molecule protease inhibitors incorporate a functional group that can react

with the active site cysteine or serine in a covalent manner that imparts high affinity with relatively low off-target reactivity (**Figure 15**).^{133, 136-137} The aminoacetonitrile group has been extensively studied and is present in a number of FDA-approved drugs and advanced clinical candidates, including vildagliptin, saxagliptin, and odanacatib.¹³⁰ In contrast to the irreversible inhibitor LHVS, the dipeptide nitriles function through a reversibly covalent mechanism (**Figure 15B**), reducing the potential for off target effects, and its low molecular weight and relatively low tPSA were considered advantageous for achieving CNS permeability.



a

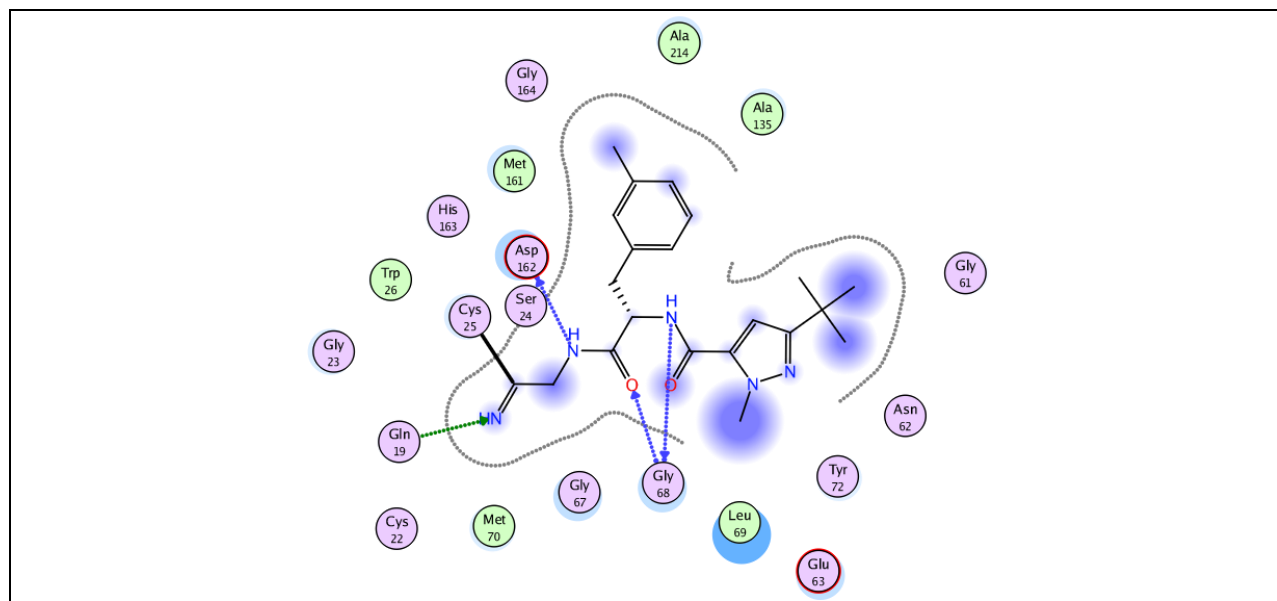


Figure 16. Ligplot diagram of 232877 in *HsCPL*

LIGPLOT diagram generated in MOE, shows key interactions between 232877 and *HsCPL*. Hydrogen bonds: blue arrows, lipophilic interactions: blue spheres. Derived from PDB: 3HHA

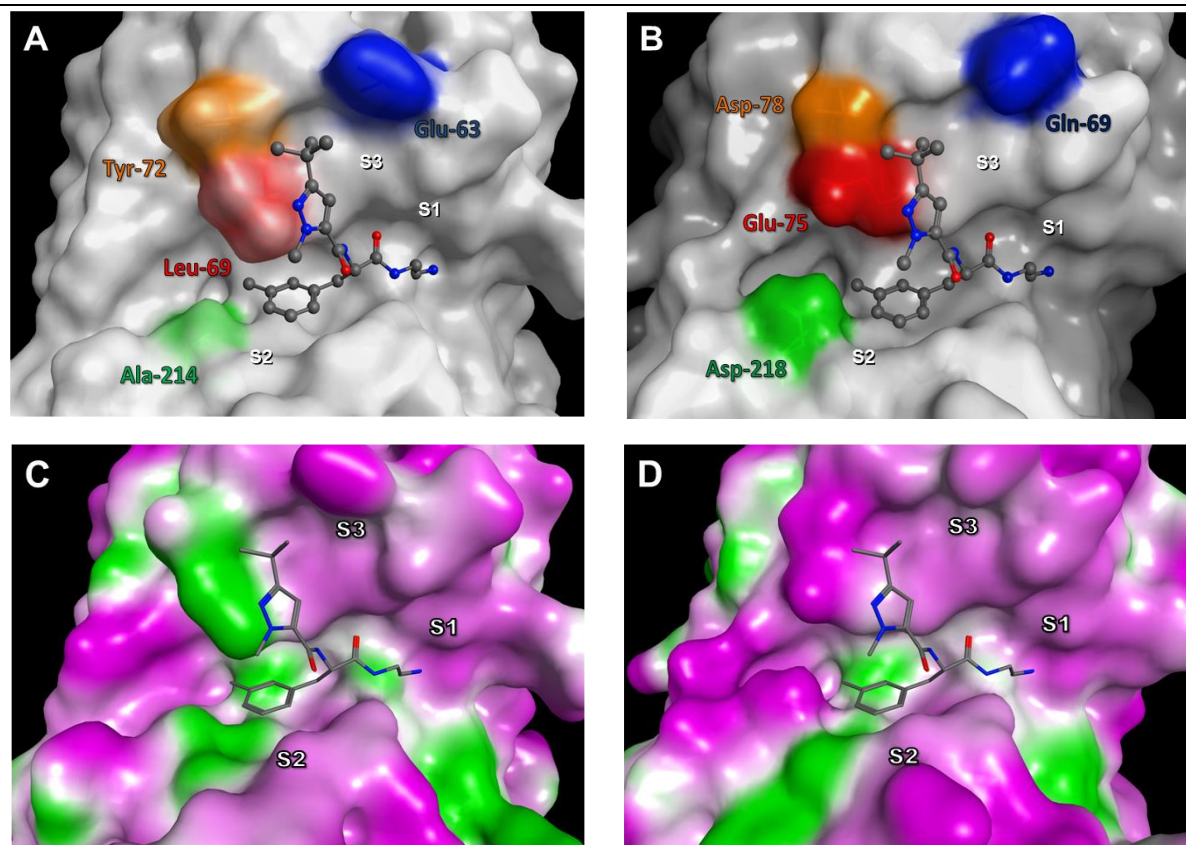


Figure 17. *TgCPL* and *HsCPL* active site comparison

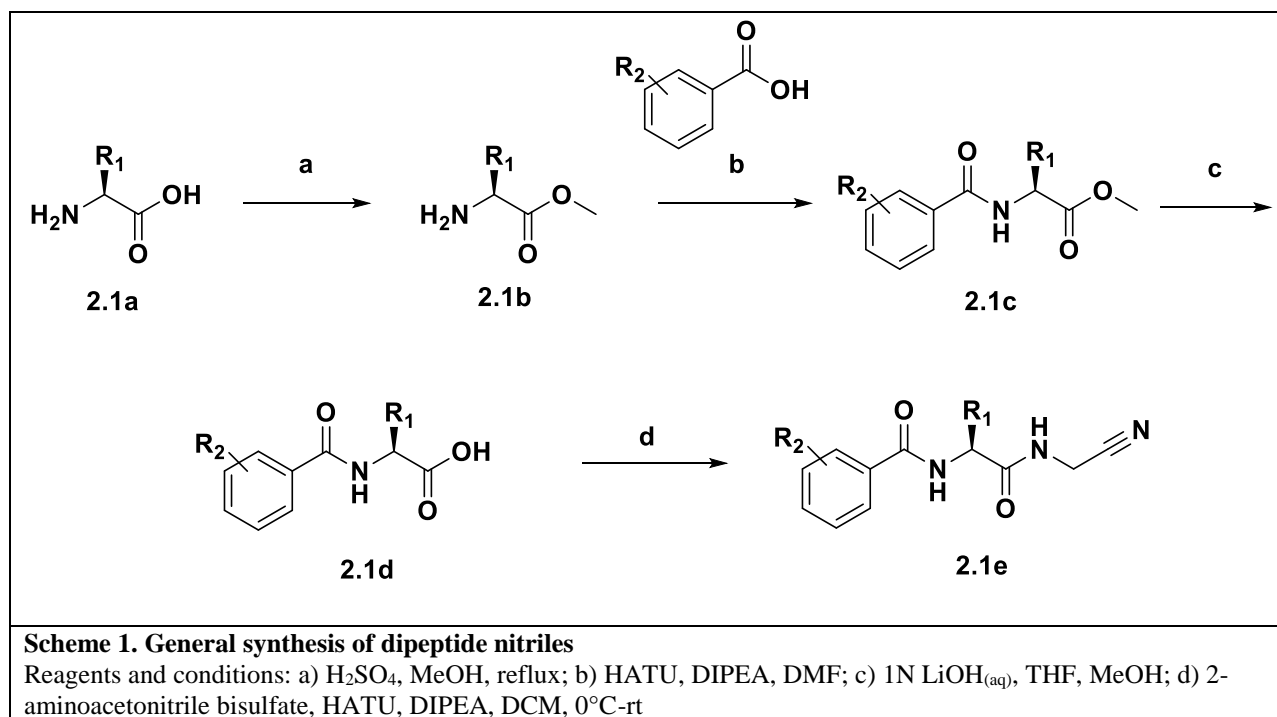
Comparison of 232877 bound to *HsCPL* (A, C) and a superposition of 232877 modeled into the active site of *TgCPL* (B, D) depicting key non-conserved residues. A) *HsCPL* with key residues colored. B) *TgCPL* with key residues colored C) Lipophilicity mapping of *HsCPL* (green: lipophilic; magenta: polar); D) Lipophilicity mapping of *TgCPL*. (Derived from PDB codes: 3HHA and 3F75)

We selected **232877** as a lead because of the availability of an X-ray co-crystal structure of it bound to human cathepsin L (*HsCPL*, (PDB: 3HHA)).¹³² Opportunely, a crystal structure of *TgCPL* was also available from our previous work, which we expected would greatly facilitate the design of *TgCPL*-selective inhibitors.^{132, 138-141} The crystal structure of **232877** bound to *HsCPL* shows that the active site Cys25 is covalently added to the nitrile, consistent with other reversibly-covalent nitrile based inhibitors of cysteine proteases, and that the ligand makes hydrogen-bonding interactions with Asp162, Gly68, and Gln19 (**Figure 16**).^{133, 136} Importantly, the bound inhibitor **232877** can be overlaid on our crystal structure of *TgCPL* to identify proximal structural differences between the cathepsins that can be exploited to achieve selective inhibition of the *T. gondii* enzyme (**Figure 17**).¹²¹ In particular this overlay reveals a smaller S2 pocket for the *Toxoplasma* cathepsin, as well as four non-conserved residues (colored in **Figures 17A,B**). Further comparison of the protein sequence alignment of *TgCPL* and the human cathepsin isoforms A-X, revealed that these key residues are either unique to *TgCPL*, or generally non-conserved across human isoforms. The S2 pocket across the human cathepsins tends to be more uniformly lipophilic (colored green in **Figures 17C,D**) than *TgCPL*, and the inclusion of a basic residue in the P2 position, which we predicted might interact strongly with non-conserved Asp218 in *TgCPL*, is generally not tolerated. With the exception of human cathepsin B, which bears a Glu245 in this respective position, the overall topology in the S2 subsite is thus substantially different than that of *TgCPL*.¹⁴² This provided excellent supporting evidence that optimization in the P2 position would be paramount in an effort to gain selectivity over the bulk of the human isoforms.

Our primary objectives in this preliminary work were: 1) to develop analogs with better predicted CNS permeability without losing potency; and 2) to determine if we can begin to shift the selectivity of **232877** away from *HsCPL* and towards *TgCPL*. Herein we report the development of a series of dipeptide nitrile probes that help to define pharmacophoric features key to improving both potency and selectivity for *TgCPL*, including one analog with CNS permeability in vivo.

First Generation Dipeptide Nitrile Inhibitors of *TgCPL*

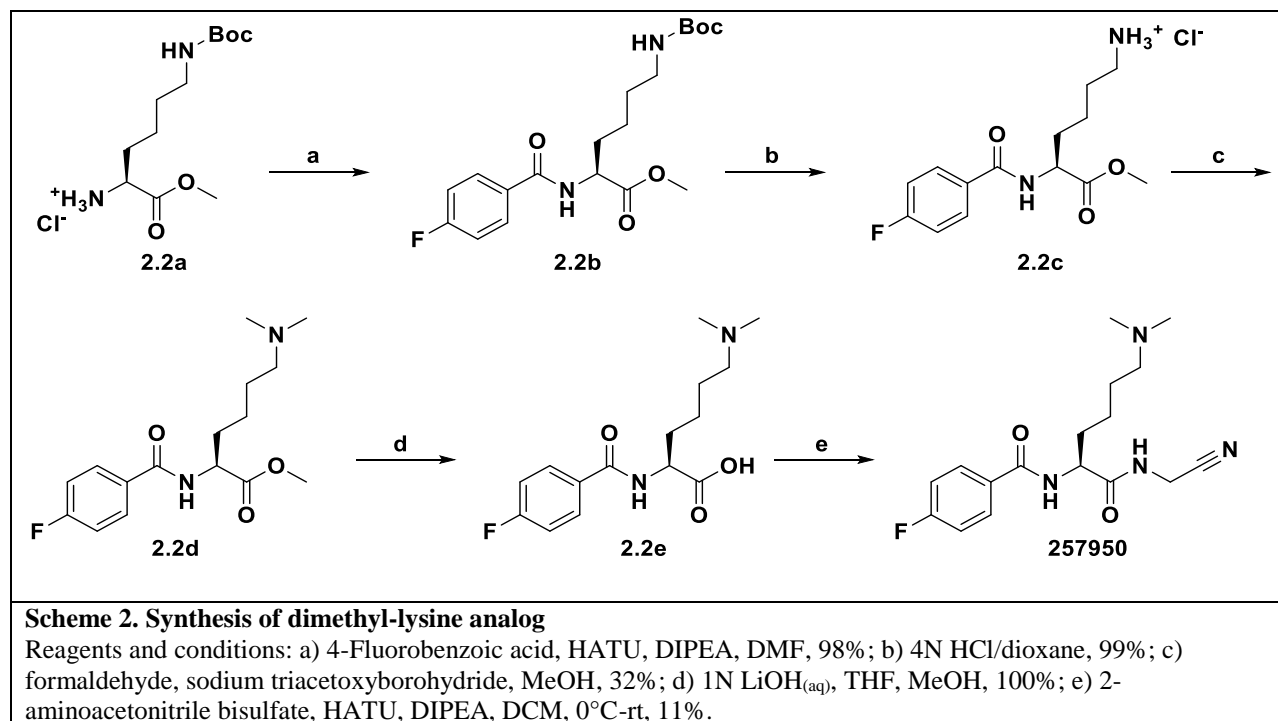
- General Synthesis of Dipeptide Nitriles



Synthesis of dipeptide nitriles (**Scheme 1**) was performed analogous to the literature precedent for the peptide-nitrile cathepsin inhibitors.^{132-133, 135, 141} We began with the esterification of various commercially available L-amino acids **2.1a** to afford their respective

methyl esters **2.1b**. Subsequent amide coupling to the appropriate aryl acids gave **2.1c**. The methyl ester was then saponified under mild conditions with LiOH in a THF:MeOH system to afford the desired free acid **2.1d**. Initial coupling with 2-aminoacetonitrile gave several unwanted side reactions and generally low yields when using DMF or THF as the solvent, regardless of the temperature or coupling reagent used. Upon changing to dichloromethane we found that, while solubility was not always ideal, the desired products (**2.1e**, 52 examples) were formed cleanly and in moderate yields.

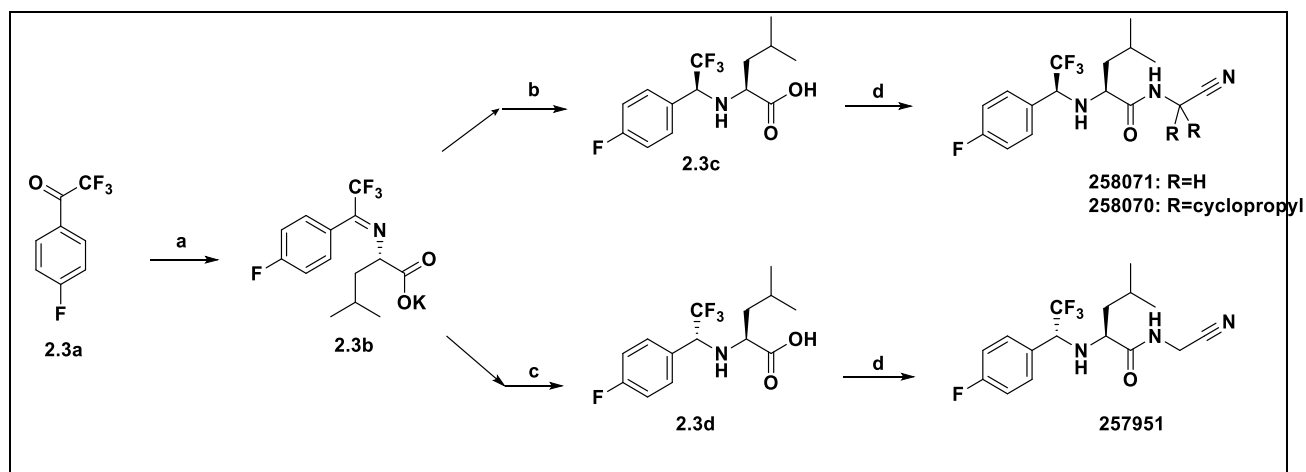
- Synthesis of Dimethyl-lysine Analog



Synthesis of **257950** was achieved as shown in **Scheme 2**. Nε-Boc-L-lysine methyl ester hydrochloride **2.2a** was coupled to 4-fluorobenzoic acid to provide intermediate **2.2b**. Boc

removal from **2.2b** afforded the HCl salt of **2.3c**, which was immediately followed by dimethylation of the side chain to provide compound **2.3d**. Saponification of **2.3d** with lithium hydroxide provided **2.3e**, and subsequent amide coupling using HATU gave the desired product **257950**.

- **Synthesis of Trifluoroethylamines**



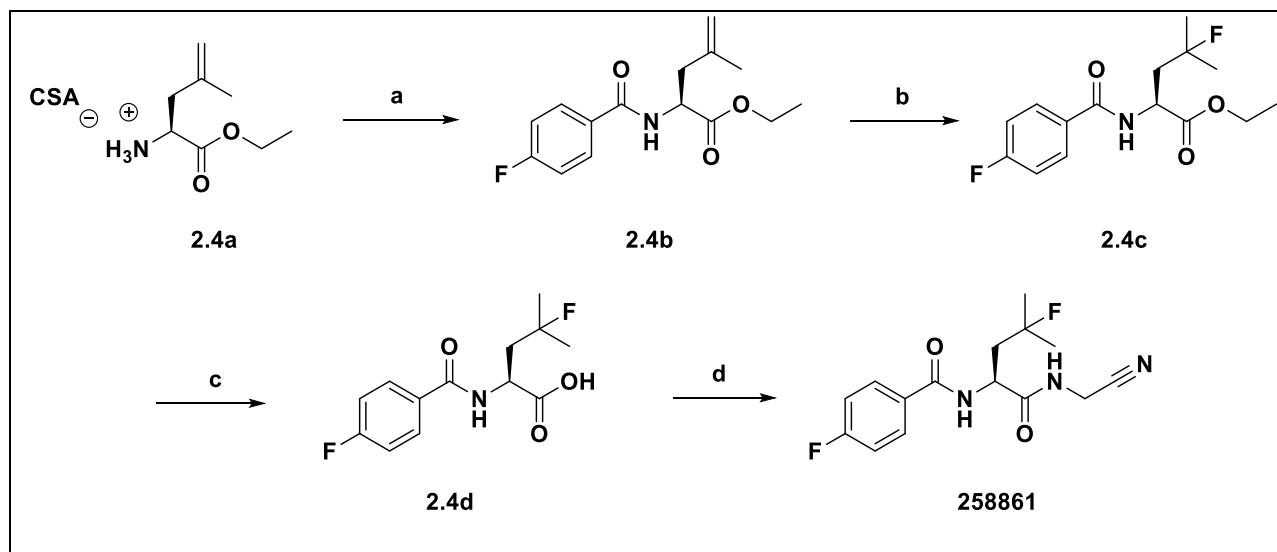
Scheme 3. Synthesis of trifluoroethylamines

Reagents and conditions: a) Leucine hydrochloride, K_2CO_3 , MeOH, $50^\circ C$, 18h; b) $Zn(BH_4)_2$, ACN/DME, $-40^\circ C$, 5h, 87%; c) $NaBH_4$, THF, 93%; d) 2-aminoacetonitrile bisulfate, or 1-aminocyclopropane-1-carbonitrile HCl, HATU, DIPEA, DCM, $0^\circ C$ -rt, 45-89%

Trifluoroethylamine analogs (**258070**, **258071**, and **257951**) were generally synthesized as shown in **Scheme 3** following previously established methods in the development of odanacatib.¹⁴³⁻¹⁴⁴ Synthesis began with the condensation of the trifluoroacetophenone **2.3a** and L-Leucine-methylester under basic conditions to afford the imine intermediate **2.3b**. The *R,S* diastereomer **2.3d**, was obtained via dropwise addition of $NaBH_4$ dissolved in THF at $-40^\circ C$ in a 10:1 dr. Alternatively the (*S,S*) diastereomer could be obtained through a chelation controlled reduction of the imine with zinc borohydride in acetonitrile/dimethoxyethane at $-40^\circ C$, providing

2.3c in an 11:1 dr. The (S,S) and (R,S) compounds **258070**, **258071**, and **257951** were obtained in 45-94% yield through the previously described amide coupling conditions (**Scheme 1**).

- **Synthesis of Fluoroleucine Dipeptide Nitrile**



Scheme 4. Synthesis of fluoroleucine dipeptide nitriles

Reagents and conditions: a) 4-fluorobenzoic acid, HATU, DIPEA, DMF, 34%; b) Selectfluor, $\text{Fe}_2(\text{SO}_4)_3$, NaBH_4 , acetonitrile:water, 0°C -rt, 27%; c) 1N $\text{LiOH}_{(\text{aq})}$, THF:EtOH, 0°C -rt, 100%; d) 2-aminoacetonitrile bisulfate, HATU, DIPEA, DCM, 0°C -rt, 18%

Fluoroleucine analog **258861** was prepared as shown in **Scheme 4** through a sequence derived from previously reported methods for analogous compounds.¹⁴⁴⁻¹⁴⁷ Dehydroleucine **2.4a**, as the CSA salt, was coupled to 4-fluorobenzoic acid to provide intermediate amide **2.4b**. Initially, we tried to achieve fluorination of **2.4c** using a variety of the previously reported conditions, predominantly using reagents that are a source of nucleophilic fluorine such as HF:Urea or HF:Pyridine. However, these conditions generally suffered from poor yields and unwanted side reactions such as cyclization or elimination. We then opted to try an electrophilic source of fluorine as an alternative approach, derived from that reported by Fanelli et. al..¹⁴⁸

Activation of the olefin with Fe(III), followed by the sequential addition of Selectfluor and NaBH₄ provided the desired product **2.4c** in moderate yield, which was then saponified to **2.4d** and directly coupled to 2-aminoacetonitrile, affording the desired compound **258861**.

SAR Analysis

- Initial Set of Dipeptide Nitriles.

All compounds were evaluated in vitro for inhibition of both *TgCPL* and *HsCPL* activity by monitoring the rates of hydrolysis of Z-Leu-Arg-7-amino-4-methylcoumarin (Z-L-R-AMC). Results are summarized in **Tables 2-5**. We first re-synthesized literature lead **232877** to benchmark its relative potency against *TgCPL* versus *HsCPL*. In vitro testing revealed low micromolar potency against *TgCPL*, and 46-fold more potent inhibition against *HsCPL* (**Table 2**).

Initially we replaced the pyrazole heterocycle in the P3 position of **232877** with phenyl in order to remove two nitrogen atoms (**232921**) and rapidly lower the tPSA of **232877**, thereby increasing the potential for CNS permeability. This exchange resulted in a 2-3-fold drop in potency against *HsCPL* while enhancing activity against *TgCPL*, improving the *TgCPL*-selectivity about 4-fold. The *t*-butyl group of **232921** was then replaced by trifluoromethyl to stabilize the now electron-rich P3 aromatic ring to potential oxidation by CYP450 enzymes, giving **232920**. This analog lost potency against *TgCPL*, but maintained effectiveness versus *HsCPL*. Since both analogs had reduced selectivity for *HsCPL* compared to lead **232877** we retained both P3 groups during our initial survey of P2.

Table 2. Cathepsin L inhibitory activity of initial P2 and P3 analogs.

		Ar	R	<i>Tg</i> CPL ^a IC ₅₀ (μM)	<i>Hs</i> CPL ^b IC ₅₀ (μM)	Selectivity for <i>Hs</i> CPL ^c
232877				2.0	0.044	46.4
232920				2.4	0.11	22.5
232921				1.4	0.13	11.3
257162				1.4	0.042	33.5
257163				1.2	0.092	13.3
257165				6.1	0.086	71
257166				4.6	0.24	18.8
257101				0.12	0.077	1.9
257085				0.12	0.32	0.4

^{a,b}IC₅₀ for *Toxoplasma gondii* Cathepsin L (*Tg*CPL) or human Cathepsin L (*Hs*CPL). Values are mean of at least 3 independent experiments. ^cSelectivity ratio for human Cathepsin L as defined by *Tg*CPL IC₅₀/*Hs*CPL IC₅₀.

The vast majority of selectivity between human cathepsin isoforms comes from the P2-S2 interaction.¹⁴⁹ The S3 and S1 subsites also play significant roles in inhibitor selectivity, while the S' subsites (toward the C-terminus of the scissile bond) are highly conserved between isoforms and generally difficult to exploit.¹²⁴ Inspection of the cathepsin crystal structures revealed several active site residues unique to the *T. gondii* isoform vs the human isoform that could potentially be exploited to gain selectivity and potency. As noted above, the *TgCPL* S2 site contains a unique aspartate residue (Asp218), as opposed to the human isoform, which bears a hydrophobic alanine in this position (colored green in **Figures 17A, B**). Overlaying *TgCPL* with the co-crystal structure of our lead compound bound to *HsCPL* indicates that the 3-methylphenylalanine (3-Me-Phe) core of **232877** sits approximately 3-4 Å from this key aspartate (Figure **17B**). Due to the proximity of the core to Asp218 we hypothesized we might be able to build in a potential H-bond to improve potency and selectivity.

The P2 3-methylphenylalanine residue of analogs **232920** and **232921** was thus replaced with 3-hydroxyphenylalanine or 3-methoxyphenylalanine (**257162**, **257163**, **257165**, and **257166**) in an attempt to pick up a selective hydrogen bonding interaction with the non-conserved Asp218 of *TgCPL*. We had hoped this would provide some initial gain in selectivity toward the parasite cathepsin, but the results were inconsequential changes in potency. This might be due to the Asp218 orienting the residue away from the S2 pocket and preventing a beneficial interaction. Without a co-crystal structure, it is difficult to determine the true positioning of this residue.

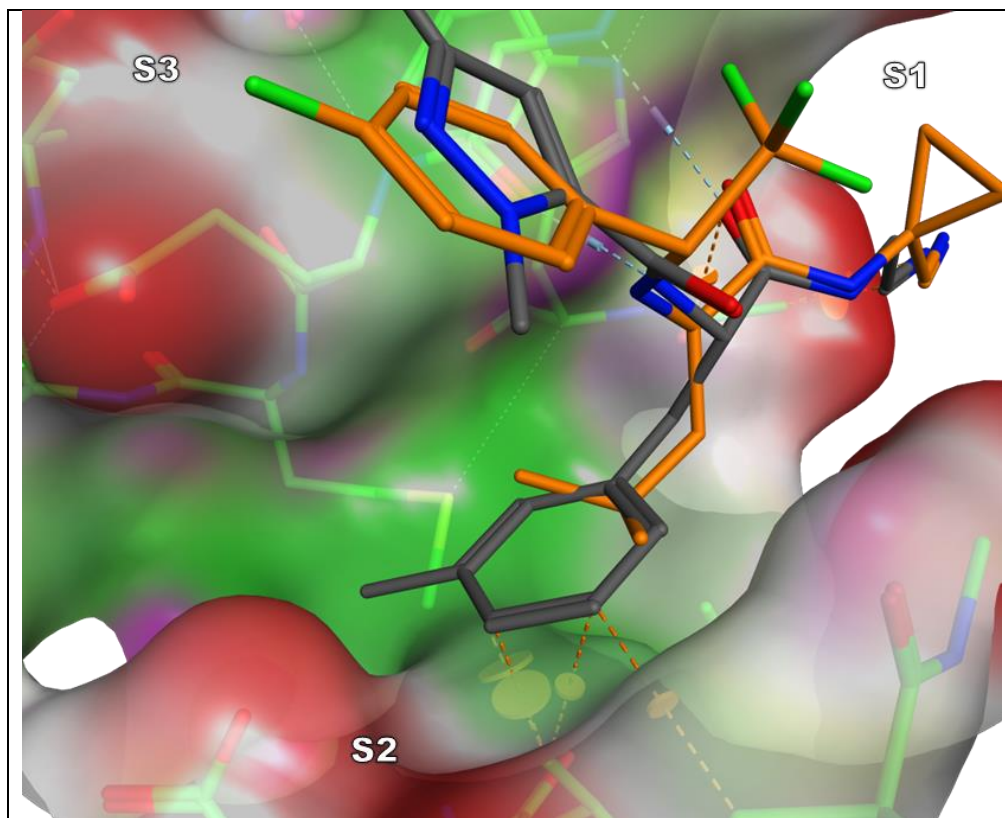


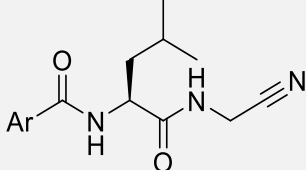
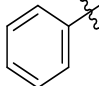
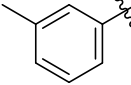
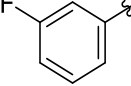
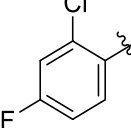
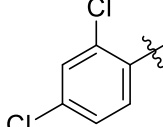
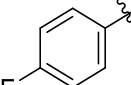
Figure 18. Overlay of 232877 and 258070 in *TgCPL*

Overlay of **232877** (gray) and **258070** (orange) into the crystal structure of *TgCPL* (PDB code: 3F75) depicting clashes with **232877** in the S2 pocket. Hydrogen bonds and clashes are represented as blue and orange dashed lines, respectively. Pocket surface coloration represents polar (purple), lipophilic (green), and solvent exposed (red) areas.

Molecular modeling also identified several predicted clashes with *HsCPL* when the larger phenylalanine side chains are in the P2 position (**232877** in **Figure 18**). We were pleased to discover that replacement of the entire aromatic P2 residue with a less bulky leucine (**257101**, and **257085**) significantly reduced selectivity for *HsCPL*, consistent with the smaller S2 subsite in the *TgCPL* as compared to the human isoform (**Table 2.3**). With this single change, we reduced the selectivity of **232877** for *HsCPL* from 10-20 fold to <2 fold. This is an excellent validation that the differences in the S2 pockets can be exploited for improving *TgCPL* selectivity.

- SAR of Additional P3 Analogs

Table 3. Inhibitory activity of additional aryl P3 substitution analogs.

	Ar	<i>TgCPL</i> ^a IC ₅₀ (μ M)	<i>HsCPL</i> ^b IC ₅₀ (μ M)	Selectivity for <i>HsCPL</i> ^c
257102		0.35	0.11	3.3
262484		0.18	0.015	11.7
257642		0.36	0.048	7.6
258072		0.54	0.28	1.9
258186		0.53	0.14	3.8
257646		0.25	0.28	0.9

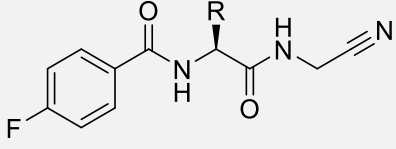
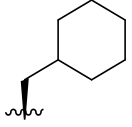
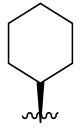
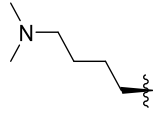
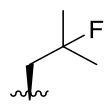
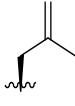
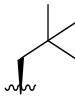

^{a,b,c}See Table 2.2 for heading definitions.

We then returned to optimization of the P3 position in an effort to reduce the molecular weight of **257085** while retaining a halogenated pendant for metabolic stability (**Table 3**). Removal of the trifluoromethyl from the P3 pendant to afford the simple phenyl (**257102**) unfortunately reversed the selectivity back to *HsCPL* over *TgCPL*. A similar trend was observed with analogs **262484**, **257072**, and **257186**, which bear a 3-methyl, 2-chloro-4-fluoro, or 2,4-dichloro substitution pattern, respectively, on the P3 pendant. Replacement of the 3-trifluoromethyl of **257085** with a fluorine (**257642**) also resulted in a large drop in potency for *TgCPL* and an increase for the human isoform. The 4-fluoro analog **257646**, however, was

equipotent at *TgCPL* and *HsCPL*, and lowered the MW below 300, making this a more promising candidate for CNS permeability as compared to the somewhat more potent and *TgCPL*-selective 4-trifluoromethyl analog **257085**.

- SAR of P2 Analogs for Metabolic Stability and Selectivity

Table 4. Inhibitory activity of additional aliphatic P2 analogs

	R	<i>TgCPL</i> ^a IC ₅₀ (μM)	<i>HsCPL</i> ^b IC ₅₀ (μM)	Selectivity for <i>HsCPL</i> ^c
257945		0.42	0.19	2.3
257706		6.6	1.2	5.7
257950		14	816	0.02
258861		4.0	2.5	1.6
258681		2.0	1.2	1.6
258921		1.2	3.5	0.3
259042		9.8	4.1	2.4

^{a,b,c}See Table 2.2 for heading definitions.

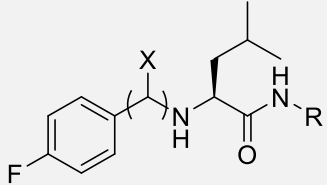
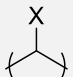
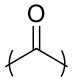
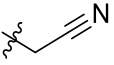
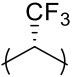
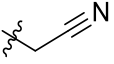
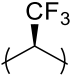
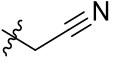
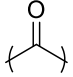

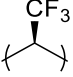
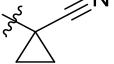
We then explored a dimethyl lysine at P2 as a basic group to establish a salt bridge with the non-conserved Asp218 of *TgCPL* (**257950** in **Table 4**). While this was predicted by modeling to be the optimal length to interact with the S2 aspartic acid, it nevertheless resulted in a major loss in potency against both isoforms. However, it should be noted that the loss in potency was significantly greater against the human isoform, demonstrating that despite the S2 pocket of these two enzymes being very similar, subtle differences at the P2 residue can offer drastic changes to the selectivity profile. Further exploration of basic residues at P2 is therefore warranted in future SAR studies.

Cyclohexyl P2 analogs have been reported as inhibitors of human protease inhibitors that offered some improvement in either binding or metabolic stability.¹⁵⁰ To further probe aliphatic SAR at the *TgCPL* P2 position, both were made (**257945** and **257706**, **Table 4**); however, neither offered any improvement. Rather, a decrease in potency and *TgCPL* selectivity was observed for both, more drastically in the case of **257706**, which is a closer mimic of valine than leucine. Substitutions much larger than leucine were thus apparently not well tolerated in *TgCPL*, consistent with the poor activity we had observed earlier with our phenylalanine analogs, so we attempted to install isosteres that were closer in size to leucine. While the use of fluoroleucine to improve metabolic issues has been successfully demonstrated in the development of odanacatib¹⁴⁴, we were surprised to see a drastic drop in potency against both *TgCPL* (IC_{50} = 4.05 μ M) and *HsCPL* (IC_{50} = 2.51 μ M) with compound **258861**. Similarly, exchange of the P2 leucine with either a neopentylglycine, or dehydroleucine (**258921**, **258681**) resulted in a significant loss of potency (IC_{50} = 1.19 μ M and 2.00 μ M respectively). Surprisingly, even the cyclopropyl analog **259042** showed a large drop in potency as compared to **257646**. While these structural changes

are minor, the substantial changes in potency clearly demonstrate the high level of sensitivity of the P2 position to steric modification. Within this initial set of dipeptide nitrile *TgCPL* inhibitors, leucine thus proved to be the most optimal residue in the P2 position for both potency and reduced selectivity for *HsCPL*.

- SAR of Analogs Designed for Improved CNS Profile

Table 5. Inhibitory activity of trifluoroethylamine and cyclopropyl-nitrile analogs

		R	<i>TgCPL</i> ^a IC ₅₀ (μM)	<i>HsCPL</i> ^b IC ₅₀ (μM)	Selectivity for <i>HsCPL</i> ^c
257646			0.25	0.28	0.9
257951			0.66	0.59	1.1
258071			0.11	0.093	1.2
258068			0.40	0.14	2.9
258070			0.16	0.084	1.9

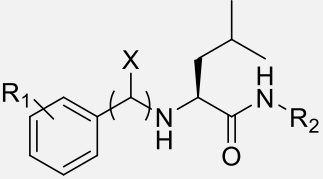
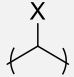
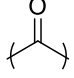
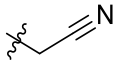
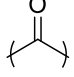
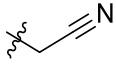
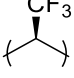
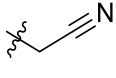
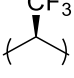
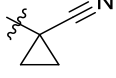
See Table 2.2 for heading definitions.

Most CNS drugs do not tolerate more than 1 or 2 hydrogen bond donors. As shown in the LIGPLOT diagram from the co-crystal structure of *HsCPL* and compound **232877** (**Figure 16**), the carbonyl of the P2-P3 amide is not actively engaged by the enzyme and therefore may be unnecessary. Replacement of this amide with the well-established trifluoroethylamine bioisostere offered an effective way to reduce our overall tPSA, greatly enhancing our chances for CNS

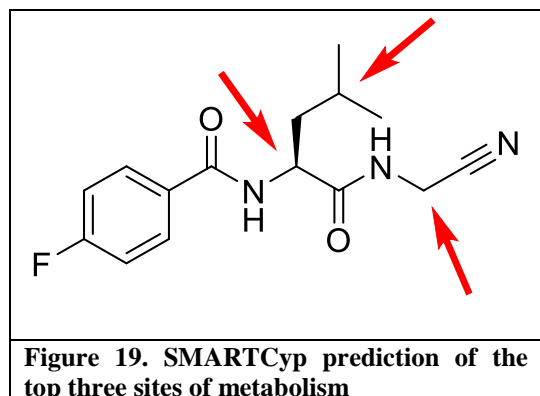
penetration.^{143-144, 151-152} We found that the (R,S) diastereomer **257951** gave a substantial drop in overall potency for both cathepsins (Table 5). The (S,S) diastereomer **258071**, however, doubled the potency against both the *Toxoplasma* and human enzymes, providing the most potent nitrile-based inhibitor to date against *TgCPL* with an IC₅₀= 110 nM. This diastereomeric preference is consistent with literature reports of other dipeptide cathepsin inhibitors incorporating the trifluoroethyl amine bioisostere.¹⁴³

Metabolic Stability and Pharmacokinetics.

Table 6. Metabolic stability of select analogs in mouse liver microsomes

	R₁	X 	R₂	MLM t_{1/2} (min)
257085	3-CF ₃			37
257646	4-F			>60
258071	4-F			4.4
258070	4-F			22

The metabolic stability of our dipeptide nitrile series was initially evaluated in mouse liver microsomes (MLM) to assess suitability for future in vivo studies and to further guide our design. Compound **257085** was evaluated to benchmark the dipeptide nitrile series (Table 6). We observed that compound **257085** had a reasonably long half-life (37 min). This parameter was further improved to >60 min with less lipophilic compound **257646**, despite several metabolic liabilities predicted by SMARTCyp (Figure 19).¹⁵³



Interestingly, while replacement of the P2 amide with a trifluoroethylamine (**258071**) removed an amide that could be a metabolic liability, the half-life in mouse liver microsome decreased to 4.4 minutes. It is likely that the increased lipophilicity simply enhanced binding to metabolizing enzymes. Two of the most likely positions for metabolism of **258071** are oxidation alpha to the nitrile warhead and hydrolysis of the P1 amide bond.¹⁵³ The incorporation of a cyclopropyl at the P1 position serves to block this site from oxidation and to slow hydrolysis of the P1 amide, a strategy successfully used in the development of odanacatib and other inhibitors of human cathepsins.^{144, 152, 154} Cyclopropyl analog **258070** indeed provided a significantly improved MLM half-life of 22 min, affording a compound more suitable for further in vivo analysis. It also retained potency for *TgCPL*, which is consistent with the predicted projection of the cyclopropyl group at P1 out into solvent (**Figure 18**).

Table 7. *In Vivo* Exposure of Compound 258070 Following IP or IV Administration to Mice^a

Time Post-Dose (IP 10 mg/kg)	30 min	2 h	4 h	7 h
Plasma Conc. (ng/mL)	110	138	10	BLQ
Brain Conc. (ng/g)	54	BLQ	BLQ	BLQ
Time Post-Dose (IV 1 mg/kg)	5 min	10 min	15 min	30 min
Plasma Conc. (ng/mL)	109	50	31	8
Brain Conc. (ng/g)	BLQ	BLQ	BLQ	BLQ

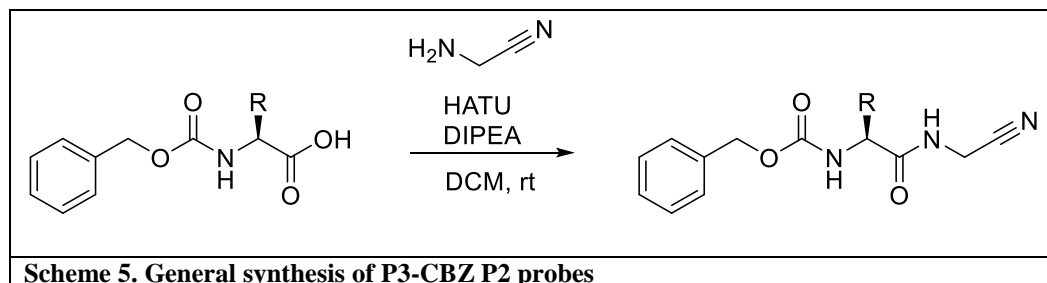
^a CD-1 mice were injected intraperitoneally with a single 10 mg/kg dose or intravenously with a single 1 mg/kg dose. The data shown are mean values from 2 mice at each time point. BLQ = Below Limit of Quantification.

Compound **258070** was advanced to an abbreviated *in vivo* pharmacokinetic study in mice (**Table 7**). Our main objective was to determine if this chemotype could penetrate the CNS. Significantly, we were able to detect compound in the brain, with a brain/plasma ratio of 0.5 at 30 minutes. Unfortunately, the overall levels in both brain and plasma were quite low, despite the fact that **258070** was shown to have good aqueous solubility (630 μ M) and excellent plasma stability (~100% parent remaining after 24h). The plasma levels and rapid disappearance indicates that this compound has a high volume of distribution, high clearance or both. Studies are currently underway to address this issue and to develop new analogs with improved pharmacokinetic profiles.

Synthesis and SAR of P3-CBZ Peptide Probes

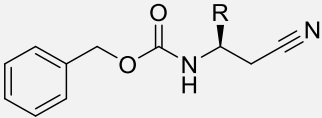
We also evaluated alternative methods and approaches to facilitate a rapid exploration of the TgCPL pharmacophore. Throughout the literature in the development of human cathepsin inhibitors, it has been demonstrated that either a Boc or CBZ group can be used as a surrogate

for the P3 pendant.¹⁵⁵⁻¹⁵⁶ This would allow for the rapid evaluation of commercially available amino acids and unnatural amino acids.



In general, analogs were synthesized via a one-step direct coupling of aminoacetonitrile to a commercially available CBZ-protected amino acid (**Scheme 6**).

Table 8. P3 CBZ probes for rapid P2 analysis

	R =	<i>TgCPL</i> IC ₅₀ ^a (μ M)	<i>HsCPL</i> IC ₅₀ ^b (μ M)
258064	<i>i</i> -Butyl	0.58	0.50
258067	<i>i</i> -Propyl	8.9	4.6
258066	Ethyl	59	16
258065	Methyl	841	108
258181	-H	N/D*	80
258182	<i>Sec</i> -Butyl	26	14
258183	-CH ₂ OH	72	44
258184	4-Hydroxyphenyl	1.3	0.083

^{a,b}IC₅₀ for *Toxoplasma gondii* Cathepsin L (*TgCPL*) or human Cathepsin L (*HsCPL*). Values are mean of at least 3 independent experiments. *N/D = No detectable activity

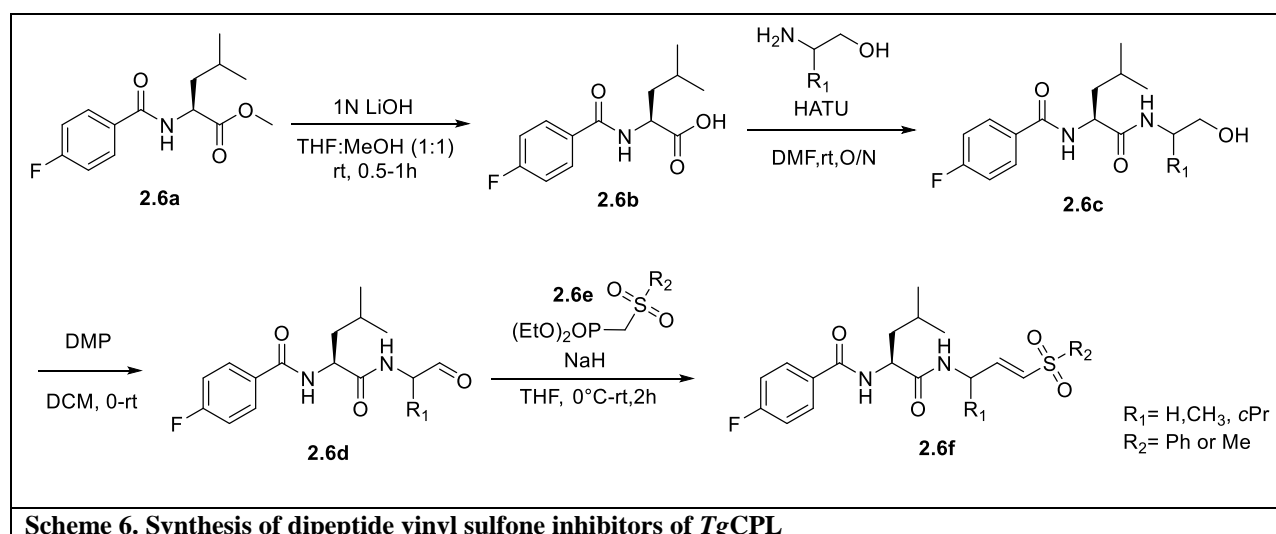
While the overall potency was significantly reduced versus the dipeptideneditriles, we were pleased to find that the SAR trends observed for these P3-CBZ surrogates aligned with those observed for the dipeptide series. The P2 SAR trends for *TgCPL* favored the leucine side chain (**258064**) above all others. The affinity was stepwise decrease in correlation to the stepwise reduction of the size of the P2 side chain (**258067**, **258066**, **258065**, **258181**). The Isoleucine

258182 and Serine **258183** were moderately tolerated by both human and parasite isoform. In agreement with the dipeptide series, selectivity in favor of *HsCPL* was observed for the tyrosine analog **258184**. This data offers validating support that this approach can be utilized to rapidly assess the potency of various P2 vectors, including unnatural amino acids that may give rise to improved potency or selectivity for *TgCPL*.

Vinyl Sulfone (VS) Inhibitors of *TgCPL*

We opted to pursue the dipeptide nitrile series based on the reasons previously explained. However, the dipeptide nitriles overall exhibited significantly lower potency versus the LHVS vinyl sulfone. Additionally, we wanted to have an irreversibly covalent control analog for comparison to the reversible analogs when moving forward into in vitro efficacy evaluation. To this end a small set of vinyl sulfone analogs was prepared (**Scheme 7**).

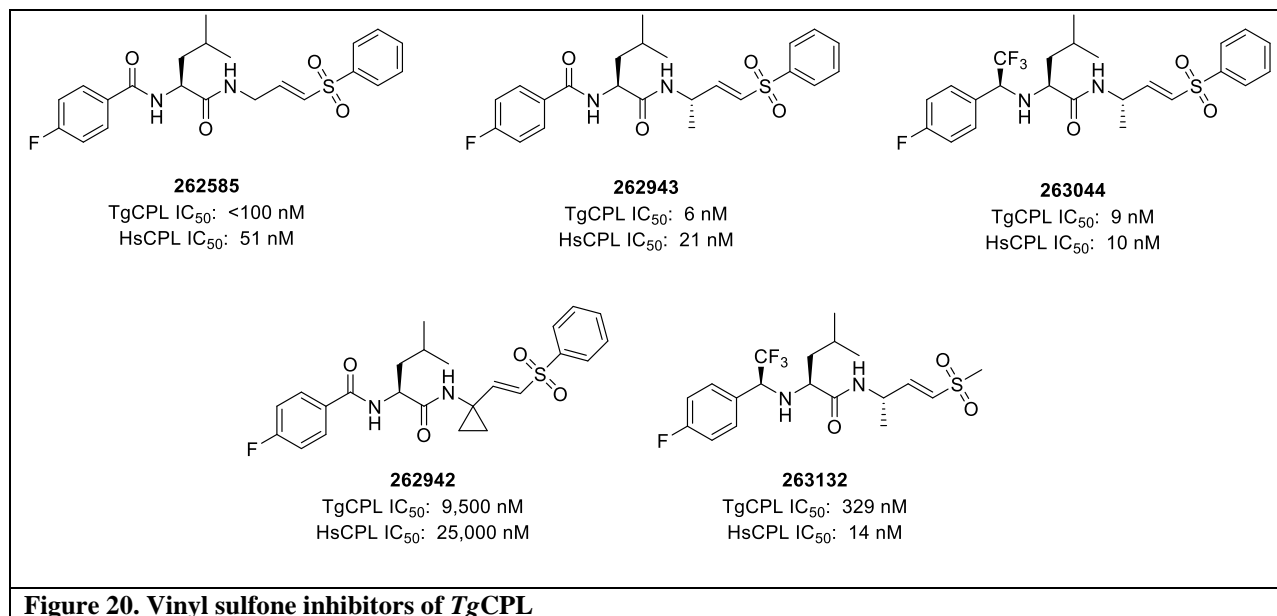
- Synthesis of VS Analogs



The optimal dipeptide methyl ester **2.6a**, was saponified using 1N lithium hydroxide (aq.) in THF:Methanol to afford intermediate **2.6b**. HATU coupling with a alkanolamines was then used to install the desired P1 R₁-group (**2.6c**). Oxidation with Dess-Martin periodinane provided the intermediate aldehydes (**2.6d**) and subsequent HWE olefination afforded the desired vinyl sulfones (**2.6f**, 5 examples).

- VS Trends and SAR

Below, **Figure 20** shows the summary set of dipeptide vinyl sulfones developed that were intended to be direct comparators to the dipeptide nitrile series.



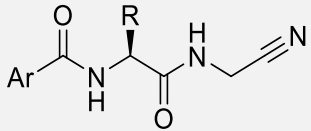
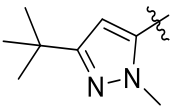
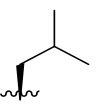
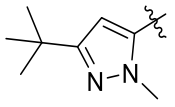
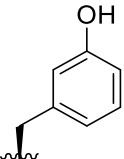
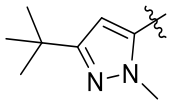
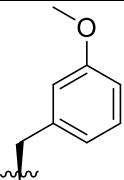
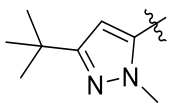
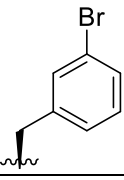
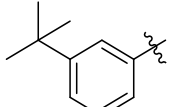
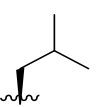
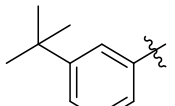
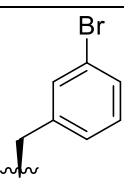
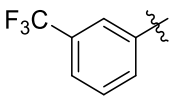
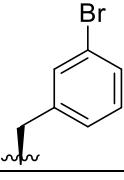
For direct comparison to the dipeptide nitrile with optimized P2/P3 (**257646**), the analogous vinyl sulfone (**262585**) was made. As expected, this compound was more potent as compared to the nitrile analog, given that it is irreversibly covalent. Interestingly, it was not as potent as

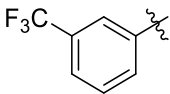
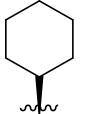
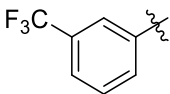
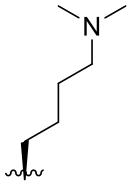
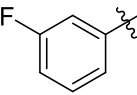
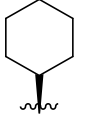
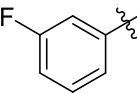
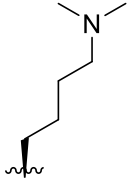
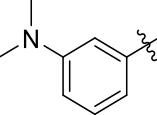
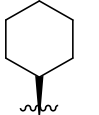
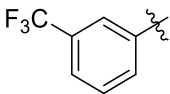
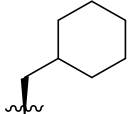
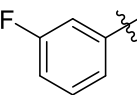
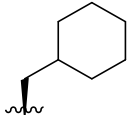
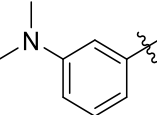
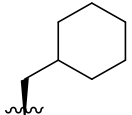
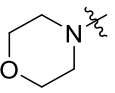
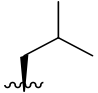
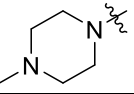
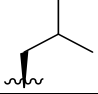
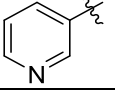
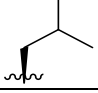
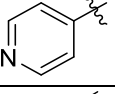
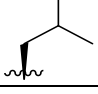
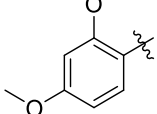
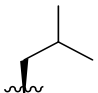
LHVS, suggesting that the nitriles and vinyl sulfones potentially bind in slightly different orientations, thus altering the affinity of the P2 and P3 vectors with the pockets. Alternative explanations for the loss in potency could be the stability of the vinyl sulfone conformational bias if the P1 methylene was left unsubstituted. The synthesis of **262585**, suffered from low yield in the last olefination step, likely due to an undesirable aldol-type reaction of the aldehyde intermediate **26a**. The addition of the methyl into the P1 position (**262943**) seemed to resolve this issue, as the synthesis became significantly easier during the HWE step, suffering from fewer side products. Substitution of the amide for a trifluoroethylamine (**263044**), while well tolerated, did not significantly alter the potency, implying that the high affinity conferred by the covalent vinyl sulfone outweighed the improvement in binding affinity from the trifluoro substitution. We were surprised to see that the incorporation of the cyclopropyl in the P1 position abolished almost all activity. A likely explanation for this is the cyclopropyl somehow precludes the active site cysteine from the necessary Michael addition to the vinyl sulfone, effectively eliminating the ‘warhead’ functionality. Finally, we tried to exchange the phenyl sulfone for a methyl sulfone, as the reduction in molecular weight could help CNS penetrance, and perhaps could be used in place of LHVS for in vivo studies if it proved to be potent and crossed the BBB. Unfortunately, this resulted in retention of activity for the human isoform and two orders of magnitude loss in potency for *TgCPL*. We additionally synthesized a BODIPY-tagged vinyl sulfone for competition assays, which will be further addressed in Chapter 4.

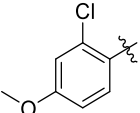
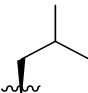
SAR of Additional Dipeptide Nitrile Inhibitors

Many additional compounds were synthesized during the development of the previously listed dipeptide nitrile inhibitors of *TgCPL*. The following table summarizes the SAR trends for those that were less potent, selective or redundant with the former.

Table 9. Cathepsin L inhibitory activity of initial P2 and P3 analogs

	Ar	R	<i>TgCPL</i> ^a IC ₅₀ (μ M)	<i>HsCPL</i> ^b IC ₅₀ (μ M)	Selectivity for <i>HsCPL</i> ^c
257084			0.33	0.15	2.2
257164			3.3	0.005	660
257167			3.1	0.049	63.3
257088			0.89	0.022	40.5
257101			0.15	0.077	1.9
257086			0.56	0.042	13.3
257087			1.3	0.052	25

257704			3.6	0.59	6.1
257948			6.6	1.6	4.1
257705			4.3	0.43	10
257949			26	372	0.07
257946			5.5	1.6	3.4
257943			0.17	0.053	3.2
257944			0.28	0.093	3.01
257947			0.98	0.27	3.6
258761			0.61	0.87	0.70
259044			0.82	0.53	1.5
259041			1.3	0.49	2.7
262467			1.4	0.53	2.6
262743			0.86	0.17	5.1

262744			4.0	0.99	4
--------	---	---	-----	------	---

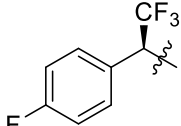
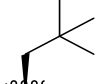

^{a,b,c}See Table 2 for heading definitions.

Various combinations of the lead *t*Bu-methyl-pyrazole (**257084**, **257164**, **257167**, and **257088**) were tested however all significantly favored *HsCPL* over *TgCPL*, highlighting the preference *HsCPL* has for this P3 vector. Analogs **257101** and **257086** were intended to lower the TPSA of the P3 pendant while retaining the *t*Bu in the 3-position. Both offered an increase in potency for *TgCPL* (0.15 μ M and 0.56 μ M respectively) but exhibited significant preference for *HsCPL*. 3-trifluoromethyl-benzyl vectors in P3 (and **257704**) generally were favorable for *TgCPL* (see **Table 3**) however, the phenylalanine isostere in P2 **257087**, **257088**, **257101**, and **257086** were not well tolerated in *TgCPL*, showing over an order of magnitude in increased potency toward *HsCPL*. The same trend was observed with the P2 cyclohexylglycine vectors in analogs **257704**, **257705**, **257946**. It is worth noting the analog **257946**, bearing the 3-dimethylaniline in P3, showed a loss of activity for *HsCPL* versus **257704**, suggesting that perhaps a basic amine in P3 may not be tolerated in *HsCPL* and could be important for achieving *TgCPL* selectivity. For reasons unknown however, this trend is not directly reflected comparing **257704** and **257947**. The P2 dimethyl lysine analogs **257948** and **257949** were not tolerated in either isoform, with their IC_{50} s landing in the μ M range. Compounds **257943** (*TgCPL* IC_{50} = 0.17 μ M) and **257944** (*TgCPL* IC_{50} = 0.17 μ M), bearing a P2 cyclohexylalanine vector, showed some of the more potent activity for *TgCPL*, yet still favored *HsCPL*. Compound **257947** decreased in potency (*TgCPL* IC_{50} = 0.98 μ M, *HsCPL* IC_{50} = 0.27 μ M) for both isoforms, like the other compounds with dimethylaniline P3 pendants. As we had established a general preference for P2 leucine, several analogs were made to determine if more polar P3 vectors could provide some

selectivity for parasite over human isoform (see **Figure 17C,D**). Unfortunately, **258761**, **259044**, **259041**, and **262467** all failed to improve either the potency or selectivity for *TgCPL*. Finally, to determine the effects of an electron rich P3 ring, **262743** and **262744** were tested, however potency was significantly reduced (*TgCPL* IC₅₀ = 0.86 μM and 4.0 μM respectively.)

Table 10. Cathepsin L inhibitory activity of initial P2 and P3 analogs

	R ₁	R ₂	R ₃	<i>TgCPL</i> ^a IC ₅₀ (μM)	<i>HsCPL</i> ^b IC ₅₀ (μM)	Selectivity for <i>HsCPL</i> ^c
232877				2.0	0.044	46.4
257161				179	0.64	279
257952				0.4	0.049	8.2
258061				1.7	0.81	2.1
258062				1.4	0.47	3
258063				0.7	0.072	9.7
258069				0.6	0.11	5.5
262608				1.1	3.1	0.35

262642				1.7	2.0	0.85
---------------	---	---	---	-----	-----	------

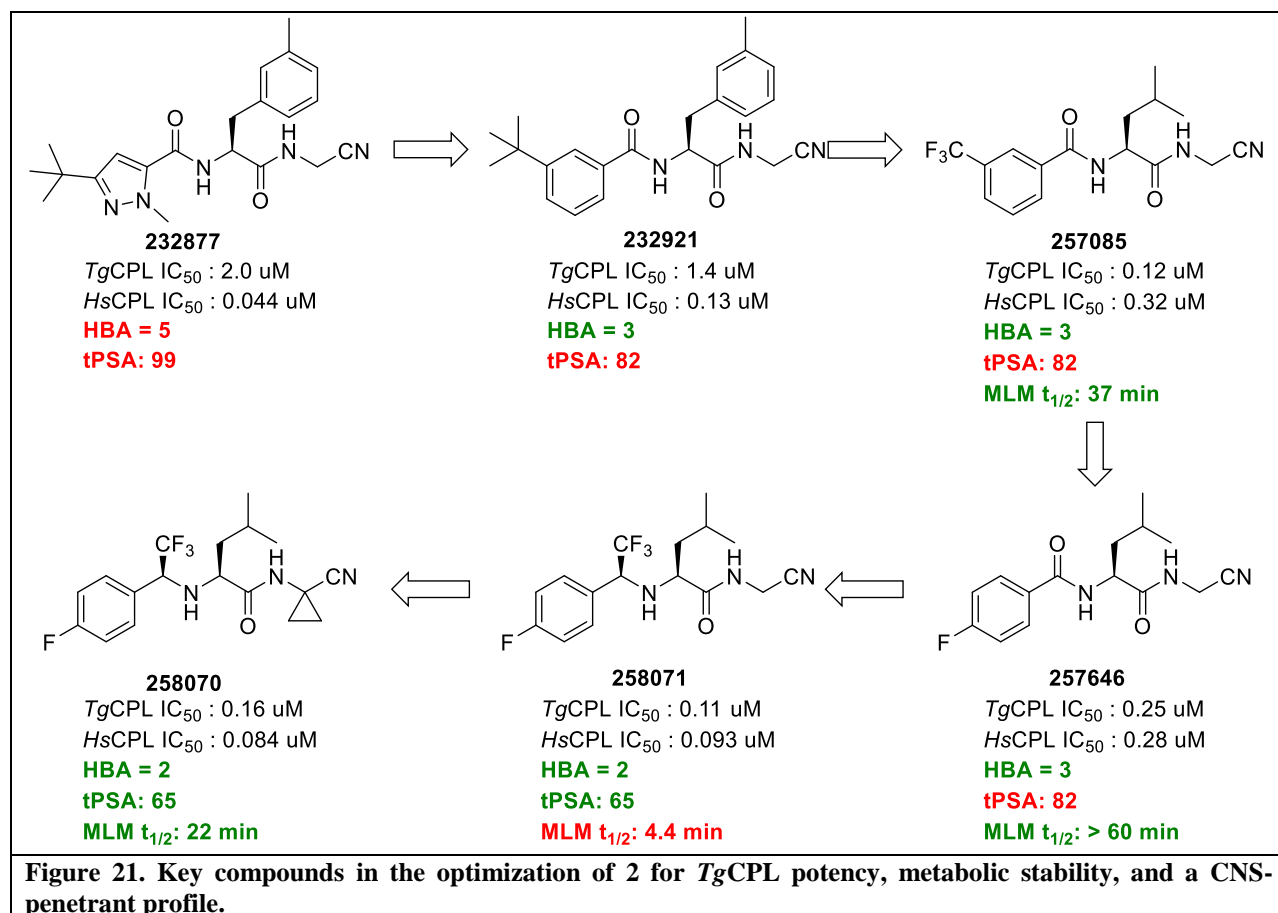
^{a,b,c}See Table 2 for heading definitions.

The alkyne analog **257161** was made as a comparator to lead compound **232877** to determine how much of the activity could be attributed to the nitrile ‘warhead’. Potency for both enzymes reduced by over an order of magnitude (*TgCPL* IC₅₀ = 179 μM and *HsCPL* IC₅₀ = 0.64 μM, respectively) highlighting the need for the covalent interaction to gain inhibitory activity against cathepsins. Trifluoroethylamine analogs (**257952**, **258061**, **258062**, **258063**, and **258069**) were synthesized as both R,S and S,S diastereomers with either a benzyl or 3-fluorobenzyl pendant in P3. While the trend remains that S,S configuration is preferential over the R,S, none of these showed improved potency or selectivity for *TgCPL*. Similarly, **262608** and **262642**, the S,S-trifluoroethylamines with a tert-butyl P2 vector all showed reduced activity from both enzymes, regardless of the nitrile warhead type. It is worth noting that the synthesis of these trifluoroethylamines with bulkier groups in P2 gave a much improved diastereomeric ratio (40:1, S,S:R,S) due to the added steric bulk better directing the zinc borohydride reduction.

Conclusions

In summary, we have demonstrated for the first time that it is possible to modify a well-established chemotype for inhibition of human cathepsins (dipeptide nitrile) and shift selectivity away from the human isoform and towards the *Toxoplasma gondii* isoform, a novel target for toxoplasmosis. Furthermore, we have demonstrated that the physical properties of the dipeptide can be adjusted to be more favorable for CNS penetration without loss of activity, particularly through reduction in tPSA and number of HBA. Key analogs in this campaign are summarized in

Figure 21. Initially, our lead compound **232877** was approximately 46-fold selective for *HsCPL* over *TgCPL*. We developed several compounds that either displayed equipotency for *HsCPL* and *TgCPL* (**257646**), or exhibited slight selectivity (up to 3-fold) for *TgCPL* over *HsCPL* (**257085**, **258921**). Notably, compound **257950** (**Table 4**) demonstrates the potential for achieving outright selectivity for *TgCPL* through the incorporation of a basic residue in the P2 position, an avenue we are exploring in future studies. Furthermore, we improved the potency of our inhibitors for the *T. gondii* enzyme from 2 μM to as low as 115 nM. Although we successfully demonstrated that compound **258070** can penetrate the blood brain barrier, it also exhibits rapid clearance in vivo. Current endeavors in our lab are aimed at further defining the pharmacophore for *TgCPL* via optimization of the P3 and P2 positions. Additionally, we are improving the pharmacokinetic profile for these inhibitors, so they may be advanced to in vivo murine infection studies in order to establish proof-of-concept that *TgCPL* is a viable target for treating the chronic form of toxoplasmosis.



Experimental Section

Chemistry General Information: All reagents were used without further purification as received from commercial sources unless noted otherwise. ^1H NMR spectra were taken in DMSO-*d*₆, MeOD, or CDCl_3 at room temperature on Varian Inova 400 MHz or Varian Inova 500 MHz instruments. Reported chemical shifts for the ^1H NMR spectra were recorded in parts per million (ppm) on the δ scale from an internal standard of residual tetramethylsilane (0 ppm). Mass spectrometry data were obtained on either a Micromass LCT or Agilent Q-TOF. An Agilent 1100 series HPLC with an Agilent Zorbax Eclipse Plus-C18 column was used to determine purity of biologically tested compounds. All tested compounds were determined to be >95% pure using a 6 minute gradient of 10-90% acetonitrile in water followed by a 2 minute hold at 90% acetonitrile with detection at 254 nm. Flash chromatographic purifications were performed using a Teledyne ISCO Combiflash RF with Redisep Gold RF columns.

General Procedure A: Fisher Esterification

The starting amino acid (1.0 eq) was dissolved in MeOH (2-4 mL/1 mmol), and catalytic 98% sulfuric acid (~0.1 eq) was then added. The mixture was heated to reflux overnight. The reaction solution was cooled to room temperature and concentrated in vacuo. The resulting crude residue was dissolved in a sat. NaHCO_3 (aq) solution, and extracted with EtOAc. The combined organic layers were washed with sat. NaHCO_3 (aq) and brine, dried over MgSO_4 and concentrated to afford the desired ester. 14-100%

General Procedure B: Amide Coupling

The aryl acid (1 eq) was dissolved into DMF (1-3 mL/1 mmol) and cooled to 0°C. HATU (1.2 eq) and DIPEA (3.5 eq) were then added and reaction was stirred at 0°C for 5-10 min. The amino acid methyl ester (1 eq) was then added and reaction was allowed to warm and stir at room temperature overnight. Reaction was poured into water, and extracted with EtOAc. The organic layers were combined and washed with a 1N HCl_(aq) solution, sat. NaHCO_{3(aq)} solution, and brine, dried over MgSO₄, and concentrated in vacuo. The crude material was purified by flash chromatography (0-100% EtOAc:Hexanes gradient). 9-99%

General Procedure C: Ester Saponification

The intermediate ester (1eq) was dissolved into a THF:MeOH:1N LiOH_(aq) 1:1:1 solution (2-3 mL/1 mmol) and stirred for 0.5-1 hr. Upon completion as determined by HPLC/TLC, the reaction was quenched with a 1N HCl_(aq) solution and volatiles were removed in vacuo. The remaining aqueous portion was extracted with EtOAc. The combined organic layer was then washed with brine, dried over MgSO₄, and concentrated in vacuo to afford the desired free acid. 95-99%

General Procedure D: Amide Coupling of Nitrile Warhead

The carboxylic acid intermediate (1 eq) was dissolved into DCM (1-3 mL/1 mmol) and cooled to 0°C. HATU (2 eq) and DIPEA (4 eq) were then added and reaction was stirred at 0°C for 5-10 min. 2-aminoacetonitrile bisulfate (2-5 eq) was then added and reaction was allowed to warm and stir at room temperature overnight. Upon completion, the reaction was poured into a 1N HCl_(aq) solution and extracted with DCM. The combined organic layers were washed with

1N HCl (aq) solution, NaHCO₃ (aq) solution, and brine then dried over MgSO₄, and concentrated. The crude material was purified by flash chromatography (0-100% EtOAc:Hexane gradient). 15-89%

Methyl (S)-2-amino-3-(m-tolyl)propanoate (4a)

General Procedure A starting from 3-Methylphenylalanine (0.5 g, 2.79 mmol) gave methyl (S)-2-amino-3-(m-tolyl)propanoate (547 mg, 85%); ¹H NMR (500 MHz, DMSO-d₆) δ 8.77 (br. s., 3H), 7.19 (t, J = 7.34 Hz, 1H), 7.07 (d, J = 7.34 Hz, 1H), 7.03 (br. s., 1H), 7.00 (d, J = 6.85 Hz, 1H), 4.18 (t, J = 6.11 Hz, 1H), 3.63 (s, 3H), 3.17 (dd, J = 5.38, 13.69 Hz, 1H), 3.05 (dd, J = 7.58, 13.94 Hz, 1H), 2.27 (s, 3H)

Methyl (S)-2-(3-(tert-butyl)-1-methyl-1H-pyrazole-5-carboxamido)-3-(m-tolyl)propanoate (5a)

General Procedure B starting from methyl (S)-2-amino-3-(m-tolyl)propanoate (0.2 g, 0.871 mmol), and 3-(tert-butyl)-1-methyl-1H-pyrazole-5-carboxylic acid (0.159 g, 0.871 mmol). Chromatography (20-80% EtOAc:Hexanes gradient) provided methyl (S)-2-(3-(tert-butyl)-1-methyl-1H-pyrazole-5-carboxamido)-3-(m-tolyl)propanoate (227 mg, 87%); ¹H NMR (500 MHz, DMSO-d₆) δ 8.23 (br. s., 1H), 7.14 (t, J = 7.34 Hz, 1H), 7.09 (s, 1H), 7.05 (d, J = 7.34 Hz, 1H), 6.99 (d, J = 7.30 Hz, 1H), 6.77 (s, 1H), 4.54 - 4.64 (m, 1H), 3.88 (s, 3H), 3.63 (s, 3H), 3.10 - 3.16 (m, 2H), 2.23 (s, 3H), 1.25 (s, 9H)

(S)-2-(3-(tert-Butyl)-1-methyl-1H-pyrazole-5-carboxamido)-3-(m-tolyl)propanoic acid (6a)

General Procedure C starting from methyl (S)-2-(3-(tert-butyl)-1-methyl-1H-pyrazole-5-carboxamido)-3-(m-tolyl)propanoate (270 mg, 0.755 mmol) gave (S)-2-(3-(tert-butyl)-1-methyl-1H-pyrazole-5-carboxamido)-3-(m-tolyl)propanoic acid (228 mg, 0.664 mmol, 88 % yield); ¹H NMR (400 MHz, MeOH-d₄) δ 7.15 (t, J = 1.00 Hz, 1H), 7.08 (s, 1H), 7.03 (t, J = 7.60 Hz, 2H), 6.58 (s, 1H), 4.77 (dd, J = 4.70, 9.78 Hz, 1H), 3.91 (s, 3H), 3.26 (t, J = 4.70 Hz, 1H), 3.00 (dd, J = 10.17, 13.69 Hz, 1H), 2.28 (s, 3H), 1.28 (s, 9H)

(S)-3-(tert-butyl)-N-(1-((cyanomethyl)amino)-1-oxo-3-(m-tolyl)propan-2-yl)-1-methyl-1H-pyrazole-5-carboxamide (2)

General Procedure D starting from (S)-2-(3-(tert-butyl)-1-methyl-1H-pyrazole-5-carboxamido)-3-(m-tolyl)propanoic acid (150 mg, 0.437 mmol) gave (S)-3-(tert-butyl)-N-(1-((cyanomethyl)amino)-1-oxo-3-(m-tolyl)propan-2-yl)-1-methyl-1H-pyrazole-5-carboxamide.

(50.7 mg, 0.133 mmol, 30.4 % yield); ¹H NMR (400 MHz, MeOH-d₄) δ 7.14 (t, J = 7.43 Hz, 1H), 7.08 (s, 1H), 7.04 (d, J = 7.43 Hz, 1H), 7.01 (d, J = 7.43 Hz, 1H), 6.63 (s, 1H), 4.73 (dd, J = 6.26, 9.00 Hz, 1H), 4.16 (d, J = 17.61 Hz, 1H), 4.11 (d, J = 17.60 Hz, 1H), 3.89 (s, 3H), 3.20 (dd, J = 6.26, 13.69 Hz, 1H), 2.97 (dd, J = 9.39, 13.69 Hz, 1H), 2.27 (s, 3H), 1.27 (s, 9H); ¹³C NMR (101 MHz, MeOH-d₄) δ 174.1, 162.0, 161.6, 139.3, 138.2, 136.7, 131.2, 129.6, 128.7, 127.5, 117.5, 105.1, 56.2, 38.7, 33.0, 31.0, 28.2, 21.6; MS (ESI+) m/z: 382.1 [M+H]⁺

(S)-3-(m-Tolyl)-2-(3-(trifluoromethyl)benzamido)propanoic acid (6b)

General Procedure B starting from (S)-3-(tert-butyl)-N-(1-((cyanomethyl)amino)-1-oxo-3-(m-tolyl)propan-2-yl)-1-methyl-1H-pyrazole-5-carboxamide (0.1 g, 0.435 mmol), and 3-(trifluoromethyl)benzoic acid (0.83 g, 0.435 mmol). gave methyl (S)-3-(m-tolyl)-2-(3-

(trifluoromethyl)benzamido)propanoate (158 mg). Compound was carried directly into General procedure C to afford (S)-3-(m-tolyl)-2-(3-(trifluoromethyl)benzamido)propanoic acid (151 mg, 0.430 mmol, 99 % yield); ¹H NMR (400 MHz, MeOH -d₄) δ 8.18 (s, 1H), 8.12 (d, *J* = 7.83 Hz, 1H), 7.85 (d, *J* = 7.83 Hz, 1H), 7.68 (t, *J* = 7.83 Hz, 1H), 4.62 - 4.72 (m, 1H), 1.67 - 1.88 (m, 3H), 1.00 (d, *J* = 5.87 Hz, 3H), 0.97 (d, *J* = 5.87 Hz, 3H)

(S)-N-(1-((Cyanomethyl)amino)-1-oxo-3-(m-tolyl)propan-2-yl)-3-(trifluoromethyl)benzamide (7a)

General Procedure D starting from (S)-3-(m-tolyl)-2-(3-(trifluoromethyl)benzamido)propanoic acid (150 mg, 0.427 mmol) provided (S)-N-(1-((cyanomethyl)amino)-1-oxo-3-(m-tolyl)propan-2-yl)-3-(trifluoromethyl)benzamide (35.3 mg, 0.091 mmol, 21.23 % yield); ¹H NMR (400 MHz, MeOH-d₄) δ 8.04 (s, 1H), 7.98 (d, *J* = 7.83 Hz, 1H), 7.81 (d, *J* = 7.83 Hz, 1H), 7.62 (t, *J* = 7.83 Hz, 1H), 7.15 (t, *J* = 7.04 Hz, 1H), 7.10 (s, 1H), 7.07 (d, *J* = 7.43 Hz, 1H), 7.01 (d, *J* = 7.43 Hz, 1H), 4.79 (dd, *J* = 6.46, 8.80 Hz, 1H), 4.14 (dd, *J* = 17.22, 25.04 Hz, 2H), 3.24 (dd, *J* = 6.26, 13.69 Hz, 1H), 3.02 (dd, *J* = 9.00, 13.69 Hz, 1H), 2.27 (s, 3H); ¹³C NMR (101 MHz, MeOH-d₄) δ 174.1, 168.7, 139.4, 138.3, 136.3, 132.3, 131.8, 131.2, 130.7, 129.6, 129.5, 128.7, 127.5, 125.5, 124.1, 117.5, 56.9, 38.7, 28.2, 21.6; MS (ESI+) *m/z*: 412.0 [M+H]⁺

Methyl (S)-2-(3-(tert-butyl)benzamido)-3-(m-tolyl)propanoate (5c)

General Procedure B starting from methyl (S)-2-amino-3-(m-tolyl)propanoate (0.1 g, 0.435 mmol), and 3-(tert-butyl)benzoic acid (0.078 g, 0.435 mmol). Chromatography (20-80 % EtOAc:Hexanes gradient) provided methyl (S)-2-(3-(tert-butyl)benzamido)-3-(m-tolyl)propanoate (95.3 mg, 0.270 mmol, 61.9 % yield); ¹H NMR (500 MHz, CDCl₃) δ 7.79 (s,

1H), 7.54 (d, $J = 7.83$ Hz, 1H), 7.46 (d, $J = 7.83$ Hz, 1H), 7.35 (t, $J = 7.58$ Hz, 1H), 7.20 (t, $J = 7.58$ Hz, 1H), 7.08 (d, $J = 7.34$ Hz, 1H), 6.97 (s, 1H), 6.95 (d, $J = 7.83$ Hz, 1H), 6.52 (d, $J = 6.85$ Hz, 1H), 5.07 (dd, $J = 6.36, 12.72$ Hz, 1H), 3.78 (s, 3H), 3.26 (dd, $J = 5.87, 13.69$ Hz, 1H), 3.20 (dd, $J = 5.38, 13.69$ Hz, 1H), 2.31 (s, 3H), 1.34 (s, 9H)

(S)-2-(3-(tert-Butyl)benzamido)-3-(m-tolyl)propanoic acid (6c)

General Procedure C starting from methyl (S)-2-(3-(tert-butyl)benzamido)-3-(m-tolyl)propanoate (95 mg, 0.269 mmol) gave (S)-2-(3-(tert-butyl)benzamido)-3-(m-tolyl)propanoic acid (86 mg, 0.253 mmol, 94 % yield); ^1H NMR (400 MHz, MeOH- d_4) δ 7.74 (s, 1H), 7.56 (d, $J = 7.83$ Hz, 1H), 7.50 (d, $J = 7.43$ Hz, 1H), 7.34 (t, $J = 7.83$ Hz, 1H), 7.04 - 7.18 (m, 3H), 7.01 (d, $J = 7.43$ Hz, 1H), 4.83 (dd, $J = 4.89, 9.59$ Hz, 1H), 3.30 (dd, $J = 4.90, 13.70$ Hz, 3H), 3.08 (dd, $J = 9.78, 13.69$ Hz, 1H), 2.27 (s, 3H), 1.33 (s, 9H)

(S)-3-(tert-Butyl)-N-(1-((cyanomethyl)amino)-1-oxo-3-(m-tolyl)propan-2-yl)benzamide (7b)

General Procedure D starting from (S)-2-(3-(tert-butyl)benzamido)-3-(m-tolyl)propanoic acid (115 mg, 0.339 mmol) provided (S)-3-(tert-butyl)-N-(1-((cyanomethyl)amino)-1-oxo-3-(m-tolyl)propan-2-yl)benzamide (55.3 mg, 0.146 mmol, 43.2 % yield) ^1H NMR (400 MHz, MeOH- d_4) δ 7.77 (s, 1H), 7.55 (t, $J = 7.83$ Hz, 2H), 7.33 (t, $J = 7.83$ Hz, 1H), 7.15 (t, $J = 7.43$ Hz, 1H), 7.10 (s, 1H), 7.07 (d, $J = 7.43$ Hz, 1H), 7.01 (d, $J = 7.43$ Hz, 1H), 4.75 - 4.82 (m, 1H), 4.12 (dd, $J = 17.61, 26.61$ Hz, 2H), 3.22 (dd, $J = 6.26, 13.69$ Hz, 1H), 3.04 (dd, $J = 8.80, 13.50$ Hz, 1H), 2.27 (s, 3H), 1.27 - 1.37 (m, 9H); ^{13}C NMR (101 MHz, MeOH- d_4) δ 174.3, 170.8, 152.8, 139.4, 138.3, 134.9, 131.3, 31.1, 130.2, 129.9, 129.5, 128.7, 127.4, 125.8, 125.5, 117.5, 56.9, 38.7, 35.8, 31.7, 28.1, 21.8; MS (ESI+) m/z : 400.1 $[\text{M}+\text{Na}]^+$

Methyl (S)-2-amino-3-(3-hydroxyphenyl)propanoate (4b)

General Procedure A starting from (S)-2-amino-3-(3-hydroxyphenyl)propanoic acid (330 mg, 1.821 mmol) gave methyl (S)-2-amino-3-(3-hydroxyphenyl)propanoate (113.2 mg, 0.580 mmol, 31.8 % yield). ¹H NMR (400 MHz, MeOH-d₄) δ 7.10 (t, *J* = 7.83 Hz, 1H), 6.62 - 6.68 (m, 2H), 6.61 (s, 1H), 3.68 - 3.71 (m, 1H), 3.67 (s, 3H), 2.93 (dd, *J* = 6.06, 13.50 Hz, 1H), 2.84 (dd, *J* = 7.04, 13.30 Hz, 1H)

(S)-3-(3-Hydroxyphenyl)-2-(3-(trifluoromethyl)benzamido)propanoic acid (6d)

General Procedure B starting from methyl (S)-2-amino-3-(3-hydroxyphenyl)propanoate hydrochloride (83 mg, 0.358 mmol) and 3-(trifluoromethyl)benzoic acid (68.1 mg, 0.358 mmol) gave methyl (S)-3-(3-hydroxyphenyl)-2-(3-(trifluoromethyl)benzamido)propanoate (130 mg, 0.354 mmol), which was carried directly into General Procedure C without further purification to afford (S)-3-(3-hydroxyphenyl)-2-(3-(trifluoromethyl)benzamido)propanoic acid (130 mg, 0.354 mmol, 99 % yield)

(S)-N-(1-((Cyanomethyl)amino)-3-(3-hydroxyphenyl)-1-oxopropan-2-yl)-3-(trifluoromethyl)benzamide (7c)

General Procedure D starting from (S)-3-(3-hydroxyphenyl)-2-(3-(trifluoromethyl)benzamido)propanoic acid (84 mg, 0.238 mmol) and 2-aminoacetonitrile bisulfate (182 mg, 1.189 mmol) gave (S)-N-(1-((cyanomethyl)amino)-3-(3-hydroxyphenyl)-1-oxopropan-2-yl)-3-(trifluoromethyl)benzamide (60.6 mg, 0.155 mmol, 65.1 % yield). ¹H NMR (400 MHz, MeOH-d₄) δ 8.05 (s, 1H), 7.97 (d, *J* = 7.83 Hz, 1H), 7.79 (d, *J* = 7.83 Hz, 1H), 7.60 (t, *J* = 7.80 Hz, 1H),

7.08 (t, $J = 8.02$ Hz, 1H), 6.70 - 6.79 (m, 2H), 6.64 (d, $J = 9.00$ Hz, 1H), 4.81 (dd, $J = 6.26, 9.00$ Hz, 1H), 4.14 (s, 2H), 3.21 (dd, $J = 6.06, 13.50$ Hz, 1H), 3.01 (dd, $J = 9.39, 13.69$ Hz, 1H); ^{13}C NMR (101 MHz, MeOH- d_4) δ 174.1, 168.7, 158.7, 139.8, 136.2, 132.4, 131.7, 130.7, 130.7, 130.4, 129.2, 125.5, 121.5, 117.5, 117.1, 114.8, 57.0, 38.6, 28.2; MS (ESI+) m/z : 414.0 $[\text{M}+\text{Na}]^+$

Methyl (S)-2-(3-(tert-butyl)benzamido)-3-(3-hydroxyphenyl)propanoate (5e)

General Procedure B starting from methyl (S)-2-amino-3-(3-hydroxyphenyl)propanoate (100 mg, 0.432 mmol), and 3-(tert-butyl)benzoic acid (77 mg, 0.432 mmol) gave methyl (S)-2-(3-(tert-butyl)benzamido)-3-(3-hydroxyphenyl)propanoate (143 mg, 0.402 mmol, 93 % yield). Product was subsequently hydrolyzed according to General procedure C, and carried directly to the next step without further purification. ^1H NMR (500 MHz, MeOH- d_4) δ 7.76 (s, 1H), 7.55 (d, $J = 7.83$ Hz, 1H), 7.52 (d, $J = 7.83$ Hz, 1H), 7.33 (t, $J = 7.58$ Hz, 1H), 7.09 (t, $J = 7.58$ Hz, 1H), 6.73 - 6.79 (m, 2H), 6.65 (d, $J = 7.83$ Hz, 1H), 4.84 (dd, $J = 4.89, 9.50$ Hz, 1H), 3.27 (dd, $J = 4.89, 13.69$ Hz, 1H), 3.08 (dd, $J = 9.50, 13.69$ Hz, 1H), 1.31 (s, 9H)

(S)-3-(tert-Butyl)-N-(1-((cyanomethyl)amino)-3-(3-hydroxyphenyl)-1-oxopropan-2-yl)benzamide (7d)

General Procedure D starting from (S)-2-(3-(tert-butyl)benzamido)-3-(3-hydroxyphenyl)propanoic acid (68 mg, 0.199 mmol) and 2-aminoacetonitrile bisulfate (153 mg, 0.996 mmol) gave (S)-3-(tert-butyl)-N-(1-((cyanomethyl)amino)-3-(3-hydroxyphenyl)-1-oxopropan-2-yl)benzamide (55.9 mg, 0.147 mmol, 74.0 % yield). ^1H NMR (400 MHz, MeOH- d_4) δ 7.77 (s, 1H), 7.57 (d, $J = 8.22$ Hz, 1H), 7.54 (d, $J = 8.22$ Hz, 1H), 7.33 (t, $J = 7.63$ Hz, 1H), 7.09 (t, $J = 8.02$ Hz, 1H), 6.71 - 6.79 (m, 2H), 6.65 (d, $J = 9.00$ Hz, 1H), 4.78 (dd, $J = 6.26, 8.61$

Hz, 1H), 4.13 (s, 2H), 3.20 (dd, $J = 6.26, 13.69$ Hz, 1H), 3.01 (dd, $J = 9.00, 13.69$ Hz, 1H), 1.31 (s, 9H); ^{13}C NMR (101 MHz, MeOH- d_4) δ 174.3, 170.9, 158.7, 152.9, 139.9, 135.0, 129.9, 125.9, 125.6, 121.5, 117.5, 117.3, 117.2, 115.1, 114.8, 56.8, 38.6, 35.8, 31.8, 31.7, 28.2; MS (ESI+) m/z : 402.1 $[\text{M}+\text{Na}]^+$

Methyl (S)-2-amino-3-(3-methoxyphenyl)propanoate (4c)

General Procedure A starting from (S)-2-amino-3-(3-methoxyphenyl)propanoic acid (440 mg, 2.254 mmol) gave methyl (S)-2-amino-3-(3-methoxyphenyl)propanoate (244.5 mg, 1.168 mmol, 51.8 % yield). ^1H NMR (500 MHz, MeOH- d_4) δ 7.19 (t, $J = 8.07$ Hz, 1H), 6.78 (d, $J = 8.31$ Hz, 1H), 6.71 - 6.76 (m, 2H), 3.74 (s, 3H), 3.68 - 3.71 (m, 1H), 3.66 (s, 3H), 2.98 (dd, $J = 5.87, 13.21$ Hz, 1H), 2.87 (dd, $J = 7.09, 13.45$ Hz, 1H)

Methyl (S)-3-(3-methoxyphenyl)-2-(3-(trifluoromethyl)benzamido)propanoate (5f)

General Procedure B starting from methyl (S)-2-amino-3-(3-methoxyphenyl)propanoate (81.5 mg, 0.389 mmol) and 3-(trifluoromethyl)benzoic acid (74.1 mg, 0.389 mmol) gave methyl (S)-3-(3-methoxyphenyl)-2-(3-(trifluoromethyl)benzamido)propanoate (145.5 mg, 0.382 mmol, 98 % yield) Product was subsequently hydrolyzed according to General Procedure C, and carried directly to the next step without further purification. ^1H NMR (400 MHz, MeOH- d_4) δ 8.01 (s, 1H), 7.94 (d, $J = 7.43$ Hz, 1H), 7.75 (d, $J = 7.83$ Hz, 1H), 7.55 (t, $J = 7.83$ Hz, 1H), 7.15 (t, $J = 8.22$ Hz, 1H), 6.81 - 6.88 (m, 2H), 6.69 - 6.76 (m, 1H), 4.91 (dd, $J = 4.70, 9.78$ Hz, 1H), 3.69 (s, 3H), 3.34 (dd, $J = 4.70, 14.09$ Hz, 1H), 3.09 (dd, $J = 9.98, 14.00$ Hz, 1H), 1.97 (s, 3H)

(S)-N-(1-((Cyanomethyl)amino)-3-(3-methoxyphenyl)-1-oxopropan-2-yl)-3-trifluoromethyl benzamide (7e)

General Procedure D starting from (S)-3-(3-methoxyphenyl)-2-(3-(trifluoromethyl)benzamido)propanoic acid (145.5 mg, 0.396 mmol) and 2-aminoacetonitrile bisulfate ((305 mg, 1.981 mmol) gave (S)-N-(1-((cyanomethyl)amino)-3-(3-methoxyphenyl)-1-oxopropan-2-yl)-3-(trifluoromethyl)benzamide (120.5 mg, 0.297 mmol, 75 % yield). ¹H NMR (500 MHz, MeOH-d₄) δ 8.04 (s, 1H), 7.97 (d, *J* = 7.34 Hz, 1H), 7.80 (d, *J* = 7.83 Hz, 1H), 7.60 (t, *J* = 7.83 Hz, 1H), 7.18 (t, *J* = 8.07 Hz, 1H), 6.84 - 6.89 (m, 2H), 6.76 (dd, *J* = 1.96, 8.31 Hz, 1H), 4.85 (s, 3H), 4.16 (dd, *J* = 17.61, 23.97 Hz, 2H), 3.72 (s, 3H), 3.26 (dd, *J* = 5.87, 13.69 Hz, 1H), 3.05 (dd, *J* = 9.29, 13.69 Hz, 1H); ¹³C NMR (126 MHz, MeOH-d₄) δ 174.1, 168.7, 161.4, 139.9, 136.2, 132.3, 130.7, 130.6, 129.4, 125.6, 122.7, 117.5, 115.9, 113.6, 56.8, 55.7, 38.7, 28.2; MS (ESI+) *m/z*: 428.0 [M+Na]⁺

(S)-2-(3-(tert-Butyl)benzamido)-3-(3-methoxyphenyl)propanoic acid (6f)

General Procedure B starting from methyl (S)-2-amino-3-(3-methoxyphenyl)propanoate (81.5 mg, 0.389 mmol) and 3-(tert-butyl)benzoic acid (69.4 mg, 0.389 mmol) gave methyl (S)-2-(3-(tert-butyl)benzamido)-3-(3-methoxyphenyl)propanoate, which was subsequently hydrolyzed according to General procedure C to afford (S)-2-(3-(tert-butyl)benzamido)-3-(3-methoxyphenyl)propanoic acid (130 mg, 0.366 mmol, 94 % yield); ¹H NMR (500 MHz, MeOH-d₄) δ 7.76 (s, 1H), 7.52 (d, *J* = 7.34 Hz, 2H), 7.30 (t, *J* = 7.83 Hz, 1H), 7.15 (t, *J* = 8.07 Hz, 1H), 6.83 - 6.88 (m, 2H), 6.70 - 6.76 (m, 1H), 4.90 (dd, *J* = 4.89, 9.80 Hz, 1H), 3.64 - 3.72 (m, 4H), 3.32 (dd, *J* = 4.65, 13.94 Hz, 1H), 3.12 (dd, *J* = 9.78, 13.90 Hz, 1H), 1.28 (s, 9H)

(S)-3-(tert-Butyl)-N-(1-((cyanomethyl)amino)-3-(3-methoxyphenyl)-1-oxopropan-2-yl)benzamide (7f)

General Procedure D starting from (S)-2-(3-(tert-butyl)benzamido)-3-(3-methoxyphenyl)propanoic acid (149.5 mg, 0.421 mmol) and 2-aminoacetonitrile bisulfate (324 mg, 2.103 mmol) gave (S)-3-(tert-butyl)-N-(1-((cyanomethyl)amino)-3-(3-methoxyphenyl)-1-oxopropan-2-yl)benzamide (140 mg, 0.356 mmol, 85 % yield); ¹H NMR (500 MHz, MeOH-d₄) δ 7.77 (s, 1H), 7.52 - 7.58 (m, 2H), 7.32 (t, *J* = 8.31 Hz, 1H), 7.17 (t, *J* = 8.07 Hz, 1H), 6.83 - 6.89 (m, 2H), 6.75 (dd, *J* = 1.71, 8.07 Hz, 1H), 4.83 (s, 2H), 4.14 (d, *J* = 7.34 Hz, 1H), 3.70 (s, 3H), 3.25 (dd, *J* = 5.87, 13.69 Hz, 1H), 3.06 (dd, *J* = 9.29, 13.69 Hz, 1H), 1.30 (s, 9H); ¹³C NMR (126 MHz, MeOH-d₄) δ 174.2, 170.8, 161.3, 152.8, 140.0, 134.9, 130.6, 130.1, 129.4, 125.7, 125.7, 122.7, 117.5, 116.0, 113.6, 56.6, 55.7, 38.7, 35.8, 31.8, 28.2, 14.6; MS (ESI+) *m/z*: 416.1 [M+Na]⁺

(S)-3-(tert-Butyl)-N-(1-((cyanomethyl)amino)-4-methyl-1-oxopentan-2-yl)benzamide (7g)

General Procedure D starting from (3-(tert-butyl)benzoyl)-L-leucine (218 mg, 0.748 mmol) and 2-aminoacetonitrile (577 mg, 3.74 mmol), gave (S)-3-(tert-butyl)-N-(1-((cyanomethyl)amino)-4-methyl-1-oxopentan-2-yl)benzamide (25.6 mg, 0.078 mmol, 10.39 % yield); ¹H NMR (500 MHz, MeOH-d₄) δ 7.93 (s, 1H), 7.67 (d, *J* = 7.34 Hz, 1H), 7.60 (d, *J* = 7.83 Hz, 1H), 7.39 (t, *J* = 7.83 Hz, 1H), 4.66 (dd, *J* = 4.65, 10.03 Hz, 1H), 4.16 (d, *J* = 6.85 Hz, 2H), 1.74 - 1.87 (m, 1H), 1.63 - 1.74 (m, 2H), 1.35 (s, 9H), 1.00 (d, *J* = 6.36 Hz, 3H), 0.98 (d, *J* = 6.36 Hz, 3H); ¹³C NMR (126 MHz, MeOH-d₄) δ 175.6, 171.0, 153.0, 134.9, 130.2, 129.4, 125.9, 125.8, 117.6, 53.7, 41.7, 35.9, 31.8, 28.2, 26.3, 23.6, 22.1; MS (ESI+) *m/z*: 352.1 [M+Na]⁺

(3-(Trifluoromethyl)benzoyl)-L-leucine (6h)

General Procedure A starting from ethyl L-leucinate, HCl (200 mg, 1.022 mmol) and 3-(trifluoromethyl)benzoic acid (194 mg, 1.022 mmol) gave ethyl (3-(trifluoromethyl)benzoyl)-L-leucinate, which was subsequently hydrolyzed according to General procedure C to afford (3-(trifluoromethyl)benzoyl)-L-leucine (299 mg, 0.986 mmol, 99 % yield); ¹H NMR (400 MHz, MeOH-d₄) δ 8.18 (s, 1H), 8.12 (d, *J* = 7.83 Hz, 1H), 7.85 (d, *J* = 7.83 Hz, 1H), 7.68 (t, *J* = 7.83 Hz, 1H), 4.62 - 4.72 (m, 1H), 1.67 - 1.88 (m, 3H), 1.00 (d, *J* = 5.87 Hz, 3H), 0.97 (d, *J* = 5.87 Hz, 3H)

(S)-N-(1-((Cyanomethyl)amino)-4-methyl-1-oxopentan-2-yl)-3-(trifluoromethyl)benzamide (7h)

General Procedure D starting from (3-(trifluoromethyl)benzoyl)-L-leucine (100 mg, 0.330 mmol) and 2-aminoacetonitrile bisulfate (252 mg, 1.649 mmol) gave (S)-N-(1-((cyanomethyl)amino)-4-methyl-1-oxopentan-2-yl)-3-(trifluoromethyl)benzamide (17.3 mg, 0.051 mmol, 15.37 % yield); ¹H NMR (400 MHz, MeOH-d₄) δ 8.21 (s, 1H), 8.13 (d, *J* = 7.83 Hz, 1H), 7.85 (d, *J* = 7.43 Hz, 1H), 7.68 (t, *J* = 7.83 Hz, 1H), 4.65 (dd, *J* = 4.70, 9.78 Hz, 1H), 4.17 (dd, *J* = 17.61, 21.52 Hz, 2H), 1.63 - 1.87 (m, 3H), 0.98 (dd, *J* = 6.26, 10.56 Hz, 6H); ¹³C NMR (101 MHz, MeOH-d₄) δ 175.4, 168.9, 136.3, 136.2, 132.5, 132.4, 130.7, 130.6, 129.6, 125.7, 117.6, 53.9, 41.6, 28.2, 26.3, 23.5, 21.9; MS (ESI+) *m/z*: 364.0 [M+Na]⁺

(S)-N-(1-((Cyanomethyl)amino)-4-methyl-1-oxopentan-2-yl)benzamide (7i)

General Procedure A starting from ethyl L-leucinate, HCl (200 mg, 1.022 mmol) and benzoic acid (125 mg, 1.022 mmol) gave ethyl benzoyl-L-leucinate, which was subsequently hydrolyzed

according to General procedure C and directly coupled to 2-aminoacetonitrile bisulfate (547 mg, 3.57 mmol) according to General Procedure D to afford (S)-N-(1-((cyanomethyl)amino)-4-methyl-1-oxopentan-2-yl)benzamide (26.5 mg, 0.097 mmol, 13.6 % yield); ¹H NMR (400 MHz, MeOH-d₄) δ 7.86 (d, *J* = 7.43 Hz, 2H), 7.53 (t, *J* = 7.43 Hz, 1H), 7.45 (t, *J* = 7.43 Hz, 2H), 4.65 (dd, *J* = 5.48, 10.17 Hz, 1H), 4.16 (dd, *J* = 17.61, 21.13 Hz, 2H), 1.59 - 1.87 (m, 3H), 0.97 (dd, *J* = 5.87, 10.56 Hz, 6H); ¹³C NMR (101 MHz, MeOH-d₄) δ 175.5, 170.5, 135.1, 133.2, 132.8, 129.8, 129.5, 128.8, 128.6, 117.7, 53.7, 41.7, 28.2, 26.2, 23.7, 23.5, 22.1, 21.9; MS (ESI+) *m/z*: 296.0 [M+Na]⁺

Ethyl (3-fluorobenzoyl)-L-leucinate (5k)

General Procedure A starting from ethyl L-leucinate, HCl (200 mg, 1.022 mmol) and ethyl L-leucinate, HCl (200 mg, 1.022 mmol) gave ethyl (3-fluorobenzoyl)-L-leucinate (285 mg, 1.012 mmol, 99 % yield); ¹H NMR (500 MHz, MeOH-d₄) δ 7.68 (d, *J* = 7.83 Hz, 1H), 7.58 (d, *J* = 9.29 Hz, 1H), 7.43 - 7.55 (m, 1H), 7.30 (dt, *J* = 2.45, 8.31 Hz, 1H), 4.64 (dd, *J* = 4.65, 10.03 Hz, 1H), 4.19 (q, *J* = 7.01 Hz, 2H), 1.66 - 1.83 (m, 3H), 1.27 (t, *J* = 7.09 Hz, 3H), 0.99 (d, *J* = 6.36 Hz, 3H), 0.94 - 0.98 (m, 3H)

(S)-N-(1-((Cyanomethyl)amino)-4-methyl-1-oxopentan-2-yl)-3-fluorobenzamide (7k)

General Procedure C starting from ethyl (3-fluorobenzoyl)-L-leucinate (280 mg, 0.995 mmol) gave (3-fluorobenzoyl)-L-leucine (250 mg, 0.987 mmol) which was subsequently coupled to 2-aminoacetonitrile bisulfate (756 mg, 4.94 mmol) according to General Procedure D to afford (S)-N-(1-((cyanomethyl)amino)-4-methyl-1-oxopentan-2-yl)-3-fluorobenzamide (139 mg, 0.477 mmol, 48.3 % yield); ¹H NMR (500 MHz, MeOH-d₄) δ 7.68 (d, *J* = 7.83 Hz, 1H), 7.58 (d, *J* =

9.29 Hz, 1H), 7.45 (dt, $J = 5.87, 7.83$ Hz, 1H), 7.25 (dt, $J = 2.45, 8.31$ Hz, 1H), 4.65 (dd, $J = 4.65, 10.03$ Hz, 1H), 4.13 - 4.23 (m, 2H), 1.61 - 1.85 (m, 3H), 0.98 (d, $J = 6.36$ Hz, 3H), 0.95 (d, $J = 6.36$ Hz, 3H); ^{13}C NMR (126 MHz, MeOH- d_4) δ 175.4, 168.8, 165.0, 163.0, 137.4, 131.5, 124.5, 119.8, 117.6, 115.7, 53.7, 41.6, 28.2, 26.2, 23.5, 22.0; MS (ESI+) m/z : 314.1 $[\text{M}+\text{Na}]^+$

Methyl (2-chloro-4-fluorobenzoyl)-L-leucinate (5l)

General Procedure B starting from methyl L-leucinate (150 mg, 1.033 mmol) and 2-chloro-4-fluorobenzoic acid (180 mg, 1.033 mmol) gave methyl (2-chloro-4-fluorobenzoyl)-L-leucinate (261 mg, 0.865 mmol, 84 % yield); ^1H NMR (500 MHz, DMSO- d_6) δ 6.71 (t, $J = 7.34$ Hz, 1H), 6.50 (d, $J = 8.80$ Hz, 1H), 6.36 (t, $J = 8.31$ Hz, 1H), 3.84 (dd, $J = 5.14, 10.03$ Hz, 1H), 2.95 (s, 3H), 0.99 (qd, $J = 6.81, 13.33$ Hz, 1H), 0.84 - 0.93 (m, 2H), 0.18 (d, $J = 6.85$ Hz, 6H)

(2-Chloro-4-fluorobenzoyl)-L-leucine (6l)

General Procedure C starting from methyl (2-chloro-4-fluorobenzoyl)-L-leucinate (130 mg, 0.431 mmol) gave (2-chloro-4-fluorobenzoyl)-L-leucine (122 mg, 0.424 mmol, 98 % yield); ^1H NMR (500 MHz, MeOH- d_4) δ 7.48 - 7.60 (m, 1H), 7.27 - 7.39 (m, 2H), 7.17 (t, $J = 8.56$ Hz, 2H), 4.63 (dd, $J = 5.87, 9.29$ Hz, 1H), 1.79 - 1.90 (m, 1H), 1.63 - 1.79 (m, 2H), 1.00 (d, $J = 6.36$ Hz, 6H)

(S)-2-Chloro-N-(1-((cyanomethyl)amino)-4-methyl-1-oxopentan-2-yl)-4-fluorobenzamide (7l)

General Procedure D starting from (2-chloro-4-fluorobenzoyl)-L-leucine (100 mg, 0.348 mmol) and 2-aminoacetone bisulfate (106 mg, 0.695 mmol) gave (S)-2-chloro-N-(1-

((cyanomethyl)amino)-4-methyl-1-oxopentan-2-yl)-4-fluorobenzamide (64.2 mg, 0.197 mmol, 56.7 % yield); ^1H NMR (500 MHz, MeOH- d_4) δ 7.55 (dd, $J = 6.36, 8.31$ Hz, 1H), 7.31 (dd, $J = 2.45, 8.80$ Hz, 1H), 7.17 (dt, $J = 2.45, 8.31$ Hz, 1H), 4.61 (dd, $J = 5.14, 10.03$ Hz, 1H), 4.23 (d, $J = 17.20$ Hz, 1H), 4.18 (d, $J = 17.12$ Hz, 1H), 1.76 - 1.86 (m, 1H), 1.68 - 1.76 (m, 1H), 1.58 - 1.66 (m, 1H), 1.00 (d, $J = 6.36$ Hz, 6H); ^{13}C NMR (126 MHz, MeOH- d_4) δ 174.8, 169.2, 164.6, 133.8, 133.6, 132.0, 118.4, 117.6, 115.4, 53.5, 41.7, 28.2, 26.1, 23.5, 22.0; MS (ESI+) m/z : 348.1 [M+Na] $^+$

(S)-N-(1-((Cyanomethyl)amino)-4-methyl-1-oxopentan-2-yl)-3-methylbenzamide (7j)

General Procedure D starting with (tert-butoxycarbonyl)-L-leucine (1 g, 4.32 mmol) gave tert-butyl (S)-(1-((cyanomethyl)amino)-4-methyl-1-oxopentan-2-yl)carbamate (1100 mg, 4.08 mmol, 94 % yield); ^1H NMR (400 MHz, DMSO- d_6) δ 8.56 (t, $J = 5.09$ Hz, 1H), 7.02 (d, $J = 8.22$ Hz, 1H), 4.11 (d, $J = 5.48$ Hz, 2H), 3.89 - 4.00 (m, 1H), 1.50 - 1.68 (m, 1H), 1.40 - 1.48 (m, 2H), 1.37 (s, 9H), 0.87 (d, $J = 6.65$ Hz, 3H), 0.84 (d, $J = 6.26$ Hz, 3H); Subsequently, in a dry round bottom flask under nitrogen, (S)-2-amino-N-(cyanomethyl)-4-methylpentanamide (27 mg, 0.160 mmol) was dissolved into acetonitrile (5 mL). 3-methylbenzoic acid (21.72 mg, 0.160 mmol), HATU (91 mg, 0.239 mmol), and DIPEA (0.070 ml, 0.399 mmol) were added to the solution and the reaction was left to stir under overnight. The solution was extracted with 3 times with EtOAc, and the combined organic layer was washed with sat. aqueous sodium bicarbonate, and brine, dried over MgSO_4 and concentrated in vacuo. Compound was purified via by flash chromatography (0-100% EtOAc:Hexanes gradient) to afford (S)-N-(1-((cyanomethyl)amino)-4-methyl-1-oxopentan-2-yl)-3-methylbenzamide (10 mg, 0.035 mmol, 21.81 % yield); ^1H NMR (400 MHz, MeOH- d_4) δ 7.69 (s, 1H), 7.65 (d, $J = 7.04$ Hz, 1H), 7.31 - 7.39 (m, 2H), 4.64 (dd, J

= 4.50, 9.98 Hz, 1H), 4.19 (d, $J = 17.61$ Hz, 1H), 4.14 (d, $J = 17.60$ Hz, 1H), 2.40 (s, 3H), 1.60 - 1.86 (m, 3H), 0.99 (d, $J = 6.26$ Hz, 3H), 0.97 (d, $J = 5.87$ Hz, 3H); ^{13}C NMR (101 MHz, MeOH- d_4) δ 175.5, 170.7, 139.6, 135.2, 133.7, 129.6, 129.2, 125.9, 117.6, 53.7, 41.7, 28.2, 26.3, 23.6, 22.1, 21.0; MS (ESI+) m/z : 288.1707 $[\text{M}+\text{H}]^+$

(S)-2,4-Dichloro-N-(1-((cyanomethyl)amino)-4-methyl-1-oxopentan-2-yl)benzamide (7m)

General Procedure D starting with (tert-butoxycarbonyl)-L-leucine (1 g, 4.32 mmol) gave tert-butyl (S)-(1-((cyanomethyl)amino)-4-methyl-1-oxopentan-2-yl)carbamate (1100 mg, 4.08 mmol, 94 % yield); ^1H NMR (400 MHz, DMSO- d_6) δ 8.56 (t, $J = 5.09$ Hz, 1H), 7.02 (d, $J = 8.22$ Hz, 1H), 4.11 (d, $J = 5.48$ Hz, 2H), 3.89 - 4.00 (m, 1H), 1.50 - 1.68 (m, 1H), 1.40 - 1.48 (m, 2H), 1.37 (s, 9H), 0.87 (d, $J = 6.65$ Hz, 3H), 0.84 (d, $J = 6.26$ Hz, 3H); Subsequently, In a dry roundbottom flask under nitrogen, tert-butyl (S)-(1-((cyanomethyl)amino)-4-methyl-1-oxopentan-2-yl)carbamate (600 mg, 2.228 mmol) was dissolved into THF (4 ml) and cooled to 0°C . methanesulfonic acid (0.723 ml, 11.14 mmol) was added and reaction was placed under a light vacuum. Reaction was left to stir for 30min. THF was removed in vacuo and residue was brought to pH ~ 10 with 1N NaOH (aq). The solution was extracted with 3 times with EtOAc, and the combined organic layer was washed with sat. aqueous sodium bicarbonate, and brine, dried over MgSO_4 and concentrated in vacuo to afford (S)-2-amino-N-(cyanomethyl)-4-methylpentanamide (250 mg, 1.477 mmol, 66.3 % yield) as an oily/semisolid residue. The residue was carried directly into the subsequent coupling following General procedure B starting from 2,4-dichlorobenzoic acid (91 mg, 0.475 mmol) and (S)-3-amino-5-methylhexanenitrile (50 mg, 0.396 mmol) gave (S)-2,4-dichloro-N-(1-((cyanomethyl)amino)-4-methyl-1-oxopentan-2-yl)benzamide (12 mg, 0.035 mmol, 8.85 % yield); ^1H NMR (500 MHz, MeOH- d_4) δ 7.54 (d, $J =$

1.47 Hz, 1H), 7.49 (d, $J = 8.31$ Hz, 1H), 7.41 (dd, $J = 1.47, 8.31$ Hz, 1H), 4.61 (dd, $J = 5.14, 10.03$ Hz, 1H), 4.23 (d, $J = 17.12$ Hz, 1H), 4.18 (d, $J = 17.61$ Hz, 1H), 1.76 - 1.86 (m, 1H), 1.67 - 1.76 (m, 1H), 1.56 - 1.67 (m, 1H), 1.00 (br. s, 3H), 0.99 (br. s, 3H); ^{13}C NMR (126 MHz, MeOH- d_4) δ 174.8, 169.1, 137.5, 135.9, 133.2, 131.4, 130.8, 128.5, 117.6, 53.5, 41.7, 28.2, 26.1, 23.5, 22.0; MS (ESI+) m/z : 364.1 $[\text{M}+\text{Na}]^+$

Ethyl (4-fluorobenzoyl)-L-leucinate (5n)

General Procedure B starting from ethyl L-leucinate, HCl (250 mg, 1.278 mmol) and 4-fluorobenzoic acid (197 mg, 1.405 mmol) gave ethyl (4-fluorobenzoyl)-L-leucinate (350 mg, 1.244 mmol, 97 % yield); ^1H NMR (500 MHz, MeOH- d_4) δ 7.91 (dd, $J = 5.38, 8.31$ Hz, 2H), 7.19 (t, $J = 8.56$ Hz, 2H), 4.57 - 4.70 (m, 1H), 4.19 (q, $J = 7.34$ Hz, 2H), 1.70 - 1.80 (m, 2H), 1.33 - 1.40 (m, 1H), 1.27 (t, $J = 7.09$ Hz, 3H), 0.99 (d, $J = 6.36$ Hz, 3H), 0.96 (d, $J = 5.87$ Hz, 3H)

(4-Fluorobenzoyl)-L-leucine (6n)

General Procedure C starting from ethyl (4-fluorobenzoyl)-L-leucinate (350 mg, 1.244 mmol) gave (4-fluorobenzoyl)-L-leucine (300 mg, 1.184 mmol, 95 % yield); ^1H NMR (500 MHz, MeOH- d_4) δ 7.77 - 7.99 (m, 2H), 7.18 (t, $J = 8.56$ Hz, 2H), 4.54 - 4.72 (m, 1H), 1.63 - 1.87 (m, 3H), 0.99 (d, $J = 5.87$ Hz, 3H), 0.97 (d, $J = 5.87$ Hz, 3H)

(S)-N-(1-((Cyanomethyl)amino)-4-methyl-1-oxopentan-2-yl)-4-fluorobenzamide (7n)

General Procedure D starting from (4-fluorobenzoyl)-L-leucine (300 mg, 1.184 mmol) and 2-aminonitrile bisulfate (907 mg, 5.92 mmol) gave (S)-N-(1-((cyanomethyl)amino)-4-methyl-1-

oxopentan-2-yl)-4-fluorobenzamide (233 mg, 0.800 mmol, 67.5 % yield). ¹H NMR (500 MHz, MeOH-d₄) δ 7.88 - 7.95 (m, 2H), 7.13 - 7.22 (m, 2H), 4.64 (dd, *J* = 4.89, 9.78 Hz, 1H), 4.12 - 4.22 (m, 2H), 1.63 - 1.82 (m, 3H), 0.98 (d, *J* = 6.36 Hz, 3H), 0.95 (d, *J* = 6.36 Hz, 3H); ¹³C NMR (126 MHz, MeOH-d₄) δ 175.5, 169.2, 167.4, 165.4, 131.4, 117.7, 116.4, 53.7, 41.7, 28.2, 26.2, 23.5, 22.0; MS (ESI+) *m/z*: 314.1 [M+Na]⁺

Methyl (S)-3-cyclohexyl-2-(4-fluorobenzamido)propanoate (5o)

General Procedure B starting from methyl (S)-2-amino-3-cyclohexylpropanoate, HCl (150 mg, 0.677 mmol) and 4-fluorobenzoic acid (104 mg, 0.744 mmol) gave methyl (S)-3-cyclohexyl-2-(4-fluorobenzamido)propanoate (200 mg, 0.651 mmol, 96 % yield). ¹H NMR (500 MHz, MeOH-d₄) δ 7.91 (dd, *J* = 5.38, 8.80 Hz, 2H), 7.20 (t, *J* = 8.56 Hz, 2H), 4.69 (dd, *J* = 6.11, 9.05 Hz, 1H), 3.74 (s, 3H), 1.84 (d, *J* = 12.72 Hz, 1H), 1.71 - 1.79 (m, 5H), 1.62 - 1.69 (m, 1H), 1.43 (dt, *J* = 3.67, 6.97 Hz, 1H), 1.38 (dd, *J* = 4.16, 6.60 Hz, 1H), 1.26 - 1.34 (m, 1H), 1.17 - 1.23 (m, 1H), 0.89 - 1.08 (m, 2H)

(S)-3-Cyclohexyl-2-(4-fluorobenzamido)propanoic acid (6o)

General Procedure C starting from methyl (S)-3-cyclohexyl-2-(4-fluorobenzamido)propanoate (140 mg, 0.455 mmol) gave (S)-3-cyclohexyl-2-(4-fluorobenzamido)propanoic acid (133 mg, 0.453 mmol, 100 % yield); ¹H NMR (500 MHz, DMSO-d₆) δ 8.59 (d, *J* = 7.83 Hz, 1H), 7.95 (dd, *J* = 5.62, 8.07 Hz, 2H), 7.30 (t, *J* = 8.80 Hz, 2H), 4.38 - 4.51 (m, 1H), 1.69 - 1.77 (m, 2H), 1.60 - 1.69 (m, 4H), 1.59 (br. s., 1H), 1.33 - 1.42 (m, 1H), 1.07 - 1.23 (m, 4H), 0.95 (d, *J* = 10.76 Hz, 1H), 0.85 (d, *J* = 9.78 Hz, 1H)

(S)-N-(1-((Cyanomethyl)amino)-3-cyclohexyl-1-oxopropan-2-yl)-4-fluorobenzamide (7o)

General Procedure D starting from (S)-3-cyclohexyl-2-(4-fluorobenzamido)propanoic acid (50 mg, 0.170 mmol), and 2-aminonitrile bisulfate (104 mg, 0.682 mmol) gave (S)-N-(1-((cyanomethyl)amino)-3-cyclohexyl-1-oxopropan-2-yl)-4-fluorobenzamide (41 mg, 0.124 mmol, 72.6 % yield); ¹H NMR (500 MHz, MeOH-d₄) δ 7.88 - 7.98 (m, 2H), 7.16 - 7.26 (m, 2H), 4.65 (dd, *J* = 5.87, 9.29 Hz, 1H), 4.12 - 4.23 (m, 2H), 1.84 (d, *J* = 12.72 Hz, 1H), 1.70 - 1.81 (m, 5H), 1.62 - 1.70 (m, 1H), 1.42 (dd, *J* = 5.38, 7.83 Hz, 1H), 1.24 - 1.36 (m, 2H), 1.17 - 1.22 (m, 1H), 0.85 - 1.08 (m, 2H); ¹³C NMR (126 MHz, MeOH-d₄) δ 175.6, 169.3, 167.5, 165.5, 131.4, 131.3, 117.6, 116.6, 116.4, 53.1, 40.3, 35.8, 34.9, 33.5, 28.2, 27.7, 27.5, 27.3; MS (ESI+) *m/z*: 354.1588 [M+Na]⁺

Methyl 2-amino-2-cyclohexylacetate (4e)

General Procedure A starting from 2-amino-2-cyclohexylacetic acid (500 mg, 3.18 mmol) gave methyl 2-amino-2-cyclohexylacetate (525 mg, 3.07 mmol, 96 % yield); ¹H NMR (400 MHz, MeOH-d₄) δ 3.88 (d, *J* = 4.70 Hz, 1H), 3.84 (s, 3H), 1.93 (ddd, *J* = 3.91, 7.92, 11.64 Hz, 1H), 1.74 - 1.88 (m, 3H), 1.69 (t, *J* = 12.72 Hz, 2H), 1.07 - 1.35 (m, 5H)

Methyl (S)-2-cyclohexyl-2-(4-fluorobenzamido)acetate (5p)

General Procedure B starting from methyl (S)-2-amino-2-cyclohexylacetate (100 mg, 0.584 mmol) and 4-fluorobenzoic acid (82 mg, 0.584 mmol) gave methyl (S)-2-cyclohexyl-2-(4-fluorobenzamido)acetate (135 mg, 0.460 mmol, 79 % yield); ¹H NMR (400 MHz, MeOH-d₄) δ 7.89 (dd, *J* = 5.28, 8.80 Hz, 2H), 7.19 (t, *J* = 8.80 Hz, 2H), 4.47 (d, *J* = 7.43 Hz, 1H), 3.70 - 3.77

(m, 3H), 1.92 (dtd, $J = 3.91, 7.68, 11.25$ Hz, 1H), 1.73 - 1.83 (m, 3H), 1.68 (br. s., 2H), 1.27 - 1.38 (m, 3H), 1.07 - 1.20 (m, 2H)

(S)-2-Cyclohexyl-2-(4-fluorobenzamido)acetic acid (6p)

General Procedure C starting from methyl (S)-2-cyclohexyl-2-(4-fluorobenzamido)acetate (100 mg, 0.341 mmol) gave (S)-2-cyclohexyl-2-(4-fluorobenzamido)acetic acid (93 mg, 0.333 mmol, 98 % yield); ^1H NMR (500 MHz, MeOH- d_4) δ 7.90 (dd, $J = 5.38, 8.80$ Hz, 2H), 7.19 (t, $J = 8.80$ Hz, 2H), 4.48 (d, $J = 6.85$ Hz, 1H), 1.89 - 1.98 (m, 1H), 1.79 (br. d, $J = 9.80$ Hz, 4H), 1.68 (br. d, $J = 12.20$ Hz, 1H), 1.26 - 1.35 (m, 2H), 1.14 - 1.22 (m, 3H)

(S)-N-(2-((Cyanomethyl)amino)-1-cyclohexyl-2-oxoethyl)-4-fluorobenzamide (7p)

General Procedure D starting from (S)-2-cyclohexyl-2-(4-fluorobenzamido)acetic acid (100 mg, 0.358 mmol) and 2 aminoacetonitrile bisulfate (274 mg, 1.790 mmol) gave (S)-N-(2-((cyanomethyl)amino)-1-cyclohexyl-2-oxoethyl)-4-fluorobenzamide (50 mg, 0.158 mmol, 44.0 % yield); ^1H NMR (500 MHz, MeOH- d_4) δ 7.88 - 7.92 (m, 2H), 7.17 - 7.22 (m, 2H), 4.34 (d, $J = 8.31$ Hz, 1H), 4.22 (d, $J = 17.61$ Hz, 1H), 4.13 (d, $J = 17.61$ Hz, 1H), 1.84 - 1.92 (m, 1H), 1.75 - 1.83 (m, 3H), 1.63 - 1.74 (m, 2H), 1.18 - 1.28 (m, 3H), 1.06 - 1.18 (m, 2H); ^{13}C NMR (126 MHz, MeOH- d_4) δ 157.4, 156.9, 131.4, 131.3, 116.6, 116.4, 60.4, 41.3, 31.0, 30.6, 28.0, 27.4, 27.1; MS (ESI+) m/z : 340.1 $[\text{M}+\text{Na}]^+$

Methyl (S)-5-((tert-butoxycarbonyl)amino)-2-(4-fluorobenzamido)pentanoate (9)

General Procedure A starting from methyl (S)-2-amino-5-((tert-butoxycarbonyl)amino)pentanoate, HCl (250 mg, 0.884 mmol) and 4-fluorobenzoic acid (136

mg, 0.973 mmol) gave methyl (S)-5-((tert-butoxycarbonyl)amino)-2-(4-fluorobenzamido)pentanoate (320 mg, 0.869 mmol, 98 % yield); ¹H NMR (500 MHz, DMSO-d₆) δ 8.71 (d, *J* = 7.34 Hz, 1H), 7.94 (dd, *J* = 5.62, 8.56 Hz, 2H), 7.30 (t, *J* = 8.80 Hz, 2H), 6.76 (br. s., 1H), 4.37 (dd, *J* = 7.34, 14.67 Hz, 1H), 3.63 (s, 3H), 2.79 - 2.95 (m, 2H), 1.66 - 1.83 (m, 2H), 1.35 - 1.43 (m, 3H), 1.33 (s, 9H), 1.25 - 1.32 (m, 1H)

Methyl (4-fluorobenzoyl)-L-lysinate (10)

In a dry round bottom flask, methyl N₆-(tert-butoxycarbonyl)-N₂-(4-fluorobenzoyl)-L-lysinate (630 mg, 1.647 mmol) was dissolved in a 6M HCl:dioxane solution and stirred at room temperature for 4h. The solvent was removed in vacuo and the resulting crude residue was purified by flash chromatography (10% MeOH in DCM + 1% triethylamine) to afford methyl (4-fluorobenzoyl)-L-lysinate (460 mg, 1.629 mmol, 99 % yield); ¹H NMR (500 MHz, MeOH-d₄) δ 7.95 (dd, *J* = 5.38, 7.83 Hz, 2H), 7.20 (t, *J* = 8.07 Hz, 2H), 4.53 - 4.66 (m, 1H), 3.65 (s, 3H), 2.95 (t, *J* = 6.60 Hz, 2H), 2.85 (s, 2H), 1.96 - 2.06 (m, 1H), 1.89 - 1.96 (m, 1H), 1.68 - 1.81 (m, 2H), 1.45 - 1.66 (m, 2H)

Methyl N₂-(4-fluorobenzoyl)-N₆,N₆-dimethyl-L-lysinate (11)

In a dry round bottom flask under nitrogen, methyl (4-fluorobenzoyl)-L-lysinate (200 mg, 0.708 mmol) was dissolved into MeOH (2 ml). Formalin (37%) (0.527 ml, 7.08 mmol) and glacial acetic acid (0.081 ml, 1.417 mmol) were then added, followed by the addition of sodium triacetoxyborohydride (601 mg, 2.83 mmol). The reaction was left to stir at room temperature overnight. The solvent was removed in vacuo and the resulting crude residue was purified by flash chromatography (10% MeOH in DCM + 1% triethylamine) to afford methyl N₂-(4-

fluorobenzoyl)-N6,N6-dimethyl-L-lysinate (70 mg, 0.226 mmol, 31.8 % yield); ¹H NMR (500 MHz, MeOH-d₄) δ 7.92 (dd, *J* = 5.62, 8.56 Hz, 2H), 7.20 (t, *J* = 8.56 Hz, 2H), 4.59 (dd, *J* = 5.14, 9.54 Hz, 1H), 3.74 (s, 3H), 2.57 (t, *J* = 7.58 Hz, 2H), 2.42 (s, 6H), 1.93 - 2.02 (m, 1H), 1.81 - 1.93 (m, 1H), 1.56 - 1.70 (m, 2H), 1.39 - 1.56 (m, 2H); ¹³C NMR (126 MHz, MeOH-d₄) δ 174.3, 169.4, 167.5, 165.5, 131.4, 131.3, 116.6, 116.4, 59.9, 54.4, 52.9, 44.9, 32.1, 27.0, 24.9

(S)-N-(1-((Cyanomethyl)amino)-6-(dimethylamino)-1-oxohexan-2-yl)-4-fluorobenzamide (13)

General Procedure C starting from methyl N2-(4-fluorobenzoyl)-N6,N6-dimethyl-L-lysinate (60 mg, 0.193 mmol) gave N2-(4-fluorobenzoyl)-N6,N6-dimethyl-L-lysine (57.3 mg, 0.193 mmol). The crude residue was carried directly into general procedure D to afford (S)-N-(1-((cyanomethyl)amino)-6-(dimethylamino)-1-oxohexan-2-yl)-4-fluorobenzamide (6.4 mg, 0.019 mmol, 11.30 % yield); ¹H NMR (400 MHz, MeOH-d₄) δ 7.95 (dd, *J* = 5.48, 8.61 Hz, 2H), 7.20 (t, *J* = 8.61 Hz, 2H), 4.56 (dd, *J* = 5.48, 9.00 Hz, 1H), 4.17 (d, *J* = 3.52 Hz, 2H), 2.90 (t, *J* = 8.02 Hz, 2H), 2.69 (s, 6H), 1.94 - 2.03 (m, 1H), 1.87 (dd, *J* = 5.28, 9.19 Hz, 1H), 1.66 - 1.81 (m, 2H), 1.39 - 1.57 (m, 2H); MS (ESI+) *m/z*: 335.2 [M+Na]⁺

Ethyl (S)-2-(4-fluorobenzamido)-4-methylpent-4-enoate (21)

General Procedure B starting from dehydroleucine (D)-(+)-camphorsulfonic acid salt (1 g, 6.36 mmol) and 4-fluorobenzoic acid (0.891 g, 6.36 mmol) gave ethyl (S)-2-(4-fluorobenzamido)-4-methylpent-4-enoate (600 mg, 2.148 mmol, 33.8 % yield); ¹H NMR (500 MHz, CDCl₃) δ 7.77 (dd, *J* = 5.38, 8.31 Hz, 2H), 7.08 (t, *J* = 8.56 Hz, 2H), 6.62 (d, *J* = 6.85 Hz, 1H), 4.87 (br. s., 1H),

4.82 - 4.86 (m, 1H), 4.79 (br. s, 1H), 4.22 (q, $J = 6.85$ Hz, 2H), 2.66 (dd, $J = 5.62, 13.94$ Hz, 1H), 2.52 (dd, $J = 8.31, 13.69$ Hz, 1H), 1.78 (s, 3H), 1.29 (t, $J = 7.34$ Hz, 3H)

(S)-N-(1-((Cyanomethyl)amino)-4-methyl-1-oxopent-4-en-2-yl)-4-fluorobenzamide (25)

General Procedure C starting from ethyl (S)-2-(4-fluorobenzamido)-4-methylpent-4-enoate (100 mg, 0.358 mmol) gave (S)-2-(4-fluorobenzamido)-4-methylpent-4-enoic acid (60 mg, 0.239 mmol). Product was carried directly into general procedure D to afford (S)-N-(1-((cyanomethyl)amino)-4-methyl-1-oxopent-4-en-2-yl)-4-fluorobenzamide (22 mg, 0.076 mmol, 31.8 % yield); ^1H NMR (500 MHz, MeOH- d_4) δ 7.89 (dd, $J = 5.38, 8.31$ Hz, 2H), 7.18 (t, $J = 8.56$ Hz, 2H), 4.84 (s, 1H), 4.83 (s, 1H), 4.76 (dd, $J = 5.14, 10.03$ Hz, 1H), 4.17 (s, 2H), 2.65 (dd, $J = 4.89, 14.00$ Hz, 1H), 2.52 (dd, $J = 10.03, 13.94$ Hz, 1H), 1.79 (s, 3H); ^{13}C NMR (126 MHz, MeOH- d_4) δ 174.6, 169.3, 166.5, 142.6, 131.4, 117.6, 116.5, 114.6, 53.4, 40.9, 28.2, 22.2; MS (ESI+) m/z : 290.1 [M+Na] $^+$

Ethyl (S)-4-fluoro-2-(4-fluorobenzamido)-4-methylpentanoate (22)

Iron (III) sulfate monohydrate (344 mg, 0.859 mmol) was stirred in H₂O (15 mL) until complete dissolution. The solution was cooled to 0 °C and degassed for 10 min. SELECTFLUOR (609 mg, 1.719 mmol) and ACN (5 mL) were added to the reaction mixture. A solution of ethyl (S)-2-(4-fluorobenzamido)-4-methylpent-4-enoate (240 mg, 0.859 mmol) in ACN (5 mL) was transferred into the reaction mixture, and sodium borohydride (104 mg, 2.75 mmol) was added at 0 °C. After 2 min, the reaction was treated with an additional portion of sodium borohydride (104 mg, 2.75 mmol). The resulting mixture was stirred for 30 min at 0 °C before being quenched by addition of 30% aq. NH₄OH (~5mL). The mixture was extracted with DCM, the organic layer

was dried over MgSO₄, and concentrated under reduced pressure. Flash chromatography (15% EtOAc:Hex isocratic) gave ethyl (S)-4-fluoro-2-(4-fluorobenzamido)-4-methylpentanoate (70 mg, 0.234 mmol, 27.2 % yield); ¹H NMR (500 MHz, CDCl₃) δ 7.79 (dd, *J* = 5.62, 8.07 Hz, 4H), 7.08 (t, *J* = 8.56 Hz, 4H), 6.90 (br. s., 1H), 4.80 (q, *J* = 6.85 Hz, 1H), 4.21 (q, *J* = 6.85 Hz, 2H), 2.12 - 2.31 (m, 2H), 1.47 (d, *J* = 9.29 Hz, 3H), 1.42 (d, *J* = 8.80 Hz, 3H), 1.28 (t, *J* = 7.09 Hz, 3H); ¹⁹F NMR (500 MHz, CDCl₃) δ -107.85 (s), -135.74 (s)

(S)-N-(1-((Cyanomethyl)amino)-4-fluoro-4-methyl-1-oxopentan-2-yl)-4-fluorobenzamide (24)

General Procedure C starting from ethyl (S)-4-fluoro-2-(4-fluorobenzamido)-4-methylpentanoate (70 mg, 0.234 mmol) gave (S)-4-fluoro-2-(4-fluorobenzamido)-4-methylpentanoic acid (63.4 mg, 0.234 mmol) (**23**). Product was carried directly into General Procedure D to afford (S)-N-(1-((cyanomethyl)amino)-4-fluoro-4-methyl-1-oxopentan-2-yl)-4-fluorobenzamide (13 mg, 0.042 mmol, 18.10 % yield); ¹H NMR (500 MHz, MeOH-d₄) δ 7.91 (dd, *J* = 5.38, 8.31 Hz, 2H), 7.20 (t, *J* = 8.56 Hz, 2H), 4.81 (dd, *J* = 3.91, 9.78 Hz, 1H), 4.16 (s, 2H), 2.13 - 2.35 (m, 2H), 1.44 (d, *J* = 6.85 Hz, 3H), 1.40 (d, *J* = 6.85 Hz, 3H); ¹³C NMR (126 MHz, MeOH-d₄) δ 174.7, 169.0, 166.5, 131.4, 117.5, 116.5, 95.8, 52.1, 42.9, 28.3, 27.8, 26.9; ¹⁹F NMR (500 MHz, MeOH-d₄) δ -110.21 (1F), 138.99 (1F); MS (ESI+) *m/z*: 310.1 [M+H]⁺

Methyl (S)-2-(4-fluorobenzamido)-4,4-dimethylpentanoate (5q)

General Procedure B starting from methyl (S)-2-amino-4,4-dimethylpentanoate (30 mg, 0.188 mmol) and 4-fluorobenzoic acid (26.4 mg, 0.188 mmol) gave methyl (S)-2-(4-fluorobenzamido)-4,4-dimethylpentanoate (45 mg, 0.160 mmol, 85 % yield); ¹H NMR (500 MHz, CDCl₃) δ 7.77

(dd, $J = 5.38, 8.31$ Hz, 2H), 7.06 (t, $J = 8.56$ Hz, 2H), 4.84 (dt, $J = 3.40, 8.80$ Hz, 1H), 3.73 (s, 3H), 1.83 (dd, $J = 3.18, 14.43$ Hz, 1H), 1.61 (dd, $J = 9.05, 14.43$ Hz, 1H), 0.98 (s, 9H)

(S)-N-(1-((Cyanomethyl)amino)-4,4-dimethyl-1-oxopentan-2-yl)-4-fluorobenzamide (7q)

General Procedure C starting from methyl (S)-2-(4-fluorobenzamido)-4,4-dimethylpentanoate (45 mg, 0.160 mmol) gave (S)-2-(4-fluorobenzamido)-4,4-dimethylpentanoic acid (42 mg, 0.157 mmol) (**6q**). Product was carried directly into General Procedure D to afford (S)-N-(1-((cyanomethyl)amino)-4,4-dimethyl-1-oxopentan-2-yl)-4-fluorobenzamide (25 mg, 0.082 mmol, 52.1 % yield); ^1H NMR (500 MHz, MeOH- d_4) δ 7.88 - 7.94 (m, 2H), 7.15 - 7.23 (m, 2H), 4.68 (dd, $J = 2.93, 8.80$ Hz, 1H), 4.15 (s, 2H), 1.75 - 1.89 (m, 2H), 1.00 (s, 9H); ^{13}C NMR (126 MHz, MeOH- d_4) δ 175.7, 168.9, 166.5, 131.6, 131.3, 116.7, 116.4, 52.9, 45.9, 31.6, 30.2, 28.3; MS (ESI+) m/z : 306.2 [M+H] $^+$

(S)-2-Amino-3-cyclopropylpropanoic acid (4h)

General procedure A from (S)-2-amino-3-cyclopropylpropanoic acid (250 mg, 1.936 mmol) gave methyl (S)-2-amino-3-cyclopropylpropanoate, HCl (348 mg, 1.936 mmol, 100 % yield); ^1H NMR (500 MHz, MeOH- d_4) δ 4.13 (t, $J = 6.10$ Hz, 1H), 3.84 (s, 3H), 1.87 - 2.01 (m, 1H), 1.74 - 1.84 (m, 1H), 0.77 - 0.93 (m, 1H), 0.53 - 0.63 (m, 2H), 0.15 - 0.25 (m, 2H)

Methyl (S)-3-cyclopropyl-2-(4-fluorobenzamido)propanoate (5r)

General procedure B starting from 4-fluorobenzoic acid (326 mg, 2.325 mmol) and methyl (S)-2-amino-3-cyclopropylpropanoate, HCl (348 mg, 1.937 mmol) gave methyl (S)-3-cyclopropyl-2-(4-fluorobenzamido)propanoate (150 mg, 0.565 mmol, 29.2 % yield); ^1H NMR (500 MHz,

MeOH-d₄) δ 7.91 (dd, $J = 5.62, 8.56$ Hz, 2H), 7.19 (t, $J = 8.56$ Hz, 2H), 4.67 (dd, $J = 5.62, 8.56$ Hz, 1H), 3.74 (s, 3H), 1.84 (td, $J = 7.46, 14.43$ Hz, 1H), 1.69 - 1.76 (m, 1H), 0.81 - 0.89 (m, 1H), 0.45 - 0.53 (m, 2H), 0.07 - 0.20 (m, 2H)

(S)-N-(1-((Cyanomethyl)amino)-3-cyclopropyl-1-oxopropan-2-yl)-4-fluorobenzamide (7r)

General Procedure C starting from (S)-3-cyclopropyl-2-(4-fluorobenzamido)propanoate (150 mg, 0.565 mmol) gave (S)-3-cyclopropyl-2-(4-fluorobenzamido)propanoic acid (140 mg, 0.557 mmol) (**6r**). Product was carried directly into General Procedure D to afford (S)-N-(1-((cyanomethyl)amino)-3-cyclopropyl-1-oxopropan-2-yl)-4-fluorobenzamide (97 mg, 0.335 mmol, 60.2 % yield); ¹H NMR (400 MHz, MeOH-d₄) δ 7.89 - 7.96 (m, 2H), 7.18 (t, $J = 8.61$ Hz, 2H), 4.60 (t, $J = 7.43$ Hz, 1H), 4.22 (d, $J = 16.82$ Hz, 1H), 4.15 (d, $J = 17.22$ Hz, 1H), 1.83 (d, $J = 1.00$ Hz, 1H), 1.60 - 1.75 (m, 1H), 0.72 - 0.89 (m, 1H), 0.44 - 0.59 (m, 2H), 0.06 - 0.25 (m, 2H); MS (ESI+) m/z : 290.1 [M+H]⁺

Potassium ((S)-2,2,2-trifluoro-1-(4-fluorophenyl)ethyl)-L-leucinate (16)

In a dry roundbottom flask, methyl L-leucinate, HCl (520 mg, 2.86 mmol) and potassium carbonate (899 mg, 6.51 mmol) were dissolved in MeOH (8 ml). 2,2,2-trifluoro-1-(4-fluorophenyl)ethan-1-one (0.365 ml, 2.60 mmol) was then added and the reaction was heated to 50°C overnight. The solution was cooled to room temperature, filtered through a plug of Celite and diluted with anhydrous acetonitrile (80mL). The solution was then cooled to -40°C. In a separate flask under inert atmosphere, a solution of freshly formed Zn(BH₄)₂ (495 mg, 5.21mmol) in DME (10mL) was cooled to -40, filtered through run through a plug of celite into an addition funnel, washed through with 10-20 mL of acetonitrile and slowly added to the

reaction mixture. The solution was placed left to stir under nitrogen at -40°C for 5 hours. 5-10 mL of acetone was then added and the reaction was allowed to slowly warm to room temperature over 1 hour. 1N HCl was slowly added to the cloudy solution until the solution was quenched and became clear. The organic solvents were removed in vacuo and the resulting aqueous solution was extracted with EtOAc 3x. The combined organic layers were wash with brine 3x, dried over MgSO_4 , and concentrated to afford potassium ((S)-2,2,2-trifluoro-1-(4-fluorophenyl)ethyl)-L-leucinate (0.859 g, 2.488 mmol, 87 % yield) as a white solid. dr = 11:1 (S,S) as determined by ^{19}F NMR. ^1H NMR (500 MHz, MeOH-d_4) δ 7.46 (dd, $J = 5.38, 8.31$ Hz, 2H), 7.03 - 7.13 (m, 2H), 4.25 (d, $J = 7.34$ Hz, 1H), 4.22 (d, $J = 7.34$ Hz, 1H), 3.46 (t, $J = 7.09$ Hz, 1H), 1.86 - 1.96 (m, 1H), 1.46 - 1.52 (m, 2H), 0.94 (d, $J = 6.85$ Hz, 3H), 0.92 (d, $J = 6.85$ Hz, 3H); ^{13}C NMR (126 MHz, MeOH-d_4) δ 178.4, 173.1, 165.5, 163.5, 132.6, 131.8, 131.7, 116.6, 116.4, 64.0, 63.7, 61.6, 60.1, 43.8, 26.0, 23.5, 23.4, 22.5, 21.0, 14.6; ^{19}F NMR (470 MHz, MeOH-d_4) δ -75.00; -114.7

((R)-2,2,2-Trifluoro-1-(4-fluorophenyl)ethyl)-L-leucine (17)

In a dry rb flask under nitrogen: methyl L-leucinate, HCl (150 mg, 0.826 mmol) and 2,2,2-trifluoro-1-(4-fluorophenyl)ethan-1-one (159 mg, 0.826 mmol) were dissolved into anhydrous MeOH (10 mL). Potassium carbonate (228 mg, 1.651 mmol) was added and the reaction was heated to reflux overnight. Solvent was removed in vacuo and the residue was resuspended in anhydrous THF (5 mL). The suspension was then added to dry roundbottom flask charged with SODIUM BOROHYDRIDE (250 mg, 6.61 mmol). 5 mL of water:THF (v/v:2/8) was added via syringe pump over 3 hours. 1N HCl was added and solution was extracted with EtOAc 3x. The combined organic layer was washed with saturated sodium bicarbonate (aq) and brine, dried over

MgSO₄ and concentrated to afford ((R)-2,2,2-trifluoro-1-(4-fluorophenyl)ethyl)-L-leucine (236 mg, 0.768 mmol, 93 % yield). dr = 12:1 (R,S) as determined by ¹⁹F NMR. ¹H NMR (500 MHz, MeOH-d₄) δ 7.50 (dd, *J* = 5.87, 8.31 Hz, 2H), 7.05 - 7.21 (m, 2H), 4.32 (q, *J* = 7.34 Hz, 1H), 2.91 (dd, *J* = 5.38, 8.80 Hz, 1H), 1.79 - 1.92 (m, 1H), 1.38 - 1.54 (m, 2H), 0.92 - 1.01 (m, 2H), 0.89 (d, *J* = 6.85 Hz, 3H), 0.75 (d, *J* = 6.36 Hz, 3H); ¹³C NMR (126 MHz, MeOH-d₄) δ 178.5, 165.9, 163.9, 132.7, 132.6, 116.6, 116.5, 63.7, 63.5, 62.5, 57.8, 44.1, 25.9, 23.6, 22.3; ¹⁹F NMR (470 MHz, MeOH-d₄) δ -76.43, -114.64

(S)-N-(Cyanomethyl)-4-methyl-2-(((R)-2,2,2-trifluoro-1-(4-fluorophenyl)ethyl)amino)pentanamide (19)

General Procedure D starting from ((R)-2,2,2-trifluoro-1-(4-fluorophenyl)ethyl)-L-leucine (50 mg, 0.163 mmol) and 2-aminoacetonitrile bisulfate (37.4 mg, 0.244 mmol) gave (S)-N-(cyanomethyl)-4-methyl-2-(((R)-2,2,2-trifluoro-1-(4-fluorophenyl)ethyl)amino)pentanamide (25 mg, 0.072 mmol, 44.5 % yield). dr= 10:1 (R,S) as shown by ¹⁹F NMR; ¹H NMR (400 MHz, MeOH-d₄) δ 7.50 (dd, *J* = 5.48, 8.22 Hz, 2H), 7.15 (t, *J* = 8.61 Hz, 2H), 4.11 - 4.21 (m, 3H), 2.97 (dd, *J* = 5.09, 9.00 Hz, 1H), 1.67 - 1.78 (m, 1H), 1.43 - 1.53 (m, 1H), 1.30 - 1.39 (m, 1H), 0.87 (d, *J* = 6.65 Hz, 3H), 0.73 (d, *J* = 6.65 Hz, 3H); ¹³C NMR (101 MHz, MeOH-d₄) δ 177.4, 166.1, 163.6, 132.5, 131.1, 128.0, 125.2, 117.7, 116.5, 63.6, 59.1, 44.1, 27.9, 25.8, 23.6, 22.2; ¹⁹F NMR (470 MHz, MeOH-d₄) δ -76.13; -114.56; MS (ESI+) *m/z*: 346.15 [M+H]⁺

(S)-N-(Cyanomethyl)-4-methyl-2-(((S)-2,2,2-trifluoro-1-(4-fluorophenyl)ethyl)amino)pentanamide (18a)

General Procedure D starting from ((S)-2,2,2-trifluoro-1-(4-fluorophenyl)ethyl)-L-leucine (100 mg, 0.325 mmol) and 2-aminoacetonitrile bisulfate (59.8 mg, 0.391 mmol) gave (S)-N-(cyanomethyl)-4-methyl-2-(((S)-2,2,2-trifluoro-1-(4-fluorophenyl)ethyl)amino)pentanamide (100 mg, 0.290 mmol, 89 % yield). dr= 7:1 (S,S) as shown by ^{19}F NMR; ^1H NMR (500 MHz, MeOH- d_4) δ 7.45 (dd, $J = 5.38, 8.31$ Hz, 2H), 7.07 - 7.14 (m, 2H), 4.13 - 4.25 (m, 1H), 4.04 (d, $J = 17.12$ Hz, 1H), 3.99 (d, $J = 17.61$ Hz, 1H), 1.74 - 1.87 (m, 1H), 1.47 - 1.54 (m, 1H), 1.33 - 1.47 (m, 1H), 0.94 (dd, $J = 3.18, 6.60$ Hz, 6H); ^{13}C NMR (126 MHz, MeOH- d_4) δ 177.6, 165.5, 163.6, 132.4, 131.9, 117.5, 116.5, 64.1, 61.0, 44.1, 39.0, 27.9, 26.0, 23.4, 22.6; ^{19}F NMR (470 MHz, MeOH- d_4) δ -75.24, -114.76; MS (ESI+) m/z : 346.1537 [M+H] $^+$

(S)-N-(1-((1-Cyanocyclopropyl)amino)-4-methyl-1-oxopentan-2-yl)-4-fluorobenzamide (26)

General Procedure D starting with (4-fluorobenzoyl)-L-leucine (250 mg, 0.987 mmol) and 1-aminocyclopropane-1-carbonitrile, HCl (140 mg, 1.184 mmol) gave (S)-N-(1-((1-cyanocyclopropyl)amino)-4-methyl-1-oxopentan-2-yl)-4-fluorobenzamide (229 mg, 0.721 mmol, 73 % yield); ^1H NMR (500 MHz, MeOH- d_4) δ 7.90 (dd, $J = 5.38, 8.31$ Hz, 2H), 7.17 (t, $J = 8.80$ Hz, 2H), 4.44 - 4.60 (m, 1H), 1.67 - 1.82 (m, 2H), 1.57 - 1.66 (m, 1H), 1.49 (dd, $J = 5.38, 7.83$ Hz, 2H), 1.24 (dd, $J = 6.36, 8.31$ Hz, 2H), 0.98 (d, $J = 6.36$ Hz, 3H), 0.95 (d, $J = 6.36$ Hz, 3H); ^{13}C NMR (126 MHz, MeOH- d_4) δ 176.4, 169.3, 167.4, 165.4, 131.3, 121.4, 116.4, 53.7, 41.7, 26.2, 23.5, 22.1, 21.5, 17.2, 16.9; MS (ESI+) m/z : 318.1 [M+H] $^+$

(S)-N-(1-Cyanocyclopropyl)-4-methyl-2-(((S)-2,2,2-trifluoro-1-(4-fluorophenyl)ethyl)amino) pentanamide (18b)

General Procedure D starting with ((S)-2,2,2-trifluoro-1-(4-fluorophenyl)ethyl)-L-leucine (100 mg, 0.325 mmol) and 1-aminocyclopropane-1-carbonitrile, HCl (46.3 mg, 0.391 mmol) gave (S)-N-(1-cyanocyclopropyl)-4-methyl-2-(((S)-2,2,2-trifluoro-1-(4-fluorophenyl)ethyl)amino) pentanamide (100 mg, 0.269 mmol, 83 % yield). dr= 11:1 (S,S) as shown by ¹⁹F NMR; ¹H NMR (500 MHz, MeOD) δ 7.43 (dd, *J* = 5.38, 8.31 Hz, 2H), 7.11 (t, *J* = 8.80 Hz, 2H), 4.10 - 4.21 (m, 1H), 3.28 (dd, *J* = 6.36, 8.31 Hz, 1H), 1.79 (td, *J* = 6.85, 13.69 Hz, 1H), 1.44 - 1.50 (m, 1H), 1.33 - 1.42 (m, 3H), 0.99 - 1.04 (m, 1H), 0.93 (d, *J* = 6.85 Hz, 6H); ¹³C NMR (126 MHz, DMSO-*d*₆) δ 178.7, 165.6, 163.6, 131.9, 121.2, 116.7, 116.6, 64.3, 61.3, 44.2, 26.0, 23.4, 22.6, 21.1, 16.9, 16.8; ¹⁹F NMR (470 MHz, MeOH-*d*₄) δ -76.29, -115.63; MS (ESI+) *m/z*: 372.1692 [M+H]⁺

Ethyl (3-(tert-butyl)-1-methyl-1H-pyrazole-5-carbonyl)-L-leucinate

General Procedure B from ethyl L-leucinate, HCl (200 mg, 1.022 mmol) and 3-(tert-butyl)-1-methyl-1H-pyrazole-5-carboxylic acid (186 mg, 1.022 mmol) gave ethyl (3-(tert-butyl)-1-methyl-1H-pyrazole-5-carbonyl)-L-leucinate (323 mg, 0.999 mmol, 98 % yield); ¹H NMR (500 MHz, CDCl₃) δ 6.33 (d, *J* = 8.31 Hz, 1H), 4.75 (d, *J* = 4.89 Hz, 1H), 4.23 (q, *J* = 7.34 Hz, 2H), 4.10 (s, 3H), 1.71 - 1.76 (m, 1H), 1.60 (br. s., 1H), 1.43 - 1.50 (m, 1H), 1.26 - 1.34 (m, 12H), 0.99 (t, *J* = 5.38 Hz, 6H)

(3-(Tert-butyl)-1-methyl-1H-pyrazole-5-carbonyl)-L-leucine

General Procedure C from ethyl (3-(tert-butyl)-1-methyl-1H-pyrazole-5-carbonyl)-L-leucinate (395 mg, 1.221 mmol) gave (3-(tert-butyl)-1-methyl-1H-pyrazole-5-carbonyl)-L-leucine (307

mg, 1.039 mmol, 85 % yield); ^1H NMR (500 MHz, MeOH- d_4) δ 6.81 (s, 1H), 4.60 (dd, J = 4.65, 10.94 Hz, 1H), 4.06 (s, 3H), 1.67 - 1.82 (m, 3H), 1.33 (s, 9H), 1.00 (d, J = 5.93 Hz, 3H), 0.97 (d, J = 5.87 Hz, 3H)

(S)-3-(Tert-butyl)-N-(1-((cyanomethyl)amino)-4-methyl-1-oxopentan-2-yl)-1-methyl-1H-pyrazole-5-carboxamide (257084)

General procedure D from (3-(Tert-butyl)-1-methyl-1H-pyrazole-5-carbonyl)-L-leucine (83 mg, 0.281 mmol) and 2-aminoacetonitrile bisulfate (51.6 mg, 0.337 mmol) gave (S)-3-(tert-butyl)-N-(1-((cyanomethyl)amino)-4-methyl-1-oxopentan-2-yl)-1-methyl-1H-pyrazole-5-carboxamide (65.6 mg, 0.197 mmol, 70 % yield); ^1H NMR (400 MHz, MeOH- d_4) δ 6.78 (s, 1H), 4.51 - 4.63 (m, 1H), 4.15 (s, 2H), 4.03 (s, 3H), 1.58 - 1.81 (m, 3H), 1.30 (s, 9H), 0.97 (dd, J = 6.06, 13.11 Hz, 6H); ^{13}C NMR (101 MHz, MeOH- d_4) δ 175.4, 164.1, 161.7, 136.8, 117.6, 105.2, 53.1, 41.5, 33.1, 31.0, 28.2, 26.2; MS (ESI+) m/z : 334.1 [$\text{M}+\text{H}$] $^+$

Ethyl (3-(tert-butyl)benzoyl)-L-leucinate

General Procedure B from ethyl L-leucinate, HCl (100 mg, 0.511 mmol) and 3-(tert-butyl)benzoic acid (91 mg, 0.511 mmol) gave ethyl (3-(tert-butyl)benzoyl)-L-leucinate (102.7 mg, 0.321 mmol, 62.9 % yield); Carried directly to next step without further purification.

(3-(Tert-butyl)-1-methyl-1H-pyrazole-5-carbonyl)-L-leucine

General Procedure C from ethyl (3-(tert-butyl)-1-methyl-1H-pyrazole-5-carbonyl)-L-leucinate (395 mg, 1.221 mmol) gave (3-(tert-butyl)-1-methyl-1H-pyrazole-5-carbonyl)-L-leucine (307 mg, 1.039 mmol, 85 % yield); ^1H NMR (500 MHz, MeOH- d_4) δ 6.81 (s, 1H), 4.60 (dd, J = 4.65,

10.94 Hz, 1H), 4.06 (s, 3H), 1.67 - 1.82 (m, 3H), 1.33 (s, 9H), 1.00 (d, $J = 5.93$ Hz, 3H), 0.97 (d, $J = 5.87$ Hz, 3H)

**(S)-3-(Tert-butyl)-N-(1-((cyanomethyl)amino)-4-methyl-1-oxopentan-2-yl)benzamide
(257101)**

General procedure D from (3-(tert-butyl)benzoyl)-L-leucine (218 mg, 0.748 mmol) and 2-((tetraoxidanyl-16-sulfanylidene)amino)acetonitrile (577 mg, 3.74 mmol) gave (S)-3-(tert-butyl)-N-(1-((cyanomethyl)amino)-4-methyl-1-oxopentan-2-yl)benzamide (25.6 mg, 0.078 mmol, 10.39 % yield); ^1H NMR (500 MHz, MeOH- d_4) δ 7.93 (s, 1H), 7.67 (d, $J = 7.34$ Hz, 1H), 7.60 (d, $J = 7.83$ Hz, 1H), 7.39 (t, $J = 7.83$ Hz, 1H), 4.66 (dd, $J = 4.65, 10.03$ Hz, 1H), 4.16 (d, $J = 6.85$ Hz, 2H), 1.74 - 1.87 (m, 1H), 1.63 - 1.74 (m, 2H), 1.35 (s, 9H), 1.00 (d, $J = 6.36$ Hz, 3H), 0.98 (d, $J = 6.36$ Hz, 3H); ^{13}C NMR (126 MHz, MeOH- d_4) δ 175.6, 171.0, 153.0, 134.9, 130.2, 129.4, 125.9, 125.8, 117.6, 53.7, 41.7, 35.9, 31.8, 28.2, 26.3, 23.6, 22.1; MS (ESI+) m/z : 352.1 $[\text{M}+\text{H}]^+$

(S)-2-(3-(Tert-butyl)-1-methyl-1H-pyrazole-5-carboxamido)-3-(3-hydroxyphenyl)propanoate

General procedure B from methyl L-phenylalaninate hydrochloride (111 mg, 0.515 mmol) and 3-(tert-butyl)-1-methyl-1H-pyrazole-5-carboxylic acid (94 mg, 0.515 mmol) gave methyl (S)-2-(3-(tert-butyl)-1-methyl-1H-pyrazole-5-carboxamido)-3-(3-hydroxyphenyl)propanoate (180 mg, 0.501 mmol, 97 % yield); ^1H NMR (500 MHz, MeOH- d_4) δ 7.08 (t, $J = 7.83$ Hz, 1H), 6.69 - 6.76 (m, 2H), 6.64 (d, $J = 9.78$ Hz, 1H), 6.61 (s, 1H), 4.79 (dd, $J = 4.65, 9.54$ Hz, 1H), 3.92 (s, 3H), 3.25 (dd, $J = 4.65, 13.94$ Hz, 1H), 2.99 (dd, $J = 10.03, 13.94$ Hz, 1H), 1.28 (s, 9H)

(S)-2-(3-(Tert-butyl)-1-methyl-1H-pyrazole-5-carboxamido)-3-(3-hydroxyphenyl)propanoic acid

General Procedure C from (S)-2-(3-(tert-butyl)-1-methyl-1H-pyrazole-5-carboxamido)-3-(3-hydroxyphenyl)propanoate (180 mg, 0.501 mmol) gave (S)-2-(3-(tert-butyl)-1-methyl-1H-pyrazole-5-carboxamido)-3-(3-methoxyphenyl)propanoic acid (0.501 mmol, 100% yield). Carried directly to next step.

(S)-3-(Tert-butyl)-N-(1-((cyanomethyl)amino)-3-(3-hydroxyphenyl)-1-oxopropan-2-yl)-1-methyl-1H-pyrazole-5-carboxamide (257164)

General procedure D from (S)-2-(3-(tert-butyl)-1-methyl-1H-pyrazole-5-carboxamido)-3-(3-hydroxyphenyl)propanoic acid (82.3 mg, 0.238 mmol) and aminoacetonitrile bisulfate (182 mg, 1.191 mmol) gave (S)-3-(tert-butyl)-N-(1-((cyanomethyl)amino)-3-(3-hydroxyphenyl)-1-oxopropan-2-yl)-1-methyl-1H-pyrazole-5-carboxamide (14 mg, 0.037 mmol, 15.32 % yield); ¹H NMR (400 MHz, MeOH-d₄) δ 7.08 (t, *J* = 7.83 Hz, 1H), 6.68 - 6.77 (m, 2H), 6.59 - 6.66 (m, 2H), 4.74 (dd, *J* = 6.06, 9.19 Hz, 1H), 4.14 (s, 2H), 3.91 (s, 3H), 3.18 (dd, *J* = 5.87, 13.69 Hz, 1H), 2.94 (dd, *J* = 9.39, 13.69 Hz, 1H), 1.27 (s, 9H); ¹³C NMR (101 MHz, MeOH-d₄) δ 174.1, 162.1, 161.6, 158.7, 139.8, 136.8, 130.7, 121.5, 117.5, 117.2, 115.0, 105.1, 56.2, 38.7, 33.0, 31.1, 28.2; MS (ESI+) *m/z*: 384.1 [M+H]⁺

(S)-2-(3-(Tert-butyl)-1-methyl-1H-pyrazole-5-carboxamido)-3-(3-methoxyphenyl)propanoic acid

General procedure B starting from methyl (S)-2-amino-3-(3-methoxyphenyl)propanoate (81.5 mg, 0.389 mmol) and 3-(tert-butyl)-1-methyl-1H-pyrazole-5-carboxylic acid (71.0 mg, 0.389 mmol) followed directly by general procedure C gave (S)-2-(3-(tert-butyl)-1-methyl-1H-pyrazole-5-carboxamido)-3-(3-methoxyphenyl)propanoic acid (136.6 mg, 0.380 mmol, 98 % yield) over two steps. ¹H NMR (500 MHz, MeOH-d₄) δ 7.15 (t, *J* = 8.07 Hz, 1H), 6.82 (br. s., 2H), 6.73 (d, *J* = 8.31 Hz, 1H), 6.62 (s, 1H), 4.84 (dd, *J* = 4.65, 10.30 Hz, 1H), 3.90 (s, 3H), 3.70 (s, 3H), 3.30 (dd, *J* = 4.65, 13.94 Hz, 1H), 3.03 (dd, *J* = 10.27, 13.90 Hz, 1H), 1.25 (s, 9H)

(S)-3-(Tert-butyl)-N-(1-((cyanomethyl)amino)-3-(3-methoxyphenyl)-1-oxopropan-2-yl)-1-methyl-1H-pyrazole-5-carboxamide (257167)

General procedure D from (S)-2-(3-(tert-butyl)-1-methyl-1H-pyrazole-5-carboxamido)-3-(3-methoxyphenyl)propanoic acid (136.6 mg, 0.380 mmol) and 2-((tetraoxidanyl-16-sulfanylidene)amino)acetonitrile (293 mg, 1.900 mmol) gave (S)-3-(tert-butyl)-N-(1-((cyanomethyl)amino)-3-(3-methoxyphenyl)-1-oxopropan-2-yl)-1-methyl-1H-pyrazole-5-carboxamide (126 mg, 0.317 mmol, 83 % yield); ¹H NMR (500 MHz, MeOH-d₄) δ 7.17 (t, *J* = 8.07 Hz, 1H), 6.82 - 6.87 (m, 2H), 6.73 - 6.78 (m, 1H), 6.63 (s, 1H), 4.77 (dd, *J* = 5.87, 9.29 Hz, 1H), 4.15 (d, *J* = 2.45 Hz, 2H), 3.89 (s, 3H), 3.72 (s, 3H), 3.22 (dd, *J* = 5.87, 13.69 Hz, 1H), 2.99 (dd, *J* = 9.29, 13.69 Hz, 1H), 1.27 (s, 9H); ¹³C NMR (126 MHz, MeOH-d₄) δ 174.0, 162.0, 161.6, 161.3, 139.9, 136.7, 130.7, 122.7, 117.5, 116.0, 113.6, 105.2, 56.0, 55.7, 38.8, 33.0, 31.0, 28.2; MS (ESI+) *m/z*: 391.1 [M+H]⁺

Methyl (S)-3-(3-bromophenyl)-2-(3-(tert-butyl)benzamido)propanoate

General procedure B from methyl (S)-2-amino-3-(3-bromophenyl)propanoate, HCl (100 mg, 0.339 mmol) and 3-(tert-butyl)benzoic acid (60.5 mg, 0.339 mmol) gave methyl (S)-3-(3-bromophenyl)-2-(3-(tert-butyl)benzamido)propanoate (140 mg, 0.335 mmol, 99 % yield) Carried directly to next step.

(S)-3-(3-Bromophenyl)-2-(3-(tert-butyl)benzamido)propanoic acid

General procedure C from methyl (S)-3-(3-bromophenyl)-2-(3-(tert-butyl)benzamido)propanoate (140 mg, 0.335 mmol) gave (S)-3-(3-bromophenyl)-2-(3-(tert-butyl)benzamido)propanoic acid (135 mg, 0.335 mmol, 100 % yield). Carried directly to next step.

(S)-N-(3-(3-bromophenyl)-1-((cyanomethyl)amino)-1-oxopropan-2-yl)-3-(tert-butyl)benzamide (257086)

General procedure D from (S)-3-(3-bromophenyl)-2-(3-(tert-butyl)benzamido)propanoic acid (140 mg, 0.346 mmol) and 2-aminoacetonitrile bisulfate (267 mg, 1.731 mmol) gave (S)-N-(3-(3-bromophenyl)-1-((cyanomethyl)amino)-1-oxopropan-2-yl)-3-(tert-butyl)benzamide (160 mg, 0.362 mmol, 104 % yield); ¹H NMR (400 MHz, MeOH-d₄) δ 7.77 (s, 1H), 7.54 (d, *J* = 7.43 Hz, 1H), 7.57 (d, *J* = 7.83 Hz, 1H), 7.49 (s, 1H), 7.31 - 7.38 (m, 2H), 7.26 (d, *J* = 7.43 Hz, 1H), 7.18 (t, *J* = 7.63 Hz, 1H), 4.81 (dd, *J* = 5.87, 9.39 Hz, 1H), 4.15 (d, *J* = 3.13 Hz, 2H), 3.28 (t, *J* = 1.00 Hz, 1H), 3.05 (dd, *J* = 9.59, 13.89 Hz, 1H), 1.32 (s, 9H); ¹³C NMR (101 MHz, MeOH-d₄) δ 173.9, 171.0, 152.9, 141.3, 134.9, 133.6, 133.5, 131.4, 131.1, 130.2, 129.4, 125.7, 125.6, 123.5, 117.5, 56.4, 38.2, 35.8, 31.8, 28.2; MS (ESI+) *m/z*: 442.0 [M+H]⁺ and 463.9 [M+Na]⁺

Methyl (S)-3-(3-bromophenyl)-2-(3-(trifluoromethyl)benzamido)propanoate

General procedure B from methyl (S)-2-amino-3-(3-bromophenyl)propanoate, HCl (500 mg, 1.697 mmol) and 3-(trifluoromethyl)benzoic acid (323 mg, 1.697 mmol) gave methyl (S)-3-(3-bromophenyl)-2-(3-(trifluoromethyl)benzamido)propanoate (715 mg, 1.662 mmol, 98 % yield)

Carried directly to next step.

(S)-3-(3-Bromophenyl)-2-(3-(trifluoromethyl)benzamido)propanoic acid

General procedure C from methyl (S)-3-(3-bromophenyl)-2-(3-(trifluoromethyl)benzamido)propanoate (715 mg, 1.662 mmol) gave (S)-3-(3-bromophenyl)-2-(3-(trifluoromethyl)benzamido)propanoic acid (692 mg, 1.662 mmol, 100 % yield). Carried directly to next step.

(S)-N-(3-(3-Bromophenyl)-1-((cyanomethyl)amino)-1-oxopropan-2-yl)-3-

(trifluoromethyl)benzamide (257087)

General procedure D from (S)-3-(3-bromophenyl)-2-(3-(trifluoromethyl)benzamido)propanoic acid (300 mg, 0.721 mmol), 2-aminoacetonitrile bisulfate (556 mg, 3.60 mmol) gave (S)-N-(3-(3-bromophenyl)-1-((cyanomethyl)amino)-1-oxopropan-2-yl)-3-(trifluoromethyl)benzamide (22 mg, 0.048 mmol, 6.72 % yield) ¹H NMR (400 MHz, MeOH-d₄) δ 8.06 (s, 1H), 7.99 (d, *J* = 7.83 Hz, 1H), 7.83 (d, *J* = 7.83 Hz, 1H), 7.61 - 7.74 (m, 1H), 7.49 (s, 1H), 7.36 (d, *J* = 8.22 Hz, 1H), 7.26 (d, *J* = 7.43 Hz, 1H), 7.19 (t, *J* = 7.83 Hz, 1H), 4.82 (dd, *J* = 5.87, 9.39 Hz, 1H), 4.08 - 4.21 (m, 2H), 3.27 (d, *J* = 5.87 Hz, 1H), 2.93 - 3.12 (m, 1H), 2.80 (s, 1H); ¹³C NMR (101 MHz, MeOH-d₄) δ 173.7, 168.8, 141.2, 136.2, 133.6, 133.5, 132.3, 132.2, 131.5, 131.2, 130.6, 129.5, 129.3, 125.6, 123.5, 117.5, 56.6, 56.5, 38.2, 28.2; MS (ESI+) *m/z*: 475.9 [M+H]⁺

(S)-3-(3-bromophenyl)-2-(3-(tert-butyl)-1-methyl-1H-pyrazole-5-carboxamido)propanoate

General procedure B from methyl (S)-2-amino-3-(3-bromophenyl)propanoate and 3-(tert-butyl)-1-methyl-1H-pyrazole-5-carboxylic acid gave methyl (S)-3-(3-bromophenyl)-2-(3-(tert-butyl)-1-methyl-1H-pyrazole-5-carboxamido)propanoate (140 mg, 0.331 mmol, 98 % yield) as off-white solid. ¹H NMR (400 MHz, MeOH-d₄) δ 7.77 (s, 1H), 7.54 (d, *J* = 7.43 Hz, 1H), 7.57 (d, *J* = 7.83 Hz, 1H), 7.49 (s, 1H), 7.31 - 7.38 (m, 2H), 7.26 (d, *J* = 7.43 Hz, 1H), 7.18 (t, *J* = 7.63 Hz, 1H), 4.81 (dd, *J* = 5.87, 9.39 Hz, 1H), 4.15 (d, *J* = 3.13 Hz, 2H), 3.28 (t, *J* = 1.00 Hz, 1H), 3.05 (dd, *J* = 9.59, 13.89 Hz, 1H), 1.32 (s, 9H)

(S)-3-(3-bromophenyl)-2-(3-(tert-butyl)-1-methyl-1H-pyrazole-5-carboxamido)propanoic acid

General procedure C from methyl (S)-3-(3-bromophenyl)-2-(3-(tert-butyl)-1-methyl-1H-pyrazole-5-carboxamido)propanoate (140 mg, 0.331 mmol) gave (S)-3-(3-bromophenyl)-2-(3-(tert-butyl)-1-methyl-1H-pyrazole-5-carboxamido)propanoic acid (135 mg, 0.331 mmol, 100 % yield) Carried directly to next step.

(S)-N-(3-(3-bromophenyl)-1-((cyanomethyl)amino)-1-oxopropan-2-yl)-3-(tert-butyl)-1-methyl-1H-pyrazole-5-carboxamide (257088)

General procedure D from (S)-3-(3-bromophenyl)-2-(3-(tert-butyl)-1-methyl-1H-pyrazole-5-carboxamido)propanoic acid (140 mg, 0.343 mmol), 2-aminoacetonitrile bisulfate (264 mg, 1.714 mmol) gave (S)-N-(3-(3-bromophenyl)-1-((cyanomethyl)amino)-1-oxopropan-2-yl)-3-(tert-butyl)-1-methyl-1H-pyrazole-5-carboxamide (52 mg, 0.117 mmol, 34.0 % yield); ¹H NMR (400 MHz, MeOH-d₄) δ 7.49 (s, 1H), 7.35 (d, *J* = 7.83 Hz, 1H), 7.25 (d, *J* = 7.43 Hz, 1H), 7.18 (t, *J* = 7.63 Hz, 1H), 6.63 (s, 1H), 4.78 (dd, *J* = 5.67, 9.59 Hz, 1H), 4.17 (s, 2H), 3.89 (s, 3H), 3.25 (dd,

$J = 5.48, 13.69$ Hz, 1H), 2.99 (dd, $J = 9.98, 13.50$ Hz, 1H), 1.27 (s, 9H); ^{13}C NMR (101 MHz, MeOH- d_4) δ 173.7, 162.0, 161.6, 141.2, 136.6, 133.7, 131.5, 131.1, 129.3, 123.4, 117.5, 105.3, 55.7, 38.9, 38.2, 33.0, 31.1, 28.2; MS (ESI+) m/z : 445.9 $[\text{M}+\text{H}]^+$

Methyl (S)-2-cyclohexyl-2-(3-(trifluoromethyl)benzamido)acetate

General procedure B from 3-(trifluoromethyl)benzoic acid (100 mg, 0.526 mmol) and methyl (S)-2-amino-2-cyclohexylacetate (90 mg, 0.526 mmol) gave Methyl (S)-2-cyclohexyl-2-(3-(trifluoromethyl)benzamido)acetate. (yield not calcd); ^1H NMR (500 MHz, MeOH- d_4) δ 8.15 (s, 1H), 8.10 (d, $J = 7.83$ Hz, 1H), 7.85 (d, $J = 7.83$ Hz, 1H), 7.66 - 7.71 (m, 1H), 4.50 (d, $J = 7.34$ Hz, 1H), 3.74 (s, 3H), 1.90 - 1.99 (m, 1H), 1.78 (d, $J = 10.76$ Hz, 3H), 1.70 (t, $J = 13.45$ Hz, 2H), 1.26 - 1.39 (m, 3H), 1.10 - 1.21 (m, 2H)

(S)-2-Cyclohexyl-2-(3-(trifluoromethyl)benzamido)acetic acid

General procedure C from methyl (S)-2-cyclohexyl-2-(3-(trifluoromethyl)benzamido)acetate (208 mg, 0.606 mmol) gave (S)-2-cyclohexyl-2-(3-(trifluoromethyl)benzamido)acetic acid (200 mg, 0.607 mmol, 100 % yield); ^1H NMR (500 MHz, MeOH- d_4) δ 8.16 (s, 1H), 8.10 (d, $J = 7.83$ Hz, 1H), 7.85 (d, $J = 7.34$ Hz, 1H), 7.64 - 7.71 (m, 1H), 4.50 (d, $J = 6.85$ Hz, 1H), 1.96 (dd, $J = 3.42, 6.85$ Hz, 1H), 1.77 - 1.84 (m, 4H), 1.69 (d, $J = 12.23$ Hz, 1H), 1.27 - 1.40 (m, 3H), 1.14 - 1.21 (m, 2H)

(S)-N-(2-((Cyanomethyl)amino)-1-cyclohexyl-2-oxoethyl)-3-(trifluoromethyl)benzamide

(257704)

General procedure D from (S)-2-cyclohexyl-2-(3-(trifluoromethyl)benzamido)acetic acid (200 mg, 0.607 mmol) and 2-aminoacetonitrile bisulfate (465 mg, 3.04 mmol) gave (S)-N-(2-((cyanomethyl)amino)-1-cyclohexyl-2-oxoethyl)-3-(trifluoromethyl)benzamide (75 mg, 0.204 mmol, 33.6 % yield); ¹H NMR (400 MHz, MeOH-d₄) δ 8.17 (s, 1H), 8.10 (d, *J* = 7.83 Hz, 1H), 7.85 (d, *J* = 7.83 Hz, 1H), 7.68 (t, *J* = 7.63 Hz, 1H), 4.31 - 4.42 (m, 1H), 4.23 (d, *J* = 16.43 Hz, 1H), 4.13 (d, *J* = 17.61 Hz, 1H), 1.84 - 1.98 (m, 2H), 1.79 (d, *J* = 10.56 Hz, 2H), 1.70 (br. s., 2H), 1.26 - 1.37 (m, 3H), 1.06 - 1.21 (m, 2H); ¹³C NMR (126 MHz, MeOH-d₄) δ 192.9, 136.5, 132.4, 130.7, 129.4, 117.5, 60.6, 41.1, 30.9, 30.7, 28.0, 27.4, 27.2, 27.1; MS (ESI+) *m/z*: 368.1 [M+H]⁺

(S)-2-Cyclohexyl-2-(3-fluorobenzamido)acetate (137 mg, 0.467 mmol, 80 % yield)

General procedure B from 3-fluorobenzoic acid (82 mg, 0.584 mmol) and methyl (S)-2-amino-2-cyclohexylacetate (100 mg, 0.584 mmol) gave methyl (S)-2-cyclohexyl-2-(3-fluorobenzamido)acetate (137 mg, 0.467 mmol, 80 % yield); ¹H NMR (400 MHz, MeOH-d₄) δ 7.66 (d, *J* = 7.83 Hz, 1H), 7.57 (d, *J* = 9.78 Hz, 1H), 7.49 (dt, *J* = 5.87, 8.02 Hz, 1H), 7.29 (dt, *J* = 1.96, 8.41 Hz, 1H), 4.42 - 4.53 (m, 1H), 3.73 (s, 3H), 1.92 (dtd, *J* = 3.72, 7.61, 11.20 Hz, 1H), 1.78 (d, *J* = 9.78 Hz, 3H), 1.69 (br. s., 2H), 1.27 - 1.40 (m, 3H), 1.07 - 1.21 (m, 2H)

(S)-2-cyclohexyl-2-(3-fluorobenzamido)acetic acid

General procedure C from methyl (S)-2-cyclohexyl-2-(3-fluorobenzamido)acetate (100 mg, 0.341 mmol) gave (S)-2-cyclohexyl-2-(3-fluorobenzamido)acetic acid (92 mg, 0.329 mmol, 97

% yield); ¹H NMR (500 MHz, MeOH-d₄) δ 7.67 (d, *J* = 7.83 Hz, 1H), 7.57 (d, *J* = 9.29 Hz, 1H), 7.45 - 7.52 (m, 1H), 7.29 (dt, *J* = 2.20, 8.44 Hz, 1H), 4.48 (d, *J* = 6.85 Hz, 1H), 1.90 - 1.98 (m, 1H), 1.79 (d, *J* = 10.27 Hz, 4H), 1.68 (d, *J* = 12.23 Hz, 1H), 1.26 - 1.38 (m, 2H), 1.12 - 1.26 (m, 3H)

(S)-N-((Cyanomethyl)amino)-1-cyclohexyl-2-oxoethyl)-3-fluorobenzamide (257705)

General procedure D from (S)-2-cyclohexyl-2-(3-fluorobenzamido)acetic acid (100 mg, 0.358 mmol) and 2 aminoacetonitrile bisulfate (274 mg, 1.790 mmol) gave (S)-N-((cyanomethyl)amino)-1-cyclohexyl-2-oxoethyl)-3-fluorobenzamide (35 mg, 0.110 mmol, 30.8 % yield); ¹H NMR (500 MHz, MeOH-d₄) δ 7.67 (d, *J* = 7.83 Hz, 1H), 7.58 (d, *J* = 9.78 Hz, 1H), 7.46 - 7.52 (m, 1H), 7.29 (dt, *J* = 2.20, 8.44 Hz, 1H), 4.35 (d, *J* = 8.31 Hz, 1H), 4.22 (d, *J* = 17.61 Hz, 1H), 4.13 (d, *J* = 17.61 Hz, 1H), 1.83 - 1.95 (m, 2H), 1.75 - 1.83 (m, *J* = 10.80 Hz, 2H), 1.70 (br. s., 2H), 1.21 - 1.31 (m, 3H), 1.06 - 1.20 (m, 2H); ¹³C NMR (126 MHz, MeOH-d₄) δ 174.2, 165.2, 131.7, 131.6, 124.6, 124.6, 119.8, 119.7, 117.5, 115.8, 115.6, 60.4, 41.2, 30.9, 30.7, 28.0, 27.4, 27.2, 27.1; MS (ESI+) *m/z*: 340.1 [M+H]⁺

Methyl N6-(tert-butoxycarbonyl)-N2-(3-(trifluoromethyl)benzoyl)-L-lysinate

General procedure B from 3-(trifluoromethyl)benzoic acid and methyl N6-(tert-butoxycarbonyl)-L-lysinate gave methyl N6-(tert-butoxycarbonyl)-N2-(3-(trifluoromethyl)benzoyl)-L-lysinate (1.4 g, 3.24 mmol, 96 % yield) as an orange sticky oil. Next, methyl N6-(tert-butoxycarbonyl)-N2-(3-(trifluoromethyl)benzoyl)-L-lysinate (700 mg, 1.619 mmol) was dissolved into 5ml HCl (6N) in dioxane and stirred at rt for 2h to afford methyl N6-(tert-butoxycarbonyl)-N2-(3-(trifluoromethyl)benzoyl)-L-lysinate (700 mg, 1.619 mmol). Carried directly to next step.

Methyl N6,N6-dimethyl-N2-(3-(trifluoromethyl)benzoyl)-L-lysinate

Methyl (3-(trifluoromethyl)benzoyl)-L-lysinate (500 mg, 1.505 mmol) was dissolved into a solution of FORMALDEHYDE (560 μ l, 7.52 mmol) and FORMIC ACID (577 μ l, 15.05 mmol) and headed to reflux overnight. Reaction was cooled, acidified with 1mL 6N HCl (aq) and concentrated in vacuo. The crude residue was dissolved into iPrOH, crashed out with Et₂O and placed in freezer for 1h. Precipitate could not be filtered, so residue was freebased with DCM/triethylamine, absorbed onto silica and purified via biotage 5-10% MeOH:DCM +1%TEA gradient to afford methyl N6,N6-dimethyl-N2-(3-(trifluoromethyl)benzoyl)-L-lysinate as a yellow oil. (yield not calcd); ¹H NMR (500 MHz, MeOH-d₄) δ 8.18 (s, 1H), 8.12 (d, *J* = 7.83 Hz, 1H), 7.87 (d, *J* = 7.83 Hz, 1H), 7.69 (t, *J* = 7.83 Hz, 1H), 4.62 (dd, *J* = 5.14, 9.54 Hz, 1H), 3.75 (s, 3H), 2.48 (t, *J* = 7.83 Hz, 2H), 2.35 (s, 6H), 1.95 - 2.00 (m, 1H), 1.89 (dt, *J* = 4.40, 9.29 Hz, 1H), 1.56 - 1.66 (m, 2H), 1.42 - 1.54 (m, 2H); ¹³C NMR (126 MHz, MeOH-d₄) δ 174.2, 168.9, 136.3, 132.4, 130.8, 129.5, 129.5, 125.6, 125.6, 60.1, 54.6, 53.0, 45.1, 32.1, 27.4, 25.0

(S)-N-(1-((Cyanomethyl)amino)-6-(dimethylamino)-1-oxohexan-2-yl)-3-(trifluoromethyl)benzamide (257948)

General procedure C from methyl N6,N6-dimethyl-N2-(3-(trifluoromethyl)benzoyl)-L-lysinate gave N6,N6-dimethyl-N2-(3-(trifluoromethyl)benzoyl)-L-lysine (99 % yield). Next, General procedure D from N6,N6-dimethyl-N2-(3-(trifluoromethyl)benzoyl)-L-lysine (500 mg, 1.444 mmol) and 2-aminoacetonitrile bisulfate (1105 mg, 7.22 mmol) Followed by purification via prep TLC 10%MeOH:DCM + 1%TEA (R_f~0.4) gave (S)-N-(1-((cyanomethyl)amino)-6-(dimethylamino)-1-oxohexan-2-yl)-3-(trifluoromethyl)benzamide (yield<5%); ¹H NMR (400

MHz, MeOH-d₄) δ 8.22 (s, 1H), 8.15 (d, $J = 7.83$ Hz, 1H), 7.87 (d, $J = 7.43$ Hz, 1H), 7.69 (t, $J = 7.83$ Hz, 1H), 4.58 (dd, $J = 5.48, 9.00$ Hz, 1H), 4.11 - 4.26 (m, 2H), 2.76 (t, $J = 7.83$ Hz, 2H), 2.58 (s, 6H), 1.93 - 2.03 (m, 1H), 1.83 - 1.90 (m, 1H), 1.61 - 1.76 (m, 2H), 1.40 - 1.56 (m, 2H); HRMS (ESI+) m/z : 385.1843 [M+H]⁺

Methyl N6-(tert-butoxycarbonyl)-N2-(3-fluorobenzoyl)-L-lysinate

General procedure B from 3-fluorobenzoic acid (260 mg, 1.853 mmol) and methyl N6-(tert-butoxycarbonyl)-L-lysinate, HCl (500 mg, 1.685 mmol) gave methyl N6-(tert-butoxycarbonyl)-N2-(3-fluorobenzoyl)-L-lysinate (644 mg, 1.684 mmol, 100 % yield); ¹H NMR (400 MHz, MeOH-d₄) δ 7.69 (d, $J = 7.83$ Hz, 1H), 7.59 (d, $J = 9.78$ Hz, 1H), 7.43 - 7.53 (m, 1H), 7.28 (dt, $J = 2.15, 8.31$ Hz, 1H), 4.52 - 4.64 (m, 1H), 3.69 - 3.76 (m, 3H), 3.04 (t, $J = 6.46$ Hz, 2H), 1.88 - 1.99 (m, 1H), 1.85 (td, $J = 4.40, 9.19$ Hz, 1H), 1.43 - 1.56 (m, 3H), 1.38 - 1.43 (m, 9H), 1.31 - 1.38 (m, 1H)

Methyl (3-fluorobenzoyl)-L-lysinate

Methyl N6-(tert-butoxycarbonyl)-N2-(3-fluorobenzoyl)-L-lysinate (600 mg, 1.569 mmol) was dissolved in 6M HCl:dioxane solution and stirred at rt for 4h. Solvent was removed in vacuo and crude residue was basified w/ MeOH/TEA, absorbed onto silica, and purified via FC 10% MeOH/DCM + 1% TEA to afford methyl (3-fluorobenzoyl)-L-lysinate (400 mg, 1.417 mmol, 90 % yield); ¹H NMR (500 MHz, DMSO-d₆) δ 8.93 (d, $J = 7.34$ Hz, 1H), 7.78 (d, $J = 7.83$ Hz, 1H), 7.73 (d, $J = 9.78$ Hz, 1H), 7.49 - 7.57 (m, 1H), 7.37 - 7.44 (m, 1H), 4.35 - 4.47 (m, 1H), 3.65 (s, 3H), 2.77 (t, $J = 7.34$ Hz, 2H), 1.74 - 1.90 (m, 2H), 1.53 - 1.67 (m, 2H), 1.33 - 1.53 (m, 2H), 1.05 (t, $J = 7.34$ Hz, 1H)

Methyl N2-(3-fluorobenzoyl)-N6,N6-dimethyl-L-lysinate

Methyl (3-fluorobenzoyl)-L-lysinate (170 mg, 0.602 mmol) was dissolved into MeOH (2 ml). FORMALDEHYDE (0.448 ml, 6.02 mmol) and ACETIC ACID (0.069 ml, 1.204 mmol) were added, followed by the addition of SODIUM TRIACETOXYBOROHYDRIDE (510 mg, 2.409 mmol). Reaction was left to stir at rt overnight and monitored by HPLC. Purified by FC 10%MeOH in DCM + 1% TEA to afford methyl N2-(3-fluorobenzoyl)-N6,N6-dimethyl-L-lysinate (175 mg, 0.564 mmol, 94 % yield); ¹H NMR (400 MHz, MeOH-d₄) δ 7.69 (d, *J* = 7.43 Hz, 1H), 7.60 (d, *J* = 9.39 Hz, 1H), 7.44 - 7.53 (m, 1H), 7.26 - 7.34 (m, 1H), 4.59 (dd, *J* = 5.09, 9.39 Hz, 1H), 3.74 (s, 3H), 2.44 (t, *J* = 7.63 Hz, 2H), 2.32 (s, 6H), 1.80 - 2.05 (m, 2H), 1.39 - 1.65 (m, 4H); ¹³C NMR (126 MHz, MeOH-d₄) δ 174.3, 169.4, 167.5, 165.5, 131.4, 131.3, 116.6, 116.4, 59.9, 54.4, 52.9, 44.9, 32.1, 27.0, 24.9; MS (ESI+) *m/z*: 311.0 [M+H]⁺

(S)-N-(1-((Cyanomethyl)amino)-6-(dimethylamino)-1-oxohexan-2-yl)-3-fluorobenzamide (257949)

General procedure D from N2-(3-fluorobenzoyl)-N6,N6-dimethyl-L-lysinate (167 mg, 0.565 mmol) and 2-aminonitrile bisulfate (433 mg, 2.83 mmol). Purification by FC (10-15% MeOH:DCM+ 1%TEA) followed by prep TLC 10%MeOH:DCM + 1%TEA gave (S)-N-(1-((cyanomethyl)amino)-6-(dimethylamino)-1-oxohexan-2-yl)-3-fluorobenzamide. (Yield not calcd <5%) HPLC: Rt=3.942; ¹H NMR (400 MHz, MeOH-d₄) δ 7.72 (d, *J* = 7.83 Hz, 1H), 7.63 (d, *J* = 9.78 Hz, 1H), 7.46 - 7.53 (m, 1H), 7.26 - 7.35 (m, 1H), 4.56 (dd, *J* = 5.48, 9.00 Hz, 1H), 4.12 - 4.25 (m, 2H), 2.93 (t, *J* = 7.83 Hz, 2H), 2.71 (s, 6H), 1.93 - 2.03 (m, 1H), 1.82 - 1.90 (m, 1H), 1.65 - 1.80 (m, 2H), 1.39 - 1.58 (m, 2H); MS (ESI+) *m/z*: 335.1876 [M+H]⁺

**(S)-N-(2-((cyanomethyl)amino)-1-cyclohexyl-2-oxoethyl)-3-(dimethylamino) benzamide
(257946)**

General procedure B from 3-(dimethylamino)benzoic acid (200 mg, 1.211 mmol) and methyl (S)-2-amino-2-cyclohexylacetate (249 mg, 1.453 mmol) was directly followed by General procedure C and General procedure D from (S)-2-cyclohexyl-2-(3-(dimethylamino)benzamido)acetic acid (96 mg, 0.315 mmol) and 2-aminoacetonitrile bisulfate (241 mg, 1.577 mmol) to afford (S)-N-(2-((cyanomethyl)amino)-1-cyclohexyl-2-oxoethyl)-3-(dimethylamino)benzamide (95 mg, 0.277 mmol, 88 % yield); ¹H NMR (400 MHz, (400 MHz, MeOH-d₄) δ 7.23 - 7.31 (m, 1H), 7.19 (s, 1H), 7.12 (d, *J* = 7.43 Hz, 1H), 6.92 (dd, *J* = 1.96, 8.22 Hz, 1H), 4.36 (d, *J* = 8.61 Hz, 1H), 4.23 (d, *J* = 17.61 Hz, 1H), 4.12 (d, *J* = 17.22 Hz, 1H), 2.92 - 3.03 (m, 6H), 1.83 - 1.95 (m, 2H), 1.78 (d, *J* = 10.96 Hz, 2H), 1.69 (br. s., 2H), 1.06 - 1.36 (m, 5H); ¹³C NMR (101 MHz, (400 MHz, MeOH-d₄) δ 174.5, 171.4, 152.3, 132.0, 130.1, 117.6, 117.1, 112.9, 112.6, 111.6, 60.2, 41.3, 40.8, 39.2, 38.9, 38.1, 28.0; MS (ESI+) *m/z*: 343.2129 [M+H]⁺

(S)-3-Cyclohexyl-2-(3-(trifluoromethyl)benzamido)propanoate

General procedure B from 3-(trifluoromethyl)benzoic acid (94 mg, 0.496 mmol) and methyl (S)-2-amino-3-cyclohexylpropanoate, HCl (100 mg, 0.451 mmol) gave methyl (S)-3-cyclohexyl-2-(3-(trifluoromethyl)benzamido)propanoate (150 mg, 0.420 mmol, 93 % yield); ¹H NMR (500 MHz, MeOH-d₄) δ 8.18 (s, 1H), 8.12 (d, *J* = 7.83 Hz, 1H), 7.87 (d, *J* = 7.83 Hz, 1H), 7.70 (t, *J* = 7.83 Hz, 1H), 4.68 - 4.77 (m, 1H), 3.74 (s, 3H), 1.85 (d, *J* = 12.72 Hz, 1H), 1.70 - 1.81 (m, 5H), 1.62 - 1.69 (m, 1H), 1.39 - 1.49 (m, 1H), 1.34 - 1.39 (m, 1H), 1.27 - 1.34 (m, 1H), 1.17 - 1.22 (m, 1H), 0.91 - 1.08 (m, 2H)

(S)-3-Cyclohexyl-2-(3-(trifluoromethyl)benzamido)propanoic acid

General procedure C from methyl (S)-3-cyclohexyl-2-(3-(trifluoromethyl)benzamido)propanoate (150 mg, 0.420 mmol) gave (S)-3-cyclohexyl-2-(3-(trifluoromethyl)benzamido)propanoic acid (131 mg, 0.382 mmol, 91 % yield); ¹H NMR (500 MHz, DMSO-d₆) δ 8.87 (d, *J* = 7.83 Hz, 1H), 8.23 (s, 1H), 8.19 (d, *J* = 7.83 Hz, 1H), 7.87 - 7.96 (m, 1H), 7.68 - 7.79 (m, 1H), 4.43 - 4.57 (m, 1H), 1.70 - 1.79 (m, 2H), 1.60 - 1.70 (m, 4H), 1.58 (br. s., 1H), 1.31 - 1.44 (m, 1H), 1.07 - 1.26 (m, 3H), 0.91 - 1.01 (m, 1H), 0.79 - 0.91 (m, 1H)

(S)-N-(1-((Cyanomethyl)amino)-3-cyclohexyl-1-oxopropan-2-yl)-3-(trifluoromethyl)benzamide (257943)

General procedure D from (S)-3-cyclohexyl-2-(3-(trifluoromethyl)benzamido)propanoic acid (50 mg, 0.146 mmol) and 2-aminoacetonitrile bisulfate (89 mg, 0.583 mmol) gave (S)-N-(1-((cyanomethyl)amino)-3-cyclohexyl-1-oxopropan-2-yl)-3-(trifluoromethyl)benzamide (50 mg, 0.131 mmol, 90 % yield); HPLC Rt: 7.276 min; ¹H NMR (500 MHz, MeOH-d₄) δ 8.22 (s, 1H), 8.14 (d, *J* = 7.83 Hz, 1H), 7.87 (d, *J* = 7.83 Hz, 1H), 7.69 (t, *J* = 7.58 Hz, 1H), 4.67 (dd, *J* = 5.87, 9.78 Hz, 1H), 4.13 - 4.23 (m, 2H), 1.85 (d, *J* = 12.72 Hz, 1H), 1.71 - 1.81 (m, 5H), 1.68 (br. s., 1H), 1.36 - 1.49 (m, 1H), 1.27 - 1.35 (m, 1H), 1.21 - 1.26 (m, 2H), 0.93 - 1.09 (m, 2H); ¹³C NMR (126 MHz, MeOH-d₄) δ 175.4, 168.9, 136.3, 132.4, 130.7, 129.5, 125.7, 125.7, 117.6, 53.2, 40.2, 35.8, 34.9, 33.5, 28.2, 27.7, 27.5, 27.4; MS (ESI+) *m/z*: 404.1558 [M+H]⁺

Methyl (S)-3-cyclohexyl-2-(3-fluorobenzamido)propanoate

General procedure B from 3-fluorobenzoic acid (69.5 mg, 0.496 mmol) and methyl (S)-2-amino-3-cyclohexylpropanoate, HCl (110 mg, 0.500 mmol) Gave methyl (S)-3-cyclohexyl-2-(3-

fluorobenzamido)propanoate (200 mg, 0.651 mmol, 144 % yield); ^1H NMR (500 MHz, MeOH-d_4) δ 7.69 (d, $J = 7.83$ Hz, 1H), 7.59 (d, $J = 9.29$ Hz, 1H), 7.45 - 7.55 (m, 1H), 7.30 (dt, $J = 1.96$, 8.31 Hz, 1H), 4.70 (dd, $J = 5.87$, 9.29 Hz, 1H), 3.74 (s, 3H), 1.84 (d, $J = 12.23$ Hz, 1H), 1.69 - 1.80 (m, 5H), 1.61 - 1.69 (m, 1H), 1.35 - 1.48 (m, 1H), 1.24 - 1.33 (m, 2H), 1.16 - 1.22 (m, 1H), 0.89 - 1.09 (m, 2H)

(S)-3-Cyclohexyl-2-(3-fluorobenzamido)propanoic acid

General procedure C from methyl (S)-3-cyclohexyl-2-(3-fluorobenzamido)propanoate (140 mg, 0.455 mmol) gave (S)-3-cyclohexyl-2-(3-fluorobenzamido)propanoic acid (134 mg, 0.457 mmol, 100 % yield); ^1H NMR (500 MHz, DMSO-d_6) δ 8.67 (d, $J = 7.34$ Hz, 1H), 7.75 (d, $J = 6.85$ Hz, 1H), 7.69 (d, $J = 9.29$ Hz, 1H), 7.54 (br. d, $J = 6.40$ Hz, 1H), 7.34 - 7.44 (m, 1H), 4.46 (br. s., 1H), 1.73 (d, $J = 10.27$ Hz, 2H), 1.65 (br. s., 4H), 1.59 (br. s., 1H), 1.38 (br. s., 1H), 1.05 - 1.28 (m, 4H), 0.90 - 1.04 (m, 1H), 0.86 (d, $J = 9.78$ Hz, 1H)

(S)-N-(1-((Cyanomethyl) amino)-3-cyclohexyl-1-oxopropan-2-yl)-3-fluorobenzamide (257944)

General procedure D from (S)-3-cyclohexyl-2-(3-fluorobenzamido)propanoic acid (50 mg, 0.170 mmol) and 2-aminoacetonitrile bisulfate (104 mg, 0.682 mmol) gave (S)-N-(1-((cyanomethyl) amino)-3-cyclohexyl-1-oxopropan-2-yl)-3-fluorobenzamide (37 mg, 0.112 mmol, 65.5 % yield); ^1H NMR (500 MHz, MeOH-d_4) δ 7.70 (d, $J = 7.34$ Hz, 1H), 7.61 (d, $J = 9.78$ Hz, 1H), 7.45 - 7.54 (m, 1H), 7.29 (t, $J = 7.83$ Hz, 1H), 4.65 (q, $J = 7.34$ Hz, 1H), 4.09 - 4.27 (m, 2H), 1.83 (d, $J = 12.23$ Hz, 1H), 1.68 - 1.80 (m, 5H), 1.67 (br. s., 1H), 1.41 (br. s., 1H), 1.23 - 1.34 (m, 2H), 1.14 - 1.21 (m, 1H), 0.90 - 1.08 (m, 2H); ^{13}C NMR (126 MHz, MeOH-d_4) δ 175.6, 169.1, 165.2,

163.2, 131.7, 131.6, 124.6, 124.6, 119.9, 119.7, 117.6, 115.8, 115.6, 53.2, 40.3, 35.8, 34.9, 33.5, 28.3, 27.7, 27.5, 27.3; MS (ESI+) m/z : 354.1589 [M+H]⁺

Methyl (S)-3-cyclohexyl-2-(3-(dimethylamino)benzamido)propanoate

General procedure B from methyl (S)-2-amino-3-cyclohexylpropanoate (100 mg, 0.540 mmol) and 3-(dimethylamino)benzoic acid (98 mg, 0.594 mmol) gave methyl (S)-3-cyclohexyl-2-(3-(dimethylamino)benzamido)propanoate (175 mg, 0.526 mmol, 98 % yield); ¹H NMR (500 MHz, MeOH-d₄) δ 7.28 (t, J = 7.83 Hz, 1H), 7.22 (s, 1H), 7.15 (d, J = 7.34 Hz, 1H), 6.94 (dd, J = 2.45, 8.31 Hz, 1H), 4.70 (dd, J = 5.38, 9.78 Hz, 1H), 3.74 (s, 3H), 2.98 (s, 6H), 1.85 (d, J = 12.72 Hz, 1H), 1.70 - 1.80 (m, 5H), 1.63 - 1.69 (m, 1H), 1.39 - 1.50 (m, 1H), 1.32 - 1.35 (m, 1H), 1.29 (dd, J = 2.93, 9.78 Hz, 1H), 1.17 - 1.23 (m, 1H), 0.89 - 1.08 (m, 2H)

(S)-3-Cyclohexyl-2-(3-(dimethylamino)benzamido)propanoic acid

General procedure C from methyl (S)-3-cyclohexyl-2-(3-(dimethylamino)benzamido)propanoate (175 mg, 0.526 mmol) gave (S)-3-cyclohexyl-2-(3-(dimethylamino)benzamido)propanoic acid (168 mg, 0.526 mmol, 100 % yield). Carried directly to next step.

(S)-N-(1-((cyanomethyl)amino)-3-cyclohexyl-1-oxopropan-2-yl)-3-(dimethylamino)benzamide (257947)

General procedure D from (S)-3-cyclohexyl-2-(3-(dimethylamino)benzamido)propanoic acid (75 mg, 0.236 mmol) and 2-aminoacetonitrile bisulfate (144 mg, 0.942 mmol). Purified on reverse phase C-18 (10-50% ACN in H₂O+ 0.1% TFA) to afford (S)-N-(1-((cyanomethyl)amino)-3-cyclohexyl-1-oxopropan-2-yl)-3-(dimethylamino)benzamide (50 mg, 0.140 mmol, 59.6 % yield);

HPLC Rt=5.561 min; ^1H NMR (500 MHz, MeOH- d_4) δ 8.00 (s, 1H), 7.85 (d, $J = 7.34$ Hz, 1H), 7.67 (d, $J = 7.83$ Hz, 1H), 7.61 (t, $J = 8.31$ Hz, 1H), 4.67 (dd, $J = 5.38, 9.78$ Hz, 1H), 4.18 (dd, $J = 18.10, 22.99$ Hz, 2H), 3.26 (s, 6H), 1.69 - 1.88 (m, 6H), 1.67 (br. s., 1H), 1.38 - 1.49 (m, 1H), 1.16 - 1.33 (m, 3H), 0.92 - 1.08 (m, 2H); ^{13}C NMR (126 MHz, MeOH- d_4) δ 175.6, 169.0, 146.3, 137.3, 131.7, 127.1, 123.2, 119.4, 117.7, 53.3, 45.8, 40.3, 35.7, 34.9, 33.5, 28.3, 27.7, 27.5, 27.3

Methyl (morpholine-4-carbonyl)-L-leucinate

To a dry rb flask was added, methyl L-leucinate, HCl (250 mg, 1.376 mmol) and DCM (3 ml). solution was cooled to 0°C then morpholine-4-carbonyl chloride (0.161 ml, 1.376 mmol) and DIPEA (0.481 ml, 2.75 mmol) were added. The reaction was allowed to warm to rt and left to stir under nitrogen overnight. Reaction was diluted 3x with DCM and washed with 1N HCl then brine, dried over MgSO_4 , and conc to afford methyl (morpholine-4-carbonyl)-L-leucinate (240 mg, 0.929 mmol, 67.5 % yield) as a white solid.; ^1H NMR (500 MHz, CDCl_3) δ 4.52 (s, 1H), 3.72 (s, 3H), 3.66 - 3.70 (m, 4H), 3.31 - 3.43 (m, 4H), 1.58 - 1.74 (m, 2H), 1.47 - 1.55 (m, 1H), 0.95 (d, $J = 2.93$ Hz, 3H), 0.94 (d, $J = 3.42$ Hz, 3H)

(Morpholine-4-carbonyl)-L-leucine

General procedure C from methyl (morpholine-4-carbonyl)-L-leucinate (200 mg, 0.774 mmol) gave (morpholine-4-carbonyl)-L-leucine (185 mg, 0.757 mmol, 98 % yield). Carried directly to next step.

**(S)-N-(1-((Cyanomethyl)amino)-4-methyl-1-oxopentan-2-yl)morpholine-4-carboxamide
(258761)**

General procedure D from (morpholine-4-carbonyl)-L-leucine (125 mg, 0.512 mmol) gave (S)-N-(1-((cyanomethyl)amino)-4-methyl-1-oxopentan-2-yl)morpholine-4-carboxamide.; ¹H NMR (400 MHz, MeOH-d₄) δ 4.29 (dd, *J* = 5.28, 9.98 Hz, 1H), 4.08 - 4.20 (m, 2H), 3.57 - 3.71 (m, 4H), 3.32 - 3.48 (m, 4H), 1.49 - 1.76 (m, 3H), 0.96 (d, *J* = 6.26 Hz, 3H), 0.93 (d, *J* = 6.26 Hz, 3H); ¹³C NMR (101 MHz, MeOH-d₄) δ 176.8, 159.8, 117.7, 67.7, 54.6, 45.4, 41.9, 28.2, 26.1, 23.6, 22.0; MS (ESI+) *m/z*: 283.1766 [M+H]⁺

Methyl (S)-2-isocyanato-4-methylpentanoate

To a mixture of L-leucine methyl ester hydrochloride (3.62 g, 20 mmol) in saturated NaHCO₃ (72 mL) and DCM (72 mL) was added triphosgene (1.96 g, 6.6 mmol). The reaction mixture was vigorously stirred under ice-water bath for 1 h and the organic layer was collected. The water layer was extracted with DCM for three times and the organic phase was combined and dried with MgSO₄. After the solvent removed under vacuum, the residue was dissolved in DCM (20 mL). This solution was then added to corresponding ortho-substituted anilines or benzylamines (21 mmol) in DCM (80 mL) under ice bath. The reaction mixture was stirred at room temperature for 12 h and then the solvent was removed under low pressure. The residue was taken up with ethyl acetate (100 mL) and washed with 1 N HCl (30 mL) and brine (30 mL). The organic phase was dried with MgSO₄. After the solvent removed, the residue without purification was directly added to a solution of potassium hydroxylamine (8.37 g, 56 mmol) in methanol (20 mL). The reaction mixture was stirred at room temperature for 1 h and then removed methanol under low pressure. The residue was taken up with 1 N HCl and extracted

with ethyl acetate. The organic phase was washed with brine and dried with MgSO₄. After the solvent removed under low pressure, the residue was separated by silica gel column chromatography to afford desired product. Carried directly to next step without further purification.

Methyl (4-methylpiperazine-1-carbonyl)-L-leucinate

methyl (S)-2-isocyanato-4-methylpentanoate (0.942 g, 5.50 mmol) was dissolved in DCM (20 ml) and the solution was cooled to 0°C. 1-methylpiperazine (0.671 ml, 6.05 mmol) was then added and reaction was allowed to warm to rt over 2.5 hours. Reaction was conc. in vacuo and purified on silica gel via chromatography w/ 5% MeOH in DCM +1% triethylamine to afford methyl (4-methylpiperazine-1-carbonyl)-L-leucinate (1.1 g, 4.05 mmol, 73.7 % yield); ¹H NMR (500 MHz, MeOH-d₄) δ 4.32 (dd, *J* = 5.14, 10.03 Hz, 1H), 3.69 (s, 3H), 3.40 - 3.55 (m, 4H), 2.35 - 2.47 (m, 4H), 2.30 (s, 3H), 1.61 - 1.76 (m, 2H), 1.51 - 1.60 (m, 1H), 0.92 (d, *J* = 6.36 Hz, 3H), 0.96 (d, *J* = 6.85 Hz, 3H)

(4-Methylpiperazine-1-carbonyl)-L-leucine

General procedure C from methyl (4-methylpiperazine-1-carbonyl)-L-leucinate (250 mg, 0.921 mmol) gave (4-methylpiperazine-1-carbonyl)-L-leucine (237 mg, 0.921 mmol, 100 % yield). Carried directly to next step without further purification.

(S)-N-(1-((cyanomethyl)amino)-4-methyl-1-oxopentan-2-yl)-4-methylpiperazine-1-carboxamide (259044)

General procedure D from (4-methylpiperazine-1-carbonyl)-L-leucine (237 mg, 0.921 mmol) and 2-aminoacetonitrile bisulfate (169 mg, 1.105 mmol). Purified via silica gel column, 5-10% MeOH:DCM gradient + 1% TEA. Desired compound came out during the final wash w/ 10% MeOH to afford (S)-N-(1-((cyanomethyl)amino)-4-methyl-1-oxopentan-2-yl)-4-methylpiperazine-1-carboxamide (100 mg, 0.339 mmol, 36.8 % yield); ¹H NMR (500 MHz, MeOH-d₄) δ 4.23 - 4.32 (m, 1H), 4.17 (d, *J* = 18.10 Hz, 1H), 4.12 (d, *J* = 18.59 Hz, 1H), 3.63 (br. s., 4H), 2.94 (br. s., 4H), 2.66 (s, 3H), 1.61 - 1.79 (m, 2H), 1.50 - 1.61 (m, 1H), 0.97 (d, *J* = 5.38 Hz, 3H), 0.93 (d, *J* = 5.38 Hz, 3H); ¹³C NMR (126 MHz, MeOH-d₄) δ 176.7, 159.1, 117.8, 54.9, 54.8, 44.8, 43.4, 41.8, 28.2, 26.1, 23.6, 22.0

(S)-N-(1-((Cyanomethyl)amino)-4-methyl-1-oxopentan-2-yl)nicotinamide (259041)

General procedure B from nicotinic acid (407 mg, 3.30 mmol) and methyl L-leucinate, HCl (500 mg, 2.75 mmol) gave methyl nicotinoyl-L-leucinate (600 mg, 2.397 mmol, 87 % yield). Next, General procedure C from methyl nicotinoyl-L-leucinate (600 mg, 2.397 mmol) gave nicotinoyl-L-leucine (566 mg, 2.396 mmol, 100 % yield). Finally, General procedure D from nicotinoyl-L-leucine (250 mg, 1.058 mmol) and 2-aminoacetonitrile bisulfate (324 mg, 2.116 mmol) followed by purification by FC (1-10% MeOH in DCM +1%TEA) gave (S)-N-(1-((cyanomethyl)amino)-4-methyl-1-oxopentan-2-yl)nicotinamide (130 mg, 0.474 mmol, 44.8 % yield); ¹H NMR (400 MHz, MeOH-d₄) δ 9.01 (s, 1H), 8.69 (d, *J* = 3.91 Hz, 1H), 8.26 - 8.31 (m, 1H), 7.54 (dd, *J* = 5.09, 7.43 Hz, 1H), 4.64 (dd, *J* = 4.50, 9.98 Hz, 1H), 4.20 (d, *J* = 17.61 Hz, 1H), 4.15 (d, *J* = 17.61 Hz, 1H), 1.61 - 1.85 (m, 2H), 1.34 - 1.39 (m, 1H), 0.99 (d, *J* = 5.87 Hz, 3H), 0.97 (d, *J* =

5.87 Hz, 3H); ^{13}C NMR (101 MHz, MeOH- d_4) δ 175.3, 168.1, 152.9, 149.5, 137.4, 131.6, 125.2, 117.6, 53.8, 41.6, 28.2, 26.2, 23.5, 22.0; MS (ESI+) m/z : 275.1566 $[\text{M}+\text{H}]^+$

(S)-N-(1-((Cyanomethyl)amino)-4-methyl-1-oxopentan-2-yl)isonicotinamide (262467)

General procedure B from isonicotinic acid (254 mg, 2.066 mmol) and methyl L-leucinate (250 mg, 1.722 mmol) gave methyl isonicotinoyl-L-leucinate (415 mg, 1.658 mmol, 96 % yield). Next General procedure C from methyl isonicotinoyl-L-leucinate (415 mg, 1.658 mmol) gave isonicotinoyl-L-leucine (392 mg, 1.659 mmol, 100 % yield). Finally, General procedure D from isonicotinoyl-L-leucine (392 mg, 1.659 mmol) and 2-aminoacetonitrile bisulfate (508 mg, 3.32 mmol) gave (S)-N-(1-((cyanomethyl)amino)-4-methyl-1-oxopentan-2-yl)isonicotinamide (360 mg, 1.312 mmol, 79 % yield); ^1H NMR (500 MHz, MeOH- d_4) δ 8.68 (d, $J = 4.89$ Hz, 2H), 7.81 (d, $J = 5.87$ Hz, 2H), 4.65 (dd, $J = 4.89, 10.27$ Hz, 1H), 4.21 (d, $J = 17.61$ Hz, 1H), 4.17 (d, $J = 17.61$ Hz, 1H), 1.64 - 1.84 (m, 3H), 0.99 (d, $J = 5.87$ Hz, 3H), 0.96 (d, $J = 5.87$ Hz, 3H); ^{13}C NMR (126 MHz, MeOH- d_4) δ 175.1, 168.0, 151.0, 143.3, 123.2, 117.6, 53.8, 41.6, 28.3, 26.2, 23.5, 22.0; MS (ESI+) m/z : 275.1504 $[\text{M}+\text{H}]^+$

Benzyl (S)-1-((cyanomethyl)amino)-4-methyl-1-oxopentan-2-yl)carbamate

General procedure D from ((benzyloxy)carbonyl)-L-leucine (2 g, 7.54 mmol) and 2-aminoacetonitrile bisulfate (2.309 g, 15.08 mmol) gave benzyl (S)-1-((cyanomethyl)amino)-4-methyl-1-oxopentan-2-yl)carbamate (1.5 g, 4.94 mmol, 65.6 % yield) as a white solid.; ^1H NMR (500 MHz, MeOH- d_4) δ 7.23 - 7.44 (m, 5H), 5.04 - 5.16 (m, 2H), 4.04 - 4.20 (m, 3H), 1.62 - 1.78 (m, 1H), 1.56 (t, $J = 6.11$ Hz, 2H), 0.95 (d, $J = 6.36$ Hz, 3H), 0.92 (d, $J = 6.36$ Hz, 3H)

(S)-2-Amino-N-(cyanomethyl)-4-methylpentanamide

In a dry rb flask under nitrogen, benzyl (S)-1-((cyanomethyl)amino)-4-methyl-1-oxopentan-2-yl)carbamate (600 mg, 1.978 mmol) was dissolved into acetonitrile (10 ml). Palladium on carbon 5% (421 mg, 0.198 mmol) was added to the solution. Nitrogen was removed by vacuum (water aspirator) and vessel was fixed with a hydrogen balloon. Reaction was stirred at rt for 2h, at which time HPLC indicated reaction was complete. Hydrogen was removed, and vessel was purged w/ nitrogen. Solution was filtered through celite and washed 2x with CAN to afford (S)-2-amino-N-(cyanomethyl)-4-methylpentanamide (335 mg, 1.978 mmol, 100 % yield) carried directly to next step.

(S)-4-Chloro-N-(1-((cyanomethyl)amino)-4-methyl-1-oxopentan-2-yl)-2-methoxybenzamide**(262743)**

After filtering (S)-2-amino-N-(cyanomethyl)-4-methylpentanamide (100 mg, 0.591 mmol) into a new flask, post-debenzylation rxn, 4-chloro-2-methoxybenzoic acid (110 mg, 0.591 mmol), HATU (337 mg, 0.886 mmol), and DIPEA (0.258 ml, 1.477 mmol) were added to the solution and left to stir under nitrogen at rt overnight. Solvent was removed via rotovap, and crude residue was dissolved into EtOAc (10mL) and washed 2x each with 1N HCl, Sat. NaHCO₃ (aq), and brine. dried over mgso₄ and concentrated onto silica gel. Purified via biotage 30-50% EtOAc:Hex gradient to afford (S)-4-Chloro-N-(1-((cyanomethyl)amino)-4-methyl-1-oxopentan-2-yl)-2-methoxybenzamide (Yield not calcd); ¹H NMR (500 MHz, DMSO-d₆) δ 7.87 (d, *J* = 7.83 Hz, 1H), 7.21 (s, 1H), 7.08 (d, *J* = 8.31 Hz, 1H), 4.59 - 4.68 (m, 1H), 4.20 (d, *J* = 17.61 Hz, 1H), 4.16 (d, *J* = 17.61 Hz, 1H), 4.00 (s, 3H), 1.61 - 1.82 (m, 3H), 1.00 (d, *J* = 6.85 Hz, 3H), 0.98 (d, *J*

= 6.36 Hz, 3H); ^{13}C NMR (126 MHz, DMSO- d_6) δ 175.2, 167.1, 159.9, 140.1, 133.6, 122.4, 121.6, 117.6, 113.8, 57.3, 53.7, 42.5, 28.2, 26.3, 23.6, 22.3; MS (ESI+) m/z : 338.129 [M+H] $^+$

(S)-2-chloro-N-(1-((cyanomethyl)amino)-4-methyl-1-oxopentan-2-yl)-4-methoxybenzamide (262744)

After filtering (S)-2-amino-N-(cyanomethyl)-4-methylpentanamide (100 mg, 0.591 mmol) into a new flask after the debenzylation rxn, 2-chloro-4-methoxybenzoic acid (110 mg, 0.591 mmol), HATU (337 mg, 0.886 mmol), and DIPEA (0.258 ml, 1.477 mmol) were added to the solution and left to stir under nitrogen at rt overnight. Solvent was removed via rotovap, and crude residue was dissolved into EtOAc (10mL) and washed 2x each with 1N HCl, Sat. NaHCO_3 (aq), and brine. dried over mgso_4 and concentrated onto silica gel. Purified via biotage 30-50% EtOAc:Hex gradient to afford (S)-2-chloro-N-(1-((cyanomethyl)amino)-4-methyl-1-oxopentan-2-yl)-4-methoxybenzamide (Yield not calcd); ^1H NMR (500 MHz, MeOH- d_4) δ 7.48 (d, J = 8.80 Hz, 1H), 7.00 (d, J = 1.96 Hz, 1H), 6.94 (dd, J = 2.45, 8.80 Hz, 1H), 4.57 (dd, J = 5.14, 10.03 Hz, 1H), 4.21 (d, J = 17.61 Hz, 1H), 4.17 (d, J = 17.61 Hz, 1H), 3.83 (s, 3H), 1.75 - 1.84 (m, 1H), 1.67 - 1.75 (m, 1H), 1.58 - 1.66 (m, 1H), 0.98 (d, J = 6.36 Hz, 6H); ^{13}C NMR (126 MHz, MeOH- d_4) δ 175.1, 170.0, 163.0, 133.2, 131.6, 128.8, 117.6, 116.6, 113.8, 56.4, 53.7, 41.6, 28.2, 26.0, 23.4, 14.5; MS (ESI+) m/z : 338.127 [M+H] $^+$

(S)-3-(Tert-butyl)-1-methyl-N-(1-oxo-1-(prop-2-yn-1-ylamino)-3-(m-tolyl)propan-2-yl)-1H-pyrazole-5-carboxamide (257161)

General procedure D from (S)-2-(3-(tert-butyl)-1-methyl-1H-pyrazole-5-carboxamido)-3-(m-tolyl)propanoic acid (137 mg, 0.399 mmol) and prop-2-yn-1-amine (0.077 ml, 1.197 mmol) gave

(S)-3-(tert-butyl)-1-methyl-N-(1-oxo-1-(prop-2-yn-1-ylamino)-3-(m-tolyl)propan-2-yl)-1H-pyrazole-5-carboxamide (85 mg, 0.223 mmol, 56.0 % yield). ¹H NMR (400 MHz, MeOH-d₄) δ 7.11 - 7.18 (m, 1H), 7.09 (s, 1H), 7.01 (d, *J* = 7.43 Hz, 1H), 7.05 (d, *J* = 7.83 Hz, 1H), 6.61 (s, 1H), 4.72 (dd, *J* = 5.87, 9.39 Hz, 1H), 3.96 (d, *J* = 1.96 Hz, 2H), 3.90 (s, 3H), 3.18 (dd, *J* = 5.87, 13.69 Hz, 1H), 2.93 (dd, *J* = 9.39, 13.69 Hz, 1H), 2.59 (t, *J* = 2.35 Hz, 1H), 2.28 (s, 3H), 1.28 (s, 9H); ¹³C NMR (101 MHz, MeOH-d₄) δ 173.4, 162.0, 161.7, 139.2, 138.5, 136.9, 131.4, 129.6, 128.7, 127.6, 105.2, 80.5, 72.7, 56.3, 39.0, 38.7, 33.0, 31.1, 29.7, 21.7; ; MS (ESI+) *m/z*: 381.1 [M+H]⁺

Potassium (S,Z)-4-methyl-2-((2,2,2-trifluoro-1-phenylethylidene)amino)pentanoate

In a dry rb flask under nitrogen, methyl L-leucinate, HCl (200 mg, 1.101 mmol), 2,2,2-trifluoro-1-phenylethan-1-one (155 μl, 1.101 mmol), potassium carbonate (304 mg, 2.202 mmol) were heated to reflux in anhydrous MeOH overnight. Reaction was cooled to rt, filtered through celite, wash with MeOH, and concentrated to afford potassium (S,Z)-4-methyl-2-((2,2,2-trifluoro-1-phenylethylidene)amino)pentanoate (358 mg, 1.101 mmol, 100 % yield). Carried directly to next step without further purification.

((S)-2,2,2-trifluoro-1-phenylethyl)-L-leucine

Potassium (S,Z)-4-methyl-2-((2,2,2-trifluoro-1-phenylethylidene)amino)pentanoate (896 mg, 2.75 mmol) was dissolved with ~1mL anhydrous MeOH and diluted with 10mL or ACN to form a white slurry. Vessel was placed under nitrogen and cooled to -40°C in ACN dry ice bath. Zinc borohydride (3305 μl, 3.30 mmol) in Et₂O was added dropwise via addition cannula under a flow on nitrogen. Reaction was stirred for 2-4h at -40°C then allowed to warm to rt.

rxn was quenched slowly using 1N HCl. More 1N HCl was added and compound was extracted with EtOAc 3x. Organic layer was dried over MgSO₄ and concentrated to afford ((S)-2,2,2-trifluoro-1-phenylethyl)-L-leucine (743 mg, 2.57 mmol, 93 % yield) dr = 1:3 (1-R,S : 3-S,S); ¹H NMR (500 MHz, MeOH-d₄) δ 7.35 - 7.51 (m, 5H), 4.99 - 5.08 (m, 1H), 4.31 (d, *J* = 7.34 Hz, 1H), 4.19 (q, *J* = 7.34 Hz, 1H), 4.10 (q, *J* = 7.34 Hz, 1H), 3.46 (t, *J* = 6.85 Hz, 1H), 1.98 - 2.03 (m, 1H), 1.91 (td, *J* = 6.79, 13.33 Hz, 1H), 1.45 - 1.54 (m, 2H), 1.23 (t, *J* = 7.09 Hz, 1H), 0.91 - 0.98 (m, 3H), 0.88 (d, *J* = 6.85 Hz, 1H), 0.74 (d, *J* = 6.85 Hz, 1H); ¹⁹F NMR MeOH-d₄) δ ppm - 79.65 (s) -76.11 (s) -75.03 (s)

(S)-N-(cyanomethyl)-4-methyl-2-(((S)-2,2,2-trifluoro-1-phenylethyl)amino)pentanamide (257952)

General procedure D from ((S)-2,2,2-trifluoro-1-phenylethyl)-L-leucine (190 mg, 0.657 mmol) and 2-aminoacetonitrile bisulfate (201 mg, 1.314 mmol) gave (S)-N-(cyanomethyl)-4-methyl-2-(((S)-2,2,2-trifluoro-1-phenylethyl)amino)pentanamide (200 mg, 0.611 mmol, 93 % yield) dr=1:3; ¹H NMR (500 MHz, MeOH-d₄) δ 7.33 - 7.44 (m, 5H), 4.16 (s, 1H), 3.98 (dd, *J* = 17.61, 30.32 Hz, 2H), 3.33 - 3.44 (m, 1H), 1.74 - 1.86 (m, 1H), 1.46 - 1.54 (m, 1H), 1.37 - 1.46 (m, 1H), 0.94 (dd, *J* = 2.69, 6.60 Hz, 6H); MS (ESI+) *m/z*: 328.1634 [M+H]⁺

((R)-2,2,2-Trifluoro-1-phenylethyl)-L-leucine

Potassium (S,Z)-4-methyl-2-((2,2,2-trifluoro-1-phenylethylidene)amino)pentanoate (358 mg, 1.100 mmol) was suspended in 5ml THF and added to dry rb flask charged with sodium tetrahydroborate (333 mg, 8.80 mmol). 5mL of water:THF (v/v:2/8) was added via syringe pump over 3h. 1N HCl was added and rxn was extracted with EtOAc 3x. Organic layer was washed

with bicarb and brine, dried over MgSO₄, and concentrated to afford ((R)-2,2,2-trifluoro-1-phenylethyl)-L-leucine (135 mg, 0.467 mmol, 42.4 % yield). Carried directly to next step

**(S)-N-(cyanomethyl)-4-methyl-2-(((R)-2,2,2-trifluoro-1-phenylethyl)amino)pentanamide
(258061)**

General procedure D from ((R)-2,2,2-trifluoro-1-phenylethyl)-L-leucine (135 mg, 0.467 mmol) and 2-aminoacetonitrile bisulfate (143 mg, 0.933 mmol) gave (S)-N-(cyanomethyl)-4-methyl-2-(((R)-2,2,2-trifluoro-1-phenylethyl)amino)pentanamide. dr = 1:15 (S,S : R,S), (yield not calcd).; ¹H NMR (400 MHz, MeOH-d₄) δ 7.43 - 7.51 (m, 2H), 7.34 - 7.43 (m, 3H), 4.15 (s, 2H), 4.06 - 4.14 (m, 1H), 3.00 (dd, *J* = 5.28, 8.80 Hz, 1H), 1.62 - 1.78 (m, 1H), 1.41 - 1.53 (m, 1H), 1.26 - 1.39 (m, 1H), 0.86 (d, *J* = 6.65 Hz, 3H), 0.71 (d, *J* = 6.65 Hz, 3H); ¹³C NMR (101 MHz, MeOH-d₄) δ 177.6, 135.1, 130.5, 130.1, 129.7, 117.7, 64.1, 59.2, 44.2, 27.9, 25.8, 23.5, 22.3; MS (ESI+) *m/z*: 328.1634 [M+H]⁺

Potassium (S,Z)-4-methyl-2-((2,2,2-trifluoro-1-(3-fluorophenyl)ethylidene)amino)pentanoate

In a dry round bottom flask under nitrogen, methyl L-leucinate, HCl (130 mg, 0.716 mmol), 2,2,2-trifluoro-1-(3-fluorophenyl)ethan-1-one (100 μl, 0.716 mmol), and potassium carbonate (198 mg, 1.431 mmol) were heated to reflux in anhydrous MeOH overnight. Reaction was cooled to rt, filtered through celite, wash with MeOH, and concentrated to afford potassium (S,Z)-4-methyl-2-((2,2,2-trifluoro-1-(3-fluorophenyl)ethylidene)amino)pentanoate (246 mg, 0.716 mmol, 100 % yield)

((R)-2,2,2-Trifluoro-1-(3-fluorophenyl)ethyl)-L-leucine

A dry round bottom flask was charged with sodium tetrahydroborate (16.53 mg, 0.437 mmol) and THF (3 ml) was then added. Potassium (S,Z)-4-methyl-2-((2,2,2-trifluoro-1-(3-fluorophenyl)ethylidene)amino)pentanoate (150 mg, 0.437 mmol) was dissolved into THF:H₂O (10:1) and added via syringe pump over 2h at rt. Reaction was quenched with 1N HCl and THF was removed in vacuo. Extracted w/ EtOAc 3x, washed organic layer 2x with 1N HCl and brine, dried over mgso₄ and conc to afford ((R)-2,2,2-trifluoro-1-(3-fluorophenyl)ethyl)-L-leucine (120 mg, 0.391 mmol, 89 % yield) and an off-white/yellow crystalline solid.; ¹H NMR (500 MHz, MeOH-d₄) δ 7.35 - 7.43 (m, 1H), 7.22 - 7.29 (m, 2H), 7.13 (t, *J* = 8.80 Hz, 1H), 4.35 (q, *J* = 7.01 Hz, 1H), 2.95 (dd, *J* = 5.38, 8.80 Hz, 1H), 1.79 - 1.94 (m, 1H), 1.38 - 1.54 (m, 2H), 0.88 (d, *J* = 6.36 Hz, 3H), 0.74 (d, *J* = 6.36 Hz, 3H); 1:12 dr (S,S:R,S) by ¹⁸F-NMR

(S)-N-(Cyanomethyl)-4-methyl-2-(((R)-2,2,2-trifluoro-1-(3-fluorophenyl)ethyl)amino)pentanamide (258062)

((R)-2,2,2-trifluoro-1-(3-fluorophenyl)ethyl)-L-leucine (120 mg, 0.391 mmol), 2-aminoacetonitrile bisulfate (120 mg, 0.781 mmol), DIPEA (0.205 ml, 1.172 mmol), HATU (163 mg, 0.430 mmol) gave (S)-N-(cyanomethyl)-4-methyl-2-(((R)-2,2,2-trifluoro-1-(3-fluorophenyl)ethyl)amino)pentanamide. (yield not calcd) 1:12 dr (S,S:R,S) by ¹⁸F-NMR; ¹H NMR (500 MHz, MeOH-d₄) δ 7.43 (s, 1H), 7.24 - 7.31 (m, 2H), 7.15 (dt, *J* = 1.96, 8.31 Hz, 1H), 4.17 - 4.22 (m, 1H), 4.17 (s, 2H), 3.01 (dd, *J* = 5.14, 9.05 Hz, 1H), 1.73 (td, *J* = 6.85, 13.69 Hz, 1H), 1.48 (ddd, *J* = 5.62, 8.80, 13.94 Hz, 1H), 1.36 (ddd, *J* = 5.38, 8.31, 13.69 Hz, 1H), 0.87 (d, *J* = 6.36 Hz, 3H), 0.73 (d, *J* = 6.36 Hz, 3H); ¹³C NMR (126 MHz, MeOH-d₄) δ 177.4, 165.4,

163.5, 137.9, 131.7, 126.4, 117.7, 117.3, 116.9, 63.9, 59.3, 44.1, 28.0, 25.8, 23.5, 22.2; HRMS (ESI+) m/z : 346.1541 [M+H]⁺

((S)-2,2,2-Trifluoro-1-(3-fluorophenyl)ethyl)-L-leucine (200 mg, 0.651 mmol, 91 % yield)

Potassium (S,Z)-4-methyl-2-((2,2,2-trifluoro-1-(3-fluorophenyl)ethylidene)amino) pentanoate (246 mg, 0.716 mmol) was dissolved with ~1mL anhydrous MeOH and diluted with 10mL or ACN to form a white slurry. Vessel was placed under nitrogen and cooled to -40°C in ACN dry ice bath. Zinc Borohydride (3582 μ l, 0.716 mmol) in Et₂O was added dropwise via addition cannula under a flow on nitrogen. Reaction was stirred for 2-4h at -40°C then allowed to warm to rt. Reaction was quenched slowly using 1N HCl. More 1N HCl was added and compound was extracted with EtOAc 3x. Organic layer was dried over MgSO₄ and concentrated to afford ((S)-2,2,2-trifluoro-1-(3-fluorophenyl)ethyl)-L-leucine (200 mg, 0.651 mmol, 91 % yield). Dr = 2:1 (S,S:R,S). Carried to final step. ¹H NMR (400 MHz, MeOH-d₄) δ 7.33 - 7.44 (m, 1H), 7.17 - 7.30 (m, 2H), 6.99 - 7.16 (m, 1H), 5.05 (q, J = 7.04 Hz, 1H), 4.07 (q, J = 7.17 Hz, 1H), 1.92 - 2.06 (m, 8H), 1.78 - 1.92 (m, 1H), 1.41 - 1.57 (m, 1H), 1.10 - 1.34 (m, 2H), 0.81 - 0.98 (m, 3H), 0.66 - 0.78 (m, 1H); ¹⁹F NMR (MeOH-d₄) δ ppm -115.08, (s) -114.38, (s), -79.62, -75.73 (s) - 75.71 (s) -74.63 (s)

(S)-N-(cyanomethyl)-4-methyl-2-(((S)-2,2,2-trifluoro-1-(3-fluorophenyl)ethyl)amino) pentanamide (258063)

General procedure D from ((S)-2,2,2-trifluoro-1-(3-fluorophenyl)ethyl)-L-leucine (200 mg, 0.651 mmol) and 2- aminoacetonitrile bisulfate (299 mg, 1.953 mmol) gave (S)-N-(cyanomethyl)-4-methyl-2-(((S)-2,2,2-trifluoro-1-(3-fluorophenyl)ethyl)amino)pentanamide

(yield not calcd) dr = 2:1 (S,S:R,S); ¹H NMR (400 MHz, MeOH-d₄) δ 7.40 (s, 1H), 7.24 - 7.30 (m, 1H), 7.18 - 7.24 (m, 1H), 7.06 - 7.17 (m, 1H), 4.18 - 4.26 (m, 1H), 4.13 - 4.18 (m, 1H), 3.92 - 4.07 (m, 2H), 1.66 - 1.87 (m, 1H), 1.29 - 1.56 (m, 2H), 0.92 (dd, *J* = 2.54, 6.46 Hz, 6H); ¹³C NMR (126 MHz, MeOH-d₄) δ 177.5, 165.2, 163.2, 138.8, 131.6, 125.8, 117.5, 117.1, 116.7, 64.2, 61.0, 44.0, 27.9, 25.9, 23.4, 22.6; HRMS (ESI+) *m/z*: 346.1539 [M+H]⁺

(S)-N-(1-Cyanocyclopropyl)-4-methyl-2-(((S)-2,2,2-trifluoro-1-phenylethyl)amino)pentanamide (258069)

General procedure D from ((S)-2,2,2-trifluoro-1-phenylethyl)-L-leucine (100 mg, 0.346 mmol) and 1-aminocyclopropane-1-carbonitrile, HCl (49.2 mg, 0.415 mmol) gave (S)-N-(1-cyanocyclopropyl)-4-methyl-2-(((S)-2,2,2-trifluoro-1-phenylethyl)amino)pentanamide as a white solid. (Yield not calcd); dr= 3:1 (S,S:R,S) by ¹⁸F-NMR; ¹H NMR (500 MHz, MeOH-d₄) δ 7.34 - 7.48 (m, 5H), 4.09 - 4.15 (m, 1H), 1.74 - 1.86 (m, 1H), 1.41 - 1.52 (m, 2H), 1.28 - 1.41 (m, 3H), 1.14 - 1.21 (m, 1H), 0.90 - 0.97 (m, 6H); ¹³C NMR (126 MHz, MeOH-d₄) δ 178.7, 136.6, 130.4, 130.2, 129.9, 129.9, 129.8, 121.2, 64.9, 61.5, 44.2, 39.0, 26.0, 23.4, 22.6, 21.1, 17.0, 16.8; HRMS (ESI+) *m/z*: 354.1793 [M+H]⁺

Potassium (R,E)-4,4-dimethyl-2-((2,2,2-trifluoro-1-(4-fluorophenyl)ethylidene)amino)pentanoate

In a dry rb flask, 2,2,2-trifluoro-1-(4-fluorophenyl)ethan-1-one (500 mg, 2.60 mmol), methyl (S)-2-amino-4,4-dimethylpentanoate, HCl (560 mg, 2.86 mmol), potassium carbonate (899 mg, 6.51 mmol) were added and refluxed overnight in anhydrous methanol. Reaction was cooled to rt, filtered through celite, washed with MeOH, and concentrated to afford potassium (R,E)-4,4-

dimethyl-2-((2,2,2-trifluoro-1-(4-fluorophenyl)ethylidene)amino)pentanoate (930 mg, 2.60 mmol, 100 % yield). Carried directly to next reaction.

Potassium (S)-4,4-dimethyl-2-(((S)-2,2,2-trifluoro-1-(4-fluorophenyl)ethyl)amino)pentanoate

In a dry round bottom flask, zinc (II) chloride (709 mg, 5.20 mmol) freshly fused (3x) dissolved in DME (~10-15mL) and , sodium tetrahydroborate (394 mg, 10.41 mmol) was added and left at rt overnight. Potassium (R,E)-4,4-dimethyl-2-((2,2,2-trifluoro-1-(4-fluorophenyl)ethylidene)amino)pentanoate (930 mg, 2.60 mmol) was cooled to rt and filtered through a plug of celite into a dry 250ml rb flask. ~80 mL dry ACN (dry over 3Å sieves) was then added. Vessel was cooled to -40°C in dry ice/ACN bath and fixed with dry addition funnel. The Zn(BH₄)₂ solution was cooled to -40, run through a plug of celite into the addition funnel and slowly added to the reaction mixture then washed through 2x w/ anhydrous ACN (2x 5-10mL each). The reaction was placed under nitrogen and left to stir at -40°C for 5h. ~5-10mL acetone was added and the reaction was left to warm to rt over 1hr. 1N HCl was slowly added to cloudy solution (became clear upon quench) and organic solvent was removed via rotovap. Extraction w/ EtOAc 3x, washed with brine, dried over MgSO₄, and conc to afford potassium (S)-4,4-dimethyl-2-(((S)-2,2,2-trifluoro-1-(4-fluorophenyl)ethyl)amino)pentanoate (640 mg, 1.781 mmol, 68.4 % yield); 40:1 dr (S,S:R,S) by ¹⁹F-NMR; ¹H NMR (500 MHz, MeOH-d₄) δ 7.45 (dd, *J* = 5.62, 8.07 Hz, 2H), 7.10 (t, *J* = 8.56 Hz, 2H), 4.85 (br. s., 2H), 4.18 (q, *J* = 7.66 Hz, 1H), 3.49 (dd, *J* = 4.40, 7.34 Hz, 1H), 1.62 (dd, *J* = 4.40, 14.18 Hz, 1H), 1.46 (dd, *J* = 7.34, 14.18 Hz, 1H), 1.00 (s, 9H); ¹³C NMR (126 MHz, MeOH-d₄) δ 178.9, 165.5, 163.6, 132.9, 131.9, 116.4, 64.0, 59.8, 48.3, 31.6, 30.4

(S)-N-(cyanomethyl)-4,4-dimethyl-2-(((S)-2,2,2-trifluoro-1-(4-fluorophenyl)ethyl)amino)pentanamide (262608)

General procedure D from potassium (S)-4,4-dimethyl-2-(((S)-2,2,2-trifluoro-1-(4-fluorophenyl)ethyl)amino)pentanoate (100 mg, 0.278 mmol) and 2-aminoacetonitrile bisulfate (128 mg, 0.835 mmol) gave (S)-N-(cyanomethyl)-4,4-dimethyl-2-(((S)-2,2,2-trifluoro-1-(4-fluorophenyl)ethyl)amino)pentanamide (87.8 mg, 0.244 mmol, 88 % yield); ¹H NMR (500 MHz, MeOH-d₄) δ 7.43 (dd, *J* = 5.62, 7.58 Hz, 2H), 7.10 (t, *J* = 8.80 Hz, 2H), 4.13 (dd, *J* = 6.85, 14.67 Hz, 1H), 4.00 (d, *J* = 17.10 Hz, 1H), 3.94 (d, *J* = 17.12 Hz, 1H), 3.40 (t, *J* = 6.11 Hz, 1H), 1.45 - 1.56 (m, 2H), 0.99 (s, 9H); ¹³C NMR (126 MHz, MeOH-d₄) δ 177.9, 177.9, 163.6, 164.5, 132.4, 131.9, 117.4, 116.6, 63.9, 60.6, 48.4, 31.5, 30.5, 27.9; HRMS (ESI⁺) *m/z*: 360.1695 [M+H]⁺

(S)-N-(1-Cyanocyclopropyl)-4,4-dimethyl-2-(((S)-2,2,2-trifluoro-1-(4-fluorophenyl)ethyl)amino)pentanamide (262642)

General procedure D from potassium (S)-4,4-dimethyl-2-(((S)-2,2,2-trifluoro-1-(4-fluorophenyl)ethyl)amino)pentanoate (100 mg, 0.278 mmol) and 1-aminocyclopropane-1-carbonitrile, HCl (99 mg, 0.835 mmol) gave (S)-N-(1-cyanocyclopropyl)-4,4-dimethyl-2-(((S)-2,2,2-trifluoro-1-(4-fluorophenyl)ethyl)amino)pentanamide (75 mg, 0.195 mmol, 69.9 % yield); ¹H NMR (500 MHz, MeOH-d₄) δ 7.38 - 7.45 (m, 2H), 7.11 (t, *J* = 8.56 Hz, 2H), 4.10 (q, *J* = 7.50 Hz, 1H), 3.32 - 3.37 (m, 1H), 1.48 (d, *J* = 5.90 Hz, 2H), 1.35 - 1.43 (m, 2H), 1.00 - 1.04 (m, 1H), 0.98 (s, 9H), 0.80 - 0.90 (m, 1H); ¹³C NMR (126 MHz, MeOH-d₄) δ 178.9, 164.7, 132.6, 131.9, 128.2, 121.2, 116.7, 64.0, 60.9, 48.4, 31.5, 30.5, 21.2, 16.9, 16.7; HRMS (ESI⁺) *m/z*: 386.1852 [M+H]⁺

Computational Modeling:

The X-ray structure of TgCPL complexed with its propeptide (PDB: 3F75) was superposed with the X-ray structure of HsCPL complexed with AZ-12878478 (PDB 3HHA), using The Molecular Operating Environment (MOE), version 2008.10, Chemical Computing Group Inc., Montreal, Quebec, Canada. The X-ray structure of *HsCPL* and the propeptide chain of TgCPL were removed to generate the figures shown.

TgCPL and *HsCPL* Inhibition Assay: Compound potency and selectivity was evaluated in vitro for both TgCPL and *HsCPL* activity in a fluorescence based assay by monitoring the hydrolysis of Cbz-Leu-Arg-aminomethylcoumarin (Z-L-R-AMC). Protein was expressed and purified as previously described. The substrate hydrolysis results in the release of fluorescent 7-amino-4-methylcoumarin (AMC) that can be monitored spectrophotometrically with linear kinetics for up to 60 min. Inhibitors were serial diluted in DMSO in a 1-to-3 dilution, spanning at least 10 concentration points in either duplicate or triplicate. The enzyme was pre-incubated with the inhibitory compounds for 5 min at 23°C, followed by the addition of the AMC substrate. The assay final conditions had a total volume of 200 μ L, consisting of 90 μ L enzyme (conc.=50 ng/mL), 100 μ L ZLR-AMC substrate (conc.= 80 μ M), and 10 μ L inhibitor or DMSO. The relative fluorescence of the AMC generation is measured over the course of 5 min (Excitation: 380 nm, Emission: 460 nm). LHVS and DMSO were used as positive and negative controls, respectively. All dose response data was obtained with at least independent three replicates (n=3). Graphpad Prism software was used to visualize inhibition curves and calculate IC₅₀ values

from the reaction mean v. Assay final concentrations in each well: 40 μ M ZLR-AMC, TgCPL or HsCPL (final conc= 0.0225 ng/ μ L). Assay Buffer: 100 mM NaAc, 2 mM EDTA, 900 mM NaCl, 50 mM DTT. Substrate: Cbz-Leu-Arg-AMC (Bachem, purchased as HCl salt).

Metabolic Stability in Mouse Liver Microsomes: The metabolic stability was assessed using CD-1 mouse liver microsomes. One micromolar of each compound was incubated with 0.5 mg/mL microsomes and 1.7 mM cofactor β -NADPH in 0.1 M phosphate buffer (pH = 7.4) containing 3.3 mM $MgCl_2$ at 37 °C. The DMSO concentration was less than 0.1% in the final incubation system. At 0, 5, 10, 15, 30, 45, and 60 min of incubation, 40 μ L of reaction mixture were taken out, and the reaction is quenched by adding 3-fold excess of cold acetonitrile containing 100 ng/mL of internal standard for quantification. The collected fractions were centrifuged at 15000 rpm for 10 min to collect the supernatant for LC–MS/ MS analysis, from which the amount of compound remaining was determined. The natural log of the amount of compound remaining was plotted against time to determine the disappearance rate and the half-life of tested compounds.

Pharmacokinetic Studies in Mice: All animal experiments in this study were approved by the University of Michigan Committee on Use and Care of Animals and Unit for Laboratory Animal Medicine. The abbreviated pharmacokinetics for **18b** was determined in female CD-1 mice following intraperitoneal (ip) injection at 10 mg/kg. Compound was dissolved in the vehicle containing 15% (v/v) DMSO, 15% (v/v) PEG-400, and 70% (v/ v) PBS. Four blood samples (50 μ L) were collected over 7 h (at 0.5h, 2h, 4h, and 7h), centrifuged at 3500 rpm for 10 min, and plasma was frozen at -80°C for later analysis. Plasma concentrations of the compounds were

determined by the LC–MS/MS method developed and validated for this study. The LC–MS/MS method consisted of a Shimadzu HPLC system, and chromatographic separation of tested compound which was achieved using a Waters Xbridge-C18 column (5 cm × 2.1 mm, 3.5 µm). An AB Sciex QTrap 4500 mass spectrometer equipped with an electrospray ionization source (ABI-Sciex, Toronto, Canada) in the positive-ion multiple reaction monitoring (MRM) mode was used for detection. All pharmacokinetic parameters were calculated by non-compartmental methods using WinNonlin, version 3.2 (Pharsight Corporation, Mountain View, CA, USA).

Chapter 3 The Identification and Optimization of Triazine Nitrile Inhibitors of *TgCPL*

Rationale

Through the development of the first SAR for the inhibition of *TgCPL* with our series of dipeptide nitriles, we were able to gain insight into the pharmacophore necessary for *TgCPL* inhibition and to improve the potency and selectivity over human isoforms. However, we were unable to advance the dipeptide series toward *in vivo* target validation due to the sub-optimal PK properties. Our optimized lead **258070** (**Figure 22**) was potent *in vitro* and CNS penetrant, but the drug was rapidly cleared *in vivo*. Although the dipeptide-nitriles are convenient to investigate SAR in the cathepsin pockets, they often exhibit less than desirable physicochemical properties for gaining blood-brain barrier (BBB) permeability, such as several rotational bonds, extensive hydrogen bonding, and high TPSA.¹⁵⁷ We thus began searching for alternative scaffolds that might exhibit better physicochemical properties to improve upon the *in vivo* PK, while maintaining the pharmacophore elements for *TgCPL* inhibition and BBB penetration.

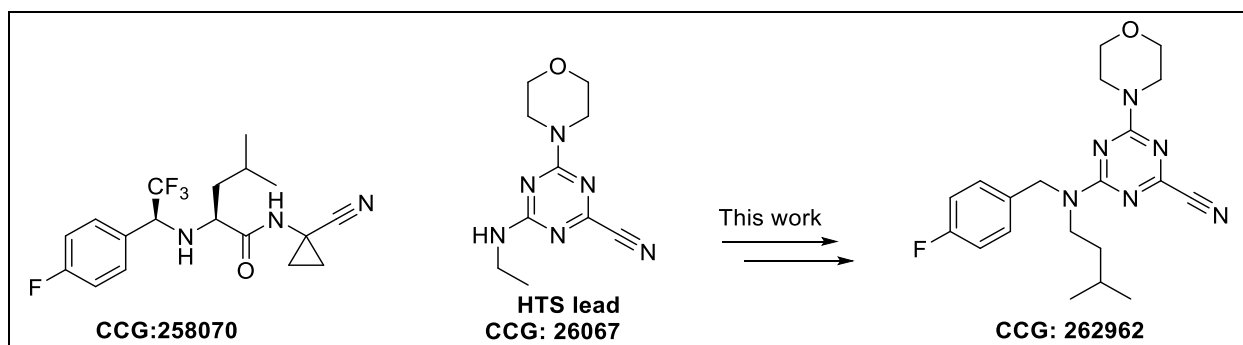


Figure 22. Inhibitors of *Toxoplasma gondii* cathepsin L

Identification of Triazine Nitriles via High-Throughput Screen

The Carruthers lab conducted a high throughput screen for *TgCPL* inhibitors at the Center for Chemical Genomics at the University of Michigan on over 140,000 small molecules. From this we identified several inhibitor classes that demonstrated promising inhibitory activity against *TgCPL*, reasonable synthetic approachability, and physiochemical profiles optimal for use as a lead scaffold in a CNS targeted campaign. To minimize potential DMPK issues in later development, we chose to exclude compounds that were peptidic in structure, or irreversibly covalent. After rigorous triage had identified several potential lead molecules, we searched the literature to determine if any of these chemotypes had any previously demonstrated activity against cysteine proteases. An extensive amount of study has been done on inhibitors of human cathepsin L (*HsCPL*). Since *Toxoplasma gondii* cathepsin L shares high homology with *HsCPL* (60% similarity and 40% identity) we considered chemotypes with precedent for inhibiting *HsCPL* as good potential leads. Among the several potential lead molecules discovered in the screen, we selected a modestly active triazine nitrile **26067** (*TgCPL* IC₅₀ = 2.5 μM, *HsCPL* IC₅₀ = 2.3 μM) as a lead candidate (**Figure 22**), given its small size, chemical profile, and literature precedent as a cathepsin inhibitor class. Several recent publications have reported triazine nitrile-based inhibitors of human cathepsins, and additionally demonstrated potent inhibition of rhodesain and falcipain.¹⁵⁸⁻¹⁶⁰ The activity reported for these analogous cysteine proteases from related apicomplexan parasites *P. falciparum* and *T. brucei* further supports the potential of this chemotype as an antiparasitic agent. Additional triazine nitriles, pyrazolopyrimidine nitriles, and related heterocyclic-nitrile motifs, have also been reported as inhibitors of rhodesain, cruzain, and falcipain.

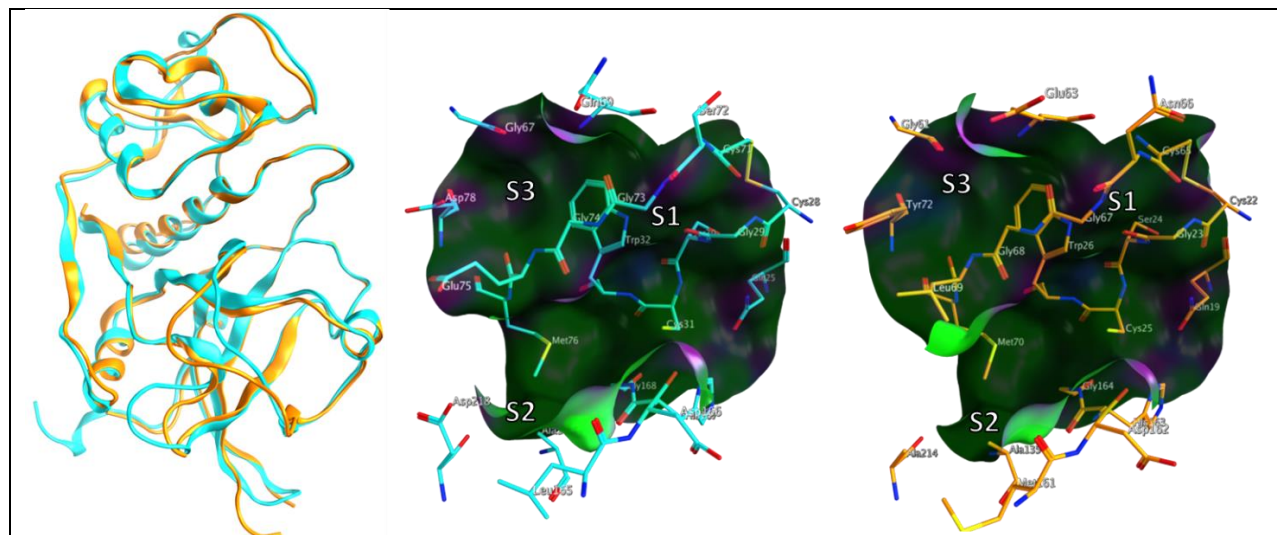
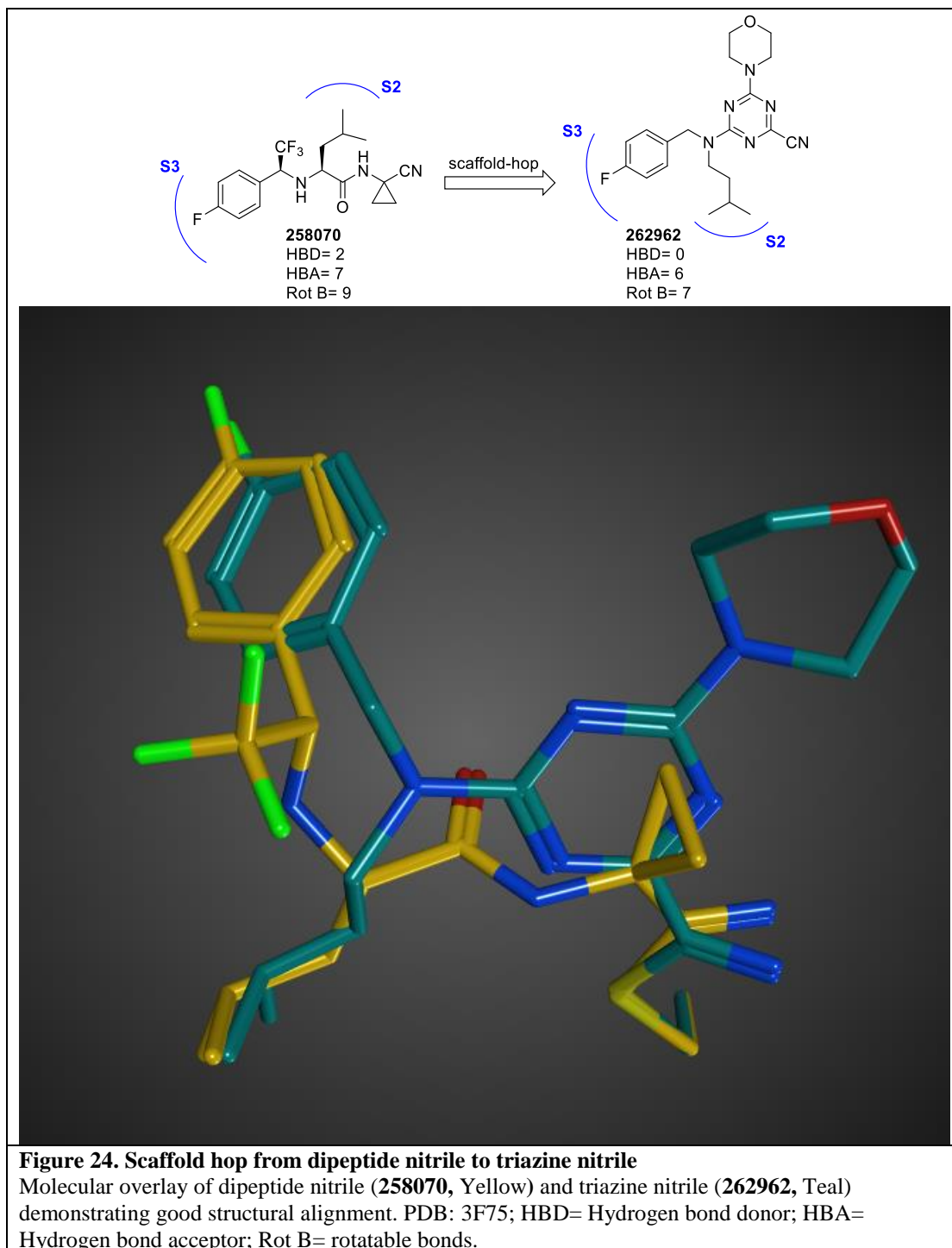


Figure 23. Structural overlay and active sites of *Tg*CPL
(Cyan; PDB-3F75) and *Hs*CPL (Orange PDB-5MAJ)

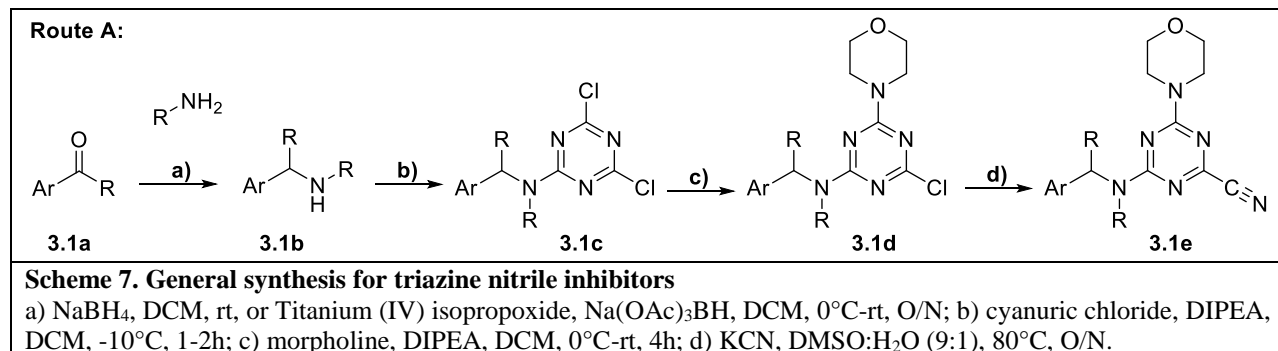
Scaffold Hop from Dipeptide to Triazine Nitrile

Although these recent studies have established the potential of this chemotype as a clinically relevant antiparasitic agent, *Toxoplasma gondii*, as well as other protozoan parasites such as *T. brucei*, establish a chronic infection in the central nervous system (CNS). Compounds with CNS targets have a somewhat constrained physicochemical profile as compared to peripheral drugs. Key among these are the minimization of hydrogen bond donors and decreasing TPSA which increase the rate of BBB penetration and unbound-drug brain concentration. Additionally, CNS drugs exhibit low MW (<450), high lipophilicity (logP <5), exclusion of acid moieties, and reduced number of rotatable bonds (RotB) (<8). The triazinyl-peptidomimetic scaffold (**26067**) was promising in that it could both retain the structural motifs necessary for binding in the S2 and S3 pockets, which we elucidated in our previous work, and potentially improve the pharmacokinetic profile by reducing the rotational degrees of freedom and hydrogen bonding as compared to the dipeptide nitrile inhibitor class (**Figure 24**). To the best of our knowledge, no

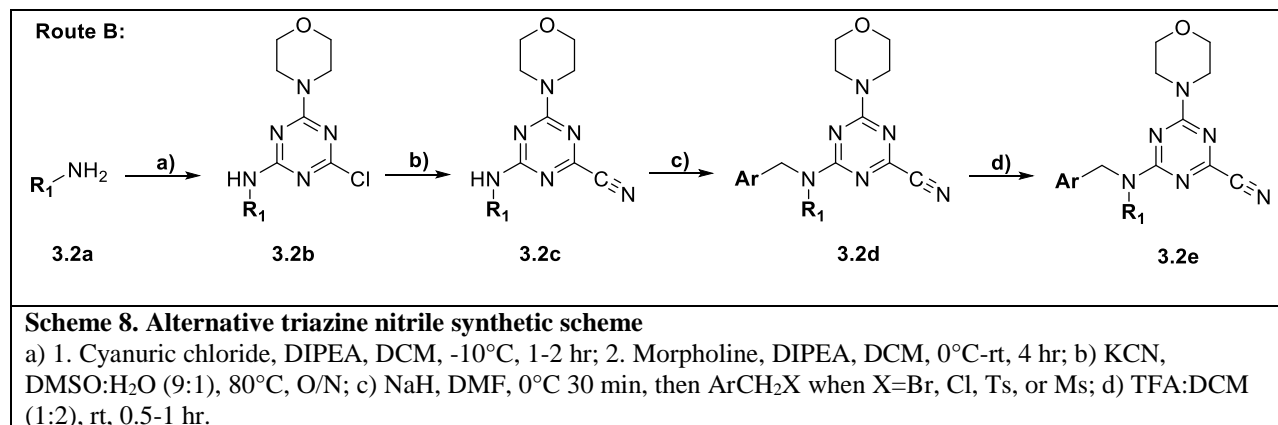
one has yet demonstrated that these triazine nitrile inhibitors targeting parasitic cathepsins are able to cross the BBB. As such, this remained one of our overarching goals in the development of *Tg*CPL inhibitors.



Synthesis of Triazine Nitriles



Under anhydrous conditions, the desired arylaldehyde or acetophenone (**3.1a**) was condensed with the desired alkylamine overnight, at which point the formed amine was reduced with sodium triacetoxyborohydride (**Scheme 7**). Next, the reaction between the secondary amine (**3.1b**) and cyanuric chloride provides intermediates (**3.1c**). Subsequent S_NAr with morpholine provides intermediates (**3.1d**). In the case of **263392**, oxetanamine was used as the P1 solubilizing group in place of morpholine. Finally, cyanation of the scaffold with potassium cyanide in DMSO provided the desired final compounds (**3.1e**).



To expedite rapid production of diverse analogs, synthetic strategy analogous to that reported by Giroud et. al. for the synthesis of triazine-nitrile *HsCPL* inhibitors was employed.¹⁵⁸

First, cyanuric chloride underwent S_NAr reactions with the desired benzyl or alkyl amines (**3.2a**) to set the various S2 and S3 vectors for intermediates (**3.2b**, **Scheme 8**). A second S_NAr step was employed to install a morpholine as a P1 solubilizing group. Cyanation of the intermediate was performed with potassium cyanide in DMSO, to afford **3.2c**. Subsequently, the anion of intermediates (**3.2c**) was generated using sodium hydride and the desired alkyl/benzyl halide was added to provide analogs (**3.2d**). In the case of analogs bearing a Boc-protected amine side chain, TFA:DCM deprotection was employed to provide the desired final compounds (**3.2e**).

Results

- Docking of Triazine Lead with *TgCPL*

The initial IC_{50} for the triazine nitrile (**26067**, **Table 11**) we identified in our HTS was benchmarked at 3.5 μ M and 2.3 μ M against *TgCPL* and *HsCPL* respectively. Considering this lead bears an ethyl as the only potential P2/3 vector, it left obvious room for improvement. Based on our previous work in exploring the SAR for selective and potent *TgCPL* inhibition with the dipeptide nitrile chemotype, we elected to first synthesize the triazine nitrile (**262962**) analogous to an optimum dipeptide nitrile from our previous work, as we expected it would bind within the previously developed pharmacophore (**Figures 24 and 25**). The triazine nitrile replaces the P1-P2 amide bond and retains the reversibly covalent nitrile interaction with the active site cysteine. In the P2 position, we previously found that leucine is the optimal amino acid, so in the respective position, we placed an isoamyl amine to achieve the same length into the S2 pocket. In P3, our most active compound previously bore a 4-fluorobenzyl, and as such, we place the same in the respective position for the triazine nitrile scaffold. An additional feature found both in our HTS lead and known literature analogs was the P1 morpholine. While the S1

pocket in *TgCPL* is absent, the morpholine in the P1 position projects into solvent and has been shown to improve the solubility of this chemotype (**Figure 25**).

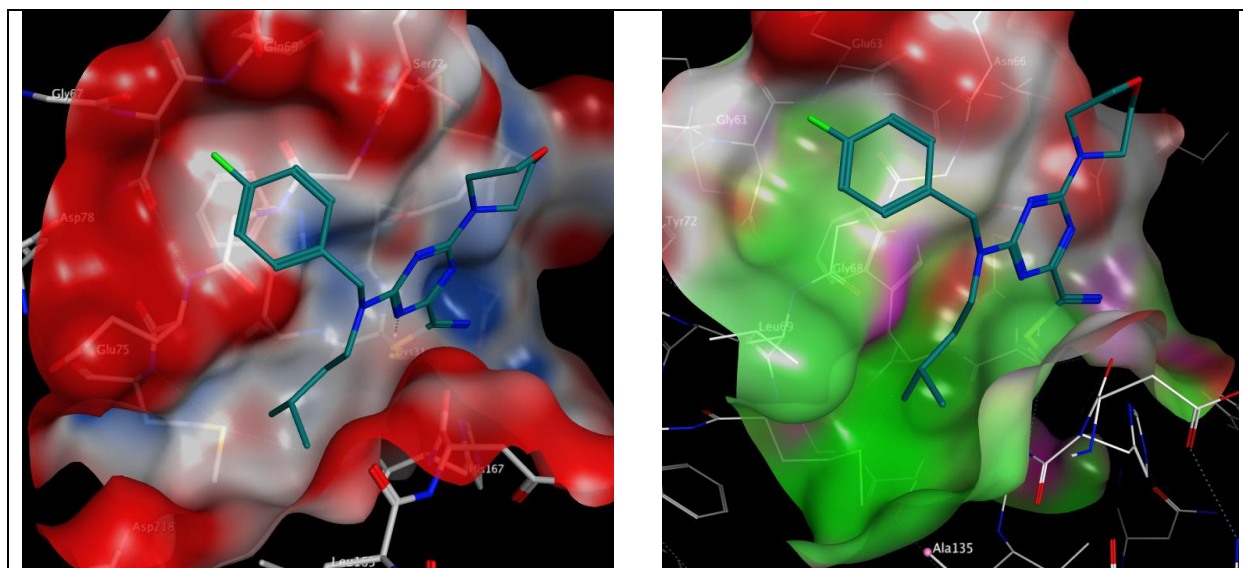


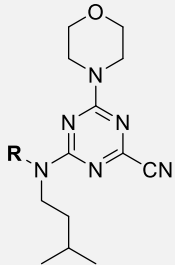
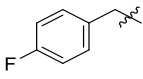
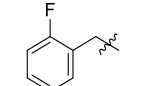
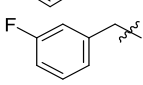
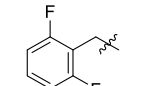
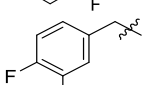
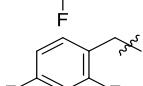
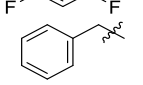
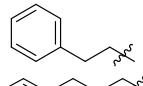
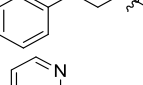
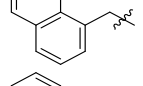
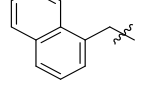
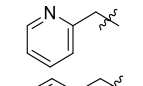
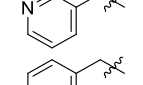
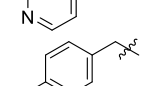
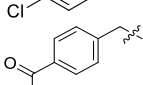

Figure 25. Covalent docking of 262962 into *TgCPL* and *HsCPL*

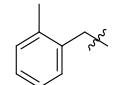
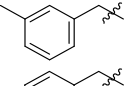
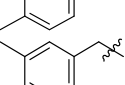
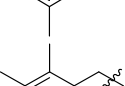
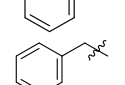
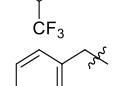
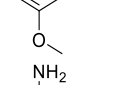
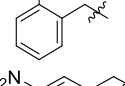
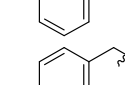
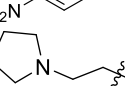
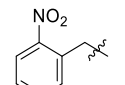
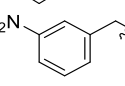
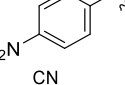
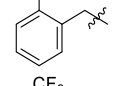
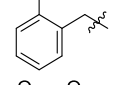
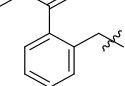
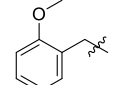
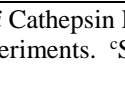
Covalent docking of **262962** into *TgCPL* active site and electrostatic surface mapping. Red= polar negative, White = neutral, Blue= polar positive. (Derived from PDB: 3F75); **Right:** Overlay of **262962** in *HsCPL* (PDB: 5MAJ). Pocket view; Red= polar negative, White= neutral, Green= lipophilic

The installment of these two pendants indeed provided over a 100-fold improvement in potency, affording an IC_{50} of 34 nM and 32 nM for *TgCPL* and *HsCPL* respectively. We were pleased to see that the pharmacophore developed for the dipeptide nitrile series, readily translated to the triazine-nitrile scaffold.

- SAR of P3 Vectors

Table 11. SAR of P3 vectors

	R	<i>TgCPL</i> ^a IC ₅₀ (μM)	<i>HsCPL</i> ^b IC ₅₀ (μM)	Selectivity for <i>HsCPL</i> ^c	n =
26067 (HTS Lead)	H	3.5	2.3	1.5	3
262962		0.034	0.032	1.1	20+
263587		0.055	0.022	2.5	2
263588		0.049	0.019	2.6	2
263579		0.51	0.039	13	2
264180		0.060	0.043	1.4	2
264181		0.064	0.04	1.6	2
264301		0.14	0.087	1.6	2
263466		0.15	0.076	2	2
263589		0.16	0.044	3.6	2
263580		92.1	0.013	7,084	2
263581		11	0.025	440	2
263462		0.088	0.034	2.6	2
263464		0.042	0.006	7	2
263468		0.13	0.039	3.3	2
263578		0.039	0.003	13	2
263582		0.095	0.036	2.6	4

264183		0.086	0.16	0.54	2
263590		0.068	0.030	2.3	2
263591		0.014	0.006	2.3	2
263583		0.037	0.041	0.9	3
263584		0.017	0.047	0.36	3
263586		0.018	0.004	4.5	2
263585		0.047	0.006	7.8	2
263659		0.29	0.100	2.9	2
263660		0.12	0.028	4.3	2
263686		0.19	0.43	0.44	2
263684		0.25	0.35	0.71	2
263592		0.027	0.103	0.26	4
263593		0.055	0.019	2.9	2
263594		0.041	0.030	1.4	2
264179		0.154	0.081	1.9	2
264184		1.42	0.361	3.9	2
264185		0.14	0.122	1.2	2
264186		1.42	0.087	16	2

^{a,b}IC₅₀ for *Toxoplasma gondii* Cathepsin L (*TgCPL*) or human Cathepsin L (*HsCPL*). Values are mean of at least 2 independent experiments. ^cSelectivity ratio for human Cathepsin L as defined by *TgCPL* IC₅₀/*HsCPL* IC₅₀.

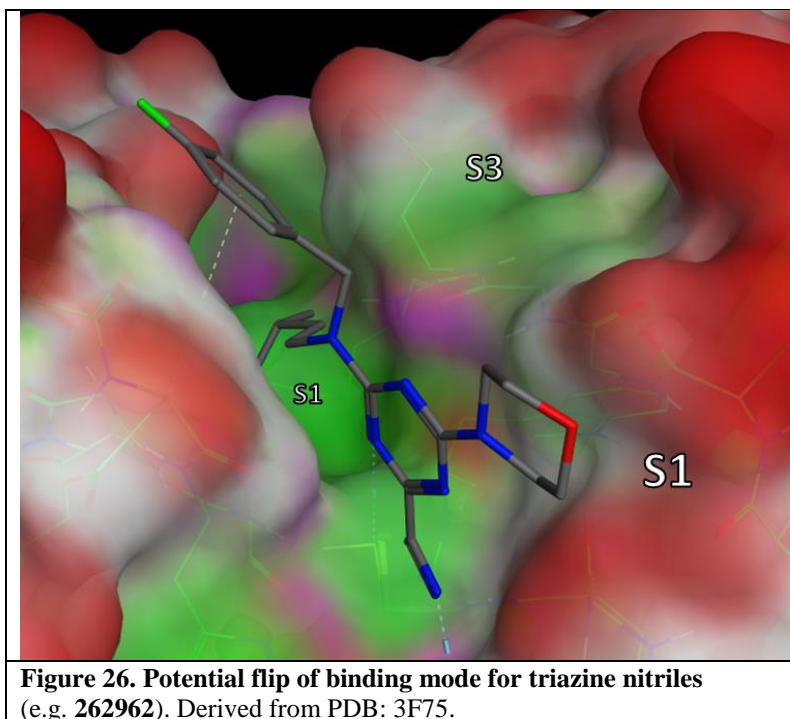
To further explore the SAR trends for the triazine nitriles and elucidate features necessary for isoform selectivity, we decided to keep an isoamyl P2 vector and first vary the P3 position (**Table 11**). A scan of fluorine mono- substitution of the P3 benzyl (**263587** and **263588**) showed retention of activity, but no significant improvement in either overall potency or selectivity. A similar trend was seen with the P3 di-fluoro analogs **263579**, **264180**, and **264181**. The non-fluorinated P3 benzyl pendant **264301** exhibited roughly a 4-fold loss of potency (*TgCPL* IC₅₀ = 0.14 μM) versus the 4-fluoro lead **262962**. Homologation of the linker from methyl to ethyl (**263466**) or propyl (**263589**), while better tolerated for the human isoform, resulted in the same reduced potency for *TgCPL*. An even greater loss of potency for the parasitic enzyme was seen when large bulky pendants like the quinoline or naphthyl of **2635780** and **263581** were installed. Taken together, this demonstrates that the parasitic isoform does not tolerate large steric vectors in the P3 position.

The P3 pocket of *TgCPL* is topologically more polar versus the human isoform. With this in mind, we tried the 2-, 3-, and 4-pyridyl pendants (**263462**, **263464**, and **263468**) in P3, with the hope that it would improve our selectivity for the parasite, as well as potentially improve our metabolic profile by decreasing the clogP. Of these, the 3-pyridyl (**263464**) retained potency (*TgCPL* IC₅₀ = 39 nM), but unfortunately did not offer any improvement in either metabolic stability (MLM t_{1/2} = 6 min), or selectivity over the human isoform (*HsCPL* IC₅₀ = 6 nM). Anilines **263659**, **263660**, and **263686** were evaluated. We had hoped to gain a meaningful interaction with Asp78, Gln69, or Glu75, but none of the anilines were very potent for *TgCPL*. However, analog **263686** did afford a small measure of selectivity toward *TgCPL* (*TgCPL* IC₅₀ = 190 nM, *HsCPL* IC₅₀ = 430 nM). Similarly, analog **263684** was tested to determine if a basic

amine might afford some difference in selectivity, but resulted in over a 5-fold loss in potency versus parent.

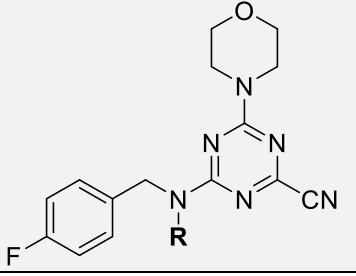
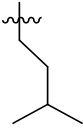
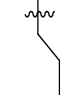
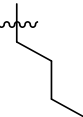
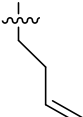
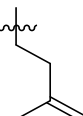
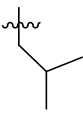
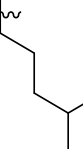

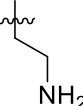
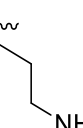
As a comparison to our 4-fluorobenzyl pendant, we tested the 4-chlorobenzyl analog **263578** to determine if the larger halogen might provide any improvement. While equally effective in *TgCPL* to the 4-fluoro, this change afforded an order of magnitude improvement in potency for *HsCPL* (*TgCPL* IC_{50} = 39 nM, *HsCPL* IC_{50} = 3 nM). Analog **263582** was synthesized to assess the effects of a moderately electron withdrawing acetophenone, but afforded a mild reduction in potency against *TgCPL* (IC_{50} = 86 nM). A methyl scan was performed to probe the space around the ring and determine if any of the substitution patterns may lead toward some selectivity for *TgCPL*. While **264183** and **263590** did not offer any improvement in potency, **263591** was nearly twice as potent (*TgCPL* IC_{50} = 14 nM) as the parent scaffold **262962**, but more significantly improved *HsCPL* inhibition (*HsCPL* IC_{50} = 6 nM). It is worth noting that the *o*-methyl benzyl, while less potent than the 4-fluorobenzyl, showed some selectivity for *TgCPL* (2-fold over *HsCPL*) for the first time in this series. Dimethyl analogs **263583** and **263584** provided more potent inhibitors and stayed consistent with the trend that an ortho substitution (**263584**) may be slightly selective for *TgCPL*. Undesirably, these also increased overall molecular weight and potential metabolic hotspots, and therefore were not further pursued. The electron withdrawing 3-trifluoromethyl **263586** provided one of the more potent *TgCPL* inhibitors, but exhibited selectivity in favor of *HsCPL*. The increased MW versus **262962** was also undesirable in trying to remain within the calculated properties for BBB permeability. The corresponding 3-methoxy analog **263585** was also tested to assess the effects of electron donation into the ring, however this did not seem to offer any significant difference in

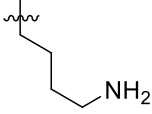
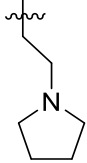
potency or selectivity as compared to **263586**. Interestingly, a nitro scan in analogs **263592**, **263593**, and **263594**, we found that the *o*-nitrobenzyl P3 vector of **263592** exhibited a 4-fold selectivity over the human isoform (*TgCPL* IC₅₀ = 27 nM, *HsCPL* IC₅₀ = 103 nM). As this was the first analog that demonstrated significant selectivity in favor of *TgCPL*, analogs **264179**, **264184**, **264185**, and **264186** were synthesized in an effort to better explain the selectivity. The nitrile (**264179**), trifluoromethyl (**264184**), and methyl ester (**264184**) vectors were tested as isosteres of the nitro. Unfortunately, none of these substituents reproduced the selectivity we saw with the *o*-nitro vector. The *o*-methoxy analog **264186** was also synthesized to determine if the observed effects were due to the electron withdrawing nature of the nitro, or a conformational change due to sterics. While tolerated in *HsCPL* (IC₅₀ = 87 nM), the potency significantly decreased against *TgCPL* (IC₅₀ = 1,420 nM). Based on our modeling (**Figure 26**), it appears that the P3 pendant may have the ability to bind outside of the S3 pocket and interact with lipophilic backbone of Asp166, giving rise to high vector tolerance.



- SAR Analysis of P2 Vectors

Table 12. Screen of various P2 vectors

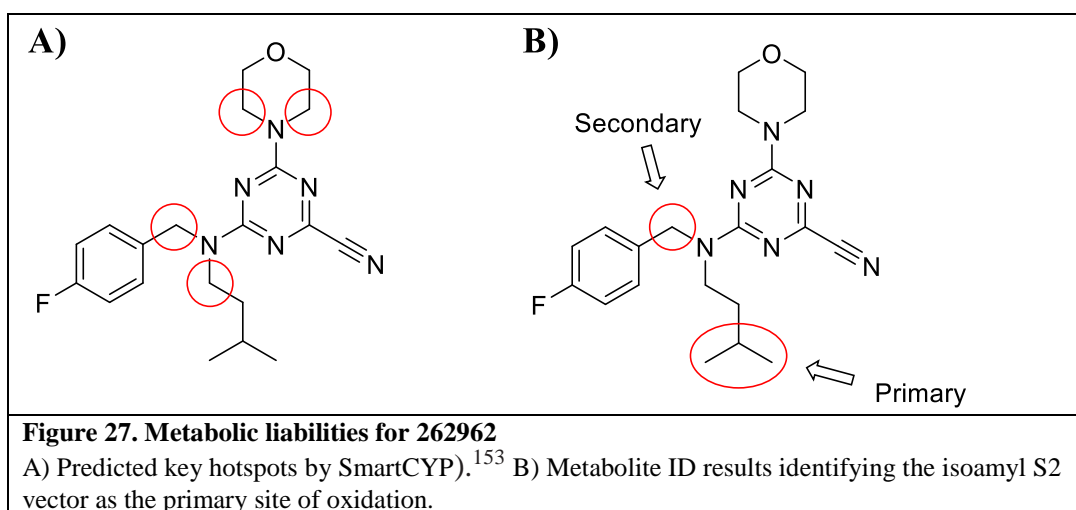
	R	<i>TgCPL</i> ^a IC ₅₀ (μ M)	<i>HsCPL</i> ^b IC ₅₀ (μ M)	Selectivity for <i>HsCPL</i> ^c	n
262962		0.034	0.032	1.1	20+
263256		0.23	0.079	2.9	2
263898		0.18	0.035	5.1	2
263255		0.19	0.071	2.7	2
263918		0.041	0.034	1.2	1
263043		0.067	0.023	29	3
263939		0.37	0.40	0.925	1
263257		1.4	0.28	5	1
264084		7.1	3.1	2.3	1
264082		2.0	2.3	0.87	2

264083		1.7	0.76	2.2	2
263661		2.1	1.8	1.2	2

^{a,b}IC₅₀ for *Toxoplasma gondii* Cathepsin L (*TgCPL*) or human Cathepsin L (*HsCPL*). Values are mean of at least 2 independent experiments. ^cSelectivity ratio for human Cathepsin L as defined by *TgCPL* IC₅₀/*HsCPL* IC₅₀.

We then turned our attention to evaluating the SAR in the S2 vectors for the triazine nitrile series. In general, the papain family proteases determine their substrate specificity from interactions in the S2 pocket.^{124, 161} Based on our previous SAR studies with the dipeptide nitriles, we had determined that leucine was the optimal amino acid for the P2 position. We were pleased to find that with (**262962**), the isoamyl sidechain in the respective position for the triazine nitriles afforded a huge improvement in potency (*TgCPL* IC₅₀ = 34 nM) as compared to the dipeptide nitriles. We wanted to determine if the previous SAR trends we found tracked in a similar fashion with this new chemotype. Initially, we evaluated the effects of shorter, aliphatic vectors. The n-propyl, n-butyl, and n-butene (**263256**, **263898**, and **263255**) were tolerated in *HsCPL*, but all decreased in potency for *TgCPL*. Consistent with our previous SAR, the isobutyl S2 vector in **263043**, which closely mimics a valine residue, slightly decreased activity for *TgCPL* to 67 nM, but enhanced *HsCPL* inhibition (IC₅₀ = 2 nM). Interestingly, the dehydroleucine analog **263918** retained nearly equivalent potency (*TgCPL* IC₅₀ = 41 nM) to **262962**, a trend that was not observed in the dipeptide series. This indicated to us that while similar, the SAR between the dipeptide and triazine chemotypes was not identical and that binding with the triazine nitrile series may be somewhat more accommodating to changes.

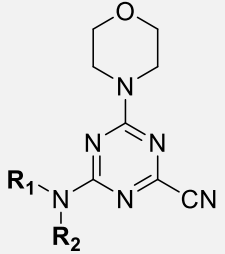
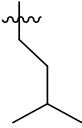
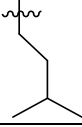
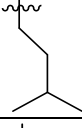
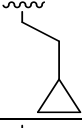
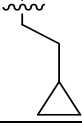
Extension of the S2 sidechain by one carbon in **263939** resulted in a significant loss of potency, we believe this may be due to a clash in the back of the S2 pocket disallowing elongated sidechains in the position. Compound **263257** was made to determine if the S2 pocket could tolerate a less lipophilic group thereby reducing overall clogP and improving compound solubility. Unfortunately, this resulted in a large decrease in potency for both enzymes (*TgCPL* IC₅₀ = 1.4 μM, *HsCPL* IC₅₀ = 0.28 μM). Given that *TgCPL* bears a unique Asp218 versus the Ala214 in *HsCPL* (**Figure 23**), we hoped the inclusion of a polar or basic group in the S2 position might afford some selectivity, as well as improve compound solubility. As such, compounds **264084**, **264082**, **264083**, and **263661** were synthesized. We had hoped that the stepwise increase in side chain length might elucidate the ideal distance required to gain a meaningful interaction with Asp2148. Unfortunately, these changes were not well tolerated and resulted in a drastic drop in potency down to the low micromolar range for both enzymes, indicating that perhaps these compounds are not binding as predicted, or the Asp218 is not oriented that way it appears in the model.

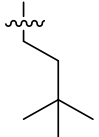
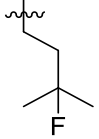
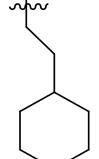
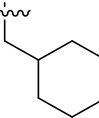
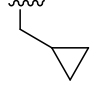
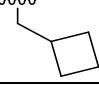
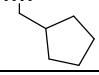
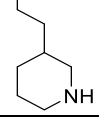
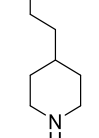
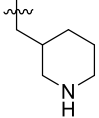
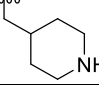
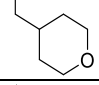
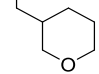


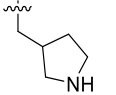
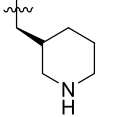
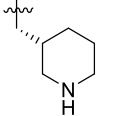
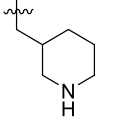
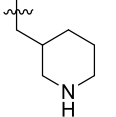
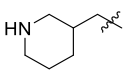
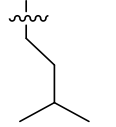
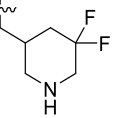
While the improvement in both potency and predicted CNS profile of the triazine scaffold was encouraging, it resulted in a significant reduction in metabolic stability compared to the dipeptide series, as measured by MLM $t_{1/2}$. (6 min versus 22 min). To aid the PK optimization of this new triazine nitrile series, a metabolite ID study was completed for **262962**. **Figure 27** shows that the hotspots for metabolism are predominantly oxidation of the P2 isoamyl vector, and the P3 benzylic methylene. With this guidance in mind, analogs were designed to retain the physiochemical profile of a CNS drug and simultaneously circumvent these potential metabolic liabilities.

- **P2 Vectors for Improved Metabolic Profile and Selectivity**

Table 13. P2 Vectors for Improved Metabolic profile and Selectivity

	R₁	R₂	TgCPL^a IC₅₀ (μM)	HsCPL^b IC₅₀ (μM)	Selectivity for HsCPL^c	n
262962	4-Fluorobenzyl		0.034	0.032	1.1	20+
263251	4-Fluoro- α -methylbenzyl		0.026	0.015	1.7	3
263392*	4-Fluoro- α -methylbenzyl		0.119	0.027	4.4	2
263698	4-Fluorobenzyl		0.19	0.15	1.3	2
264079	4-Fluoro- α -methylbenzyl		0.143	0.103	1.4	3

263806	4-Fluorobenzyl		0.068	0.16	0.43	3
263919	4-Fluorobenzyl		0.019	0.030	0.63	2
263682	4-Fluorobenzyl		100	130.8	0.76	2
263683	4-Fluorobenzyl		0.026	0.095	0.27	4
263253	4-Fluorobenzyl		3.6	0.066	54.5	3
263254	4-Fluorobenzyl		0.11	0.090	1.2	2
264503	4-Fluorobenzyl		0.035	0.069	0.51	2
264039	4-Fluorobenzyl		2.24	1.295	1.7	1
264038	4-Fluorobenzyl		0.29	0.98	0.30	2
264081	4-Fluorobenzyl		0.107	1.02	0.10	3
264182	4-Fluorobenzyl		1.21	1.86	0.65	2
264224	4-Fluorobenzyl		0.60	0.14	4.3	2
264239	4-Fluorobenzyl		0.039	0.19	0.21	2

264225	4-Fluorobenzyl		0.93	0.53	1.8	2
264501	4-Fluorobenzyl		1.02	1.95	0.52	2
264502	4-Fluorobenzyl		1.1	1.5	0.73	2
264261	2-Nitrobenzyl		2.8	1.2	2.3	3
264504	H		9.1	4.6	2.0	3
264521			0.164	0.12	1.4	3
264522	4-Fluorobenzyl		1.7	0.75	2.3	2
^{a,b} IC ₅₀ for <i>Toxoplasma gondii</i> Cathepsin L (<i>TgCPL</i>) or human Cathepsin L (<i>HsCPL</i>). Values are mean of at least 2 independent experiments. ^c Selectivity ratio for human Cathepsin L as defined by <i>TgCPL</i> IC ₅₀ / <i>HsCPL</i> IC ₅₀ . *S1 vector = oxetanamine in place of morpholine						

We installed an α -methyl in analog **263251** to determine if substitution on the benzyl position was tolerated, as it may be necessary to modulate the metabolic profile. We were happy to see that this change was well tolerated and provided a small improvement in overall potency, however the potency improvement was 2-fold greater for *HsCPL*. Due to the added MW and lipophilicity, compound solubility significantly decreased versus the parent compound (**262962** = 41.9 μ M, **263251** = 16.4 μ M). To resolve this, we tried replacing the S1 morpholine group with oxetanamine in analog **263392**. While the potency decreased to 119 nM for *TgCPL*, the MW was reduced, and solubility improved to 42.2 μ M. Analogs **263698**, **263806**, and **263919** were all

synthesized with the intent of blocking oxidation of the isoamyl CH. The cyclopropyl leucine mimic (**263698**) lost an order of magnitude in potency (*TgCPL* IC₅₀ = 190 nM compared to **262962**), and the tertbutyl analog, **263806**, while 2-fold selective for *TgCPL*, decreased to 68 nM at *TgCPL*. It should be noted however, that these respective changes in the dipeptide nitrile series were not tolerated nearly as well, giving us confidence that the triazine nitriles are a superior scaffold with regards to potential for improving DMPK properties. Furthermore, this data suggests these two chemotypes are not binding in the same manner. Compound **264079** was synthesized to determine if the cyclopropyl and 4-fluoro- α -methylbenzyl combination in P2 and P3 respectively would be sufficient to slow metabolism. Unfortunately, this decreased the compound half-life in mouse liver microsomes to 4.37 min, indicating a switch to another metabolic site, such as N-dealkylation of the P2 sidechain or the P1-morpholine. Compound **263919**, bearing a fluoroleucine in S2 (a vector also not tolerated in the dipeptide series), demonstrated excellent potency for *TgCPL* (IC₅₀ = 19 nM) and *HsCPL* (IC₅₀ = 30 nM), although MLM stability was decreased to $t_{1/2}$ = 3.2 min, further indicating that blocking the primary metabolic site alone is insufficient for improving stability. The ethyl-cyclohexyl vector of **263682** resulted in a significant decrease in potency for both cathepsins, likely due to the same steric clash in the S2 pocket observed for compound **263939** (Table 12). We were excited to discover that shortening the pendant by one carbon to the methyl-cyclohexyl (**263683**) both retained potency for *TgCPL* (IC₅₀ = 26 nM) and achieved 4-fold selectivity for the parasite isoform over human. The P2 cyclopentyl in **264503** is close to the cyclohexyl in terms of potency, but slightly less selective. The smaller ring size in analogs **263253** and **263254**, decreased potency for *TgCPL* and were not further pursued.

Docking of **263683** showed that the P2 cyclohexyl ring was 3-4Å from Asp218. In hopes of gaining a favorable ionic interaction with this residue, compounds **264182** and **264081** were synthesized. Interestingly, the 4-piperidine of **264182** resulted in lost activity against both enzymes, while the 3-piperidine **264081** demonstrated moderate selectivity (10-fold) for *TgCPL*. Despite a slight decrease in overall potency to 0.107 μM, **264081** exhibited a vastly improved microsomal stability with $t_{1/2} > 60$ minutes. The addition of an extra carbon in the sidechain for analog **264039** decreased potency to 2.2 μM for *TgCPL*, analogous to the ethyl cyclohexane analog **263682**. The ethyl 4-piperidine P2 vector **264038** similarly resulted in a decrease of potency, although not as drastically (*TgCPL* $IC_{50} = 0.29$). It is difficult to explain the potency differences between, **263682**, **264038**, and **264039**, but is likely the result of changes in binding mode placing the P2 vector outside the S2 site, perhaps in the S3 pocket. The respective tetrahydropyran (THP) analogs **264224** and **264239** were made to determine if the basic amine was important for this observed activity. These displayed a similar potency and selectivity profile, with heteroatom being tolerated at the 3-position (**264239** *TgCPL* $IC_{50} = 0.040$ μM), but not at the 4-position (**264224** *TgCPL* $IC_{50} = 0.60$ μM). Unfortunately, compound **264239** was not stable to mouse liver microsomes. Reduction of the piperidine ring size to a pyrrolidine in analog **264225** abolished the selectivity and potency profile (*TgCPL* $IC_{50} = 0.93$ μM). We were curious if we might see an enhanced selectivity ratio if only the 3-piperidine sidechain was utilized, removing the S2-S3 mutually preferable 4-fluorobenzyl P3 vector. As such, analog **264504** was tested, but activity was reduced to the low micromolar range for both parasite and human isoforms. We were also interested in combining the most selective P2 (methyl 3-piperidine) and P3 (*o*-nitro benzyl) vectors we have seen in analog **264261**. Unfortunately, these

effects were not synergistic and resulted in a loss of both selectivity and potency, strongly suggesting that the two congeners are not binding the same way. In an attempt to elucidate the preferred enantiomer of the P2 3-piperidine analog, compounds **264501** and **264502** were synthesized. Curiously, activity for both decrease to the low micromolar range and they no longer exhibited the selectivity found in the racemate **264081**. While only n=2, these compounds as well as the parent racemate are currently being evaluated in the biochemical assay to rule out any potential issues with the previous assay runs.

At this point we questioned if the P2 and P3 vectors could rotate about the triazine carbon-nitrogen bond to exchange positions in the active site, offering variable binding modes between the enzymes and potentially explaining the high P2 tolerance in *HsCPL*. As we previously found with the dipeptide nitriles, *HsCPL* can bind aromatic phenylalanine-like pendants in P2, while *TgCPL* prefers leucine residues. Analog **264521** was synthesized, combining the *TgCPL* P2 preferred isoamyl with the 3-piperidine. While it appears the piperidine pendant is tolerated as a P3 vector, we observed an overall loss in potency for both isoforms (*TgCPL* IC₅₀ = 164 nM, *HsCPL* IC₅₀ = 120 nM).

Microsomal Stability and Pharmacokinetics

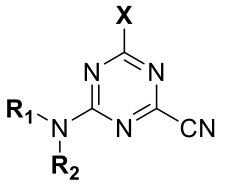
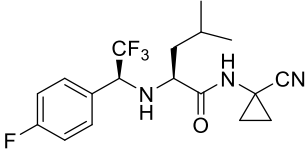
	R ₁	R ₂	X	MLM t _{1/2} (min)
262962	4-Fluorobenzyl	isoamyl	Morpholine	7
263392	4-Fluoro- α -methylbenzyl	isoamyl	Amino-oxetane	5
263919	4-Fluorobenzyl	2-fluoro-2-methylpentane	Morpholine	3.5
264079	4-Fluoro- α -methylbenzyl	propylcyclopropane	Morpholine	4.4
263464	3-pyridyl	isoamyl	Morpholine	2
263683	4-Fluorobenzyl	methyl-cyclohexyl	Morpholine	15
264081	4-Fluorobenzyl	methyl-3-piperidine	Morpholine	>60
264239	4-Fluorobenzyl	methyl-3-tetrahydropyran	Morpholine	3.5
258070				22

Figure 28. Mouse liver microsome half-life of select inhibitors

The previously developed dipeptide nitrile **258070** exhibited a fair level of stability toward mouse liver microsomes with half-life of $t_{1/2} = 22$ min (**Figure 28**). The scaffold hop to the triazine nitrile **262962** resulted in a significant drop in metabolic stability ($t_{1/2} = 7$ min). The predicted metabolic liabilities by SmartCyp (**Figure 27A**) led us to install the α -methyl and exchange the P1 solubilizing group with an oxetane in analog **263392**. Unfortunately, this did not offer any improvement to the microsomal stability profile for this series ($t_{1/2} = 5$ min). Our subsequent metabolite ID study (**Figure 27B**) indicated that the primary site of metabolism was the isoamyl P2 vector. Compound **263919** was synthesized, as the fluoroleucine has been shown to be an effective strategy in blocking the metabolism of a leucine sidechain in the development of odanacatib.¹⁶² This exchange resulted in a decrease in compound half-life to $t_{1/2} = 3.5$ min. In

an attempt to block both the P2 and benzylic oxidation sites, compound **264079** was made. Unfortunately, this did not seem to have any improvement on microsomal stability with at $t_{1/2} = 4.4$ min. Compound **263464** was tested to determine if metabolism could be reduced by decreasing lipophilicity. Compound lipophilicity was lowered to $\text{clogP} = 1.90$ (versus $\text{clogP} = 3.39$ for **262962**) but resulted in an even worse half-life ($t_{1/2} = 2$ min). We were pleased to find that the methyl-cyclohexyl analog **263683** offered an improvement in metabolic stability ($t_{1/2} = 15$ min), likely due to steric bulk of P2 impeding CYP binding, as well as retained potency and gained 4-fold selectivity for TgCPL. The related P2 3-piperidine analog **264081** drastically improved the microsomal stability to $t_{1/2} > 60$ min, presumably due simply to reducing ClogD. Similarly, the 3-tetrahydropyran analog **264239** was tested, but exhibited a significantly worse stability ($t_{1/2} = 3.5$ min). The drastic improvement seen for compound **264081** is likely due to the added charge of the basic amine impeding CYP binding.

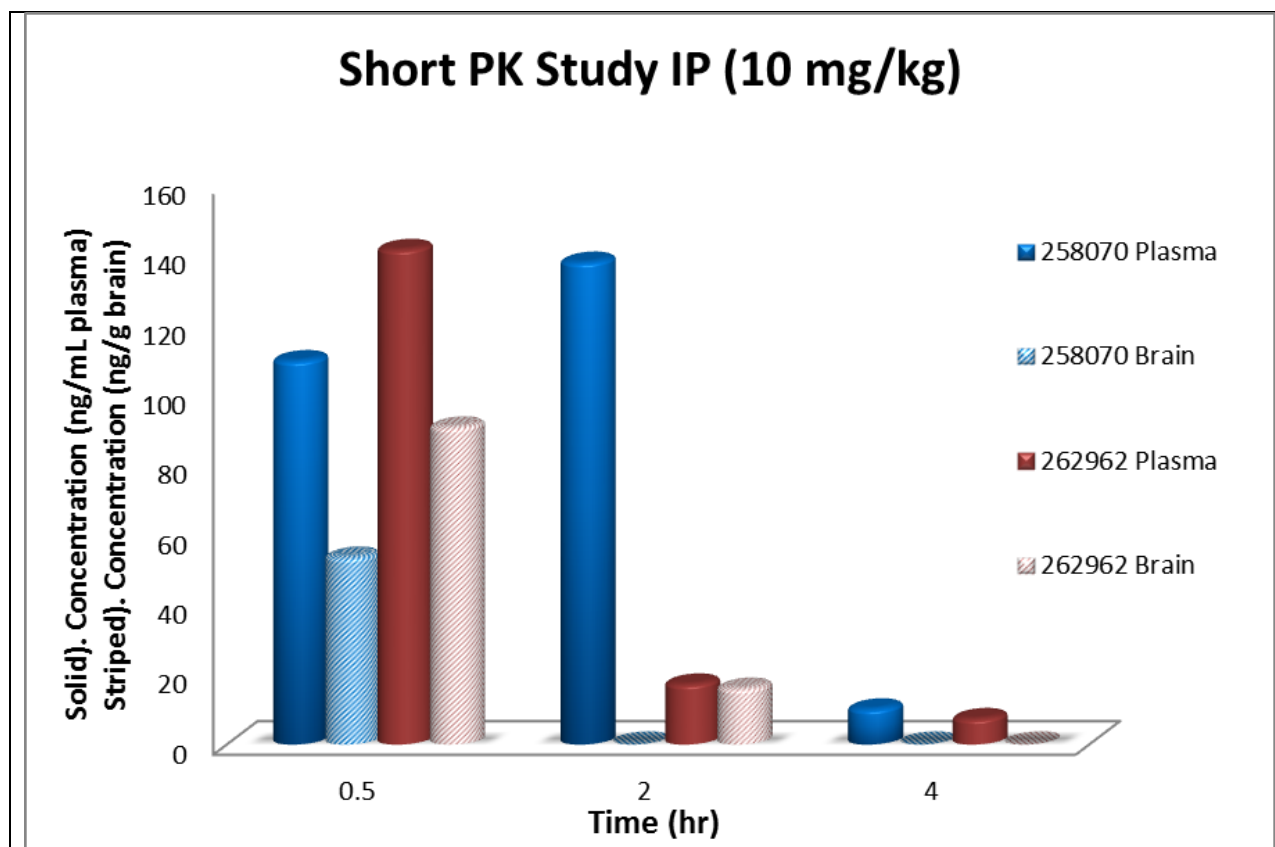
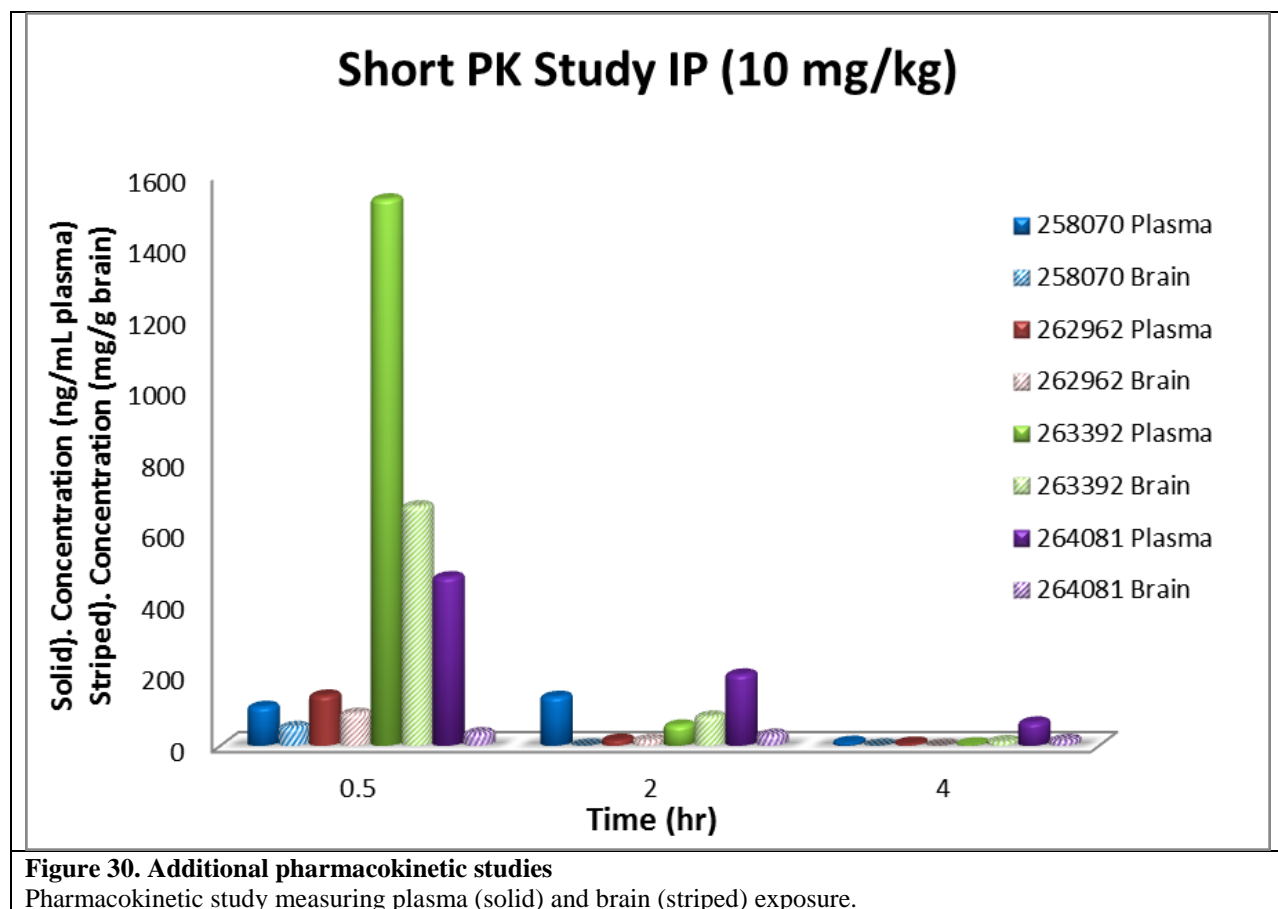


Figure 29. Initial Pharmacokinetic studies

Pharmacokinetic study measuring plasma (solid, ng/mL) and brain (striped, ng/g) exposure.

Compound **262962** was evaluated in a mouse PK study to benchmark the CNS profile of the triazine nitrile chemotype and compare it to that of the dipeptide nitrile **258070** (**Figure 29**). We were pleased to find that this **262962** does in fact access the brain with approximately a 1:1 ratio brain/plasma at 2h. However, the compound levels are decreased rather quickly, likely due to a combination of high volume of distribution and metabolic instability. Nonetheless, this was a promising result indicating that the triazine nitrile scaffold has the physicochemical profile needed to cross the BBB. We hoped that by increasing the metabolic stability of the scaffold, we might gain a better pharmacokinetic profile. We attempted to evaluate compound **263683**, as this analog exhibited an improved half-life, retained potency, and demonstrated some selectivity for *TgCPL*, but unfortunately its poor solubility precluded in vivo dosing. As mentioned above, the

replacement of the P1 morpholine of **263251** with a 3-amino-oxetane in compound **263392**, offered an improvement in solubility (16.4 μM to 42.2 μM respectively). We decided to run a short PK study on **263392** to determine if the additional hydrogen bond donor of the oxetanamine would impact our CNS penetrance, or if this could be a viable strategy to improve the solubility of future compounds (**Figure 30**).



We were very pleased to find that in addition to retaining a brain to plasma ratio of ~1 after 2 hr, the overall exposure levels were significantly increased compared to **262962** (**Figure 30**). Often, the incorporation of a basic amine can improve the CNS access of a drug, as well as increase compound solubility. Given that the 3-piperidine P2 vector in **264081** significantly

improved the metabolic stability of this compound, we decided to also profile this analog in a short PK. While the exposure levels were improved in plasma versus **262962**, this compound no longer exhibited BBB penetrance. The difluoro-3-piperidine compound **264522** was synthesized with the intent of tuning the basicity of this sidechain in an effort to overcome the PgP efflux (**Table 14**) observed with **264081**. Unfortunately, this change was not well tolerated and potency was reduced to low micromolar for this compound (T_gCPL $IC_{50} = 1.7 \mu M$).

- **MDR1/MDCK Permeability and Efflux**

Because of their strikingly divergent brain:plasma ratios observed in the PK studies, compounds **264801** and **263392** were assessed *in vitro* to determine whether they are potential substrates of P-glycoprotein (P-gp). We suspected this might be the case, as the incorporation of the basic amine in **264801** impedes CNS access and is often associated with P-gp substrates. Evaluation in an MDR1/MDCK permeability assay demonstrates that compound **263392** is favorably permeable toward the basal chamber with a concentration ratio of 4.25 (**Table 14**) and does not appear to be PgP substrate. This would be expected to translate to good CNS penetrance, which is in agreement with our PK results. **264801** conversely showed a concentration ratio of 0.06, indicating this compound is incapable of CNS penetrance and is likely a PgP substrate.

Table 14. MDR1 / MDCK Assay results

Sample	Concentration ^a (μM)	Conc. Ratio (B-A)/(A-B)
263392 (A-B)	0.017 ± 0.004	0.24
263392 (B-A)	0.004 ± 0.001	
264801 (A-B)	0.012 ± 0.002	15
264801 (B-A)	0.18 ± 0.08	

^a Concentration is shown as the average of two sample measurements of the acceptor wells from three replicate assays.

Conclusions

A high throughput screen was conducted to identify new chemotypes capable of the inhibition of *Toxoplasma gondii* cathepsin L. The low μM triazine nitrile scaffold (**26067**) was selected based on the previously established literature precedent of this chemotype as inhibitors of human cathepsins and the predicted BBB penetrant properties of this scaffold. Translation of the pharmacophore developed from the dipeptide nitrile series to the triazine nitrile scaffold resulted in an instantaneous gain of potency (*TgCPL* $\text{IC}_{50} = 34 \text{ nM}$), but reduced metabolic stability relative to the corresponding dipeptide. 71 analogs in this series were synthesized with varying S2 and S3 vectors to optimize metabolic stability, CNS permeability, and selectivity over human isoforms. Out of the nine analogs bearing an amine in P2, all exhibited IC_{50} s for *HsCPL* of $>0.5 \mu\text{M}$, supporting that the human isoform does not tolerate a basic amine in this position. *TgCPL*, conversely, appears to be able to better accommodate either a nitrogen or oxygen in S2. Future analogs will be designed to exploit these features and further explore the SAR trends with various basic and polar groups in P2. Overall, we improved potency against *TgCPL* to as low as 5 nM and identified features that can be exploited to gain selectivity vs *HsCPL* (up to 5-8 fold), and significantly improved metabolic stability (up to $t_{1/2} >60 \text{ min}$ in MLM). While CNS penetrant (1:1 B/P over 2 hr) with moderate initial exposure, **263392** was probably cleared too rapidly for efficacy studies *in vivo* (**Figure 30**). By design, we were able to improve selectivity and microsomal stability with analog **264081** ($t_{1/2} >60 \text{ min}$; *Tg/Hs* $\text{IC}_{50} = 0.10$), however this analog is an apparent Pgp substrate, precluding *in vivo* target validation. Synthesis of new analogs to circumvent this issue is currently underway to advance this series toward *in vivo* studies.

Experimental

Chemistry General Information: All reagents were used without further purification as received from commercial sources unless noted otherwise. ^1H NMR spectra were taken in DMSO-*d*₆, MeOD, or CDCl₃ at room temperature on Varian Inova 400 MHz or Varian Inova 500 MHz instruments. Reported chemical shifts for the ^1H NMR spectra were recorded in parts per million (ppm) on the δ scale from an internal standard of residual tetramethylsilane (0 ppm). Mass spectrometry data were obtained on either a Micromass LCT or Agilent Q-TOF. An Agilent 1100 series HPLC with an Agilent Zorbax Eclipse Plus-C18 column was used to determine purity of biologically tested compounds. Unless otherwise noted, all tested compounds were determined to be >95% pure using a 6 minute gradient of 10-90% acetonitrile in water followed by a 2 minute hold at 90% acetonitrile with detection at 254 nm. Flash chromatographic purifications were performed using a Teledyne ISCO Combiflash RF with Redisep Gold RF columns.

General Procedure A1: Reductive Amination

To a dry round bottom flask with DCM was added arylaldehyde (1 eq), followed by the addition of the desired primary amine (1 eq), final reaction concentration of 0.1-0.3 mM. The vessel was then stirred under a nitrogen atmosphere at room temperature overnight. Sodium triacetoxyborohydride (3 eq) was then added and reaction was stirred at room temperature for 1-3 hr. The reaction was quenched slowly with water then poured into water and extracted 3x with DCM. The combined organic layer was dried over sodium sulfate and concentrated *in-vacuo*. The crude product was further purified by column chromatography (0-10% MeOH in DCM + 0.1% TEA) to afford the desired secondary amine.

General Procedure A2: S_NAr

Under a dry nitrogen atmosphere, cyanuric chloride (1 eq) was added a roundbottom flask along with DCM (final conc. = 0.1-0.3 mM). The vessel was cooled to -10°C (Ice/Brine) and the desired secondary amine (1 eq) and DIPEA (1 eq) were then added. Reaction was stirred at -10°C for 1 h. The reaction was poured into water and extracted 3x with DCM. Combined organic layers were dried over MgSO₄ and concentrated in vacuo. The crude product was further purified by column chromatography (0-100% EtOAc in Hexanes gradient) to afford the desired intermediate.

General Procedure A3: S_NAr

Under a dry nitrogen atmosphere, dichloro triazine intermediate (1 eq) was added a roundbottom flask along with DCM to a final reaction concentration of 0.1 mM. The vessel was cooled to -10°C (Ice/Brine) and DIPEA (1 eq) and morpholine (1 eq) were then added. Reaction was stirred and allowed to warm to room temperature over 6-12 h. The reaction was poured into water and extracted 3x with DCM. Combined organic layers were dried over MgSO₄ and concentrated in vacuo. The crude product was further purified by column chromatography (0-100% EtOAc in Hexanes gradient) to afford the desired intermediate.

General Procedure A4: Cyanation

A dry pressure vessel was charged with the appropriate triazinyl chloride (1.0 eq), and suspended in DMSO/H₂O 9:1. KCN (1.1 eq.) and 1,4-diazabicyclo[2.2.2]octane (DABCO, 2.0 eq.) were added and the reaction was heated to 80°C. Reaction was left to stir at this temperature

until LC/MS showed completion of the reaction (6-12 h). Reaction was cooled to room temperature, diluted with EtOAc, and washed thoroughly with brine (3-5 x). The organic layer was separated, dried over MgSO₄, filtered, and evaporated. The crude product was further purified by column chromatography (0-100% EtOAc in Hexanes gradient) to afford the desired product.

General Procedure B1: One-pot double S_NAr

Under a dry nitrogen atmosphere, cyanuric chloride (1 eq) was added a roundbottom flask along with DCM (final conc. = 0.1-0.3 mM). The vessel was cooled to -10°C (Ice/Brine) and DIPEA (1 eq) followed by the desired primary amine (1eq) were then added. Reaction was stirred at for 1-3 hr, until TLC/HPLC indicated substitution was complete. Next, DIPEA (1 eq) was added followed by morpholine (1 eq) and reaction was allowed to stir and warm to rt over 4-12h until TLC/HPLC indicated substitution was complete. The reaction was poured into water and extracted 3x with DCM. Combined organic layers were dried over MgSO₄ and concentrated in vacuo. The crude product was further purified by column chromatography (0-100% EtOAc in Hexanes gradient) to afford the desired intermediate.

General Procedure B2: Cyanation

A dry pressure vessel was charged with the appropriate triazinyl chloride (1.0 eq), and suspended in DMSO/H₂O 9:1. KCN (1.1 eq) and 1,4-diazabicyclo[2.2.2]octane (DABCO, 2.0 eq) were added and the reaction was heated to 80°C. Reaction was left to stir at this temperature until LC/MS showed completion of the reaction (6-12 h). Reaction was cooled to room temperature, diluted with EtOAc and washed thoroughly with brine (3-5 x). The organic layer

was separated, dried over MgSO₄, filtered, and evaporated. The crude product was further purified by column chromatography (0-100% EtOAc in Hexanes gradient) to afford the desired secondary amine.

General Procedure B3: Alkylation with NaH and aryl/alkyl X/Ms/Ts

The triazinyl-nitrile (1 eq) was dissolved in DMF and cooled to -10°C (Ice/Brine bath). 60% NaH in mineral oil (1-1.5 eq) was added and reaction was stirred for 30 min. The appropriate alkyl or aryl Br/Cl/Ms/Ts (1-2 eq) was then added. The reaction was allowed to slowly warm to room temperature and left to stir (2-12 hr) until HPLC indicated reaction was complete. The solution was poured into EtOAc, washed 3x with brine, dried over NaSO₄, and concentrated. Crude residue was purified by flash chromatography EtOAc:Hexanes 0-100% gradient.

General Procedure B4: Boc-Deprotection

The Boc-protected amine (1 eq) was dissolved into a 1:2 mixture of TFA:DCM (~0.1-0.3 mM) and allowed to stir at room temperature for 0.5-2h, until HPLC or TLC indicated reaction was complete. Solvent was removed in vacuo and compound was purified by reverse phase chromatography (C18, 10-100% ACN in water + 0.1% TFA gradient) and concentrated to afford desired product as the TFA salt.

All final compounds exist as rotamers on the NMR timescale.

N-(4-Fluorobenzyl)-3-methylbutan-1-amine

General Procedure A1 from 4-fluorobenzaldehyde (0.5 ml, 4.66 mmol), 3-methylbutan-1-amine (0.541 ml, 4.66 mmol), and sodium triacetoxyborohydride (2470 mg, 11.65 mmol) gave N-(4-fluorobenzyl)-3-methylbutan-1-amine (870 mg, 4.46 mmol, 96 % yield).; ¹H NMR (CDCl₃, 500 MHz) δ 7.27 (dd, *J* = 5.62, 8.07 Hz, 2H), 6.99 (t, *J* = 8.56 Hz, 2H), 3.75 (s, 2H), 2.62 (t, *J* = 7.34 Hz, 2H), 1.56 - 1.69 (m, 1H), 1.34 - 1.45 (m, 2H), 0.89 (d, *J* = 6.36 Hz, 6H)

4,6-Dichloro-N-(4-fluorobenzyl)-N-isopentyl-1,3,5-triazin-2-amine

General Procedure A2 from 2,4,6-trichloro-1,3,5-triazine (142 mg, 0.768 mmol), N-(4-fluorobenzyl)-3-methylbutan-1-amine (150 mg, 0.768 mmol), and DIPEA (0.134 ml, 0.768 mmol) gave 4,6-dichloro-N-(4-fluorobenzyl)-N-isopentyl-1,3,5-triazin-2-amine (243 mg, 0.708 mmol, 92 % yield).; ¹H NMR (CDCl₃, 500 MHz) δ 7.23 (dd, *J* = 5.38, 8.31 Hz, 2H), 7.03 (t, *J* = 8.56 Hz, 2H), 4.79 (s, 2H), 3.51 - 3.56 (m, 2H), 1.49 - 1.61 (m, 1H), 1.40 - 1.48 (m, 2H), 0.92 (d, *J* = 6.36 Hz, 6H)

4-Chloro-N-(4-fluorobenzyl)-N-isopentyl-6-morpholino-1,3,5-triazin-2-amine

General procedure A3 from 4,6-dichloro-N-(4-fluorobenzyl)-N-isopentyl-1,3,5-triazin-2-amine (243 mg, 0.708 mmol), morpholine (0.062 ml, 0.708 mmol), and DIPEA (0.124 ml, 0.708 mmol) gave 4-chloro-N-(4-fluorobenzyl)-N-isopentyl-6-morpholino-1,3,5-triazin-2-amine (205 mg, 0.520 mmol, 73.5 % yield). Product could be recrystallized from hot EtOAc:Hexanes (2:1).; ¹H NMR (CDCl₃, 500 MHz) δ 7.15 - 7.25 (m, 2H), 6.99 (t, *J* = 8.56 Hz, 2H), 4.74 (s, 2H), 3.73 - 3.88 (m, 4H), 3.60 - 3.73 (m, 5H), 3.49 - 3.56 (m, 1H), 3.39 - 3.46 (m, 1H), 1.47 - 1.61 (m, 1H), 1.39 - 1.46 (m, 2H), 0.89 (t, *J* = 6.85 Hz, 6H)

4-((4-Fluorobenzyl)(isopentyl)amino)-6-morpholino-1,3,5-triazine-2-carbonitrile (262962)

General Procedure A4 starting from 4-chloro-N-(4-fluorobenzyl)-N-isopentyl-6-morpholino-1,3,5-triazin-2-amine (200 mg, 0.508 mmol) and DABCO (114 mg, 1.016 mmol) gave 4-((4-fluorobenzyl)(isopentyl)amino)-6-morpholino-1,3,5-triazine-2-carbonitrile (136 mg, 0.354 mmol, 69.7 % yield); ¹H NMR (CDCl₃, 400 MHz) δ 7.13 - 7.25 (m, 2H), 7.00 (t, J = 8.22 Hz, 2H), 4.73 (d, J = 19.17 Hz, 2H), 3.74 - 3.87 (m, 4H), 3.60 - 3.74 (m, 6H), 3.52 (t, J = 7.43 Hz, 1H), 3.43 (t, J = 7.83 Hz, 1H), 1.48 - 1.60 (m, 1H), 1.37 - 1.48 (m, 2H), 0.90 (t, J = 5.87 Hz, 6H); ¹³C NMR (DMSO-*d*₆, 101 MHz, 80°C) δ 163.2, 162.7, 161.1, 150.9, 133.2, 129.0, 115.0, 114.6, 65.2, 48.5, 44.4, 43.2, 25.0, 21.7; HRMS-ESI (m/z): [M+H]⁺ calcd for C₂₀H₂₅FN₆O, 385.2147; found, 385.2144

4-Chloro-N-(4-fluorobenzyl)-6-morpholino-1,3,5-triazin-2-amine

General procedure B1 from 2,4,6-trichloro-1,3,5-triazine (1 g, 5.42 mmol), (4-fluorophenyl)methanamine (0.620 ml, 5.42 mmol), DIPEA (1.894 ml, 10.84 mmol), and morpholine (0.472 ml, 5.42 mmol) gave 4-chloro-N-(4-fluorobenzyl)-6-morpholino-1,3,5-triazin-2-amine (1.07 g, 3.30 mmol, 60.9 % yield). Product could be recrystallized from hot EtOAc:Hexanes (2:1).; ¹H NMR (CDCl₃, 500 MHz) δ 7.17 - 7.35 (m, 2H), 6.89 - 7.11 (m, 2H), 6.26 (br. s., 1H), 4.46 - 4.68 (m, 2H), 3.73 - 3.86 (m, 4H), 3.70 (br. s., 4H)

4-((4-Fluorobenzyl)amino)-6-morpholino-1,3,5-triazine-2-carbonitrile

General procedure B2 from 4-chloro-N-(4-fluorobenzyl)-6-morpholino-1,3,5-triazin-2-amine (4, 12.35 mmol), potassium cyanide (0.885 g, 13.59 mmol), and DABCO (2.77 g, 24.71 mmol) gave 4-((4-fluorobenzyl)amino)-6-morpholino-1,3,5-triazine-2-carbonitrile (2.7 g, 8.59 mmol, 69.5 % yield).; ¹H NMR (CDCl₃, 500 MHz) δ 7.21 - 7.30 (m, 2H), 6.93 - 7.06 (m, 2H), 4.49 - 4.61 (m, 2H), 3.73 - 3.86 (m, 4H), 3.69 (br. s., 4H)

4-Chloro-N-isopentyl-6-morpholino-1,3,5-triazin-2-amine

General procedure B1 from 2,4,6-trichloro-1,3,5-triazine (5, 27.1 mmol), 3-methylbutan-1-amine (3.15 ml, 27.1 mmol), DIPEA (9.48 ml, 54.2 mmol), and morpholine (2.362 ml, 27.1 mmol) gave 4-chloro-N-isopentyl-6-morpholino-1,3,5-triazin-2-amine (7.5 g, 26.2 mmol, 97 % yield). Product could be recrystallized from hot EtOAc:Hexanes (2:1). ¹H NMR (CDCl₃, 500 MHz) δ 6.06 (br. s., 1H), 3.63 - 3.88 (m, 8H), 3.33 - 3.46 (m, 2H), 1.56 - 1.68 (m, 1H), 1.44 (q, *J* = 7.01 Hz, 2H), 0.91 (d, *J* = 6.36 Hz, 6H)

4-(Isopentylamino)-6-morpholino-1,3,5-triazine-2-carbonitrile

General procedure B2 from 4-chloro-N-isopentyl-6-morpholino-1,3,5-triazin-2-amine (3.24 g, 11.34 mmol), potassium cyanide (0.812 g, 12.47 mmol), and DABCO (2.54 g, 22.68 mmol) gave 4-(isopentylamino)-6-morpholino-1,3,5-triazine-2-carbonitrile (2.1 g, 7.60 mmol, 68.7 % yield).; ¹H NMR (CDCl₃, 500 MHz) δ 3.77 - 3.91 (m, 3H), 3.64 - 3.77 (m, 5H), 3.32 - 3.49 (m, 2H), 1.65 (qd, *J* = 6.62, 13.39 Hz, 1H), 1.39 - 1.53 (m, 2H), 0.85 - 1.01 (m, 6H)

4-((2-Fluorobenzyl)(isopentyl)amino)-6-morpholino-1,3,5-triazine-2-carbonitrile (263587)

General Procedure B3 starting from 4-(isopentylamino)-6-morpholino-1,3,5-triazine-2-carbonitrile (100 mg, 0.362 mmol), sodium hydride (15.92 mg, 0.398 mmol), and 1-(bromomethyl)-2-fluorobenzene (68.4 mg, 0.362 mmol) gave 4-((2-fluorobenzyl)(isopentyl)amino)-6-morpholino-1,3,5-triazine-2-carbonitrile (67.6 mg, 0.176 mmol, 48.6 % yield) ¹H NMR (CDCl₃, 500 MHz) δ 7.24 - 7.30 (m, 1H), 7.14 - 7.21 (m, 1H), 7.01 - 7.12 (m, 2H), 4.86 (s, 1H), 4.80 (s, 1H), 3.82 (br. s., 1H), 3.78 (br. s., 2H), 3.70 - 3.75 (m, 2H), 3.67 (br. s., 2H), 3.64 (br. s., 1H), 3.55 - 3.60 (m, 1H), 3.46 - 3.52 (m, 1H), 1.56 (qd, J = 6.60, 16.38 Hz, 1H), 1.41 - 1.49 (m, 2H), 0.91 (t, J = 7.34 Hz, 6H); ¹³C NMR (CDCl₃, 126 MHz) δ 164.2, 164.1, 163.6, 163.4, 161.9, 161.8, 160.0, 159.8, 130.0, 129.9, 129.2, 129.0, 128.9, 124.3, 124.2, 115.6, 115.5, 115.4, 115.2, 66.7, 66.4, 45.6, 45.0, 43.9, 43.4, 43.3, 36.26, 35.43, 26.01, 25.88, 22.51, 22.47; HRMS-ESI (m/z): [M+H]⁺ calcd for C₂₀H₂₅FN₆O, 385.2147; found, 385.2150

4-((3-Fluorobenzyl)(isopentyl)amino)-6-morpholino-1,3,5-triazine-2-carbonitrile (263588)

General Procedure B3 starting from 4-(isopentylamino)-6-morpholino-1,3,5-triazine-2-carbonitrile (100 mg, 0.362 mmol), sodium hydride (21.71 mg, 0.543 mmol), and 1-(bromomethyl)-3-fluorobenzene (68.4 mg, 0.362 mmol) gave 4-((3-fluorobenzyl)(isopentyl)amino)-6-morpholino-1,3,5-triazine-2-carbonitrile (104 mg, 0.271 mmol, 74.8 % yield); ¹H NMR (CDCl₃, 500 MHz) δ 7.21 - 7.32 (m, 1H), 6.97 - 7.02 (m, 1H), 6.93 - 6.97 (m, 1H), 6.91 (d, J = 9.29 Hz, 1H), 4.79 (s, 1H), 4.72 (s, 1H), 3.81 - 3.85 (m, 1H), 3.79 (br. s., 2H), 3.71 - 3.75 (m, 2H), 3.68 (br. s., 1H), 3.60 - 3.66 (m, 2H), 3.51 - 3.60 (m, 1H), 3.41 - 3.50 (m, 1H), 1.48 - 1.60 (m, 1H), 1.39 - 1.48 (m, 2H), 0.90 (t, J = 7.09 Hz, 6H); ¹³C NMR (CDCl₃, 126 MHz) δ 164.2, 164.0, 163.9, 163.6, 163.4, 161.9, 152.0, 151.9, 140.2, 140.1, 140.0,

139.9, 130.1, 130.0, 123.2, 122.8, 122.7, 115.5, 114.4, 114.3, 114.2, 114.1, 114.0, 66.6, 66.3, 49.4, 49.3, 45.5, 44.8, 43.9, 43.8, 43.4, 36.2, 35.4, 26.0, 25.8, 22.5, 22.4; HRMS–ESI (m/z): [M+H]⁺ calcd for C₂₀H₂₅FN₆O, 385.2147; found, 385.2151

**4-((2,6-Difluorobenzyl)(isopentyl)amino)-6-morpholino-1,3,5-triazine-2-carbonitrile
(263579)**

General Procedure B3 starting from 4-(isopentylamino)-6-morpholino-1,3,5-triazine-2-carbonitrile (100 mg, 0.362 mmol), sodium hydride (28.9 mg, 0.724 mmol), and 2-(bromomethyl)-1,3-difluorobenzene (74.9 mg, 0.362 mmol) gave 4-((2,6-difluorobenzyl)(isopentyl)amino)-6-morpholino-1,3,5-triazine-2-carbonitrile (51.6 mg, 0.128 mmol, 35.4 % yield); ¹H NMR (CDCl₃, 500 MHz) δ 7.20 - 7.34 (m, 1H), 6.79 - 6.94 (m, 2H), 4.95 (s, 1H), 4.85 (s, 1H), 3.74 - 3.86 (m, 4H), 3.66 - 3.74 (m, 4H), 3.55 (t, J = 7.80 Hz, 1H), 3.43 (t, J = 7.80 Hz, 1H), 1.46 - 1.59 (m, 1H), 1.34 - 1.46 (m, 2H), 0.90 (d, J = 6.36 Hz, 3H), 0.87 (d, J = 6.85 Hz, 3H); ¹³C NMR (CDCl₃, 126 MHz) δ 163.8, 163.7, 163.6, 163.4, 163.0, 163.0, 162.9, 162.8, 161.0, 160.9, 160.8, 151.9, 151.6, 129.8, 129.7, 129.6, 129.5, 115.6, 112.9, 111.5, 111.4, 111.3, 66.7, 66.4, 45.1, 44.2, 43.9, 43.4, 37.9, 36.1, 35.2, 26.0, 25.9, 22.5; HRMS–ESI (m/z): [M+H]⁺ calcd for C₂₀H₂₄F₂N₆O, 403.2058; found, 403.2055

**4-((3,4-Difluorobenzyl)(isopentyl)amino)-6-morpholino-1,3,5-triazine-2-carbonitrile
(264180)**

General Procedure B3 starting from 4-(isopentylamino)-6-morpholino-1,3,5-triazine-2-carbonitrile (50 mg, 0.181 mmol), sodium hydride (7.96 mg, 0.199 mmol), and 4-(bromomethyl)-1,2-difluorobenzene (0.023 ml, 0.181 mmol) gave 4-((3,4-

difluorobenzyl)(isopentyl)amino)-6-morpholino-1,3,5-triazine-2-carbonitrile (62 mg, 0.154 mmol, 85 % yield); ^1H NMR (CDCl_3 , 500 MHz) δ 7.10 (q, $J = 8.80$ Hz, 1H), 7.00 - 7.06 (m, 1H), 6.89 - 6.98 (m, 1H), 4.73 (s, 1H), 4.68 (s, 1H), 3.76 - 3.87 (m, 3H), 3.62 - 3.74 (m, 5H), 3.50 - 3.56 (m, 1H), 3.41 - 3.48 (m, 1H), 1.48 - 1.58 (m, 1H), 1.38 - 1.46 (m, 2H), 0.90 (t, $J = 6.60$ Hz, 6H); ^{13}C NMR (CDCl_3 , 126 MHz) δ 164.2, 164.0, 163.6, 163.5, 152.1, 151.9, 151.3, 150.7, 150.6, 149.3, 148.8, 148.6, 148.5, 134.5, 134.4, 123.7, 123.6, 123.2, 123.1, 117.4, 117.3, 117.2, 116.6, 116.4, 116.2, 116.1, 115.5, 115.4, 66.6, 66.3, 48.9, 45.4, 44.8, 44.0, 43.9, 43.4, 36.2, 35.4, 31.5, 26.0, 25.9, 22.6, 22.5, 22.4; ^{19}F NMR (CDCl_3 , 470 MHz) δ -137.2 (m), -139.53 (m); HRMS-ESI (m/z): $[\text{M}+\text{H}]^+$ calcd for, $\text{C}_{20}\text{H}_{24}\text{F}_2\text{N}_6\text{O}$; 403.2058; found, 403.2055

4-((2,4-Difluorobenzyl)(isopentyl)amino)-6-morpholino-1,3,5-triazine-2-carbonitrile

(264181)

General Procedure B3 starting from 4-(isopentylamino)-6-morpholino-1,3,5-triazine-2-carbonitrile (75 mg, 0.271 mmol), sodium hydride (11.94 mg, 0.299 mmol), and 1-(bromomethyl)-2,4-difluorobenzene (0.033 ml, 0.271 mmol) gave 4-((2,4-difluorobenzyl)(isopentyl)amino)-6-morpholino-1,3,5-triazine-2-carbonitrile (86 mg, 0.214 mmol, 79 % yield); ^1H NMR (CDCl_3 , 500 MHz) δ 7.13 - 7.33 (m, 1H), 6.78 - 6.86 (m, 2H), 4.80 (s, 1H), 4.75 (s, 1H), 3.76 - 3.86 (m, 3H), 3.63 - 3.74 (m, 5H), 3.52 - 3.60 (m, 1H), 3.45 - 3.52 (m, 1H), 1.51 - 1.60 (m, 1H), 1.40 - 1.49 (m, 2H), 0.92 (t, $J = 6.36$ Hz, 6H); ^{13}C NMR (CDCl_3 , 126 MHz) δ 164.2, 164.1, 163.6, 163.5, 163.4, 163.3, 163.1, 162.0, 161.9, 161.8, 161.7, 161.4, 161.3, 161.2, 160.0, 159.9, 159.8, 159.7, 152.0, 151.8, 131.2, 131.1, 130.0, 129.9, 120.4, 120.3, 120.2, 115.5, 111.6, 111.5, 111.4, 111.3, 104.0, 103.9, 103.8, 103.7, 103.6, 103.5, 66.7, 66.4, 45.6, 45.1, 44.0, 43.4, 42.9, 42.8, 36.3, 35.5, 26.0, 25.9, 22.5, 22.4; ^{19}F NMR (CDCl_3 , 470 MHz)

δ -114.58 (m), -111.04 (m); HRMS–ESI (m/z): $[M+H]^+$ calcd for, $C_{20}H_{24}F_2N_6O$; 403.2058; found, 403.2054

4-(Benzyl(isopentyl)amino)-6-morpholino-1,3,5-triazine-2-carbonitrile (JRH-1-34B/264301)

General Procedure B3 starting from 4-(isopentylamino)-6-morpholino-1,3,5-triazine-2-carbonitrile (100 mg, 0.362 mmol) and (bromomethyl)benzene (92.8 mg, 0.543 mmol) gave 4-(benzyl(isopentyl)amino)-6-morpholino-1,3,5-triazine-2-carbonitrile (89.1 mg, 0.243 mmol, 67.2 % yield); 1H NMR ($CDCl_3$, 500 MHz) δ 7.37 – 7.16 (m, 4H), 4.78 (d, J = 27.6 Hz, 2H), 3.89 – 3.58 (m, 8H), 3.58 – 3.50 (m, 1H), 3.50 – 3.39 (m, 1H), 1.54 (m, 1H), 1.44 (qd, J = 7.0, 1.4 Hz, 2H), 0.90 (dd, J = 7.8, 6.5 Hz, 6H).); ^{13}C NMR ($CDCl_3$, 126 MHz) δ 164.05, 163.69, 163.54, 152.05, 137.43, 137.31, 128.61, 128.58, 127.77, 127.50, 127.39, 127.32, 115.61, 49.74, 45.29, 44.67, 36.23, 35.37, 26.05, 25.91, 22.56, 22.51. HRMS–ESI (m/z): $[M+H]^+$ calcd for $C_{20}H_{26}N_6O$, 367.2241; found, 367.2284

4-(Isopentyl(phenethyl)amino)-6-morpholino-1,3,5-triazine-2-carbonitrile (263466)

General Procedure B3 starting from 4-(isopentylamino)-6-morpholino-1,3,5-triazine-2-carbonitrile (100 mg, 0.362 mmol), sodium hydride (28.9 mg, 0.724 mmol), and (2-bromoethyl)benzene (49.2 μ l, 0.362 mmol) gave 4-(isopentyl(phenethyl)amino)-6-morpholino-1,3,5-triazine-2-carbonitrile (15.2 mg, 0.040 mmol, 11.04 % yield); 1H NMR ($CDCl_3$, 500 MHz) δ 7.27 (dd, J = 4.65, 6.11 Hz, 1H), 7.21 (d, J = 6.85 Hz, 1H), 4.75 (br. s., 7H), 3.78 (br. s., 3H), 3.58 - 3.73 (m, 4H), 3.42 - 3.52 (m, 1H), 3.33 - 3.42 (m, 1H), 2.85 (br. s., 1H), 2.03 (br. s., 2H), 1.49 - 1.62 (m, 1H), 1.36 - 1.47 (m, 2H), 0.77 - 1.00 (m, 6H); ^{13}C NMR ($CDCl_3$, 126 MHz) δ 163.5, 163.4, 151.7, 138.9, 138.8, 128.8, 128.6, 128.5, 128.4, 126.4, 126.3, 115.6, 66.6, 66.3,

49.2, 48.8, 46.0, 45.9, 43.8, 43.3, 39.0, 38.0, 36.6, 35.9, 34.3, 33.5, 25.9, 25.8, 22.5, 22.4;
HRMS–ESI (m/z): [M+H]⁺ calcd for, C₂₁H₂₈N₆O; 381.2403; found, 381.2401

4-(Isopentyl(3-phenylpropyl)amino)-6-morpholino-1,3,5-triazine-2-carbonitrile (263589)

General Procedure B3 starting from 4-(isopentylamino)-6-morpholino-1,3,5-triazine-2-carbonitrile (100 mg, 0.362 mmol), sodium hydride (21.71 mg, 0.543 mmol), and (3-bromopropyl)benzene (72.0 mg, 0.362 mmol) gave 4-(isopentyl(3-phenylpropyl)amino)-6-morpholino-1,3,5-triazine-2-carbonitrile (113 mg, 0.286 mmol, 79 % yield); ¹H NMR (CDCl₃, 500 MHz) δ 7.25 - 7.34 (m, 2H), 7.14 - 7.25 (m, 3H), 3.80 (br. s., 1H), 3.76 (br. s., 2H), 3.69 - 3.73 (m, 2H), 3.67 (br. s., 1H), 3.63 (br. s., 1H), 3.50 - 3.58 (m, 2H), 3.41 - 3.50 (m, 3H), 2.60 - 2.70 (m, 2H), 1.87 - 1.97 (m, 2H), 1.49 - 1.62 (m, 1H), 1.35 - 1.48 (m, 2H), 0.93 (t, *J* = 7.58 Hz, 6H); ¹³C NMR (CDCl₃, 126 MHz) δ 163.4, 163.3, 151.7, 141.3, 128.3, 128.2, 125.9, 125.8, 115.6, 66.6, 66.3, 46.8, 46.4, 45.7, 45.5, 43.8, 43.7, 43.3, 43.1, 36.6, 35.8, 33.2, 32.9, 29.2, 28.4, 26.0, 25.8, 22.5; HRMS–ESI (m/z): [M+H]⁺ calcd for, C₂₂H₃₀N₆O; 395.2559; found, 395.2557

4-(Isopentyl(quinolin-8-ylmethyl)amino)-6-morpholino-1,3,5-triazine-2-carbonitrile (263580)

General Procedure B3 starting from 4-(isopentylamino)-6-morpholino-1,3,5-triazine-2-carbonitrile (100 mg, 0.362 mmol), sodium hydride (28.9 mg, 0.724 mmol), and 8-(bromomethyl)quinoline (80 mg, 0.362 mmol) gave 4-(isopentyl(quinolin-8-ylmethyl)amino)-6-morpholino-1,3,5-triazine-2-carbonitrile (41.3 mg, 0.099 mmol, 27.3 % yield); ¹H NMR (CDCl₃, 500 MHz) δ 8.90 - 8.98 (m, 1H), 8.14 - 8.22 (m, 1H), 7.74 (d, *J* = 7.83 Hz, 1H), 7.40 - 7.52 (m, 3H), 5.52 (s, 1H), 5.48 (s, 1H), 3.82 (br. s., 2H), 3.73 (br. s., 3H), 3.66 - 3.70 (m, 1H), 3.57 - 3.66

(m, 2H), 3.45 (br. s., 2H), 1.49 - 1.63 (m, 3H), 0.90 (d, $J = 5.87$ Hz, 3H), 0.88 (d, $J = 5.87$ Hz, 3H); ^{13}C NMR (CDCl_3 , 126 MHz) δ 164.3, 163.6, 163.5, 151.9, 149.4, 146.5, 146.3, 136.4, 136.2, 135.4, 135.1, 128.2, 127.2, 127.1, 126.9, 126.4, 126.3, 121.1, 115.7, 115.6, 66.7, 66.6, 66.4, 66.2, 46.1, 46.0, 45.6, 43.9, 43.8, 43.4, 43.2, 36.5, 35.6, 26.1, 25.9, 22.5; HRMS–ESI (m/z): $[\text{M}+\text{H}]^+$ calcd for, $\text{C}_{23}\text{H}_{27}\text{N}_7\text{O}$; 418.2355; found, 418.2365

4-(Isopentyl(naphthalen-1-ylmethyl)amino)-6-morpholino-1,3,5-triazine-2-carbonitrile (263581)

General Procedure B3 starting from 4-(isopentylamino)-6-morpholino-1,3,5-triazine-2-carbonitrile (100 mg, 0.362 mmol), sodium hydride (21.71 mg, 0.543 mmol), and 1-(bromomethyl)naphthalene (80 mg, 0.362 mmol) gave 4-(isopentyl(naphthalen-1-ylmethyl)amino)-6-morpholino-1,3,5-triazine-2-carbonitrile (41.3 mg, 0.099 mmol, 27.4 % yield); ^1H NMR (CDCl_3 , 500 MHz) δ 7.96 - 8.05 (m, 1H), 7.85 - 7.93 (m, 1H), 7.81 (d, $J = 8.31$ Hz, 1H), 7.48 - 7.57 (m, 2H), 7.39 - 7.45 (m, 1H), 7.22 - 7.29 (m, 1H), 5.29 (s, 1H), 5.22 (s, 1H), 3.85 (br. s., 1H), 3.79 (br. s., 2H), 3.73 (br. s., 2H), 3.68 (br. s., 1H), 3.59 (br. s., 1H), 3.50 - 3.57 (m, 2H), 3.40 - 3.48 (m, 1H), 1.45 - 1.56 (m, 1H), 1.36 - 1.45 (m, 2H), 0.86 (d, $J = 6.85$ Hz, 3H), 0.84 (d, $J = 6.36$ Hz, 3H); ^{13}C NMR (CDCl_3 , 126 MHz) δ 194.0, 193.9, 164.2, 164.0, 163.6, 163.5, 152.6, 152.6, 152.0, 151.9, 143.5, 133.4, 133.1, 133.0, 132.9, 126.3, 125.8, 124.7, 124.1, 123.9, 115.6, 115.5, 82.3, 66.7, 66.4, 49.0, 45.5, 44.7, 44.3, 44.2, 44.0, 43.9, 43.4, 38.9, 28.3, 28.2, 22.5; HRMS–ESI (m/z): $[\text{M}+\text{H}]^+$ calcd for, $\text{C}_{24}\text{H}_{28}\text{N}_6\text{O}$; 417.2397; found, 417.2398

**4-((1-(4-Fluorophenyl)ethyl)(isopentyl)amino)-6-morpholino-1,3,5-triazine-2-carbonitrile
(263251)**

General Procedure A4 from 4-chloro-N-(1-(4-fluorophenyl)ethyl)-N-isopentyl-6-morpholino-1,3,5-triazin-2-amine (200 mg, 0.490 mmol), DABCO (110 mg, 0.981 mmol), and potassium cyanide (35.1 mg, 0.539 mmol) in DMSO (2 ml) gave 4-((1-(4-fluorophenyl)ethyl)(isopentyl)amino)-6-morpholino-1,3,5-triazine-2-carbonitrile (72 mg, 0.181 mmol, 36.9 % yield); ¹H NMR (CDCl₃, 500 MHz) δ 7.21 - 7.30 (m, 2H), 7.01 (t, *J* = 8.56 Hz, 2H), 6.15 (q, *J* = 6.85 Hz, 0.5H), 5.93 (q, *J* = 6.85 Hz, 0.5H), 3.67 - 3.85 (m, 8H), 3.31 - 3.41 (m, 0.5H), 3.21 - 3.29 (m, 0.5H), 3.02 - 3.18 (m, 1H), 1.51 - 1.63 (m, 3H), 1.38 - 1.49 (m, 1H), 1.29 - 1.38 (m, 1H), 1.11 - 1.23 (m, 1H), 0.76 - 0.85 (m, 6H); ¹³C NMR (CDCl₃, 126 MHz) δ 163.7, 163.6, 163.5, 163.4, 163.0, 161.1, 152.0, 151.7, 136.6, 136.4, 129.0, 128.7, 128.6, 115.6, 115.3, 115.1, 66.7, 66.4, 52.2, 51.9, 44.0, 43.4, 42.5, 41.9, 37.7, 36.6, 26.7, 26.4, 22.5, 22.4, 22.3, 17.0, 16.9; HRMS–ESI (m/z): [M+H]⁺ calcd for, C₂₁H₂₇FN₆O; 399.2303; found, 399.2302

N-(1-(4-Fluorophenyl)ethyl)-3-methylbutan-1-amine

1-(4-Fluorophenyl)ethan-1-one (0.5 ml, 4.12 mmol), 3-methylbutan-1-amine (1.434 ml, 12.36 mmol), and titanium(iv) isopropoxide (1.810 ml, 6.18 mmol) were added to a flask containing MeOH (5 ml) and allowed to stir at room temperature overnight. The next morning, the reaction was cooled to 0°C and sodium borohydride (467 mg, 12.36 mmol) was added slowly. The reaction was allowed to warm back to room temperature and stirred for 4-6 h. Reaction was then quenched slowly with H₂O and solvent was removed *in vacuo*. Crude residue was taken up in aqueous bicarbonate, extracted with EtOAc 3x, dried over MgSO₄ and concentrated to afford N-

(1-(4-fluorophenyl)ethyl)-3-methylbutan-1-amine (745 mg, 3.56 mmol, 86 % yield); ¹H NMR (CDCl₃, 500 MHz) δ 7.20 - 7.30 (m, 2H), 7.13 (d, *J* = 4.40 Hz, 1H), 7.00 (br. t, *J* = 7.80 Hz, 2H), 6.14 (br. d, *J* = 6.80 Hz, 1H), 4.92 - 5.08 (m, 1H), 4.76 - 4.92 (m, 2H), 4.58 - 4.73 (m, 2H), 3.19 - 3.39 (m, 1H), 2.98 - 3.17 (m, 1H), 1.52 - 1.59 (m, 3H), 1.39 - 1.48 (m, 1H), 1.28 - 1.37 (m, 1H), 1.12 - 1.20 (m, 1H), 0.75 - 0.87 (m, 6H)

6-Chloro-N2-(1-(4-fluorophenyl)ethyl)-N2-isopentyl-N4-(oxetan-3-yl)-1,3,5-triazine-2,4-diamine

General procedure B1 from 2,4,6-trichloro-1,3,5-triazine (100 mg, 0.542 mmol), N-(1-(4-fluorophenyl)ethyl)-3-methylbutan-1-amine (114 mg, 0.542 mmol), DIPEA (189 μl, 1.085 mmol), and oxetan-3-amine (39.6 mg, 0.542 mmol) gave 6-chloro-N2-(1-(4-fluorophenyl)ethyl)-N2-isopentyl-N4-(oxetan-3-yl)-1,3,5-triazine-2,4-diamine (155 mg, 0.394 mmol, 72.6 % yield); ¹H NMR (CDCl₃, 500 MHz) δ 7.20 - 7.30 (m, 2H), 7.13 (d, *J* = 4.40 Hz, 1H), 7.00 (br. t, *J* = 7.80 Hz, 2H), 6.14 (br. d, *J* = 6.80 Hz, 1H), 4.92 - 5.08 (m, 1H), 4.76 - 4.92 (m, 2H), 4.58 - 4.73 (m, 2H), 3.19 - 3.39 (m, 1H), 2.98 - 3.17 (m, 1H), 1.52 - 1.59 (m, 3H), 1.39 - 1.48 (m, 1H), 1.28 - 1.37 (m, 1H), 1.12 - 1.20 (m, 1H), 0.75 - 0.87 (m, 6H)

4-((1-(4-Fluorophenyl)ethyl)(isopentyl)amino)-6-(oxetan-3-ylamino)-1,3,5-triazine-2-carbonitrile (11-90 (263392))

General procedure B2 from 6-chloro-N2-(1-(4-fluorophenyl)ethyl)-N2-isopentyl-N4-(oxetan-3-yl)-1,3,5-triazine-2,4-diamine (155 mg, 0.394 mmol), potassium cyanide (28.2 mg, 0.433 mmol), and DABCO (88 mg, 0.787 mmol) gave 4-((1-(4-fluorophenyl)ethyl)(isopentyl)amino)-6-(oxetan-3-ylamino)-1,3,5-triazine-2-carbonitrile (72 mg, 0.187 mmol, 47.6 % yield); ¹H NMR

(DMSO-d₆, 400 MHz) δ 7.30 - 7.37 (m, 2H), 7.12 (t, J = 8.80 Hz, 2H), 5.91 (br. s., 1H), 4.86 (br. s., 1H), 4.70 (br. s., 2H), 4.53 (br. s., 2H), 3.31 (br. s., 1H), 3.20 (br. s., 1H), 2.99 (br. s., 1H), 1.55 (d, J = 7.04 Hz, 3H), 1.40 - 1.50 (m, 1H), 1.28 - 1.40 (m, 1H), 1.05 - 1.15 (m, 1H), 0.81 (d, J = 7.04 Hz, 3H), 0.79 (d, J = 7.00 Hz, 3H); ¹³C NMR (CDCl₃, 126 MHz) δ 178.1, 163.8, 163.6, 163.4, 163.2, 162.8, 160.8, 151.4, 135.9, 128.8, 128.5, 128.4, 115.2, 115.1, 114.9, 78.1, 77.6, 72.2, 61.3, 52.1, 51.8, 45.6, 42.2, 41.8, 40.1, 39.9, 39.6, 39.4, 37.3, 36.5, 26.4, 26.1, 22.2, 16.8; [M+H]⁺ calcd for, C₂₀H₂₅FN₆O; 385.2147; found, 385.2149

**4-(Isopentyl(pyridin-2-ylmethyl)amino)-6-morpholino-1,3,5-triazine-2-carbonitrile
(263462)**

General procedure B3 from 4-(isopentylamino)-6-morpholino-1,3,5-triazine-2-carbonitrile (50 mg, 0.181 mmol), sodium hydride (14.47 mg, 0.362 mmol), and 2-(bromomethyl)pyridine, HBr (45.8 mg, 0.181 mmol) gave 4-(isopentyl(pyridin-2-ylmethyl)amino)-6-morpholino-1,3,5-triazine-2-carbonitrile (16.8 mg, 0.046 mmol, 25.3 % yield); ¹H NMR (CDCl₃, 500 MHz) δ 8.55 (d, J = 4.40 Hz, 1H), 7.64 (d, J = 6.85 Hz, 1H), 7.23 (d, J = 7.83 Hz, 0.5H), 7.16 - 7.22 (m, 1H), 7.11 (d, J = 7.83 Hz, 0.5H), 4.90 (s, 1H), 4.84 (s, 1H), 3.75 - 3.85 (m, 3H), 3.70 - 3.75 (m, 2H), 3.63 - 3.70 (m, 2H), 3.54 - 3.61 (m, 3H), 1.51 - 1.64 (m, 1H), 1.42 - 1.51 (m, 2H), 0.93 (d, J = 6.36 Hz, 3H), 0.90 (d, J = 6.85 Hz, 3H); ¹³C NMR (CDCl₃, 126 MHz) δ 164.2, 164.0, 163.6, 163.4, 157.6, 157.4, 152.0, 151.9, 149.3, 136.7, 136.6, 122.4, 122.2, 122.0, 120.8, 115.6, 115.5, 66.7, 66.6, 66.4, 66.3, 52.3, 51.9, 46.3, 45.6, 44.0, 43.4, 36.4, 35.5, 26.0, 25.9, 22.6, 22.5; HRMS-ESI (m/z): [M+H]⁺ calcd for, C₁₉H₂₅N₇O; 368.2193; found, 368.2200

4-(Isopentyl(pyridin-3-ylmethyl)amino)-6-morpholino-1,3,5-triazine-2-carbonitrile

(263464)

General procedure B3 from 4-(isopentylamino)-6-morpholino-1,3,5-triazine-2-carbonitrile (50 mg, 0.181 mmol), sodium hydride (14.47 mg, 0.362 mmol), and 3-(bromomethyl)pyridine, HBr (45.8 mg, 0.181 mmol), gave 4-(isopentyl(pyridin-2-ylmethyl)amino)-6-morpholino-1,3,5-triazine-2-carbonitrile (35 mg, 0.095 mmol, 52.6 % yield); ¹H NMR (CDCl₃, 500 MHz) δ 8.47 - 8.56 (m, 2H), 7.45 - 7.64 (m, 1H), 7.21 - 7.29 (m, 1H), 4.79 (s, 1H), 4.74 (s, 1H), 3.83 (br. s., 1H), 3.78 (br. s., 2H), 3.70 - 3.74 (m, 2H), 3.68 (br. s., 1H), 3.63 (br. s., 2H), 3.53 - 3.59 (m, 1H), 3.43 - 3.49 (m, 1H), 1.49 - 1.63 (m, 1H), 1.38 - 1.49 (m, 2H), 0.91 (d, *J* = 6.60 Hz, 3H), 0.90 (d, *J* = 6.60 Hz, 4H); ¹³C NMR (CDCl₃, 126 MHz) δ 164.2, 164.1, 163.6, 163.4, 152.0, 151.9, 149.2, 149.1, 149.0, 148.9, 135.6, 134.8, 133.1, 133.0, 123.5, 115.5, 115.4, 66.7, 66.6, 66.4, 66.3, 47.6, 47.5, 45.7, 44.9, 44.0, 43.9, 43.4, 36.3, 35.5, 26.0, 25.9, 22.5; HRMS–ESI (*m/z*): [M+H]⁺ calcd for, C₁₉H₂₅N₇O; 368.2193; found, 368.2194

4-(Isopentyl(pyridin-4-ylmethyl)amino)-6-morpholino-1,3,5-triazine-2-carbonitrile

(263468)

General procedure B3 from 4-(isopentylamino)-6-morpholino-1,3,5-triazine-2-carbonitrile (100 mg, 0.362 mmol), sodium hydride (28.9 mg, 0.724 mmol), and 4-(chloromethyl)pyridine, HCl (59.4 mg, 0.362 mmol) gave 4-(isopentyl(pyridin-4-ylmethyl)amino)-6-morpholino-1,3,5-triazine-2-carbonitrile (82.4 mg, 0.224 mmol, 62.0 % yield); ¹H NMR (CDCl₃, 500 MHz) δ 8.48 - 8.59 (m, 2H), 7.09 (dd, *J* = 4.89, 9.78 Hz, 2H), 4.78 (s, 1H), 4.70 (s, 1H), 3.82 (br. s., 1H), 3.74 - 3.80 (m, 2H), 3.71 (br. s., 2H), 3.65 (br. s., 1H), 3.51 - 3.61 (m, 3H), 3.41 - 3.50 (m, 1H), 1.48 - 1.62 (m, 1H), 1.36 - 1.48 (m, 2H), 0.90 (d, *J* = 6.85 Hz, 3H), 0.88 (d, *J* = 6.85 Hz, 3H); ¹³C NMR

(CDCl₃, 126 MHz) δ 164.3, 164.2, 163.5, 163.3, 152.0, 151.9, 149.9, 146.7, 146.5, 122.2, 121.8, 115.4, 115.3, 66.6, 66.5, 66.3, 66.2, 49.3, 49.1, 46.1, 45.3, 43.9, 43.8, 43.4, 43.3, 36.4, 35.5, 25.9, 25.8, 22.5, 22.4; HRMS–ESI (m/z): [M+H]⁺ calcd for, C₁₉H₂₅N₇O; 368.2193; found, 368.2195

4-((4-Chlorobenzyl)(isopentyl)amino)-6-morpholino-1,3,5-triazine-2-carbonitrile (263578)

General procedure B3 from 4-(isopentylamino)-6-morpholino-1,3,5-triazine-2-carbonitrile (100 mg, 0.362 mmol), sodium hydride (28.9 mg, 0.724 mmol), and 1-(bromomethyl)-4-chlorobenzene (74.4 mg, 0.362 mmol) gave 4-((4-chlorobenzyl)(isopentyl)amino)-6-morpholino-1,3,5-triazine-2-carbonitrile (60.6 mg, 0.151 mmol, 41.8 % yield); ¹H NMR (CDCl₃, 500 MHz) δ 7.25 - 7.32 (m, 2H), 7.11 - 7.19 (m, 2H), 4.76 (s, 1H), 4.70 (s, 1H), 3.83 (br. s., 1H), 3.79 (br. s., 2H), 3.71 - 3.75 (m, 2H), 3.69 (br. s., 1H), 3.64 (br. s., 2H), 3.53 (t, *J* = 7.80 Hz, 1H), 3.44 (t, *J* = 7.80 Hz, 1H), 1.48 - 1.59 (m, 1H), 1.39 - 1.47 (m, 2H), 0.90 (t, *J* = 6.60 Hz, 6H); ¹³C NMR (CDCl₃, 126 MHz) δ 164.2, 164.0, 163.6, 163.5, 152.1, 151.9, 135.9, 135.8, 133.3, 133.1, 131.5, 129.1, 128.7, 128.6, 115.6, 115.5, 66.7, 66.4, 49.2, 45.4, 44.7, 44.0, 43.4, 36.2, 35.4, 26.0, 25.9, 22.5; HRMS–ESI (m/z): [M+H]⁺ calcd for, C₂₀H₂₅ClN₆O; 401.1857; found, 401.1867

4-((4-Acetylbenzyl)(isopentyl)amino)-6-morpholino-1,3,5-triazine-2-carbonitrile (263582)

From 4-(isopentylamino)-6-morpholino-1,3,5-triazine-2-carbonitrile (100 mg, 0.362 mmol), sodium hydride (21.71 mg, 0.543 mmol), and 1-(4-(bromomethyl)phenyl)ethan-1-one (77 mg, 0.362 mmol) gave 4-((4-acetylbenzyl)(isopentyl)amino)-6-morpholino-1,3,5-triazine-2-carbonitrile (31.1 mg, 0.076 mmol, 21.04 % yield); ¹H NMR (CDCl₃, 500 MHz) δ 7.91 (d, *J* = 7.34 Hz, 2H), 7.23 - 7.32 (m, 2H), 4.84 (s, 1H), 4.78 (s, 1H), 3.83 (br. s., 1H), 3.79 (br. s., 1H), 3.73 (d, *J* = 4.40 Hz, 2H), 3.64 - 3.70 (m, 2H), 3.59 - 3.64 (m, 2H), 3.56 (t, *J* = 7.80 Hz, 1H),

3.46 (t, $J = 7.80$ Hz, 1H), 2.59 (s, 3H), 1.49 - 1.61 (m, 1H), 1.38 - 1.49 (m, 2H), 0.90 (t, $J = 7.58$ Hz, 6H); ^{13}C NMR (CDCl_3 , 126 MHz) δ 197.6, 164.3, 164.1, 163.6, 163.4, 152.0, 151.9, 143.0, 142.9, 136.4, 136.3, 129.8, 128.7, 127.9, 127.6, 127.2, 115.5, 70.7, 70.6, 70.4, 70.3, 69.2, 68.7, 66.7, 66.6, 66.4, 66.3, 49.7, 45.7, 45.1, 44.0, 43.9, 43.4, 36.3, 35.4, 26.6, 26.0, 25.9, 22.5; HRMS–ESI (m/z): $[\text{M}+\text{H}]^+$ calcd for, $\text{C}_{22}\text{H}_{28}\text{N}_6\text{O}$; 409.2347; found, 409.2350

4-(isopentyl(2-methylbenzyl)amino)-6-morpholino-1,3,5-triazine-2-carbonitrile (264183)

General Procedure B3 starting from 4-(isopentylamino)-6-morpholino-1,3,5-triazine-2-carbonitrile (100 mg, 0.362 mmol) and 1-(bromomethyl)-2-methylbenzene (100 mg, 0.543 mmol) gave 4-(isopentyl(2-methylbenzyl)amino)-6-morpholino-1,3,5-triazine-2-carbonitrile (78.7 mg, 0.207 mmol, 57.2 % yield); ^1H NMR (CDCl_3 , 500 MHz) δ 7.22 – 7.10 (m, 3H), 7.08 – 6.98 (m, 1H), 4.79 (d, $J = 28.6$ Hz, 2H), 3.91 – 3.56 (m, 8H), 3.52 (s, 1H), 3.49 – 3.40 (m, 1H), 2.30 (d, $J = 4.5$ Hz, 3H), 1.59 – 1.48 (m, 1H), 1.48 – 1.37 (m, 2H), 0.90 (dd, $J = 6.6, 5.3$ Hz, 6H). ^{13}C NMR (CDCl_3 , 126 MHz) δ 164.03, 163.70, 151.96, 136.29, 135.91, 134.88, 134.78, 130.50, 130.43, 127.36, 127.31, 127.19, 127.17, 126.11, 126.02, 115.60, 66.37, 47.73, 47.52, 44.97, 44.64, 36.15, 35.32, 26.12, 25.98, 22.58, 22.53, 19.21. HRMS–ESI (m/z): $[\text{M}+\text{H}]^+$ calcd for $\text{C}_{21}\text{H}_{28}\text{N}_6\text{O}$, 381.2397; found, 381.2401

4-(Isopentyl(3-methylbenzyl)amino)-6-morpholino-1,3,5-triazine-2-carbonitrile (263590)

General procedure B3 from 4-(isopentylamino)-6-morpholino-1,3,5-triazine-2-carbonitrile (100 mg, 0.362 mmol), sodium hydride (21.71 mg, 0.543 mmol), and 1-(bromomethyl)-3-methylbenzene (67.0 mg, 0.362 mmol) gave 4-(isopentyl(3-methylbenzyl)amino)-6-morpholino-1,3,5-triazine-2-carbonitrile (69.7 mg, 0.183 mmol, 50.6 % yield); ^1H NMR (CDCl_3 , 500 MHz) δ

7.21 (t, $J = 7.58$ Hz, 1H), 7.09 (d, $J = 7.34$ Hz, 1H), 6.97 - 7.04 (m, 2H), 4.77 (s, 1H), 4.72 (s, 1H), 3.83 (br. s., 1H), 3.80 (br. s., 2H), 3.71 - 3.75 (m, 2H), 3.69 (br. s., 2H), 3.65 (br. s., 1H), 3.51 - 3.57 (m, 1H), 3.43 - 3.48 (m, 1H), 2.34 (d, $J = 2.93$ Hz, 3H), 1.49 - 1.60 (m, 1H), 1.40 - 1.48 (m, 2H), 0.91 (t, $J = 7.09$ Hz, 6H); ^{13}C NMR (CDCl_3 , 126 MHz) δ 164.1, 163.9, 163.6, 163.5, 152.0, 151.9, 138.2, 137.3, 137.1, 128.5, 128.4, 128.2, 128.1, 128.0, 115.6, 66.7, 66.6, 66.4, 49.6, 49.5, 45.1, 44.5, 43.9, 43.4, 36.1, 35.3, 26.0, 25.9, 22.5, 21.4; HRMS–ESI (m/z): $[\text{M}+\text{H}]^+$ calcd for, 381.2397; $\text{C}_{21}\text{H}_{28}\text{N}_6\text{O}$; found, 381.2398

4-(Isopentyl(4-methylbenzyl)amino)-6-morpholino-1,3,5-triazine-2-carbonitrile (263591)

General procedure B3 from 4-(isopentylamino)-6-morpholino-1,3,5-triazine-2-carbonitrile (100 mg, 0.362 mmol), sodium hydride (21.71 mg, 0.543 mmol), and 1-(bromomethyl)-4-methylbenzene (67.0 mg, 0.362 mmol) gave 4-(isopentyl(4-methylbenzyl)amino)-6-morpholino-1,3,5-triazine-2-carbonitrile (88 mg, 0.231 mmol, 63.9 % yield); ^1H NMR (CDCl_3 , 500 MHz) δ 7.07 - 7.20 (m, 4H), 4.76 (s, 1H), 4.71 (s, 1H), 3.82 (br. s., 1H), 3.79 (br. s., 2H), 3.71 - 3.74 (m, 2H), 3.69 (br. s., 2H), 3.65 (br. s., 1H), 3.49 - 3.57 (m, 1H), 3.40 - 3.49 (m, 1H), 2.34 (s, 3H), 1.50 - 1.59 (m, 1H), 1.41 - 1.50 (m, 2H), 0.91 (t, $J = 6.36$ Hz, 6H); ^{13}C NMR (CDCl_3 , 126 MHz) δ 164.1, 163.9, 163.6, 163.5, 152.0, 151.9, 137.1, 137.0, 134.2, 129.2, 127.7, 127.3, 115.6, 66.6, 66.4, 60.3, 49.4, 49.3, 45.0, 44.5, 43.9, 43.8, 43.4, 36.1, 35.3, 26.0, 25.9, 22.5, 21.1, 21.0; $[\text{M}+\text{H}]^+$ calcd for, 381.2397; $\text{C}_{21}\text{H}_{28}\text{N}_6\text{O}$; found, 381.2399

4-((3,5-Dimethylbenzyl)(isopentyl)amino)-6-morpholino-1,3,5-triazine-2-carbonitrile

(263583)

General procedure B3 from 4-(isopentylamino)-6-morpholino-1,3,5-triazine-2-carbonitrile (100 mg, 0.362 mmol), sodium hydride (21.71 mg, 0.543 mmol) and 1-(bromomethyl)-3,5-dimethylbenzene (72.0 mg, 0.362 mmol) gave 4-((3,5-dimethylbenzyl)(isopentyl)amino)-6-morpholino-1,3,5-triazine-2-carbonitrile (34.4 mg, 0.087 mmol, 24.10 % yield); ¹H NMR (CDCl₃, 500 MHz) δ 6.92 (s, 1H), 6.83 (s, 2H), 4.74 (s, 1H), 4.69 (s, 1H), 3.78 - 3.87 (m, 3H), 3.68 - 3.76 (m, 4H), 3.62 - 3.68 (m, 1H), 3.51 - 3.57 (m, 1H), 3.42 - 3.49 (m, 1H), 2.31 (br. s., 3H), 2.30 (br. s., 3H), 1.55 (td, *J* = 6.66, 13.57 Hz, 1H), 1.41 - 1.49 (m, 2H), 0.93 (d, *J* = 7.10 Hz, 3H), 0.91 (d, *J* = 7.10 Hz, 3H); ¹³C NMR (CDCl₃, 126 MHz) δ 164.1, 163.9, 163.6, 163.5, 152.0, 151.9, 138.1, 138.1, 137.2, 137.0, 129.1, 129.0, 125.4, 125.1, 115.6, 115.6, 66.6, 66.4, 49.4, 49.4, 45.0, 44.4, 43.9, 43.4, 36.1, 35.2, 26.0, 25.9, 22.5, 22.5, 21.3; HRMS–ESI (*m/z*): [M+H]⁺ calcd for, C₂₂H₃₀N₆O; 395.2554; found, 395.2554

4-((2,3-Dimethylbenzyl)(isopentyl)amino)-6-morpholino-1,3,5-triazine-2-carbonitrile

(263584)

General procedure B3 from 4-(isopentylamino)-6-morpholino-1,3,5-triazine-2-carbonitrile (100 mg, 0.362 mmol), sodium hydride (21.71 mg, 0.543 mmol), and 1-(bromomethyl)-2,3-dimethylbenzene (72.0 mg, 0.362 mmol) gave 4-((2,3-dimethylbenzyl)(isopentyl)amino)-6-morpholino-1,3,5-triazine-2-carbonitrile (63.5 mg, 0.161 mmol, 44.5 % yield); ¹H NMR (CDCl₃, 500 MHz) δ 7.10 (d, *J* = 7.34 Hz, 1H), 7.05 (t, *J* = 7.58 Hz, 1H), 6.89 (dd, *J* = 7.58, 15.41 Hz, 1H), 4.82 (s, 1H), 4.77 (s, 1H), 3.82 (d, *J* = 14.18 Hz, 3H), 3.74 (d, *J* = 4.40 Hz, 2H), 3.69 (br. s., 1H), 3.64 (br. s., 2H), 3.45 - 3.50 (m, 1H), 3.40 - 3.45 (m, 1H), 2.31 (s, 3H), 2.18 (d, *J* = 6.36 Hz,

3H), 1.52 (qd, $J = 6.66, 13.27$ Hz, 1H), 1.37 - 1.46 (m, 2H), 0.89 (d, $J = 3.91$ Hz, 3H), 0.88 (d, $J = 3.91$ Hz, 3H); ^{13}C NMR (CDCl_3 , 126 MHz) δ 163.9, 163.7, 163.5, 152.0, 151.9, 137.2, 137.1, 134.8, 134.6, 134.5, 129.1, 125.5, 125.4, 125.3, 125.1, 115.7, 115.6, 66.7, 66.4, 48.2, 47.9, 44.6, 44.4, 43.9, 43.4, 36.0, 35.2, 26.1, 25.9, 22.5, 20.5, 20.4, 14.8; HRMS–ESI (m/z): $[\text{M}+\text{H}]^+$ calcd for, $\text{C}_{22}\text{H}_{30}\text{N}_6\text{O}$; 395.2554; found, 395.2555

4-(Isopentyl(3-methoxybenzyl)amino)-6-morpholino-1,3,5-triazine-2-carbonitrile (263585)

General procedure B3 from 4-(isopentylamino)-6-morpholino-1,3,5-triazine-2-carbonitrile (100 mg, 0.362 mmol), sodium hydride (21.71 mg, 0.543 mmol), and 1-(bromomethyl)-3-methoxybenzene (72.8 mg, 0.362 mmol) gave 4-(isopentyl(3-methoxybenzyl)amino)-6-morpholino-1,3,5-triazine-2-carbonitrile (70.2 mg, 0.177 mmol, 48.9 % yield); ^1H NMR (CDCl_3 , 500 MHz) δ 7.17 - 7.30 (m, 1H), 6.74 - 6.83 (m, 3H), 4.77 (s, 1H), 4.71 (s, 1H), 3.82 (br. s., 1H), 3.79 (d, $J = 6.36$ Hz, 5H), 3.70 - 3.74 (m, 2H), 3.68 (br. s., 2H), 3.63 (br. s., 1H), 3.51 - 3.58 (m, 1H), 3.42 - 3.49 (m, 1H), 1.49 - 1.60 (m, 1H), 1.40 - 1.49 (m, 2H), 0.91 (t, $J = 6.85$ Hz, 6H); ^{13}C NMR (CDCl_3 , 126 MHz) δ 164.1, 164.0, 163.6, 163.5, 159.8, 152.0, 151.9, 139.0, 138.9, 129.6, 129.5, 120.0, 119.6, 115.6, 115.5, 113.6, 113.4, 112.4, 112.1, 66.7, 66.3, 55.2, 49.6, 45.2, 44.7, 43.9, 43.8, 43.4, 36.2, 35.3, 26.0, 25.9, 22.5; HRMS–ESI (m/z): $[\text{M}+\text{H}]^+$ calcd for, $\text{C}_{21}\text{H}_{28}\text{N}_6\text{O}_2$; 397.2352; found, 397.2356

4-(Isopentyl(3-(trifluoromethyl)benzyl)amino)-6-morpholino-1,3,5-triazine-2-carbonitrile (263586)

General procedure B3 from 4-(isopentylamino)-6-morpholino-1,3,5-triazine-2-carbonitrile (100 mg, 0.362 mmol), sodium hydride (21.71 mg, 0.543 mmol), and 1-(bromomethyl)-3-

(trifluoromethyl)benzene (86 mg, 0.362 mmol) gave 4-(isopentyl(3-(trifluoromethyl)benzyl)amino)-6-morpholino-1,3,5-triazine-2-carbonitrile (119 mg, 0.274 mmol, 76 % yield); ¹H NMR (CDCl₃, 500 MHz) δ 7.52 - 7.58 (m, 1H), 7.43 - 7.52 (m, 2H), 7.36 - 7.43 (m, 1H), 4.85 (s, 1H), 4.78 (s, 1H), 3.82 - 3.88 (m, 1H), 3.77 - 3.82 (m, 2H), 3.71 - 3.77 (m, 2H), 3.68 (br. s., 1H), 3.56 - 3.66 (m, 3H), 3.45 - 3.51 (m, 1H), 1.50 - 1.61 (m, 1H), 1.37 - 1.50 (m, 2H), 0.92 (d, *J* = 6.36 Hz, 3H), 0.90 (d, *J* = 6.36 Hz, 3H); ¹³C NMR (CDCl₃, 126 MHz) δ 164.2, 164.1, 163.6, 163.4, 152.0, 151.9, 138.7, 138.4, 131.0, 130.7, 130.4, 129.1, 124.3, 124.2, 124.1, 115.5, 115.4, 66.6, 66.3, 66.2, 49.7, 49.5, 45.8, 44.9, 43.9, 43.4, 43.3, 36.3, 35.4, 26.0, 25.8, 22.5, 22.4; HRMS–ESI (m/z): [M+H]⁺ calcd for, C₂₁H₂₅F₃N₆O; 435.2115; found, 435.2095

4-(Isopentyl(2-nitrobenzyl)amino)-6-morpholino-1,3,5-triazine-2-carbonitrile (263592)

General procedure B3 from 4-(isopentylamino)-6-morpholino-1,3,5-triazine-2-carbonitrile (150 mg, 0.543 mmol), sodium hydride (32.6 mg, 0.814 mmol), 1-(bromomethyl)-2-nitrobenzene (117 mg, 0.543 mmol) gave 4-(isopentyl(2-nitrobenzyl)amino)-6-morpholino-1,3,5-triazine-2-carbonitrile (46.8 mg, 0.114 mmol, 20.95 % yield); ¹H NMR (CDCl₃, 500 MHz) δ 8.01 - 8.13 (m, 1H), 7.57 (t, *J* = 7.58 Hz, 1H), 7.39 - 7.48 (m, 1H), 7.20 (t, *J* = 9.30 Hz, 1H), 5.15 (s, 1H), 5.03 (s, 1H), 3.82 (br. s., 2H), 3.73 (br. s., 3H), 3.57 - 3.67 (m, 2H), 3.46 - 3.57 (m, 2H), 3.42 (br. s., 1H), 1.53 - 1.62 (m, 1H), 1.45 - 1.53 (m, 2H), 0.92 (d, *J* = 6.36 Hz, 3H), 0.90 (d, *J* = 6.36 Hz, 3H); ¹³C NMR (CDCl₃, 126 MHz) δ 164.4, 164.3, 163.5, 163.3, 152.0, 151.9, 148.3, 148.2, 133.6, 133.4, 133.3, 128.1, 128.0, 127.9, 127.8, 125.3, 125.0, 115.4, 115.2, 66.6, 66.5, 66.3, 66.1, 47.8, 47.7, 46.5, 45.9, 43.9, 43.8, 43.4, 43.2, 36.4, 35.5, 26.0, 25.9, 22.5, 22.4; HRMS–ESI (m/z): [M+H]⁺ calcd for, C₂₀H₂₅N₇O₃; 412.2092; found, 412.2094

4-(Isopentyl(3-nitrobenzyl)amino)-6-morpholino-1,3,5-triazine-2-carbonitrile (263593)

General procedure B3 from 4-(isopentylamino)-6-morpholino-1,3,5-triazine-2-carbonitrile (150 mg, 0.543 mmol), sodium hydride (32.6 mg, 0.814 mmol), and 1-(bromomethyl)-3-nitrobenzene (117 mg, 0.543 mmol) gave 4-(isopentyl(3-nitrobenzyl)amino)-6-morpholino-1,3,5-triazine-2-carbonitrile (43.2 mg, 0.105 mmol, 19.34 % yield); ^1H NMR (CDCl_3 , 500 MHz) δ 8.09 (br. s., 1H), 7.99 - 8.08 (m, 1H), 7.56 (t, $J = 7.83$ Hz, 1H), 7.49 (t, $J = 8.31$ Hz, 1H), 4.86 (s, 1H), 4.80 (s, 1H), 3.75 - 3.84 (m, 3H), 3.70 (br. s., 2H), 3.54 - 3.66 (m, 4H), 3.44 - 3.53 (m, 1H), 1.52 (tt, $J = 6.60, 12.96$ Hz, 1H), 1.39 - 1.48 (m, 2H), 0.88 (t, $J = 6.36$ Hz, 6H); ^{13}C NMR (CDCl_3 , 126 MHz) δ 164.1, 164.0, 163.4, 163.3, 151.9, 151.8, 148.2, 139.8, 139.7, 133.6, 133.2, 129.5, 122.3, 122.2, 122.1, 122.0, 115.3, 66.5, 66.4, 66.2, 66.1, 60.2, 49.3, 49.2, 45.8, 45.1, 43.8, 43.3, 36.2, 35.3, 25.8, 25.7, 22.4, 22.3, 20.8; HRMS-ESI (m/z): $[\text{M}+\text{H}]^+$ calcd for, $\text{C}_{20}\text{H}_{25}\text{N}_7\text{O}_3$; 412.2092; found, 412.2091

4-(Isopentyl(4-nitrobenzyl)amino)-6-morpholino-1,3,5-triazine-2-carbonitrile (263594)

General procedure B3 from 4-(isopentylamino)-6-morpholino-1,3,5-triazine-2-carbonitrile (100 mg, 0.362 mmol), sodium hydride (21.71 mg, 0.543 mmol), and 1-(bromomethyl)-4-nitrobenzene (78 mg, 0.362 mmol) gave 4-(isopentyl(4-nitrobenzyl)amino)-6-morpholino-1,3,5-triazine-2-carbonitrile (49 mg, 0.119 mmol, 32.9 % yield); ^1H NMR (CDCl_3 , 500 MHz) δ 8.18 (d, $J = 7.83$ Hz, 2H), 7.32 - 7.41 (m, 2H), 4.88 (s, 1H), 4.82 (s, 1H), 3.84 (br. s., 1H), 3.79 (br. s., 2H), 3.72 - 3.74 (m, 2H), 3.68 (br. s., 1H), 3.55 - 3.62 (m, 3H), 3.46 - 3.52 (m, 1H), 1.52 - 1.60 (m, 1H), 1.39 - 1.50 (m, 2H), 0.91 (t, $J = 6.85$ Hz, 6H); ^{13}C NMR (CDCl_3 , 126 MHz) δ 164.4, 164.2, 163.6, 163.5, 152.1, 152.0, 147.4, 147.3, 145.2, 145.1, 128.2, 127.7, 123.9, 115.4, 66.7,

66.6, 66.4, 66.2, 49.6, 46.0, 45.3, 44.0, 43.9, 43.5, 43.4, 36.4, 35.5, 26.0, 25.9, 22.5; HRMS–ESI (m/z): [M+H]⁺ calcd for, C₂₀H₂₅N₇O₃; 412.2092; found, 412.2097

4-((2-Aminobenzyl)(isopentyl)amino)-6-morpholino-1,3,5-triazine-2-carbonitrile (263659)

In a round bottom flask, 4-(isopentyl(2-nitrobenzyl)amino)-6-morpholino-1,3,5-triazine-2-carbonitrile (50 mg, 0.122 mmol) was dissolved into acetone (10 ml). Zinc dust (159 mg, 2.430 mmol) was then added, followed by the addition of aq. ammonium chloride (0.694 ml, 4.86 mmol). Reaction was left to stir for 30 min until TLC indicated starting material was consumed. Reaction was poured into water and extracted 3x with EtOAc. Combined organic layers were dried over sodium sulfate and concentrated in vacuo. Crude residue was purified by flash chromatography (0-100% EtOAc:Hexanes gradient) to afford 4-((2-aminobenzyl)(isopentyl)amino)-6-morpholino-1,3,5-triazine-2-carbonitrile (42 mg, 0.110 mmol, 91 % yield); ¹H NMR (CDCl₃, 500 MHz) δ 7.09 - 7.17 (m, 1H), 7.06 (d, *J* = 7.34 Hz, 1H), 6.70 (q, *J* = 7.83 Hz, 1H), 6.65 (d, *J* = 7.83 Hz, 1H), 4.68 (br. s, 2H), 4.34 (br. s., 1H), 3.83 (br. s., 2H), 3.76 (br. s., 2H), 3.71 (br. s., 4H), 3.39 - 3.50 (m, 2H), 1.47 - 1.57 (m, 1H), 1.33 - 1.44 (m, 2H), 0.89 (d, *J* = 6.36 Hz, 6H); ¹³C NMR (CDCl₃, 126 MHz) δ 163.5, 163.4, 163.1, 152.2, 151.6, 146.0, 145.6, 131.4, 131.4, 129.4, 129.3, 119.7, 119.6, 117.8, 117.5, 115.7, 115.4, 115.4, 66.7, 66.4, 47.3, 47.0, 44.0, 43.8, 43.6, 43.5, 35.4, 34.7, 26.2, 26.0, 22.5, 22.5; HRMS–ESI (m/z): [M+H]⁺ calcd for, C₂₀H₂₇N₇O; 382.2350; found, 382.2344

4-((3-Aminobenzyl)(isopentyl)amino)-6-morpholino-1,3,5-triazine-2-carbonitrile (263660)

In a round bottom flask, 4-(isopentyl(3-nitrobenzyl)amino)-6-morpholino-1,3,5-triazine-2-carbonitrile (50 mg, 0.122 mmol) was dissolved into acetone (10 ml). Zinc dust (159 mg, 2.430

mmol) was then added, followed by the addition of aq. ammonium chloride (0.694 ml, 4.86 mmol). Reaction was left to stir for 30 min until TLC indicated starting material was consumed. Reaction was poured into water and extracted 3x with EtOAc. Combined organic layers were dried over sodium sulfate and concentrated in vacuo. Crude residue was purified by flash chromatography (0-100% EtOAc:Hexanes gradient) to afford 4-((3-aminobenzyl)(isopentyl)amino)-6-morpholino-1,3,5-triazine-2-carbonitrile (32 mg, 0.084 mmol, 69.0 % yield); ^1H NMR (CDCl_3 , 500 MHz) δ 7.03 - 7.16 (m, 1H), 6.56 - 6.63 (m, 2H), 6.54 (s, 0.5H), 6.49 (s, 0.5H), 4.71 (s, 1H), 4.66 (s, 1H), 3.82 (br. s., 1H), 3.79 (br. s., 2H), 3.71 - 3.75 (m, 2H), 3.62 - 3.71 (m, 5H), 3.50 - 3.56 (m, 1H), 3.41 - 3.47 (m, 1H), 1.48 - 1.59 (m, 1H), 1.39 - 1.48 (m, 2H), 0.91 (t, $J = 7.09$ Hz, 6H); ^{13}C NMR (CDCl_3 , 126 MHz) δ 164.1, 163.9, 163.6, 163.5, 152.0, 151.9, 146.7, 138.6, 138.5, 129.5, 129.4, 118.0, 117.5, 115.6, 115.6, 114.3, 114.1, 114.1, 113.5, 66.7, 66.7, 66.4, 49.5, 49.5, 45.1, 44.5, 43.9, 43.9, 43.4, 36.1, 35.3, 26.0, 25.9, 22.6, 22.5; HRMS-ESI (m/z): $[\text{M}+\text{H}]^+$ calcd for, $\text{C}_{20}\text{H}_{27}\text{N}_7\text{O}$; 382.2350; found, 382.2348

4-((4-Aminobenzyl)(isopentyl)amino)-6-morpholino-1,3,5-triazine-2-carbonitrile (263686)

In a round bottom flask, 4-(isopentyl(4-nitrobenzyl)amino)-6-morpholino-1,3,5-triazine-2-carbonitrile (100 mg, 0.243 mmol) was dissolved into acetone (10 ml). Zinc dust (318 mg, 4.86 mmol) was then added, followed by the addition of aq. ammonium chloride (1.389 ml, 9.72 mmol). Reaction was left to stir for 30 min until TLC indicated starting material was consumed. Reaction was poured into water and extracted 3x with EtOAc. Combined organic layers were dried over sodium sulfate and concentrated in vacuo. Crude residue was purified by flash chromatography (0-100% EtOAc:Hexanes gradient) to afford 4-((4-aminobenzyl)(isopentyl)amino)-6-morpholino-1,3,5-triazine-2-carbonitrile (45.6mg, 0.120 mmol, 49.2 % yield); ^1H

NMR (CDCl₃, 500 MHz) δ 7.04 (d, J = 8.31 Hz, 1H), 7.01 (d, J = 8.31 Hz, 1H), 6.63 (d, J = 7.34 Hz, 2H), 4.67 (s, 1H), 4.63 (s, 1H), 3.80 (br. s., 2H), 3.76 (br. s., 2H), 3.69 - 3.73 (m, 3H), 3.67 (br. s., 3H), 3.46 - 3.53 (m, 1H), 3.39 - 3.45 (m, 1H), 1.47 - 1.59 (m, 1H), 1.36 - 1.45 (m, 2H), 0.90 (t, J = 6.11 Hz, 6H); ¹³C NMR (CDCl₃, 126 MHz) δ 163.9, 163.7, 163.6, 163.5, 151.9, 151.8, 145.8, 129.2, 128.7, 127.0, 115.6, 115.0, 66.7, 66.4, 49.2, 49.0, 44.7, 44.2, 43.9, 43.9, 43.4, 36.1, 35.2, 26.0, 25.9, 22.5; HRMS–ESI (m/z): [M+H]⁺ calcd for, C₂₀H₂₇N₇O; 382.2350; found, 382.2348

**4-(Isopentyl(2-(pyrrolidin-1-yl)ethyl)amino)-6-morpholino-1,3,5-triazine-2-carbonitrile
(263684)**

General procedure B3 from 4-(isopentylamino)-6-morpholino-1,3,5-triazine-2-carbonitrile (100 mg, 0.362 mmol), sodium hydride (21.71 mg, 0.543 mmol), and 1-(2-chloroethyl)pyrrolidine (48.4 mg, 0.362 mmol). Compound was purified by flash chromatography (1-10% MeOH:DCM) to afford 4-(isopentyl(2-(pyrrolidin-1-yl)ethyl)amino)-6-morpholino-1,3,5-triazine-2-carbonitrile (25 mg, 0.067 mmol, 18.50 % yield); ¹H NMR (CDCl₃, 500 MHz) δ 3.71 - 3.84 (m, 4H), 3.66 - 3.71 (m, 4H), 3.56 - 3.66 (m, 2H), 3.45 - 3.56 (m, 2H), 2.62 (t, J = 7.09 Hz, 2H), 2.51 - 2.58 (m, 4H), 1.70 - 1.84 (m, 4H), 1.48 - 1.62 (m, 1H), 1.37 - 1.48 (m, 2H), 0.91 (t, J = 5.62 Hz, 6H); ¹³C NMR (CDCl₃, 126 MHz) δ 163.5, 151.7, 115.6, 66.6, 66.4, 57.8, 54.4, 54.3, 54.1, 53.7, 52.9, 51.2, 46.3, 46.2, 46.1, 45.9, 43.8, 43.3, 36.6, 35.8, 26.0, 25.8, 23.4, 22.5; HRMS–ESI (m/z): [M+H]⁺ calcd for, C₁₉H₃₁N₇O; 374.2668; found, 374.5659

4-((2-Cyanobenzyl)(isopentyl)amino)-6-morpholino-1,3,5-triazine-2-carbonitrile (264179)

General procedure B3 from 4-(isopentylamino)-6-morpholino-1,3,5-triazine-2-carbonitrile (100 mg, 0.362 mmol), sodium hydride (15.92 mg, 0.398 mmol), and 2-(bromomethyl)benzonitrile (70.9 mg, 0.362 mmol) gave 4-((2-cyanobenzyl)(isopentyl)amino)-6-morpholino-1,3,5-triazine-2-carbonitrile (108 mg, 0.276 mmol, 76 % yield); ¹H NMR (CDCl₃, 500 MHz) δ 7.64 (d, *J* = 7.34 Hz, 1H), 7.49 - 7.58 (m, 1H), 7.33 - 7.40 (m, 1H), 7.29 (dd, *J* = 7.83, 24.94 Hz, 1H), 5.00 (s, 1H), 4.93 (s, 1H), 3.79 (br. s., 2H), 3.74 (br. s., 1H), 3.70 (br. s., 2H), 3.53 - 3.66 (m, 4H), 3.45 - 3.53 (m, 1H), 1.54 (s, 1H), 1.39 - 1.50 (m, 2H), 0.89 (t, *J* = 6.85 Hz, 6H); ¹³C NMR (CDCl₃, 126 MHz) δ 164.1, 163.4, 163.2, 151.9, 151.7, 141.4, 141.2, 133.0, 132.9, 132.7, 128.0, 127.8, 127.6, 127.2, 117.2, 117.1, 115.3, 115.2, 111.5, 111.1, 66.4, 66.2, 66.1, 48.1, 47.9, 46.0, 45.3, 43.8, 43.7, 43.3, 43.2, 36.2, 35.3, 25.8, 25.7, 22.3; HRMS-ESI (*m/z*): [M+H]⁺ calcd for, C₂₁H₂₅N₇O; 392.2193; found, 392.2195

4-(Isopentyl(2-(trifluoromethyl)benzyl)amino)-6-morpholino-1,3,5-triazine-2-carbonitrile (264184)

General Procedure B3 starting from 4-(isopentylamino)-6-morpholino-1,3,5-triazine-2-carbonitrile (100 mg, 0.362 mmol) and 1-(bromomethyl)-2-(trifluoromethyl)benzene (130 mg, 0.543 mmol) gave 4-(isopentyl(2-(trifluoromethyl)benzyl)amino)-6-morpholino-1,3,5-triazine-2-carbonitrile (89.8 mg, 0.207 mmol, 57.1 % yield); ¹H NMR (CDCl₃, 500 MHz) δ 7.67 (d, *J* = 7.6 Hz, 1H), 7.55 - 7.45 (m, 1H), 7.36 (s, 1H), 7.19 (d, *J* = 7.8 Hz, 1H), 4.97 (d, *J* = 46.9 Hz, 2H), 3.90 - 3.69 (m, 4H), 3.69 - 3.37 (m, 5H), 1.65 - 1.40 (m, 3H), 1.25 (t, *J* = 7.1 Hz, 1H), 0.91 (dd, *J* = 16.1, 6.5 Hz, 6H). ¹³C NMR (CDCl₃, 126 MHz) δ 164.44, 163.70, 163.47, 152.10, 136.15, 132.15, 132.07, 131.59, 127.81, 127.21, 127.08, 127.05, 126.04, 125.99, 115.58, 115.44, 66.58,

66.25, 46.59, 46.56, 46.18, 46.08, 46.06, 45.16, 44.01, 43.90, 43.49, 43.28, 36.34, 35.33, 26.04, 25.93, 22.46, 22.44. ¹⁹F NMR (470 MHz, Chloroform-d) δ -58.77, -59.85, -60.32. HRMS–ESI (m/z): [M+H]⁺ calcd for C₂₁H₂₅F₃N₆O, 435.2114; found, 435.2135

Methyl 2-(((4-cyano-6-morpholino-1,3,5-triazin-2-yl)(isopentyl)amino)methyl)benzoate (264185)

General Procedure B3 starting from 4-(isopentylamino)-6-morpholino-1,3,5-triazine-2-carbonitrile (250 mg, 0.905 mmol) and methyl 2-(bromomethyl)benzoate (311 mg, 1.36 mmol) gave methyl 2-(((4-cyano-6-morpholino-1,3,5-triazin-2-yl)(isopentyl)amino)methyl)benzoate (41.2 mg, 0.097 mmol, 10.7 % yield); ¹H NMR (CDCl₃, 500 MHz) δ 7.99 (ddd, J = 12.2, 7.8, 1.4 Hz, 1H), 7.45 (td, J = 7.6, 1.4 Hz, 1H), 7.36 – 7.28 (m, 1H), 7.11 (d, J = 7.9 Hz, 1H), 5.22 (s, 1H), 5.13 (s, 1H), 3.92 (d, J = 4.0 Hz, 3H), 3.87 – 3.68 (m, 4H), 3.68 – 3.40 (m, 5H), 1.63 – 1.43 (m, 3H), 1.33 – 1.19 (m, 1H), 0.90 (dd, J = 9.0, 6.4 Hz, 6H). ¹³C NMR (CDCl₃, 126 MHz) δ 164.33, 163.67, 163.49, 152.00, 139.49, 139.48, 132.49, 132.44, 131.14, 130.96, 128.78, 128.53, 126.96, 126.91, 126.77, 126.66, 115.65, 66.72, 66.43, 66.32, 52.10, 48.54, 48.43, 46.21, 45.70, 43.96, 43.84, 43.45, 43.30, 36.41, 35.52, 26.12, 25.98, 22.55, 22.50. HRMS–ESI (m/z): [M+H]⁺ calcd for C₂₂H₂₈N₆O₃, 425.2296; found, 425.2301

4-(Isopentyl(2-methoxybenzyl)amino)-6-morpholino-1,3,5-triazine-2-carbonitrile (264186)

General Procedure B3 starting from 4-(isopentylamino)-6-morpholino-1,3,5-triazine-2-carbonitrile (100 mg, 0.362 mmol) and 1-(chloromethyl)-2-methoxybenzene (85.0 mg, 0.543 mmol) gave 4-(isopentyl(2-methoxybenzyl)amino)-6-morpholino-1,3,5-triazine-2-carbonitrile (47.8 mg, 0.121 mmol, 33.3 % yield); ¹H NMR (CDCl₃, 500 MHz) δ 7.29 – 7.16 (m, 1H), 7.16 –

7.04 (m, 1H), 6.96 – 6.81 (m, 2H), 4.80 (d, J = 24.9 Hz, 2H), 3.85 (s, 3H), 3.83 – 3.59 (m, 7H), 3.59 – 3.45 (m, 2H), 1.60 – 1.51 (m, 1H), 1.50 – 1.43 (m, 2H), 0.92 (dd, J = 6.5, 4.4 Hz, 6H). ¹³C NMR (CDCl₃, 126 MHz) δ 164.11, 163.66, 157.40, 128.51, 128.46, 128.34, 128.07, 125.40, 125.22, 120.52, 120.48, 115.69, 110.26, 110.23, 55.29, 45.54, 45.19, 44.55, 44.34, 36.34, 35.52, 26.13, 25.97, 22.60, 22.55. HRMS–ESI (m/z): [M+H]⁺ calcd for C₂₁H₂₈N₆O₂, 397.2346; found, 397.2379

4-((4-Fluorobenzyl)(propyl)amino)-6-morpholino-1,3,5-triazine-2-carbonitrile (263256)

In a dry reaction vial, 4-((4-fluorobenzyl)amino)-6-morpholino-1,3,5-triazine-2-carbonitrile (50 mg, 0.159 mmol) was dissolved into DMF (1 ml). Cesium carbonate (104 mg, 0.318 mmol) and 1-bromopropane (0.029 ml, 0.318 mmol) were added to the solution and the reaction was left to stir at 80°C overnight. Reaction was cooled to room temperature, poured into EtOAc and washed 3x with brine. Organic layers were combined, dried over sodium sulfate, and concentrated. Crude residue was purified by flash chromatography (0-100% EtOAc:Hexanes gradient) to afford 4-((4-fluorobenzyl)(propyl)amino)-6-morpholino-1,3,5-triazine-2-carbonitrile (24 mg, 0.067 mmol, 42.3 % yield); ¹H NMR (CDCl₃, 500 MHz) δ 7.11 - 7.25 (m, 2H), 6.97 - 7.04 (m, 2H), 4.77 (s, 1H), 4.72 (s, 1H), 3.82 (br. s., 1H), 3.77 (br. s., 1H), 3.71 - 3.74 (m, 2H), 3.62 - 3.71 (m, 3H), 3.44 - 3.51 (m, 1H), 3.35 - 3.43 (m, 1H), 1.53 - 1.59 (m, 2H), 0.85 - 0.91 (m, 3H); ¹³C NMR (CDCl₃, 126 MHz) δ 164.2, 164.1, 163.6, 163.5, 163.1, 163.0, 161.2, 161.1, 152.0, 151.9, 133.1, 129.4, 128.9, 128.8, 115.6, 115.5, 115.3, 68.2, 66.6, 66.4, 66.3, 49.3, 49.2, 48.5, 48.0, 43.9, 43.7, 43.4, 20.7, 20.1, 11.5, 11.2, 10.4; HRMS–ESI (m/z): [M+H]⁺ calcd for, C₁₈H₂₁FN₆O; 357.1834; found, 357.1834

4-(Butyl(4-fluorobenzyl)amino)-6-morpholino-1,3,5-triazine-2-carbonitrile (263898)

General procedure B3 from 4-((4-fluorobenzyl)amino)-6-morpholino-1,3,5-triazine-2-carbonitrile (100 mg, 0.318 mmol), sodium hydride (19.09 mg, 0.477 mmol) and 1-bromobutane (43.6 mg, 0.318 mmol) gave 4-(butyl(4-fluorobenzyl)amino)-6-morpholino-1,3,5-triazine-2-carbonitrile (97 mg, 0.262 mmol, 82 % yield); ¹H NMR (CDCl₃, 500 MHz) δ 7.14 - 7.25 (m, 2H), 6.99 (t, *J* = 8.56 Hz, 2H), 4.76 (s, 1H), 4.72 (s, 1H), 3.75 - 3.88 (m, 3H), 3.59 - 3.75 (m, 5H), 3.51 (t, *J* = 7.58 Hz, 1H), 3.43 (t, *J* = 7.58 Hz, 1H), 1.53 (t, *J* = 7.34 Hz, 2H), 1.23 - 1.37 (m, 2H), 0.86 - 0.97 (m, 3H); ¹³C NMR (CDCl₃, 126 MHz) δ 164.2, 164.0, 163.6, 163.4, 163.1, 163.0, 161.2, 161.0, 152.0, 151.9, 133.1, 129.4, 129.3, 128.9, 128.8, 115.5, 115.4, 115.3, 115.2, 66.6, 66.3, 49.1, 46.5, 45.9, 43.9, 43.4, 29.5, 28.8, 20.1, 19.9, 13.8, 13.7; ¹⁹F NMR (CDCl₃, 470 MHz) δ -115.01; HRMS-ESI (m/z): [M+H]⁺ calcd for, C₁₉H₂₃FN₆O; 371.1990; found, 371.1989

4-(But-3-en-1-yl(4-fluorobenzyl)amino)-6-morpholino-1,3,5-triazine-2-carbonitrile (263255)

In a dry reaction vessel, 4-((4-fluorobenzyl)amino)-6-morpholino-1,3,5-triazine-2-carbonitrile (50 mg, 0.159 mmol) was dissolved into DMF (1 ml). Potassium carbonate (44.0 mg, 0.318 mmol) and 4-bromobut-1-ene (43.0 mg, 0.318 mmol) were added to the solution and the reaction was left to stir at 80°C overnight. Reaction was cooled to room temperature, poured into EtOAc and washed 3x with brine. Organic layers were combined, dried over sodium sulfate, and concentrated. Crude residue was purified by flash chromatography (0-100% EtOAc:Hexanes gradient) to afford 4-(but-3-en-1-yl(4-fluorobenzyl)amino)-6-morpholino-1,3,5-triazine-2-carbonitrile (25 mg, 0.068 mmol, 42.7 % yield); ¹H NMR (CDCl₃, 500 MHz) δ 7.15 - 7.24 (m, 2H), 6.97 - 7.04 (m, 2H), 5.66 - 5.84 (m, 1H), 5.00 - 5.09 (m, 2H), 4.78 (s, 1H), 4.73 (s, 1H), 3.75 - 3.87 (m, 3H), 3.63 - 3.75 (m, 5H), 3.59 (t, *J* = 7.34 Hz, 1H), 3.50 (t, *J* = 7.34 Hz, 1H), 2.25

- 2.36 (m, 2H); ^{13}C NMR (CDCl_3 , 126 MHz) δ 164.1, 163.5, 152.0, 143.6, 135.0, 134.9, 133.0, 129.5, 129.0, 128.9, 117.1, 116.9, 115.6, 115.4, 49.6, 49.5, 46.4, 46.0, 44.0, 43.9, 43.4, 32.0, 31.3; HRMS–ESI (m/z): $[\text{M}+\text{H}]^+$ calcd for, $\text{C}_{19}\text{H}_{21}\text{FN}_6\text{O}$; 369.1834; found, 369.1842

4-((4-Fluorobenzyl)(3-methylbut-3-en-1-yl)amino)-6-morpholino-1,3,5-triazine-2-carbonitrile (263918)

General procedure B3 from 4-((4-fluorobenzyl)amino)-6-morpholino-1,3,5-triazine-2-carbonitrile (100 mg, 0.318 mmol), sodium hydride (19.09 mg, 0.477 mmol), and 3-methylbut-3-en-1-yl 4-methylbenzenesulfonate (76 mg, 0.318 mmol) gave 4-((4-fluorobenzyl)(3-methylbut-3-en-1-yl)amino)-6-morpholino-1,3,5-triazine-2-carbonitrile (50.3 mg, 0.132 mmol, 41.3 % yield); ^1H NMR (CDCl_3 , 500 MHz) δ 7.14 - 7.25 (m, 2H), 6.95 - 7.07 (m, 2H), 4.77 (br. s., 2H), 4.73 (s, 1H), 4.66 (br. s., 1H), 3.76 - 3.86 (m, 3H), 3.72 (br. s., 3H), 3.59 - 3.69 (m, 3H), 3.54 (t, $J = 7.58$ Hz, 1H), 2.24 (q, $J = 7.83$ Hz, 2H), 1.74 (d, $J = 21.52$ Hz, 3H); ^{13}C NMR (CDCl_3 , 126 MHz) δ 164.2, 164.0, 163.6, 163.5, 163.2, 163.1, 161.3, 152.0, 142.6, 142.5, 133.0, 129.5, 129.5, 129.0, 128.9, 115.6, 115.5, 115.4, 112.2, 66.7, 66.4, 66.3, 49.4, 49.2, 45.4, 45.2, 44.0, 43.9, 43.4, 35.6, 34.8, 22.5, 22.4; HRMS–ESI (m/z): $[\text{M}+\text{H}]^+$ calcd for, $\text{C}_{20}\text{H}_{23}\text{FN}_6\text{O}$; 383.1990; found, 383.1989

4-((4-Fluorobenzyl)(isobutyl)amino)-6-morpholino-1,3,5-triazine-2-carbonitrile (263043)

General procedure A4 from 4-chloro-N-(4-fluorobenzyl)-N-isobutyl-6-morpholino-1,3,5-triazin-2-amine (65 mg, 0.171 mmol), DABCO (38.4 mg, 0.342 mmol), and potassium cyanide (12.26 mg, 0.188 mmol) gave 4-((4-fluorobenzyl)(isobutyl)amino)-6-morpholino-1,3,5-triazine-2-carbonitrile (48 mg, 0.130 mmol, 76 % yield); ^1H NMR (CDCl_3 , 500 MHz) δ 7.08 - 7.23 (m,

2H), 6.98 (t, $J = 8.31$ Hz, 2H), 4.78 (s, 1H), 4.73 (s, 1H), 3.77 (br. s., 3H), 3.70 (br. s., 3H), 3.63 (br. s., 2H), 3.37 (d, $J = 7.34$ Hz, 1H), 3.27 (d, $J = 7.34$ Hz, 1H), 2.05 - 2.14 (m, 1H), 0.83 - 0.94 (m, 6H); ^{13}C NMR (CDCl_3 , 126 MHz) δ 164.6, 164.6, 163.4, 161.1, 151.9, 151.9, 133.0, 132.9, 129.4, 129.3, 128.8, 128.8, 115.5, 115.5, 115.4, 115.3, 115.3, 66.6, 66.4, 66.3, 53.8, 53.4, 49.7, 49.6, 46.5, 43.8, 43.3, 37.1, 36.6, 31.5, 27.0, 26.7, 21.0, 20.3, 20.0, 20.0, 14.8, 14.1, 14.0, 13.9; HRMS–ESI (m/z): $[\text{M}+\text{H}]^+$ calcd for, $\text{C}_{19}\text{H}_{23}\text{FN}_6\text{O}$; 371.1996; found, 371.2060

4-((4-Fluorobenzyl)(4-methylpentyl)amino)-6-morpholino-1,3,5-triazine-2-carbonitrile (1-2P/263939)

General Procedure B3 starting from 4-((4-fluorobenzyl)amino)-6-morpholino-1,3,5-triazine-2-carbonitrile (70.0 mg, 0.223 mmol) and 1-bromo-4-methylpentane (55.1 mg, 0.334 mmol) gave 4-((4-fluorobenzyl)(4-methylpentyl)amino)-6-morpholino-1,3,5-triazine-2-carbonitrile (48.0 mg, 0.120 mmol, 54.1 % yield); ^1H NMR (CDCl_3 , 500 MHz) δ 7.14-7.24 (m, 2H), 7.00 (t, $J = 8.61$ Hz, 2H), 4.76 (s, 1H), 4.72 (s, 1H), 3.74 - 3.86 (m, 3H), 3.61 - 3.74 (m, 5H), 3.48 (t, $J = 7.43$ Hz, 1H), 3.39 (t, $J = 7.63$ Hz, 1H), 1.46 - 1.60 (m, 3H), 1.05 - 1.19 (m, 2H), 0.86 (d, $J = 6.65$ Hz, 3H), 0.84 (d, $J = 6.70$ Hz, 3H). ^{13}C NMR (CDCl_3 , 126 MHz) δ 164.2, 164.0, 163.6, 163.5, 163.4, 163.3, 152.0, 151.9, 133.1, 129.7, 129.6, 129.2, 128.7, 128.7, 115.7, 115.6, 115.6, 115.5, 115.4, 115.1, 66.7, 66.4, 49.6, 49.4, 49.3, 49.1, 47.0, 46.8, 46.7, 43.9, 43.4, 36.3, 36.1, 35.9, 35.7, 35.5, 27.7, 27.6, 27.5, 25.2, 24.4, 22.7, 22.5, 22.4, 22.2. ^{19}F NMR (376 MHz, Chloroform- d) δ -115.07, -114.99. HRMS–ESI (m/z): $[\text{M}+\text{H}]^+$ calcd for $\text{C}_{21}\text{H}_{27}\text{FN}_6\text{O}$, 399.2303; found, 399.2302

**4-((Cyclopropylmethyl)(4-fluorobenzyl)amino)-6-morpholino-1,3,5-triazine-2-carbonitrile
(263253)**

In a dry reaction vessel, 4-((4-fluorobenzyl)amino)-6-morpholino-1,3,5-triazine-2-carbonitrile (50 mg, 0.159 mmol) was dissolved into DMF (0.5 ml). Potassium carbonate (44.0 mg, 0.318 mmol) and (bromomethyl)cyclopropane (0.031 ml, 0.318 mmol) were added to the solution and the reaction was left to stir at 80°C overnight. Reaction was cooled to room temperature, poured into EtOAc and washed 3x with brine. Organic layers were combined, dried over sodium sulfate, and concentrated. Crude residue was purified by flash chromatography (0-100% EtOAc:Hexanes gradient) to afford 4-((cyclopropylmethyl)(4-fluorobenzyl)amino)-6-morpholino-1,3,5-triazine-2-carbonitrile (15 mg, 0.041 mmol, 25.6 % yield); ¹H NMR (CDCl₃, 500 MHz) δ 7.15 - 7.25 (m, 2H), 7.01 (t, *J* = 8.56 Hz, 2H), 4.89 (s, 1H), 4.85 (s, 1H), 3.63 - 3.86 (m, 8H), 3.46 (d, *J* = 6.85 Hz, 1H), 3.37 (d, *J* = 6.85 Hz, 1H), 0.98 - 1.08 (m, 1H), 0.49 (dd, *J* = 5.38, 12.72 Hz, 2H), 0.25 (q, *J* = 4.89 Hz, 1H), 0.19 (q, *J* = 4.89 Hz, 1H); ¹³C NMR (CDCl₃, 126 MHz) δ 164.3, 163.6, 163.5, 163.1, 163.0, 161.2, 161.0, 152.0, 133.2, 133.1, 129.3, 129.2, 128.8, 128.7, 115.5, 115.4, 115.3, 115.2, 115.0, 71.5, 66.6, 66.4, 66.3, 50.9, 50.3, 49.2, 49.1, 43.9, 43.7, 43.4, 14.2, 9.6, 9.1, 3.6; HRMS-ESI (m/z): [M+H]⁺ calcd for, C₁₉H₂₁FN₆O; 369.1834; found, 369.1835

**4-((Cyclobutylmethyl)(4-fluorobenzyl)amino)-6-morpholino-1,3,5-triazine-2-carbonitrile
(263254)**

In a dry reaction vial, 4-((4-fluorobenzyl)amino)-6-morpholino-1,3,5-triazine-2-carbonitrile (50 mg, 0.159 mmol) was dissolved into DMF (1 ml). Potassium carbonate (44.0 mg, 0.318 mmol) and (bromomethyl)cyclobutane (47.4 mg, 0.318 mmol) were added to the solution and the reaction was left to stir at 80°C overnight. Reaction was cooled to room temperature, poured into

EtOAc and washed 3x with brine. Organic layers were combined, dried over sodium sulfate, and concentrated. Crude residue was purified by flash chromatography (0-100% EtOAc:Hexanes) to afford 4-((cyclobutylmethyl)(4-fluorobenzyl)amino)-6-morpholino-1,3,5-triazine-2-carbonitrile (17 mg, 0.044 mmol, 27.9 % yield); ¹H NMR (CDCl₃, 500 MHz) δ 7.10 - 7.22 (m, 2H), 7.00 (t, *J* = 7.83 Hz, 2H), 4.76 (s, 1H), 4.71 (s, 1H), 3.80 (br. s., 3H), 3.73 (br. s., 2H), 3.69 (br. s., 1H), 3.64 (br. s., 2H), 3.60 (d, *J* = 7.34 Hz, 1H), 3.51 (d, *J* = 7.34 Hz, 1H), 2.53 - 2.69 (m, 1H), 1.97 (br. s., 2H), 1.79 - 1.92 (m, 2H), 1.64 - 1.79 (m, 2H); ¹³C NMR (CDCl₃, 126 MHz) δ 164.5, 164.4, 163.6, 163.5, 163.2, 161.2, 161.1, 152.0, 151.9, 133.2, 129.3, 129.3, 128.7, 128.7, 115.6, 115.5, 115.3, 66.6, 66.4, 66.3, 51.7, 51.1, 49.5, 43.9, 43.4, 34.3, 34.0, 26.8, 26.5, 18.6, 18.5; HRMS-ESI (m/z): [M+H]⁺ calcd for, C₂₀H₂₃FN₆O; 383.1990; found, 383.1994

4-(Cyclopentyl(4-fluorobenzyl)amino)-6-morpholino-1,3,5-triazine-2-carbonitrile (263022)

General procedure A4 from 4-chloro-N-cyclopentyl-N-(4-fluorobenzyl)-6-morpholino-1,3,5-triazin-2-amine (150 mg, 0.383 mmol), DABCO (86 mg, 0.766 mmol), and potassium cyanide (27.4 mg, 0.421 mmol) gave 4-(cyclopentyl(4-fluorobenzyl)amino)-6-morpholino-1,3,5-triazine-2-carbonitrile (20.5 mg, 0.054 mmol, 14.00 % yield); ¹H NMR (CDCl₃, 500 MHz) δ 7.04 - 7.22 (m, 2H), 6.90 - 7.01 (m, 2H), 4.68 - 4.79 (m, 1H), 4.61 (s, 1H), 3.56 - 3.90 (m, 6H), 3.48 (d, *J* = 15.16 Hz, 2H), 1.75 - 1.92 (m, 2H), 1.63 - 1.75 (m, 2H), 1.43 - 1.63 (m, 6H); ¹³C NMR (CDCl₃, 126 MHz) δ 164.3, 163.3, 162.6, 160.6, 151.8, 134.3, 128.1, 127.5, 115.6, 115.1, 66.6, 57.2, 46.1, 43.8, 29.2, 23.7; HRMS-ESI (m/z): [M+H]⁺ calcd for, C₂₀H₂₃FN₆O; 383.1990; found, 383.1992

**4-((Cyclopentylmethyl)(4-fluorobenzyl)amino)-6-morpholino-1,3,5-triazine-2-carbonitrile
(264503)**

General procedure B3 from 4-((4-fluorobenzyl)amino)-6-morpholino-1,3,5-triazine-2-carbonitrile (100 mg, 0.318 mmol), sodium hydride (14.00 mg, 0.350 mmol), and (bromomethyl)cyclopentane (0.039 ml, 0.318 mmol) gave 4-((cyclopentylmethyl)(4-fluorobenzyl)amino)-6-morpholino-1,3,5-triazine-2-carbonitrile (31.6 mg, 0.080 mmol, 25.05 % yield); ¹H NMR (CDCl₃, 500 MHz) δ 1.22 (m) 1.54 (m) 1.64 (m) 2.27 (m) 3.42 (d) 3.51 (d) 3.66 (m) 3.72 (m) 3.79 (m) 4.76 (s) 4.81 (s) 7.00 (t) 7.18 (m); ¹³C NMR (CDCl₃, 126 MHz) δ 164.5, 163.5, 163.1, 163.0, 161.2, 161.0, 151.9, 133.1, 133.0, 129.4, 129.3, 128.8, 128.7, 115.6, 115.5, 115.3, 66.7, 66.4, 66.3, 50.9, 50.3, 49.3, 49.2, 43.9, 43.4, 38.7, 38.2, 30.5, 30.3, 24.9, 24.8; ¹⁹F NMR (CDCl₃, 470 MHz) δ -115.16 (m); HRMS–ESI (m/z): [M+H]⁺ calcd for, C₂₁H₂₅FN₆O ; 397.2147; found, 397.2141

**4-((Cyclohexylmethyl)(4-fluorobenzyl)amino)-6-morpholino-1,3,5-triazine-2-carbonitrile
(263683)**

General procedure B3 from 4-((4-fluorobenzyl)amino)-6-morpholino-1,3,5-triazine-2-carbonitrile (100 mg, 0.318 mmol), sodium hydride (15.27 mg, 0.382 mmol), and (bromomethyl)cyclohexane (0.043 ml, 0.318 mmol) gave 4-((cyclohexylmethyl)(4-fluorobenzyl)amino)-6-morpholino-1,3,5-triazine-2-carbonitrile (105 mg, 0.256 mmol, 80 % yield); ¹H NMR (CDCl₃, 500 MHz) δ 7.11 - 7.22 (m, 2H), 6.92 - 7.05 (m, 2H), 4.79 (s, 1H), 4.73 (s, 1H), 3.78 - 3.87 (m, 2H), 3.76 (br. s., 1H), 3.71 - 3.75 (m, 2H), 3.60 - 3.70 (m, 3H), 3.40 (d, *J* = 7.83 Hz, 1H), 3.30 (d, *J* = 7.34 Hz, 1H), 1.68 - 1.83 (m, 3H), 1.57 - 1.68 (m, 3H), 1.15 - 1.24 (m, 3H), 0.88 - 1.04 (m, 2H); ¹³C NMR (CDCl₃, 126 MHz) δ 164.7, 164.6, 164.1, 163.8, 163.5,

161.2, 161.1, 152.0, 151.9, 133.1, 133.0, 129.4, 128.8, 115.6, 115.5, 115.4, 115.3, 66.7, 66.4, 66.3, 52.6, 52.2, 49.8, 49.7, 44.0, 43.4, 36.5, 36.3, 31.2, 30.7, 26.3, 25.8; HRMS–ESI (m/z): [M+H]⁺ calcd for, C₂₂H₂₇FN₆O; 411.2303; found, 411.2300

4-((2-Cyclopropylethyl)(4-fluorobenzyl)amino)-6-morpholino-1,3,5-triazine-2-carbonitrile (263698)

General procedure B3 from 4-((4-fluorobenzyl)amino)-6-morpholino-1,3,5-triazine-2-carbonitrile (100 mg, 0.318 mmol), sodium hydride (19.09 mg, 0.477 mmol), and 2-cyclopropylethyl 4-methylbenzenesulfonate (76 mg, 0.318 mmol) gave 4-((2-cyclopropylethyl)(4-fluorobenzyl)amino)-6-morpholino-1,3,5-triazine-2-carbonitrile (58 mg, 0.152 mmol, 47.7 % yield); ¹H NMR (CDCl₃, 500 MHz) δ 7.13 - 7.26 (m, 2H), 7.00 (t, *J* = 8.31 Hz, 2H), 4.78 (s, 1H), 4.73 (s, 1H), 3.75 - 3.85 (m, 3H), 3.70 - 3.74 (m, 2H), 3.68 (br. s., 2H), 3.65 (br. s., 1H), 3.59 (t, *J* = 7.40 Hz, 1H), 3.51 (t, *J* = 7.34 Hz, 1H), 1.40 - 1.51 (m, 2H), 0.52 - 0.69 (m, 1H), 0.43 (d, *J* = 7.83 Hz, 2H), 0.02 - 0.07 (m, 1H), -0.02 - 0.02 (m, 1H); ¹³C NMR (CDCl₃, 126 MHz) δ 164.1, 164.0, 163.6, 163.5, 163.0, 161.2, 161.1, 152.0, 151.9, 133.1, 133.1, 129.5, 129.4, 128.9, 115.6, 115.5, 115.3, 66.7, 66.6, 66.4, 66.3, 49.5, 47.1, 46.4, 43.9, 43.4, 32.5, 31.8, 8.5, 8.4, 4.4, 4.3; HRMS–ESI (m/z): [M+H]⁺ calcd for, C₂₀H₂₃FN₆O; 383.1990; found, 383.1986

4-((3,3-Dimethylbutyl)(4-fluorobenzyl)amino)-6-morpholino-1,3,5-triazine-2-carbonitrile (263806)

General procedure B3 from 4-((4-fluorobenzyl)amino)-6-morpholino-1,3,5-triazine-2-carbonitrile (100 mg, 0.318 mmol), sodium hydride (19.09 mg, 0.477 mmol), and 1-bromo-3,3-

dimethylbutane (0.068 ml, 0.477 mmol) gave 4-((3,3-dimethylbutyl)(4-fluorobenzyl)amino)-6-morpholino-1,3,5-triazine-2-carbonitrile (26 mg, 0.065 mmol, 20.51 % yield); ^1H NMR (CDCl_3 , 500 MHz) δ 7.15 - 7.25 (m, 2H), 6.98 - 7.04 (m, 2H), 4.74 (s, 1H), 4.69 (s, 1H), 3.76 - 3.86 (m, 3H), 3.72 (br. s., 3H), 3.63 - 3.70 (m, 2H), 3.47 - 3.53 (m, 1H), 3.39 - 3.47 (m, 1H), 1.37 - 1.46 (m, 2H), 0.91 (d, $J = 7.83$ Hz, 9H); ^{13}C NMR (CDCl_3 , 126 MHz) δ 163.7, 163.5, 162.8, 162.7, 156.1, 151.9, 133.1, 129.6, 129.5, 129.1, 129.0, 115.6, 115.4, 66.7, 66.4, 49.1, 43.5, 43.4, 42.8, 40.5, 39.6, 29.6, 29.3; ^{19}F NMR (CDCl_3 , 470 MHz) δ -114.89 (m); HRMS–ESI (m/z): $[\text{M}+\text{H}]^+$ calcd for, $\text{C}_{21}\text{H}_{27}\text{FN}_6\text{O}$; 399.2303; found, 399.2301

4-((3-Fluoro-3-methylbutyl)(4-fluorobenzyl)amino)-6-morpholino-1,3,5-triazine-2-carbonitrile (263919)

4-((4-fluorobenzyl)amino)-6-morpholino-1,3,5-triazine-2-carbonitrile (100 mg, 0.318 mmol), sodium hydride (19.09 mg, 0.477 mmol), and 3-fluoro-3-methylbutyl 4-methylbenzenesulfonate (83 mg, 0.318 mmol) gave 4-((3-fluoro-3-methylbutyl)(4-fluorobenzyl)amino)-6-morpholino-1,3,5-triazine-2-carbonitrile (59 mg, 0.147 mmol, 46.1 % yield); ^1H NMR (CDCl_3 , 500 MHz) δ 7.17 - 7.25 (m, 2H), 7.00 (t, $J = 8.31$ Hz, 2H), 4.76 (s, 1H), 4.72 (s, 1H), 3.75 - 3.87 (m, 3H), 3.67 - 3.74 (m, 4H), 3.63 - 3.67 (m, 1H), 3.60 - 3.63 (m, 1H), 3.54 - 3.60 (m, 1H), 1.77 - 1.91 (m, 2H), 1.37 (d, $J = 18.10$ Hz, 3H), 1.33 (d, $J = 18.10$ Hz, 3H); ^{13}C NMR (CDCl_3 , 126 MHz) δ 164.1, 163.9, 163.6, 163.4, 163.2, 163.1, 161.2, 161.1, 152.0, 151.9, 132.9, 129.6, 129.5, 129.1, 115.5, 115.4, 115.3, 95.1, 94.8, 93.8, 93.4, 66.6, 66.3, 49.3, 49.2, 43.9, 43.7, 43.4, 42.5, 42.0, 41.9, 38.3, 38.2, 37.6, 37.4, 26.8, 26.7, 26.6, 26.5; ^{19}F NMR (CDCl_3 , 470 MHz) δ -114.71 (m), -140.96 (m), -139.84 (m); HRMS–ESI (m/z): $[\text{M}+\text{H}]^+$ calcd for, $\text{C}_{20}\text{H}_{24}\text{F}_2\text{N}_6\text{O}$; 403.2052; found, 403.2051

4-((2-Cyclohexylethyl)(4-fluorobenzyl)amino)-6-morpholino-1,3,5-triazine-2-carbonitrile (263682)

General procedure B3 from 4-((4-fluorobenzyl)amino)-6-morpholino-1,3,5-triazine-2-carbonitrile (100 mg, 0.318 mmol), sodium hydride (19.09 mg, 0.477 mmol), and (2-bromoethyl)cyclohexane (122 mg, 0.636 mmol) gave 4-((2-cyclohexylethyl)(4-fluorobenzyl)amino)-6-morpholino-1,3,5-triazine-2-carbonitrile (84.1 mg, 0.198 mmol, 62.3 % yield); ¹H NMR (CDCl₃, 500 MHz) δ 7.14 - 7.26 (m, 2H), 7.00 (t, *J* = 8.56 Hz, 2H), 4.75 (s, 1H), 4.71 (s, 1H), 3.76 - 3.88 (m, 3H), 3.60 - 3.76 (m, 5H), 3.49 - 3.57 (m, 1H), 3.39 - 3.49 (m, 1H), 1.59 - 1.74 (m, 5H), 1.36 - 1.48 (m, 2H), 1.11 - 1.24 (m, 4H), 0.82 - 0.98 (m, 2H); ¹³C NMR (CDCl₃, 126 MHz) δ 164.1, 163.9, 163.6, 163.5, 163.2, 163.0, 161.2, 161.1, 152.0, 151.9, 133.1, 129.5, 129.4, 129.0, 128.9, 115.5, 115.3, 66.7, 66.4, 49.0, 44.8, 44.2, 43.9, 43.4, 35.5, 35.3, 34.7, 33.9, 33.2, 33.1, 26.4, 26.1, 14.1; HRMS-ESI (m/z): [M+H]⁺ calcd for, C₂₃H₂₉FN₆O; 425.2460; found, 425.2453

4-((4-Fluorobenzyl)((3-methyloxetan-3-yl)methyl)amino)-6-morpholino-1,3,5-triazine-2-carbonitrile (263257)

In a dry reaction vial, 4-((4-fluorobenzyl)amino)-6-morpholino-1,3,5-triazine-2-carbonitrile (50 mg, 0.159 mmol) was dissolved into DMF (1 ml). Cesium carbonate (104 mg, 0.318 mmol) and 3-(bromomethyl)-3-methyloxetane (0.037 ml, 0.318 mmol) were added to the solution and the reaction was left overnight at 80°C. Crude was purified by FC (1-100% EtOAc:Hexanes gradient) to afford 4-((4-fluorobenzyl)((3-methyloxetan-3-yl)methyl)amino)-6-morpholino-1,3,5-triazine-2-carbonitrile (16.9 mg, 0.042 mmol, 26.7 % yield); ¹H NMR (CDCl₃, 500 MHz) δ 7.09 - 7.19 (m, 2H), 7.01 (t, *J* = 8.56 Hz, 2H), 4.78 (s, 1H), 4.71 (s, 1H), 4.50 - 4.63 (m, 2H),

4.36 - 4.42 (m, 1H), 4.24 - 4.30 (m, 2H), 3.82 (dd, $J = 4.89, 9.78$ Hz, 2H), 3.69 - 3.79 (m, 4H), 3.65 (d, $J = 7.34$ Hz, 2H), 2.93 (s, 2H), 1.36 (s, 3H); ^{13}C NMR (CDCl_3 , 126 MHz) δ 165.1, 163.5, 155.5, 152.0, 151.9, 132.3, 129.2, 129.1, 128.7, 115.7, 115.6, 115.5, 115.3, 115.2, 81.5, 81.3, 79.5, 79.3, 72.4, 69.3, 66.6, 66.3, 52.7, 51.5, 50.3, 50.2, 43.9, 43.5, 43.4, 41.0, 40.7, 39.3, 39.2, 22.6, 22.1, 20.9; HRMS-ESI (m/z): $[\text{M}+\text{H}]^+$ calcd for, $\text{C}_{20}\text{H}_{23}\text{FN}_6\text{O}_2$; 399.1939; found, 399.1939

**4-((2-Aminoethyl)(4-fluorobenzyl)amino)-6-morpholino-1,3,5-triazine-2-carbonitrile
(264084)**

General Procedure B3 starting from 4-((4-fluorobenzyl)amino)-6-morpholino-1,3,5-triazine-2-carbonitrile (150 mg, 0.477 mmol) and tert-butyl (2-bromoethyl)carbamate (160 mg, 0.716 mmol) gave tert-butyl(2-((4-cyano-6-morpholino-1,3,5-triazin-2-yl)(4-fluorobenzyl)amino)ethyl)carbamate (25.0 mg, 0.055 mmol, 11 % yield). Carried directly through General Procedure B4 to give 4-((2-aminoethyl)(4-fluorobenzyl)amino)-6-morpholino-1,3,5-triazine-2-carbonitrile (4.0 mg, 0.055 mmol, 20.0 % yield); ^1H NMR (CDCl_3 , 500 MHz) δ 7.21 (t, $J = 7.2$ Hz, 2H), 7.01 (t, $J = 8.3$ Hz, 2H), 4.75 (s, 2H), 3.86 - 3.59 (m, 9H), 3.13 (s, 2H), 1.33 - 1.17 (m, 2H). ^{13}C NMR (CDCl_3 , 126 MHz) δ 163.20, 132.03, 129.42, 129.35, 115.92, 115.75, 66.53, 49.84, 44.12, 43.67, 14.20, 1.01. ^{19}F NMR (470 MHz, Chloroform- d) δ -75.70, -113.97. HRMS-ESI (m/z): $[\text{M}+\text{H}]^+$ calcd for $\text{C}_{17}\text{H}_{20}\text{FN}_7\text{O}$, 358.1786; found, 358.1785

4-((3-Aminopropyl)(4-fluorobenzyl)amino)-6-morpholino-1,3,5-triazine-2-carbonitrile

(264082)

General Procedure B3 starting from 4-((4-fluorobenzyl)amino)-6-morpholino-1,3,5-triazine-2-carbonitrile (150 mg, 0.477 mmol) and tert-butyl (3-bromopropyl)carbamate (170 mg, 0.716 mmol) gave tert-butyl(3-((4-cyano-6-morpholino-1,3,5-triazin-2-yl)(4-fluorobenzyl)amino)propyl)carbamate (97.6 mg, 0.207 mmol, 43.4 % yield). Carried directly through General Procedure B4 to give 4-((3-aminopropyl)(4-fluorobenzyl)amino)-6-morpholino-1,3,5-triazine-2-carbonitrile (19.0 mg, 0.085 mmol, 60.0 % yield); ¹H NMR (CDCl₃, 500 MHz) δ 7.23 – 7.09 (m, 2H), 6.99 (t, J = 8.5 Hz, 2H), 4.82 – 4.64 (m, 2H), 3.90 – 3.43 (m, 9H), 2.93 (s, 2H), 1.90 (s, 3H), 1.26 (s, 1H). ¹³C NMR (CDCl₃, 126 MHz) δ 164.42, 162.98, 161.36, 151.47, 132.19, 129.16, 129.09, 115.82, 115.65, 66.51, 66.21, 49.08, 43.65, 42.48, 25.02. ¹⁹F NMR (470 MHz, Chloroform-d) δ -74.98, -76.05, -113.87 – -115.03 (m). HRMS–ESI (m/z): [M+H]⁺ calcd for C₁₈H₂₂FN₇O, 372.1943; found, 372.1943

4-((4-Aminobutyl)(4-fluorobenzyl)amino)-6-morpholino-1,3,5-triazine-2-carbonitrile

(264083)

General Procedure B3 starting from 4-((4-fluorobenzyl)amino)-6-morpholino-1,3,5-triazine-2-carbonitrile (150 mg, 0.477 mmol) and tert-butyl (4-bromobutyl)carbamate (180 mg, 0.716 mmol) gave tert-butyl(4-((4-cyano-6-morpholino-1,3,5-triazin-2-yl)(4-fluorobenzyl)amino)butyl)carbamate (40 mg, 0.082 mmol, 17 % yield). Carried directly through General Procedure B4 to give 4-((4-aminobutyl)(4-fluorobenzyl)amino)-6-morpholino-1,3,5-triazine-2-carbonitrile (4.9 mg, 0.013 mmol, 15 % yield); ¹H NMR (CDCl₃, 500 MHz) δ 7.19 (d, J = 6.3 Hz, 2H), 7.00

(d, $J = 4.4$ Hz, 2H), 4.73 (d, $J = 15.5$ Hz, 2H), 3.91 – 3.58 (m, 8H), 3.50 (s, 2H), 2.95 (d, $J = 54.8$ Hz, 2H), 1.62 (s, 4H). ^{13}C NMR (CDCl_3 , 126 MHz) δ 164.20, 163.32, 151.81, 129.50, 129.08, 129.01, 115.68, 115.51, 49.27, 45.42, 39.34, 24.04. ^{19}F NMR (470 MHz, Chloroform- d) δ -75.87, -114.63. HRMS–ESI (m/z): $[\text{M}+\text{H}]^+$ calcd for $\text{C}_{19}\text{H}_{24}\text{FN}_7\text{O}$, 386.2099; found, 386.2095

4-((4-Fluorobenzyl)(2-(pyrrolidin-1-yl)ethyl)amino)-6-morpholino-1,3,5-triazine-2-carbonitrile (263661)

General procedure B3 from 4-((4-fluorobenzyl)amino)-6-morpholino-1,3,5-triazine-2-carbonitrile (100 mg, 0.318 mmol), sodium hydride (19.09 mg, 0.477 mmol), and 1-(2-chloroethyl)pyrrolidine (85 mg, 0.636 mmol) gave 4-((4-fluorobenzyl)(2-(pyrrolidin-1-yl)ethyl)amino)-6-morpholino-1,3,5-triazine-2-carbonitrile (92 mg, 0.224 mmol, 70.3 % yield); ^1H NMR (CDCl_3 , 500 MHz) δ 7.15 - 7.25 (m, 2H), 6.94 - 7.05 (m, 2H), 4.80 (s, 1H), 4.78 (s, 1H), 3.81 (br. s., 1H), 3.78 (br. s., 2H), 3.68 - 3.74 (m, 3H), 3.62 - 3.68 (m, 3H), 3.58 (t, $J = 7.34$ Hz, 1H), 2.56 - 2.67 (m, 2H), 2.42 - 2.56 (m, 4H), 1.76 (br. s., 4H); ^{13}C NMR (CDCl_3 , 126 MHz) δ 164.2, 164.1, 163.6, 163.5, 163.2, 163.0, 161.2, 161.1, 152.0, 151.9, 133.1, 133.0, 129.6, 129.5, 129.0, 128.9, 115.5, 115.3, 66.6, 66.4, 66.3, 54.4, 54.3, 53.6, 52.7, 49.8, 49.7, 45.7, 45.4, 43.9, 43.4, 23.5, 23.4; HRMS–ESI (m/z): $[\text{M}+\text{H}]^+$ calcd for, $\text{C}_{21}\text{H}_{26}\text{FN}_7\text{O}$; 412.2256; found, 412.2255

4-((4-Fluorobenzyl)(2-(piperidin-3-yl)ethyl)amino)-6-morpholino-1,3,5-triazine-2-carbonitrile (264039)

General procedure B4 from tert-butyl 3-(2-((4-cyano-6-morpholino-1,3,5-triazin-2-yl)(4-fluorobenzyl)amino)ethyl)piperidine-1-carboxylate (80 mg, 0.152 mmol) gave 4-((4-fluorobenzyl)(2-(piperidin-3-yl)ethyl)amino)-6-morpholino-1,3,5-triazine-2-carbonitrile (45.6

mg, 0.107 mmol, 70.4 % yield); ^1H NMR (CDCl_3 , 500 MHz) δ 7.12 - 7.24 (m, 2H), 6.92 - 7.09 (m, 2H), 4.57 - 4.86 (m, 2H), 3.53 - 3.99 (m, 10H), 3.31 - 3.52 (m, 2H), 2.84 (br. s., 1H), 2.56 (br. s., 1H), 1.85 - 2.02 (m, 2H), 1.78 (br. s., 2H), 1.35 - 1.62 (m, 2H), 1.03 - 1.26 (m, 1H); ^{13}C NMR (CDCl_3 , 126 MHz) δ 169.9, 168.6, 164.4, 164.1, 164.0, 163.6, 163.4, 161.3, 161.0, 160.8, 151.9, 129.5, 129.0, 115.7, 115.5, 107.8, 66.6, 66.3, 49.0, 44.7, 44.0, 43.6, 43.4, 31.6, 31.5, 30.8, 30.5, 28.9, 28.8, 22.0; ^{19}F NMR (CDCl_3 , 470 MHz) δ -114.80 (s), -75.85 (s); HRMS–ESI (m/z): $[\text{M}+\text{H}]^+$ calcd for, $\text{C}_{22}\text{H}_{28}\text{FN}_7\text{O}$; 426.2412 ; found, 426.2398

4-((4-Fluorobenzyl)(2-(piperidin-4-yl)ethyl)amino)-6-morpholino-1,3,5-triazine-2-carbonitrile (264038)

General procedure B4 from tert-butyl 4-(2-((4-cyano-6-morpholino-1,3,5-triazin-2-yl)(4-fluorobenzyl)amino)ethyl)piperidine-1-carboxylate (80 mg, 0.152 mmol) gave 4-((4-fluorobenzyl)(2-(piperidin-4-yl)ethyl)amino)-6-morpholino-1,3,5-triazine-2-carbonitrile (12 mg, 0.028 mmol, 18.53 % yield); ^1H NMR (CDCl_3 , 500 MHz) δ 7.15 - 7.24 (m, 2H), 7.02 (t, $J = 8.31$ Hz, 2H), 4.77 (s, 1H), 4.72 (s, 1H), 3.84 (br. s, 2H), 3.70 - 3.78 (m, 4H), 3.63 - 3.70 (m, 2H), 3.56 (t, $J = 7.09$ Hz, 1H), 3.44 - 3.52 (m, 1H), 3.24 - 3.34 (m, 2H), 2.69 - 2.86 (m, 2H), 1.73 - 1.92 (m, 2H), 1.39 - 1.58 (m, 5H); ^{19}F NMR (CDCl_3 , 470 MHz) δ -114.58 (m) -75.84 (m); HRMS–ESI (m/z): $[\text{M}+\text{H}]^+$ calcd for, $\text{C}_{22}\text{H}_{28}\text{FN}_7\text{O}$; 426.2412 ; found, 426.2408

4-((4-Fluorobenzyl)(piperidin-3-ylmethyl)amino)-6-morpholino-1,3,5-triazine-2-carbonitrile (264081)

General procedure B4 from tert-butyl 3-(((4-cyano-6-morpholino-1,3,5-triazin-2-yl)(4-fluorobenzyl)amino)methyl) piperidine-1-carboxylate (80 mg, 0.156 mmol) gave 4-((4-

fluorobenzyl)(piperidin-3-ylmethyl)amino)-6-morpholino-1,3,5-triazine-2-carbonitrile, TFA (47 mg, 0.089 mmol, 57.2 % yield). ¹H NMR (CDCl₃, 500 MHz) δ 7.10 - 7.24 (m, 2H), 7.00 (t, *J* = 7.83 Hz, 2H), 4.84 - 4.99 (m, 1H), 4.49 - 4.68 (m, 1H), 3.60 - 3.93 (m, 9H), 3.22 - 3.54 (m, 4H), 2.81 - 3.02 (m, 1H), 2.57 - 2.81 (m, 1H), 2.29 (br. s., 1H), 1.93 (br. s., 1H), 1.70 - 1.87 (m, 2H), 1.14 - 1.40 (m, 1H); ¹³C NMR (CDCl₃, 126 MHz) δ 164.9, 164.8, 163.4, 163.3, 163.2, 161.3, 152.0, 151.8, 132.2, 132.1, 129.5, 129.1, 129.0, 115.8, 115.5, 115.3, 115.2, 66.5, 66.2, 49.5, 49.1, 48.3, 47.7, 47.2, 44.6, 44.5, 43.9, 43.5, 43.3, 32.5, 32.4, 28.1, 26.8, 26.3, 21.8, 21.3; ¹⁹F NMR (CDCl₃, 470 MHz) δ -75.94, -114.44; HRMS–ESI (*m/z*): [M+H]⁺ calcd for, C₂₁H₂₆FN₇O; 412.2256 ; found, 412.2255

4-((4-Fluorobenzyl)(piperidin-4-ylmethyl)amino)-6-morpholino-1,3,5-triazine-2-carbonitrile (264182)

General procedure B4 from tert-butyl 4-(((4-cyano-6-morpholino-1,3,5-triazin-2-yl)(4-fluorobenzyl)amino)methyl)piperidine-1-carboxylate (33 mg, 0.065 mmol) gave 4-((4-fluorobenzyl)(piperidin-4-ylmethyl)amino)-6-morpholino-1,3,5-triazine-2-carbonitrile, TFA (23.5 mg, 0.045 mmol, 69.3 % yield). ¹H NMR (CDCl₃, 500 MHz) δ 7.12 - 7.24 (m, 2H), 7.01 (t, *J* = 8.31 Hz, 2H), 4.79 (s, 1H), 4.74 (s, 1H), 3.82 (br. s., 2H), 3.72 (br. s., 4H), 3.67 (br. s., 2H), 3.34 - 3.53 (m, 4H), 2.86 (br. s., 2H), 1.94 - 2.16 (m, 1H), 1.72 - 1.90 (m, 2H), 1.57 (br. s., 2H); ¹³C NMR (CDCl₃, 126 MHz) δ 165.0, 164.8, 163.5, 163.4, 161.4, 161.3, 152.0, 132.4, 129.5, 129.4, 129.0, 128.9, 115.8, 115.7, 115.6, 115.3, 66.6, 66.3, 51.5, 50.6, 50.4, 49.8, 44.0, 43.9, 43.5, 43.4, 32.9, 32.8, 26.6, 26.4; ¹⁹F NMR (CDCl₃, 470 MHz) δ -75.82(m), -114.32 (m); HRMS–ESI (*m/z*): [M+H]⁺ calcd for, C₂₁H₂₆FN₇O; 412.2256 ; found, 412.2257

4-((4-Fluorobenzyl)((tetrahydro-2H-pyran-4-yl)methyl)amino)-6-morpholino-1,3,5-triazine-2-carbonitrile (264224)

General procedure B3 from 4-((4-fluorobenzyl)amino)-6-morpholino-1,3,5-triazine-2-carbonitrile (100 mg, 0.318 mmol), sodium hydride (15.27 mg, 0.382 mmol) and 4-(bromomethyl)tetrahydro-2H-pyran (0.042 ml, 0.318 mmol) gave 4-((4-fluorobenzyl)((tetrahydro-2H-pyran-4-yl)methyl)amino)-6-morpholino-1,3,5-triazine-2-carbonitrile (68 mg, 0.165 mmol, 51.8 % yield); ¹H NMR (CDCl₃, 500 MHz) δ 7.11 - 7.23 (m, 2H), 6.99 (t, *J* = 8.31 Hz, 2H), 4.79 (s, 1H), 4.74 (s, 1H), 3.89 - 4.02 (m, 2H), 3.58 - 3.86 (m, 9H), 3.43 (d, *J* = 7.34 Hz, 1H), 3.37 (d, *J* = 7.34 Hz, 1H), 3.26 - 3.35 (m, 2H), 1.93 - 2.02 (m, 1H), 1.46 - 1.57 (m, 2H), 1.27 - 1.41 (m, 2H); ¹³C NMR (CDCl₃, 126 MHz) δ 164.8, 164.7, 163.5, 163.2, 163.1, 161.3, 161.1, 152.0, 132.9, 132.8, 129.4, 128.9, 128.8, 115.6, 115.5, 115.4, 77.3, 77.1, 76.8, 67.6, 66.6, 66.4, 66.3, 52.4, 51.5, 50.2, 49.8, 44.0, 43.4, 34.0, 33.8, 31.0, 30.6 ¹⁹F NMR (CDCl₃, 470 MHz) δ -114.74 (m); HRMS-ESI (m/z): [M+H]⁺ calcd for, C₂₁H₂₅FN₆O₂; 413.2096; found, 413.2098

4-((4-Fluorobenzyl)(pyrrolidin-3-ylmethyl)amino)-6-morpholino-1,3,5-triazine-2-carbonitrile (264225)

General procedure B4 from tert-butyl 3-(((4-cyano-6-morpholino-1,3,5-triazin-2-yl)(4-fluorobenzyl)amino)methyl)pyrrolidine-1-carboxylate (30 mg, 0.060 mmol) gave 4-((4-fluorobenzyl)(pyrrolidin-3-ylmethyl)amino)-6-morpholino-1,3,5-triazine-2-carbonitrile, TFA (23 mg, 0.045 mmol, 74.6 % yield); ¹H NMR (CDCl₃, 500 MHz) δ 7.12 - 7.24 (m, 2H), 7.00 (t, *J* = 8.31 Hz, 2H), 4.64 - 4.85 (m, 2H), 3.77 - 3.88 (m, 2H), 3.53 - 3.75 (m, 8H), 3.45 (br. s., 1H), 3.32 (br. s., 2H), 2.94 - 3.13 (m, 1H), 2.65 - 2.84 (m, 1H), 1.99 - 2.15 (m, 1H), 1.67 - 1.82 (m, *J*

= 7.60, 12.00 Hz, 1H); ^{13}C NMR (CDCl_3 , 126 MHz) δ 164.8, 163.5, 163.3, 161.4, 161.3, 152.0, 151.8, 132.4, 132.3, 129.5, 129.0, 115.8, 115.6, 115.3, 115.2, 66.6, 66.3, 49.8, 48.6, 48.0, 47.4, 45.2, 45.0, 44.0, 43.5, 43.4, 37.3, 37.0, 28.5, 28.1; ^{19}F NMR (CDCl_3 , 470 MHz) δ -75.83 (m), -114.24 (m); HRMS–ESI (m/z): $[\text{M}+\text{H}]^+$ calcd for, $\text{C}_{20}\text{H}_{24}\text{FN}_7\text{O}$; 398.2099; found, 398.2102

4-((4-fluorobenzyl)((tetrahydro-2H-pyran-3-yl)methyl)amino)-6-morpholino-1,3,5-triazine-2-carbonitrile (264239)

General procedure B3 from 4-((4-fluorobenzyl)amino)-6-morpholino-1,3,5-triazine-2-carbonitrile (100 mg, 0.318 mmol), sodium hydride (15.27 mg, 0.382 mmol), and (tetrahydro-2H-pyran-3-yl)methyl 4-methylbenzenesulfonate (86 mg, 0.318 mmol) gave 4-((4-fluorobenzyl)((tetrahydro-2H-pyran-3-yl)methyl)amino)-6-morpholino-1,3,5-triazine-2-carbonitrile (57 mg, 0.138 mmol, 43.4 % yield); ^1H NMR (CDCl_3 , 500 MHz) δ 7.52 - 7.58 (m, 1H), 7.43 - 7.52 (m, 2H), 7.36 - 7.43 (m, 1H), 4.85 (s, 1H), 4.78 (s, 1H), 3.82 - 3.88 (m, 1H), 3.77 - 3.82 (m, 2H), 3.71 - 3.77 (m, 2H), 3.68 (br. s., 1H), 3.56 - 3.66 (m, 3H), 3.45 - 3.51 (m, 1H), 1.50 - 1.61 (m, 1H), 1.37 - 1.50 (m, 2H), 0.92 (d, $J = 6.36$ Hz, 3H), 0.90 (d, $J = 6.36$ Hz, 3H); ^{13}C NMR (CDCl_3 , 126 MHz) δ 164.2, 164.1, 163.6, 163.4, 152.0, 151.9, 138.7, 138.4, 131.0, 130.7, 130.4, 129.1, 124.3, 124.2, 124.1, 115.5, 115.4, 66.6, 66.3, 66.2, 49.7, 49.5, 45.8, 44.9, 43.9, 43.4, 36.3, 35.4, 26.0, 25.8, 22.5, 22.4; HRMS–ESI (m/z): $[\text{M}+\text{H}]^+$ calcd for, $\text{C}_{21}\text{H}_{25}\text{FN}_6\text{O}_2$; 413.2096; found, 413.2149

(R)-4-((4-fluorobenzyl)(piperidin-3-ylmethyl)amino)-6-morpholino-1,3,5-triazine-2-carbonitrile (264501)

General procedure B4 from tert-butyl (R)-3-(((4-cyano-6-morpholino-1,3,5-triazin-2-yl)(4-fluorobenzyl)amino)methyl)piperidine-1-carboxylate (10.5 mg, 0.021 mmol) gave (R)-4-((4-fluorobenzyl)(piperidin-3-ylmethyl)amino)-6-morpholino-1,3,5-triazine-2-carbonitrile, TFA (5 mg, 9.51 μ mol, 46.4 % yield). ^1H NMR (CDCl_3 , 500 MHz) δ 7.10 - 7.24 (m, 2H), 7.00 (t, $J = 7.83$ Hz, 2H), 4.84 - 4.99 (m, 1H), 4.49 - 4.68 (m, 1H), 3.60 - 3.93 (m, 9H), 3.22 - 3.54 (m, 4H), 2.81 - 3.02 (m, 1H), 2.57 - 2.81 (m, 1H), 2.29 (br. s., 1H), 1.93 (br. s., 1H), 1.70 - 1.87 (m, 2H), 1.14 - 1.40 (m, 1H); ^{13}C NMR (CDCl_3 , 126 MHz) δ 164.9, 164.8, 163.4, 163.3, 163.2, 161.3, 152.0, 151.8, 132.2, 132.1, 129.5, 129.1, 129.0, 115.8, 115.5, 115.3, 115.2, 66.5, 66.2, 49.5, 49.1, 48.3, 47.7, 47.2, 44.6, 44.5, 43.9, 43.5, 43.3, 32.5, 32.4, 28.1, 26.8, 26.3, 21.8, 21.3; ^{19}F NMR (CDCl_3 , 470 MHz) δ -75.94, -114.44; HRMS-ESI (m/z): $[\text{M}+\text{H}]^+$ calcd for, $\text{C}_{21}\text{H}_{26}\text{FN}_7\text{O}$; 412.2256 ; found, 412.2255

(S)-4-((4-fluorobenzyl)(piperidin-3-ylmethyl)amino)-6-morpholino-1,3,5-triazine-2-carbonitrile (264502)

General procedure B4 from tert-butyl (S)-3-(((4-cyano-6-morpholino-1,3,5-triazin-2-yl)(4-fluorobenzyl)amino)methyl)piperidine-1-carboxylate (26.7 mg, 0.052 mmol) gave (S)-4-((4-fluorobenzyl)(piperidin-3-ylmethyl)amino)-6-morpholino-1,3,5-triazine-2-carbonitrile (20 mg, 0.049 mmol, 93 % yield); ^1H NMR (CDCl_3 , 500 MHz) δ 7.10 - 7.24 (m, 2H), 7.00 (t, $J = 7.83$ Hz, 2H), 4.84 - 4.99 (m, 1H), 4.49 - 4.68 (m, 1H), 3.60 - 3.93 (m, 9H), 3.22 - 3.54 (m, 4H), 2.81 - 3.02 (m, 1H), 2.57 - 2.81 (m, 1H), 2.29 (br. s., 1H), 1.93 (br. s., 1H), 1.70 - 1.87 (m, 2H), 1.14 - 1.40 (m, 1H); ^{13}C NMR (CDCl_3 , 126 MHz) δ 164.9, 164.8, 163.4, 163.3, 163.2, 161.3, 152.0,

151.8, 132.2, 132.1, 129.5, 129.1, 129.0, 115.8, 115.5, 115.3, 115.2, 66.5, 66.2, 49.5, 49.1, 48.3, 47.7, 47.2, 44.6, 44.5, 43.9, 43.5, 43.3, 32.5, 32.4, 28.1, 26.8, 26.3, 21.8, 21.3; ¹⁹F NMR (CDCl₃, 470 MHz) δ -75.94, -114.44; HRMS-ESI (m/z): [M+H]⁺ calcd for, C₂₁H₂₆FN₇O; 412.2256 ; found, 412.2255

***tert*-Butyl 3-(((4-chloro-6-morpholino-1,3,5-triazin-2-yl)amino)methyl)piperidine-1-carboxylate**

General procedure B1 from 2,4,6-trichloro-1,3,5-triazine (0.25 g, 1.356 mmol), *tert*-butyl 3-(aminomethyl)piperidine-1-carboxylate (0.292 ml, 1.356 mmol), DIPEA (0.474 ml, 2.712 mmol) and morpholine (0.118 ml, 1.356 mmol) gave *tert*-butyl 3-(((4-chloro-6-morpholino-1,3,5-triazin-2-yl)amino)methyl)piperidine-1-carboxylate (300 mg, 0.727 mmol, 53.6 % yield).; ¹H NMR (CDCl₃, 500 MHz) δ 3.71 - 3.83 (m, 5H), 3.59 - 3.71 (m, 6H), 3.22 - 3.41 (m, 3H), 1.72 - 1.81 (m, 2H), 1.56 - 1.67 (m, 1H), 1.41 (br. s, 2H), 1.38 (s, 9H)

***tert*-Butyl 3-(((4-cyano-6-morpholino-1,3,5-triazin-2-yl)amino)methyl)piperidine-1-carboxylate**

General procedure B2 from *tert*-butyl 3-(((4-chloro-6-morpholino-1,3,5-triazin-2-yl)amino)methyl)piperidine-1-carboxylate (722 mg, 1.749 mmol), potassium cyanide (125 mg, 1.923 mmol), and DABCO (392 mg, 3.50 mmol) gave *tert*-butyl 3-(((4-cyano-6-morpholino-1,3,5-triazin-2-yl)amino)methyl)piperidine-1-carboxylate (126 mg, 0.312 mmol, 17.86 % yield)

4-morpholino-6-((2-nitrobenzyl)(piperidin-3-ylmethyl)amino)-1,3,5-triazine-2-carbonitrile (264261)

General procedure B4 from tert-butyl 3-(((4-cyano-6-morpholino-1,3,5-triazin-2-yl)(2-nitrobenzyl)amino)methyl)piperidine-1-carboxylate (40 mg, 0.074 mmol) gave 4-morpholino-6-((2-nitrobenzyl)(piperidin-3-ylmethyl)amino)-1,3,5-triazine-2-carbonitrile, TFA (25 mg, 0.045 mmol, 60.9 % yield); ^1H NMR (CDCl_3 , 500 MHz) δ 8.03 - 8.12 (m, 1H), 7.58 (t, $J = 7.34$ Hz, 1H), 7.46 (t, $J = 6.85$ Hz, 1H), 7.15 (br. s., 1H), 5.14 - 5.30 (m, 1H), 4.93 - 5.13 (m, 1H), 3.86 (br. s., 1H), 3.78 (d, $J = 18.59$ Hz, 4H), 3.67 (br. s., 1H), 3.56 (br. s., 1H), 3.34 - 3.51 (m, 3H), 3.03 (br. s., 1H), 2.89 (br. s., 1H), 2.28 - 2.50 (m, 1H), 1.94 - 2.06 (m, 1H), 1.74 - 1.94 (m, 2H), 1.35 - 1.49 (m, 1H), 1.16 - 1.35 (m, 2H); ^{13}C NMR (CDCl_3 , 126 MHz) δ 165.3, 165.0, 163.4, 163.2, 152.0, 151.8, 148.4, 133.9, 133.8, 132.5, 132.2, 128.5, 128.4, 128.1, 127.7, 125.5, 125.3, 115.0, 66.5, 66.1, 49.5, 49.4, 48.1, 47.9, 47.2, 44.9, 44.7, 43.9, 43.3, 33.0, 32.7, 26.8, 26.2, 21.8, 21.2, 17.7; ^{19}F NMR (CDCl_3 , 470 MHz) δ -75.82; HRMS-ESI (m/z): $[\text{M}+\text{H}]^+$ calcd for, $\text{C}_{21}\text{H}_{26}\text{N}_8\text{O}_3$; 439.2201; found, 439.2208

4-Morpholino-6-((piperidin-3-ylmethyl)amino)-1,3,5-triazine-2-carbonitrile, TFA (264504)

General procedure B4 from tert-butyl 3-(((4-cyano-6-morpholino-1,3,5-triazin-2-yl)amino)methyl)piperidine-1-carboxylate (80 mg, 0.198 mmol) gave 4-morpholino-6-((piperidin-3-ylmethyl)amino)-1,3,5-triazine-2-carbonitrile, TFA (80 mg, 0.192 mmol, 97 % yield); ^1H NMR (CDCl_3 , 500 MHz) δ 8.78 (br. s., 0.5H), 8.41 (br. s., 0.5H), 6.50 (br. s., 2H), 3.76 - 3.85 (m, 4H), 3.73 (br. s., 4H), 3.37 - 3.52 (m, 3H), 3.23 - 3.35 (m, 1H), 2.79 - 2.91 (m, 1H), 2.62 (q, $J = 10.92$ Hz, 1H), 2.11 - 2.27 (m, 1H), 1.86 - 2.01 (m, 2H), 1.72 - 1.86 (m, 1H), 1.17 - 1.36 (m, 1H); ^{13}C NMR (CDCl_3 , 126 MHz) δ 163.9, 162.9, 161.4, 161.1, 150.6, 116.7,

114.8, 114.4, 66.5, 66.2, 47.5, 44.4, 44.1, 43.6, 43.3, 33.9, 26.5, 21.8; HRMS–ESI (m/z): [M+H]⁺ calcd for, C₁₄H₂₁N₇O; 304.1880; found, 304.1884

4-(isopentyl(piperidin-3-ylmethyl)amino)-6-morpholino-1,3,5-triazine-2-carbonitrile, TFA (264521)

General procedure B4 from tert-butyl 3-(((4-cyano-6-morpholino-1,3,5-triazin-2-yl)(isopentyl)amino)methyl)piperidine-1-carboxylate gave 4-(isopentyl(piperidin-3-ylmethyl)amino)-6-morpholino-1,3,5-triazine-2-carbonitrile, TFA (98 % yield); ¹H NMR (CDCl₃, 500 MHz) δ 8.80 - 9.12 (m, 2H), 3.68 - 3.84 (m, 8H), 3.64 (dd, J = 8.31, 14.18 Hz, 1H), 3.47 - 3.58 (m, 1H), 3.31 - 3.46 (m, 3H), 3.18 - 3.31 (m, 1H), 2.77 - 2.94 (m, 1H), 2.57 - 2.74 (m, 1H), 2.22 - 2.40 (m, 1H), 1.92 (br. s., 1H), 1.74 - 1.89 (m, 2H), 1.55 (tt, J = 6.30, 13.02 Hz, 1H), 1.37 - 1.48 (m, 2H), 1.18 - 1.37 (m, 1H), 0.85 - 0.99 (m, 6H); ¹³C NMR (CDCl₃, 126 MHz) δ 164.3, 164.1, 163.3, 151.8, 151.6, 115.5, 115.3, 66.6, 66.3, 49.3, 49.0, 47.4, 47.0, 46.4, 45.8, 44.3, 44.2, 43.9, 43.4, 36.1, 35.3, 33.0, 32.9, 26.9, 26.6, 26.1, 25.9, 22.5, 22.4, 21.8, 21.6; HRMS–ESI (m/z): [M+H]⁺ calcd for, C₁₉H₃₁N₇O; 374.2663; found, 374.2666

4-(((5,5-difluoropiperidin-3-yl)methyl)(4-fluorobenzyl)amino)-6-morpholino-1,3,5-triazine-2-carbonitrile, TFA (264522)

General procedure B4 from tert-butyl 5-(((4-cyano-6-morpholino-1,3,5-triazin-2-yl)(4-fluorobenzyl)amino)methyl)-3,3-difluoropiperidine-1-carboxylate (31.6 mg, 0.058 mmol) gave 4-(((5,5-difluoropiperidin-3-yl)methyl)(4-fluorobenzyl)amino)-6-morpholino-1,3,5-triazine-2-carbonitrile, TFA (29 mg, 0.052 mmol, 89 % yield); ¹H NMR (CDCl₃, 500 MHz) δ 7.13 - 7.23 (m, 2H), 7.02 (t, J = 8.31 Hz, 2H), 4.83 - 4.97 (m, 1H), 4.55 - 4.75 (m, 1H), 3.77 - 3.94 (m, 2H),

3.65 - 3.77 (m, 7H), 3.60 (br. s., 1H), 3.40 - 3.55 (m, 1H), 3.34 (d, $J = 12.23$ Hz, 1H), 3.07 - 3.26 (m, 1H), 2.85 (t, $J = 11.98$ Hz, 1H), 2.66 - 2.78 (m, 1H), 2.59 (br. s., 1H), 2.25 (br. s., 1H), 1.67 - 1.91 (m, 1H); ^{13}C NMR (CDCl_3 , 126 MHz) δ 165.1, 165.0, 163.5, 163.3, 152.1, 151.9, 131.9, 129.7, 129.6, 129.2, 129.1, 115.9, 115.9, 115.8, 115.7, 115.1, 66.6, 66.2, 49.8, 49.1, 47.5, 47.3, 46.0, 45.7, 44.1, 43.6, 43.5, 30.6, 30.3; ^{19}F NMR (CDCl_3 , 470 MHz) δ ppm -113.98 (s) -101.29 (s) -100.74 (s) -100.27 (s) -99.79 (s) -99.25 (s) -98.70 (s) -75.80 (s); HRMS-ESI (m/z): $[\text{M}+\text{H}]^+$ calcd for, $\text{C}_{19}\text{H}_{31}\text{N}_7\text{O}$; 448.2069; found, 448.2069

Computational Modeling: The X-ray structure of mature *TgCPL* in complex with its propeptide (PDB: 3F75) was superposed with the X-ray structure of *HsCPL* (PDB: 5MAJ) using The Molecular Operating Environment (MOE), version 2008.10, Chemical Computing Group Inc., Montreal, Quebec, Canada. Ligands The X-ray structure of *HsCPL* and the propeptide chain of *TgCPL* were removed to generate the docking model for figures shown.

***TgCPL* and *HsCPL* Inhibition Assay:** Compound potency and selectivity was evaluated in vitro for both *TgCPL* and *HsCPL* activity in a fluorescence based assay by monitoring the hydrolysis of Cbz-Leu-Arg-aminomethylcoumarin (Z-L-R-AMC). Protein was expressed and purified as previously described. The substrate hydrolysis results in the release of fluorescent 7-amino-4-methylcoumarin (AMC) that can be monitored spectrophotometrically with linear kinetics for up to 60 min. Inhibitors were serial diluted in DMSO in a 1-to-3 dilution, spanning at least 10 concentration points in either duplicate or triplicate. The enzyme was pre-incubated with

the inhibitory compounds for 5 min at 23°C, followed by the addition of the AMC substrate. The assay final conditions had a total volume of 200 μ L, consisting of 90 μ L enzyme (conc.=50 ng/mL), 100 μ L ZLR-AMC substrate (conc.= 80 μ M), and 10 μ L inhibitor or DMSO. The relative fluorescence of the AMC generation is measured over the course of 5 min (Excitation: 380 nm, Emission: 460 nm). LHVS and DMSO were used as positive and negative controls, respectively. All dose response data was obtained with at least independent three replicates (n=3). Graphpad Prism software was used to visualize inhibition curves and calculate IC₅₀ values from the reaction mean v. Assay final concentrations in each well: 40 μ M ZLR-AMC, *TgCPL* or *HsCPL* (final conc= 0.0225 ng/ μ L). Assay Buffer: 100 mM NaAc, 2 mM EDTA, 900 mM NaCl, 50 mM DTT. Substrate: Cbz-Leu-Arg-AMC (Bachem, purchased as HCl salt).

Metabolic Stability in Mouse Liver Microsomes: The metabolic stability was assessed using CD-1 mouse liver microsomes. One micromolar of each compound was incubated with 0.5 mg/mL microsomes and 1.7 mM cofactor β -NADPH in 0.1 M phosphate buffer (pH = 7.4) containing 3.3 mM MgCl₂ at 37 °C. The DMSO concentration was less than 0.1% in the final incubation system. At 0, 5, 10, 15, 30, 45, and 60 min of incubation, 40 μ L of reaction mixture were taken out, and the reaction is quenched by adding 3-fold excess of cold acetonitrile containing 100 ng/mL of internal standard for quantification. The collected fractions were centrifuged at 15000 rpm for 10 min to collect the supernatant for LC–MS/ MS analysis, from which the amount of compound remaining was determined. The natural log of the amount of compound remaining was plotted against time to determine the disappearance rate and the half-life of tested compounds.

Pharmacokinetic Studies in Mice: All animal experiments in this study were approved by the University of Michigan Committee on Use and Care of Animals and Unit for Laboratory Animal Medicine. The abbreviated pharmacokinetics for compounds was determined in female CD-1 mice following intraperitoneal (ip) injection at 10 mg/kg. Compound was dissolved in the vehicle containing 15% (v/v) DMSO, 15-20% (v/v) PEG-400, and 70% (v/v) PBS. Four blood samples (50 μ L) were collected over 7 h (at 0.5h, 2h, 4h, and 7h), centrifuged at 3500 rpm for 10 min, and plasma was frozen at -80°C for later analysis. Plasma concentrations of the compounds were determined by the LC-MS/MS method developed and validated for this study. The LC-MS/MS method consisted of a Shimadzu HPLC system, and chromatographic separation of tested compound which was achieved using a Waters Xbridge-C18 column (5 cm \times 2.1 mm, 3.5 μ m). An AB Sciex QTrap 4500 mass spectrometer equipped with an electrospray ionization source (ABI-Sciex, Toronto, Canada) in the positive-ion multiple reaction monitoring (MRM) mode was used for detection. All pharmacokinetic parameters were calculated by non-compartmental methods using WinNonlin, version 3.2 (Pharsight Corporation, Mountain View, CA, USA).

MDR1/MDCK Assay: A 12-well transwell plate was seeded with MDCKII-MDR1 cells (0.5 million/well) and cultured for 24h. Cells were washed with DMEM 3 times (both sides). 0.5 ml of 1 μ M CCG drug in DMEM was added to apical side (A to B) or basolateral side (B to A) (donor side) and 0.5ml of DMEM+0.1% DMSO to basolateral side (A to B). Cells were incubated for 4h and 2 \times 200 μ L was sampled from the receiving sides and stored at -20°C for future use. For calibration standard, compound standards were dissolved in DMSO then further

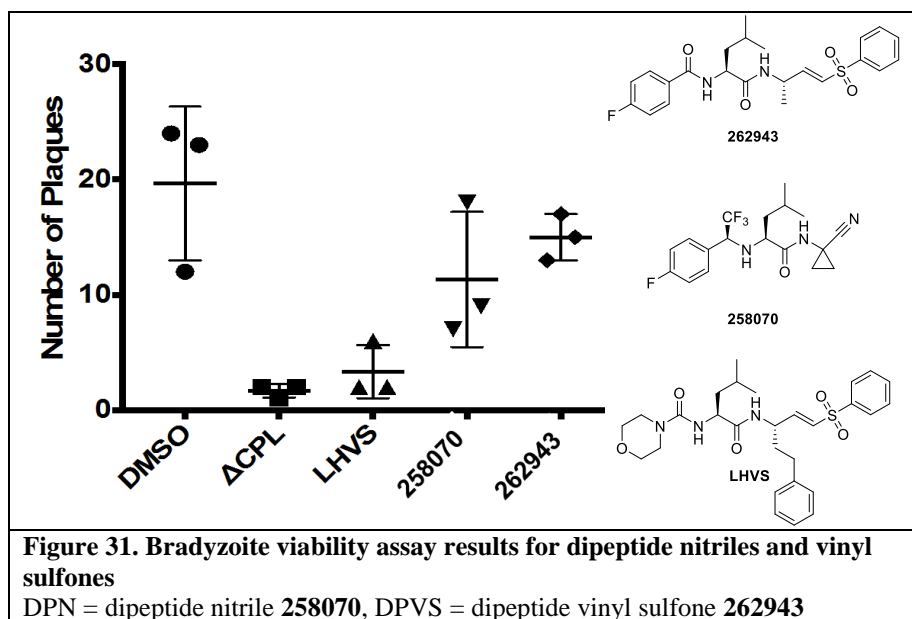
diluted in acetonitrile to a concentration of 10 µg/mL. Calibration standards were prepared from this stock with internal standard (5 nM CE302). Samples were prepared by protein precipitation from media followed by addition of internal standard. Samples were analyzed by LC–MS/MS. The LC–MS/MS method consisted of a Shimadzu HPLC system, and chromatographic separation of tested compound which was achieved using a Waters Xbridge-C18 column (5 cm × 2.1 mm, 3.5 µm). An AB Sciex QTrap 4500 mass spectrometer equipped with an electrospray ionization source (ABI-Sciex, Toronto, Canada) in the positive-ion multiple reaction monitoring (MRM) mode was used for detection.

Chapter 4 Design of Fluorescent Probes and *In Vitro* Activity

Dipeptides, Bradyzoite Viability, and Rationale

The Carruthers lab has developed an *in vitro* assay to assess the effects of compounds on bradyzoite viability. In this assay, human foreskin fibroblast cells (HFF) are infected with *T. gondii*, and the parasite is converted from tachyzoite to bradyzoite life stage. Following conversion, the parasite is treated daily with the inhibitor of interest for 1 week, replacing the conversion media containing the inhibitor/compound of interest every 24 hours. The parasite cyst is then harvested from the HFF cells, and subsequently assessed for viability in a plaque formation assay. The number of plaques formed, due to the parasite infection, is normalized to the *T. gondii* genomes per dose (as measured by qPCR) to provide the number of plaques per 1000 genomes as a measure of parasite viability. While this provides a good measure of compound efficacy, this assay is unfortunately very low throughput (~ 4-5 wks/assay), and therefore only select analogs were evaluated in this manner.

Our dipeptide nitrile inhibitor (**258070**) was a potent *TgCPL* inhibitor *in vitro* with an improved CNS profile versus LHVS. Curiously, treatment of intracellular bradyzoite cysts failed to decrease parasite viability (**Figure 31**). A similar results was observed for the dipeptide vinyl sulfone **262943**.

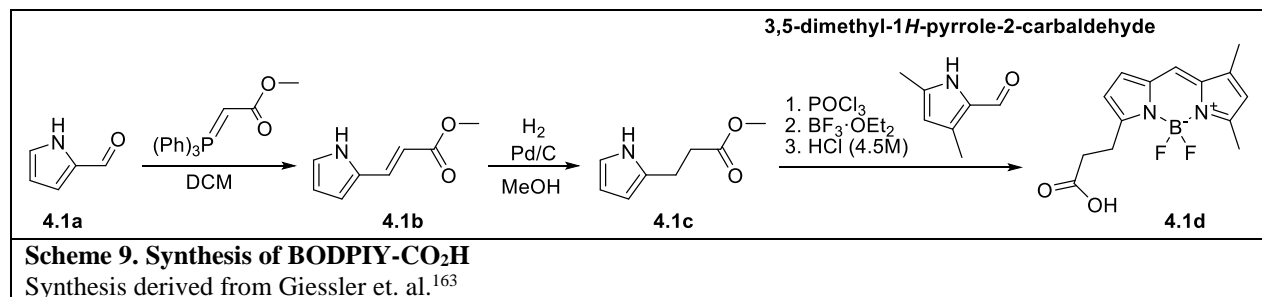


We reasoned that this lack of efficacy in bradyzoite cysts may be a result of the dipeptide compounds being unable to reach the target enzyme localized within the parasite vacuole. While these compounds were potent against *TgCPL* in our biochemical assay, there are several potential barriers to accessing the desired site of action. To reach *TgCPL*, these inhibitors need to be able to pass through the host cell membrane, cystic wall, parasite cell membrane, and enter the parasite vacuole. The inability to reduce intracellular cyst viability may be due to a lack of permeability in the human fibroblast host cells.

An additional possibility posed was that the inhibition of *TgCPL* by a reversible inhibitor (**258070**), may be inadequate for complete *TgCPL* inhibition. The viability reduction exhibited by LHVS could be due to the irreversible covalent inhibition of the vinyl sulfone warhead. However, the vinyl sulfone analog **262943** also failed to reduce bradyzoite viability. This indicates that the lack of activity may be due to other issues such as permeability. Second generation triazine nitrile analogs exhibited both improved potency and significantly higher

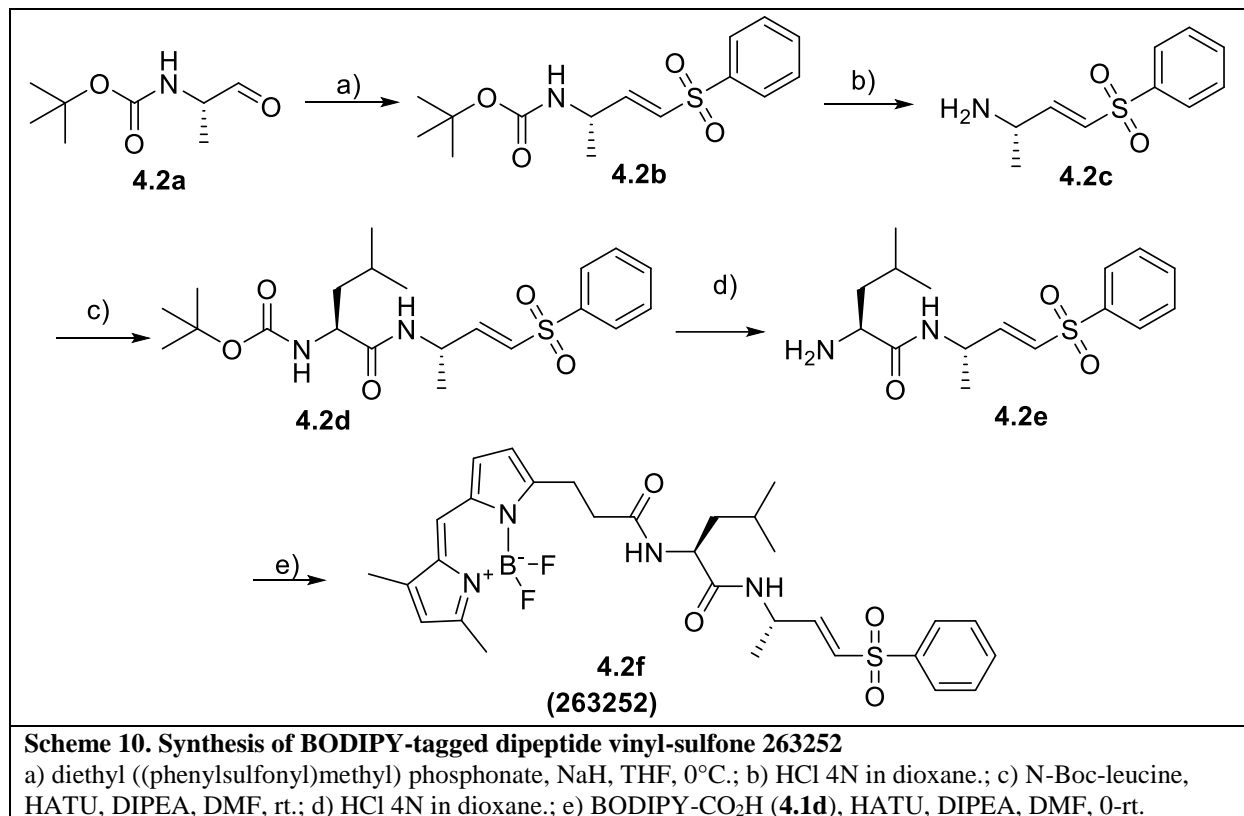
exposure levels versus the dipeptide nitrile **258070**, and a 1:1 brain:plasma ratio at 2 hr. While these features were improved, the triazine nitrile is also a reversibly covalent inhibitor. As such, we wanted to confirm two things before advancing this series further. First, we needed to verify that these compounds were able to reach and bind *TgCPL* in the parasite. Second, we wanted to understand if irreversible inhibition of *TgCPL* was necessary to reduce parasite viability. To this purpose, a set of BODIPY-linked fluorescent probes **263252** (Vinyl sulfone / irreversible) and **263473** (Triazine nitrile / reversible) were synthesized.

Synthesis of BODIPY-CO₂H



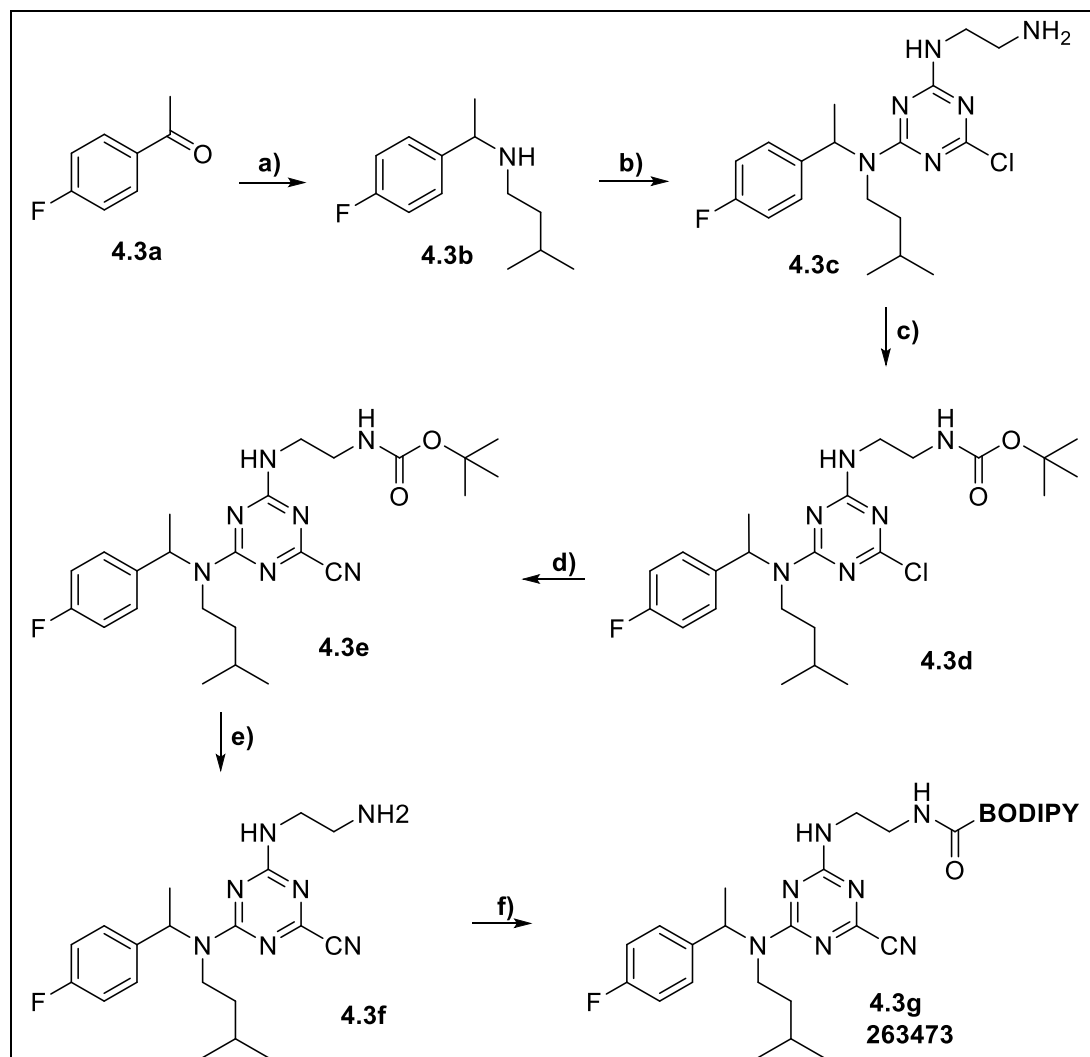
1H-pyrrole-2-carbaldehyde (**4.1a**) underwent a Wittig olefination with methyl (triphenylphosphoranylidene)acetate to provide intermediate **4.1b**. The product was then reduced over Pd/C 10% to afford **4.1c**. The intermediate then was subjected to Vilsmeier-type reaction with 3,5-dimethyl-1H-pyrrole-2-carbaldehyde to form the conjugate dipyrromethene intermediate. Treatment with boron trifluoride etherate formed the chelated BODIPY complex, which was subsequently hydrolyzed under acidic conditions with 4.5 M HCl to provide the desired BODIPY free acid **4.1d**.

Synthesis of VS-BODIPY Probe



A Horner–Wadsworth–Emmons reaction between Boc-L-alanine (**4.2a**) and diethyl ((phenylsulfonyl)methyl) phosphonate provides intermediate vinyl sulfone **4.2b**. Removal of the Boc to afford amine **4.2c** and subsequent HATU coupling provides the dipeptide **4.2d**. Deprotection with HCl dioxane gave **4.2e**, which underwent a final HATU coupling with BODIPY-CO₂H to provide the fluorescent probe (**4.f** / **263252**).

Synthesis of Triazine Nitrile BODIPY Probe



Scheme 11. Synthesis of BODIPY-tagged triazine nitrile probe 263473

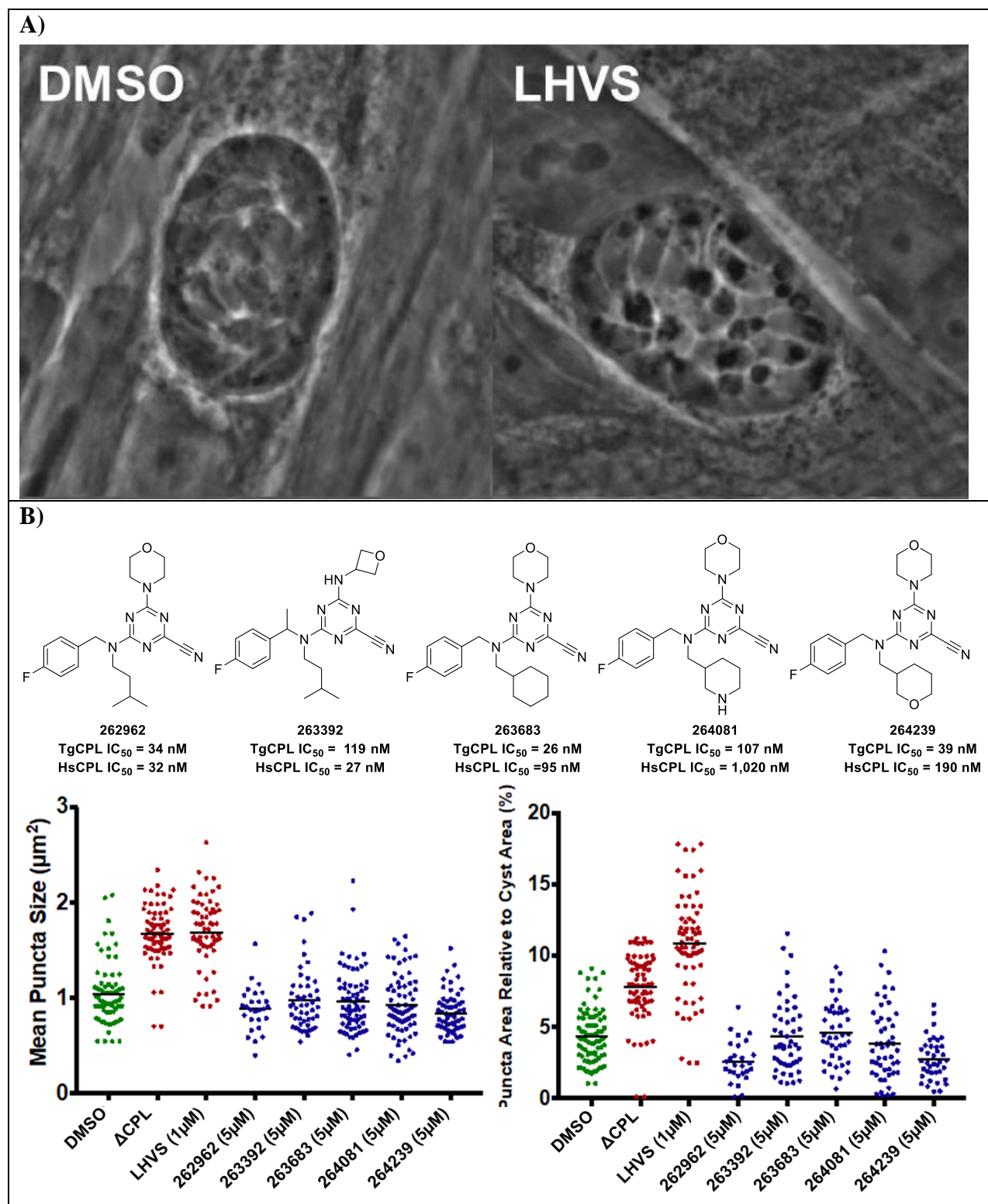
a) Isoamylamine, $\text{Ti}(\text{iPrO})_4$, NaBH_4 , MeOH, rt, O/N; b) (i) Cyanuric chloride, (ii) ethylenediamine, DIPEA, DCM, -10°C -rt, O/N; c) Boc-anhydride, DIPEA, DCM, 0-rt, O/N; d) KCN, DABCO, DMSO:H₂O (9:1), 80°C , O/N; e) 4N HCl, dioxane, rt, 1 hr; f) BODIPY-CO₂H, HATU, DIPEA, DMF, 0°C -rt, O/N.

4-Fluoro acetophenone (**4.3a**) was condensed overnight with isoamylamine in the presence of titanium isopropoxide, and the resulting imine was subsequently reduced with sodium borohydride to afford secondary amine **4.3b**. Subsequent reaction with cyanuric chloride, followed by a second $\text{S}_{\text{N}}\text{Ar}$ with ethylenediamine in one pot provided intermediate **4.3c**. Amine **4.3c** was then protected with Boc-anhydride (**4.3d**) and subjected to cyanation with potassium

cyanide in DMSO:H₂O to give **4.3e**. Finally, deprotection and subsequent amide coupling to BODIPY-CO₂H gave the triazine nitrile fluorescent probe **4.3g** (**263473**; *TgCPL* IC₅₀= 503 nM).

Puncta Formation and Autophagy in *TgCPL* Deficient Bradyzoite Cysts

T. gondii cathepsin L (*TgCPL*) is localized in the plant-like vacuole (VAC), a lysosomal-like organelle within the apical region of the parasite. This digestive enzyme plays a key role within the VAC and is necessary for persistence during neural infection. It is critical in the turnover of autophagosomes, a key structure found during the intracellular degradation cytoplasmic contents (autophagy). The formation of small, dark puncta has been observed in the *CPL* knockout strain of *T. gondii*, or when the bradyzoite cysts are treated with covalent inhibitor LHVS (**Figure 32A**). Presumably these are the buildup of autophagosomes, indicating the parasite is unable to properly turnover its organelles. While not a direct measure of parasite viability, as described above, it has been assumed that the buildup of these puncta are a prelude to cyst death and indicative of lysosomal dysfunction. As this response takes significantly less time than the complete viability assay, it was used as an initial evaluation for compound efficacy. Curiously, treatment of the bradyzoite cysts with select triazine nitriles from Chapter 3 did not result in the formation of these dark granules observed in other instances of *TgCPL* deficiency (**Figure 32B**). Similar to the viability assay with the dipeptide nitrile **258070**, we wondered if this is a result of poor permeability or an issue of covalence.



As a follow up to this observed lack of puncta formation, compounds were evaluated via Cyto-ID to better visualize the presence (or lack thereof) of autophagosomes. The Cyto-ID autophagy detection kit (Enzo life sciences) selectively stains accumulated autophagic vacuoles and monitors autophagic flux in lysosomally inhibited live cells. These “autolysosomes” are formed during the cellular process of autophagocytosis in which the cell disassembles unnecessary or dysfunctional components. Staining of bradyzoite cysts with CytoID shows a similar result observed with the dark granule formation observed by microscopy (**Figure 33**).

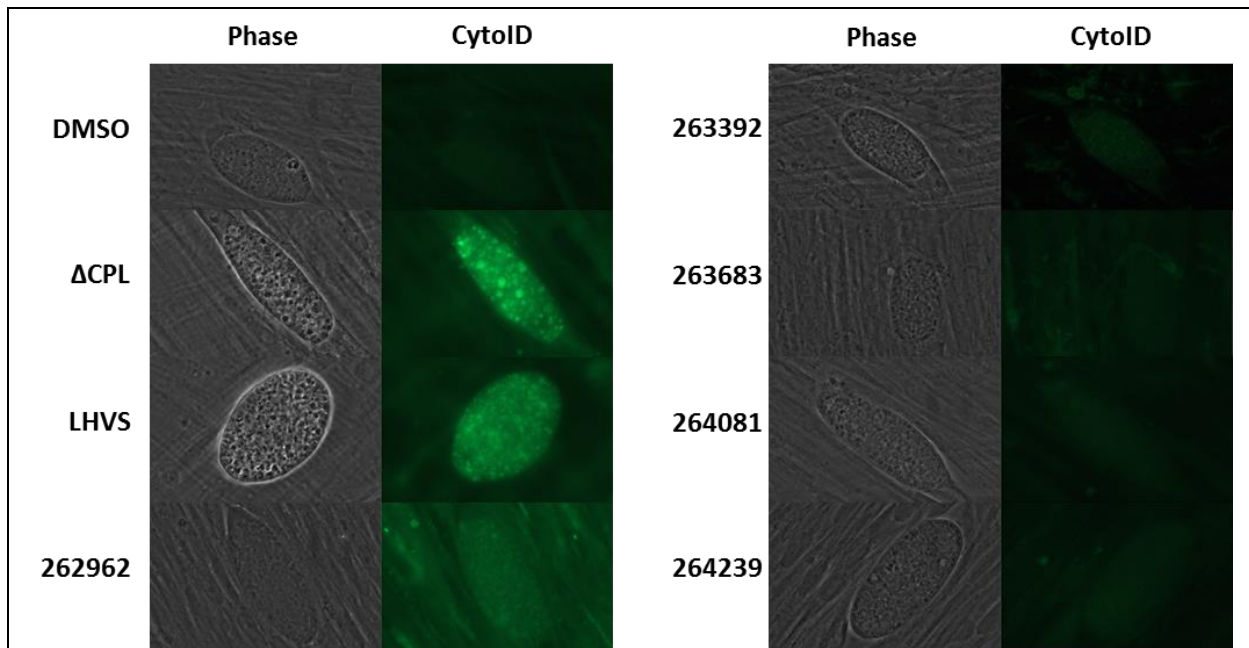


Figure 33. CytoID staining of bradyzoite cysts

CytoID staining of bradyzoite cysts treated with Triazine nitrile *TgCPL* inhibitors. CytoID stains for autophagy (stains for autolysosomes). Thus, *CPL* knockout bradyzoites and LHVS-treated bradyzoites are cytoID positive. This is likely due to the loss of autophagosome turnover in these bradyzoites, resulting in an increase in “autolysosomes”.

The *TgCPL* knockout bradyzoites and LHVS-treated bradyzoites are cytoID positive. This increase in autophagic vacuoles is likely due to the loss of autophagosome turnover in these bradyzoites due to the loss of the digestive enzyme *TgCPL*. It is unclear why we do not see the

same phenotypic response when the cysts are treated with triazine nitrile inhibitors. One possibility could be that the inhibitors fail to reach the cathepsin target within the parasite.

BODIPY Labeling of *TgCPL* in Bradyzoite Cysts

To determine if our inhibitors of *TgCPL* were able to reach the target organelle (VAC), bradyzoite cysts (ME49 strain) were incubated with BODIPY tagged inhibitors of *TgCPL* (**BO-LHVS** and **263252**) as shown in **Figure 34**.

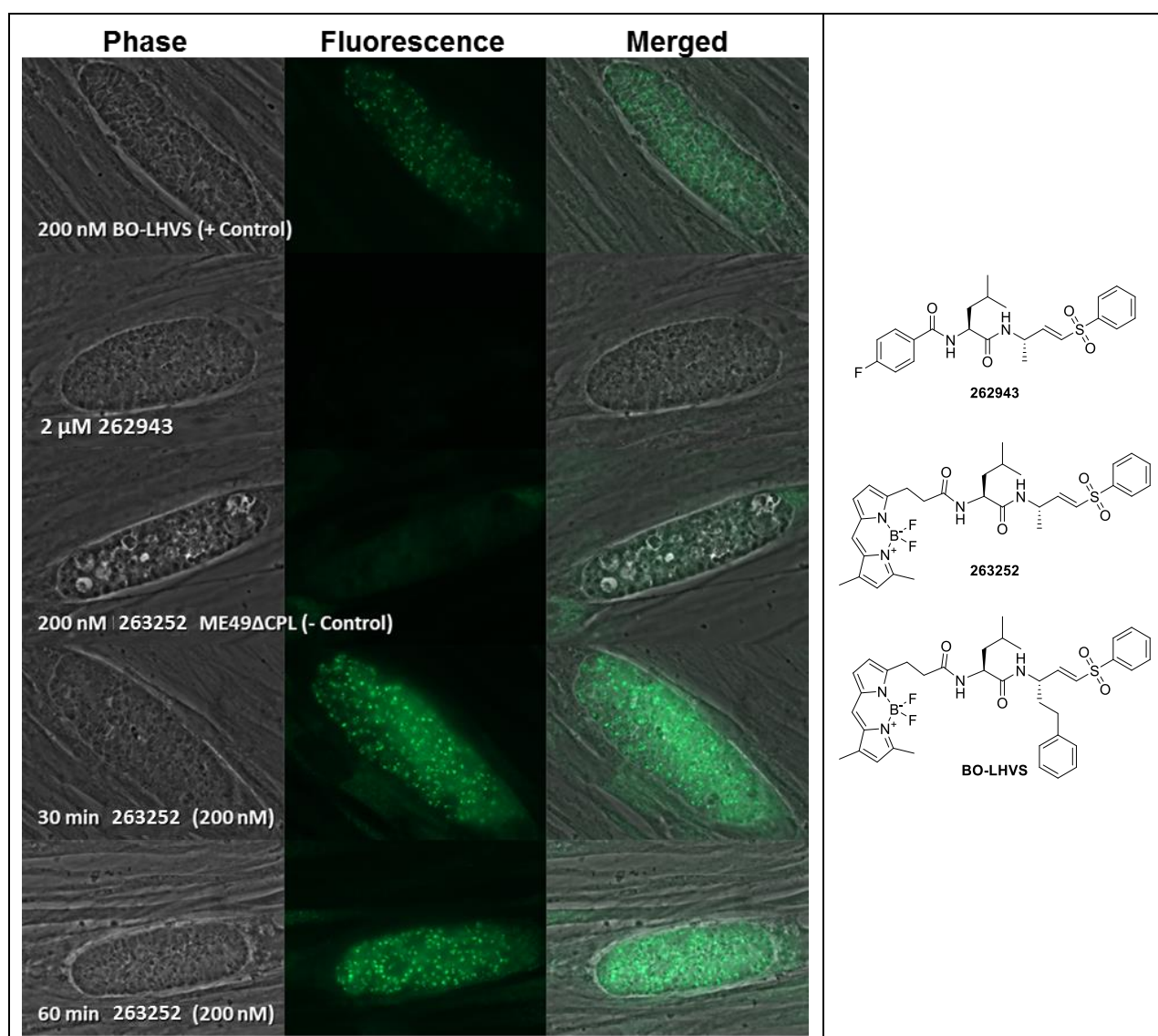


Figure 34. BODIPY vinyl sulfone probe 263252 enters bradyzoite cyst and binds to *TgCPL*

The BO-LHVS control is positive for green fluorescence (distinct puncta) and has previously been shown to primarily label *TgCPL*.¹²¹ The lack of fluorescence in the DPVS (**262943**) negative control is to demonstrate that the fluorescence shown in other samples is the result of the BODIPY tag. After incubation of the bradyzoites with **263252** (BO-DPVS), fluorescent puncta are detectable within 30 minutes of treatment, suggesting that BO-DPVS gets into the cyst within 30 mins. The puncta appear to be localizing to discrete organelles within the parasite, presumably the vacuolar compartment. In the ME49ΔCPL knockout strain of *T. gondii*, minimal fluorescence is observed when treated with BO-DPVS. This demonstrates that positive fluorescence in other BO-DPVS treated samples correlates with the presence of *TgCPL* in the parental cell line. In contrast, this fluorescent labeling of intracellular bradyzoites in human fibroblast cells was not observed with the BODIPY tagged triazine nitrile **263473**.

This data still does not answer the question as to why we do not observe the formation of inclusion bodies following treatment with the triazine nitrile inhibitors. Taken together, this data highlights a few key features. First, dark puncta as well as autophagosome accumulation is observed with inhibition by vinyl sulfones (LHVS) or *TgCPL* knockout, but not with the reversible nitrile inhibitors. Second, it appears the BODIPY tagged inhibitors bearing a covalent, irreversible warhead are capable of labeling *TgCPL* in intracellular cysts, while the BODIPY triazine nitrile **263473** failed to label the bradyzoites when subjected to the same assay. This could be a result of poor solubility, or permeability due to the increased lipophilicity added by the BODIPY tag. More plausible, is that the accumulation of puncta in the BODIPY assay is a result of the irreversibility of the vinyl sulfone tagged probes.

Fluorescent Labeling Competition Assay

One way to determine if the unlabeled probes are reaching *TgCPL* in the bradyzoites is through competition experiments with the BODIPY tags that are successful at labeling *TgCPL* (i.e. the VS probes). To demonstrate that our untagged inhibitors primarily target *TgCPL*, we performed a competition assay in which *ex vivo* bradyzoites were treated with both BODIPY-labeled and unlabeled inhibitors, with stepwise increases in the concentration of the latter. The *ex vivo* bradyzoites were harvested from the brains of mice infected with *Toxoplasma* and treated with compounds directly, effectively circumventing the additional barrier of the HFF cells in the intracellular cysts used in the previous labeling assays. **Figure 35** shows that the dipeptide-vinyl sulfone **262943** (right) can compete with the labeling of *TgCPL* by **263252**, similar to LHVS (left) and **BO-LHVS**. Fluorescent signals can be competed away with increasing concentrations of unlabeled **262943** in a dose dependent manner

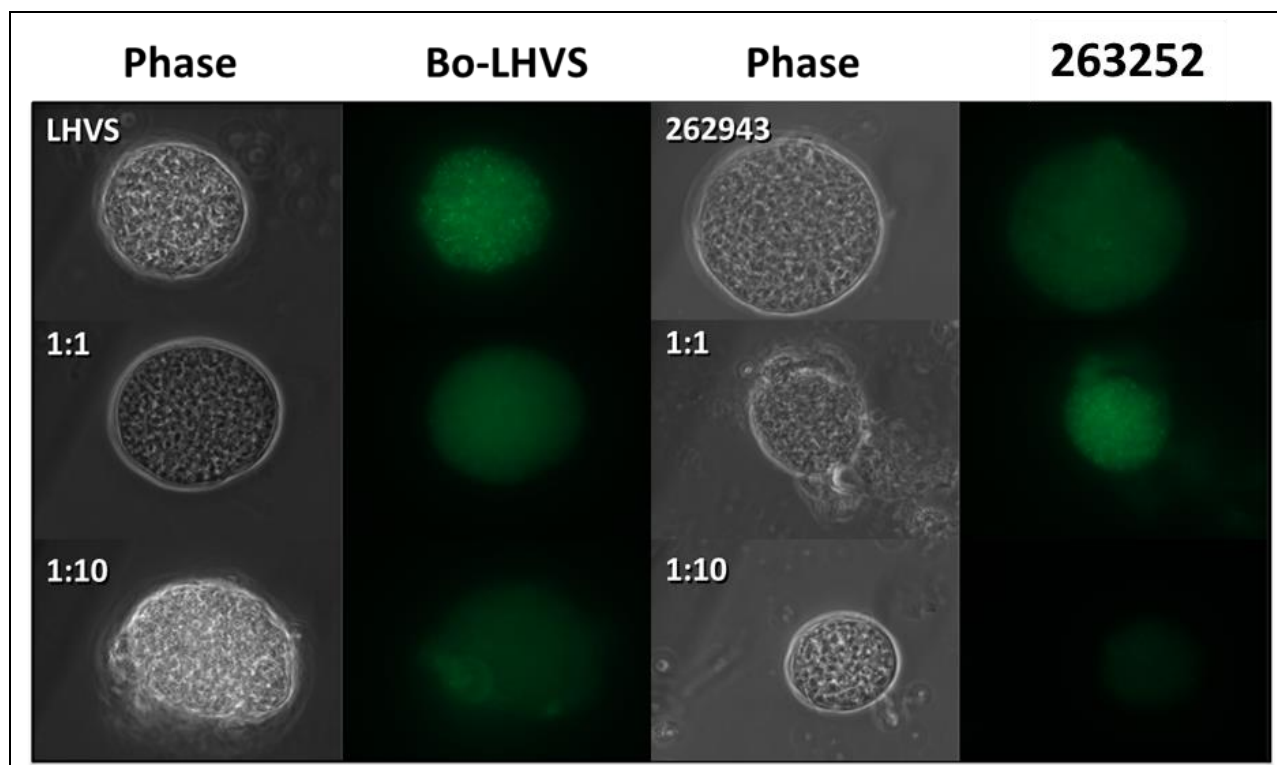


Figure 35. Competition assay between labeled and unlabeled *TgCPL* vinyl sulfone inhibitors indicates they compete for the same target. Ex vivo *T. gondii* cysts were pre-incubated with **LHVS** (left) or dipeptide vinyl sulfone **262943** (right) (200 nM for 1:1, or 2 μ M for 1:10) for 30 min, then 200 nM Bo-dipeptide vinyl sulfone **263252**, or 200 nM **Bo-LHVS** were added to the respective samples and left to incubate for 30 min (at room temperature). Imaged at x100

This is an interesting result in contrast to the previous autophagosome and viability assays. When the bradyzoite cyst is within the HFF cells, the dipeptide vinyl-sulfone **262943** failed to reduce bradyzoite viability and does not result in the formation of dark puncta and autophagosomes. These competition results show that when treating these *ex vivo* cysts, **262943** is capable of reaching *TgCPL*. This suggests the lack of efficacy previously seen is a result of HFF cells precluding the compound from reaching the bradyzoites, likely due to lowering the cLogP. The BODIPY labeled triazine nitrile **263473** was previously unable to label *TgCPL* in intracellular cysts in HFF cells. It was unclear if the lack of labeling was due to poor permeability or lack of covalency. The competition assays are performed directly on *ex vivo* bradyzoite cysts, which eliminates permeability issues that could be imparted by the HFF cells.

This bradyzoite competition experiment was therefore attempted with the BODIPY triazine nitrile **263473** and unlabeled triazine inhibitor **262962** (Figure 36).

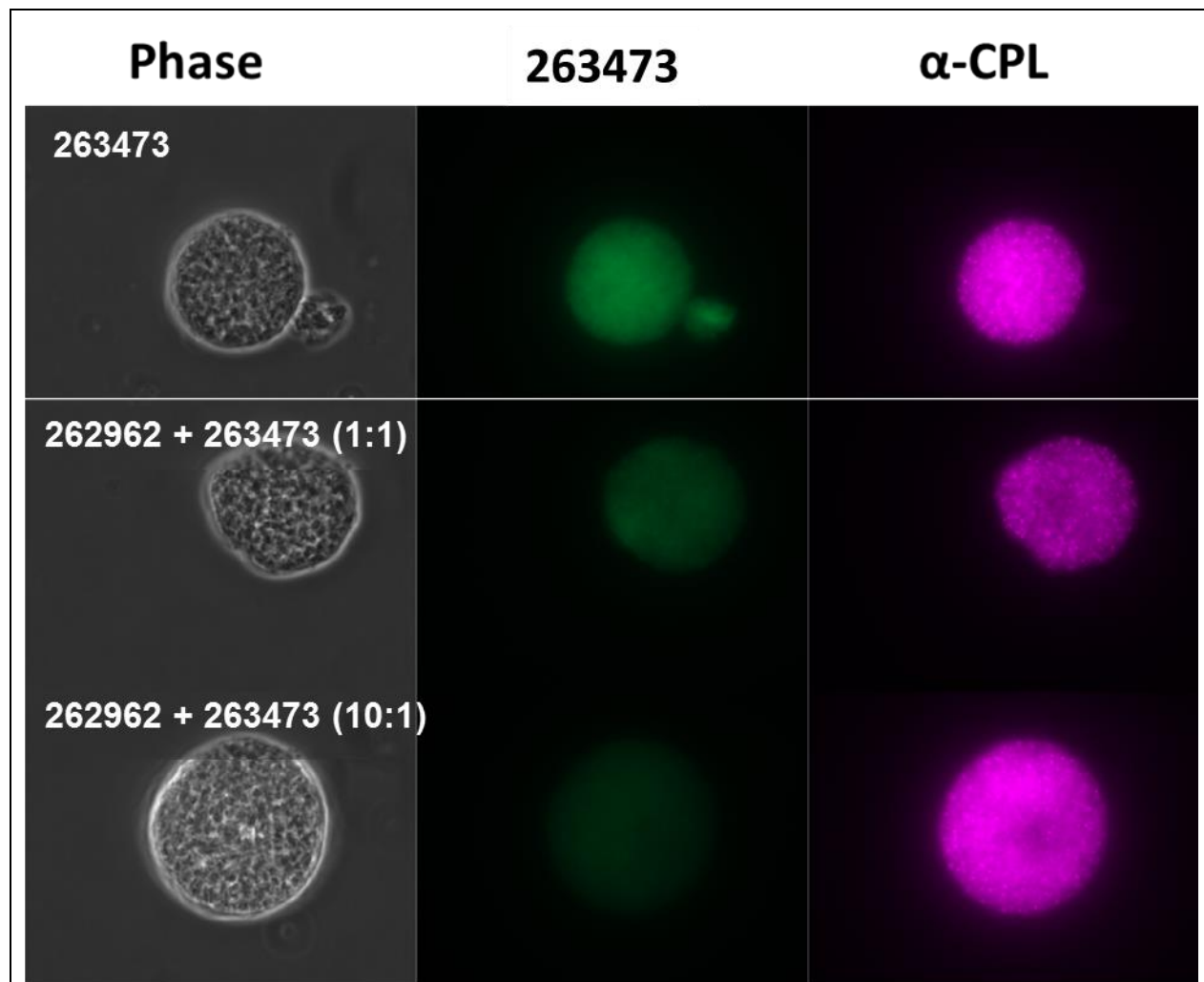


Figure 36. Competition assay between BODIPY labeled (263473) and unlabeled (262962) *TgCPL* triazine nitrile inhibitors suggests they compete for the same target.

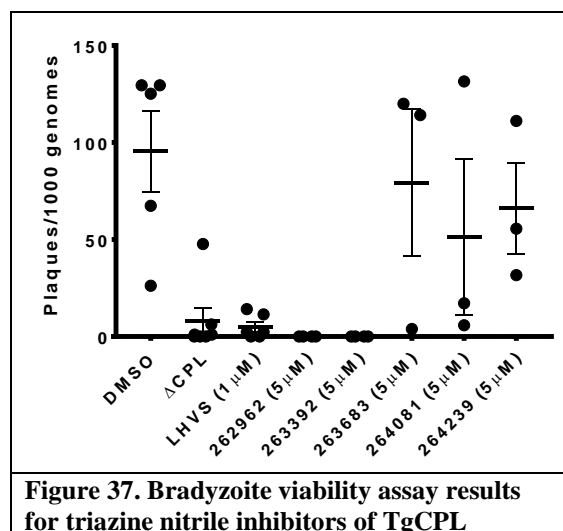
Ex vivo T. gondii cysts were pre-incubated with **262962** (200 nM or 2 μ M) for 30 min, then 200 nM **263473** was added to samples and samples left to incubate for a further 30 min (at room temperature). Cysts were also stained to show cathepsin L, using Rb α -*TgCPL* primary Ab. Cysts were imaged at x100 magnification.

Interestingly, the competition assay between labeled and unlabeled triazine nitrile *TgCPL* inhibitors showed similar results as with the vinyl sulfone type inhibitors. This implies that the triazine nitrile inhibitor **262962** is competing for the same target as the BODIPY labeled **263473**,

presumably *TgCPL*. Importantly, this suggests that the BODIPY-TRZ probe **263473** is capable of labeling *TgCPL* in extracellular bradyzoites but is impeded from accessing the cyst in intracellular cysts in some manner. Perhaps the lack of covalency prevents the BODIPY probe from accumulating in the VAC with sufficient levels for imaging. A similar intracellular competition assay between BO-LHVS (able to accumulate and label intracellular *TgCPL*) and unlabeled triazine nitrile inhibitor **262962** is currently underway.

Bradyzoite Cyst Viability Assay

In the competition assays in *ex vivo* cysts, it appears the triazine nitrile compounds can compete for the same target as the BODIPY labeled probes, indicating they are capable of inhibiting *TgCPL*. The lack of dark puncta and autophagosomes in our previous experiments may simply be due to the reversible nature of the nitrile warhead. We were pleased, therefore, to find that the triazine nitrile *TgCPL* inhibitors (**262962** and **263392**) exhibit strong efficacy in our plaque-forming, bradyzoite viability assay (**Figure 37**). They successfully reduced *T. gondii* bradyzoite viability with the same efficacy as the genetic knockout of *TgCPL* (Δ CPL) and inhibition by the irreversibly covalent LHVS.



To our knowledge, this is the first example of a CNS penetrant inhibitor of TgCPL showing efficacy against the chronic stage *Toxoplasma*. Newer triazine nitrile analogs **263683**, **264081**, and **264239** showed variable efficacy when treating the bradyzoite. The reason for this observation is unclear but may be a result of the frequency of dosing (once per day), or duration of treatment (1 wk). Replicates of these assays are currently underway to evaluate these possibilities.

Conclusion

Triazine nitrile and vinyl sulfone BODIPY fluorescent probes were synthesized in order to confirm that our compounds were able to reach and bind to our cathepsin target within the parasite vacuole. Genetic knockouts of TgCPL and treatment of intracellular bradyzoites in human fibroblast cells with the irreversibly covalent inhibitor LHVS each resulted in the development of dark granules and stain positive for autophagosome accumulation. Curiously, this response is not observed when TgCPL intracellular bradyzoites are treated with our

dipeptide nitrile, dipeptide vinyl sulfone, or triazine nitrile *TgCPL* inhibitors. Treatment of intracellular bradyzoites with the BODIPY-tagged dipeptide vinyl sulfone probe **263252** results in the fluorescent labeling of distinct areas within the parasite, presumably labeling *TgCPL* in the VAC organelle. This phenomenon was not observed when treating intracellular cysts with the triazine nitrile BODIPY probe **263473**, potentially due to issues with solubility, permeability of HFF cells, or lack of covalency. Competition assays between BODIPY labeled versus unlabeled *TgCPL* inhibitors with both the vinyl sulfone and triazine nitrile compounds were performed on *ex vivo* bradyzoites. In this cell-free environment, we were able to demonstrate fluorescent labeling within the bradyzoite with our triazine nitrile probe, and that both vinyl sulfone and triazine nitrile inhibitors apparently compete for the same *TgCPL* target. Importantly, we then demonstrated for the first time that treatment of chronic stage *T. gondii* bradyzoite cysts with triazine nitrile inhibitors reduces parasite viability with efficacy equivalent to a *TgCPL* genetic knockout. Although the BODIPY-tagged probe was unable to form fluorescent puncta in the intracellular cysts (potentially due to permeability or solubility issues), the untagged version (**263392**) was able reach the parasite VAC in sufficient concentration to cause parasite death. This is the first example of a CNS penetrant, reversible *TgCPL* inhibitor showing efficacy in an *in vitro* model of the chronic stage parasite. Current studies are underway to confirm these results and to advance the triazine nitrile series toward an *in vivo* model of latent *Toxoplasma* infection.

Experimental

Chemistry General Information: All reagents were used without further purification as received from commercial sources unless noted otherwise. ¹H NMR spectra were taken in DMSO-*d*₆, MeOD, or CDCl₃ at room temperature on Varian Inova 400 MHz or Varian Inova 500 MHz instruments. Reported chemical shifts for the ¹H NMR spectra were recorded in parts per million (ppm) on the δ scale from an internal standard of residual tetramethylsilane (0 ppm). Mass spectrometry data were obtained on either a Micromass LCT or Agilent Q-TOF. An Agilent 1100 series HPLC with an Agilent Zorbax Eclipse Plus-C18 column was used to determine purity of biologically tested compounds. Unless otherwise noted, all tested compounds were determined to be >95% pure using a 6 minute gradient of 10-90% acetonitrile in water followed by a 2 minute hold at 90% acetonitrile with detection at 254 nm. Flash chromatographic purifications were performed using a Teledyne ISCO Combiflash RF with Redisep Gold RF columns.

Chemistry:

Tert-butyl (S,E)-(4-(phenylsulfonyl)but-3-en-2-yl)carbamate

In a dry round bottom flask containing 2 mL anhydrous THF was added diethyl ((phenylsulfonyl)methyl)phosphonate (494 mg, 1.689 mmol). The solution was cooled to 0°C, sodium hydride (67.5 mg, 1.689 mmol) was added and reaction was stirred at this temperature for 30 min. Next, tert-butyl (S)-(1-oxopropan-2-yl)carbamate (225 mg, 1.299 mmol) in THF (1-2mL) was added and the reaction was allowed to warm to room temperature and stirred for 1h. Reaction was poured into EtOAc and washed with 1N HCl, sat. NaHCO₃, and brine. Organic

layer was dried over MgSO_4 and concentrated. Crude was purified by FC (1-100% EtOAc:Hexanes gradient) to afford tert-butyl (S,E)-(4-(phenylsulfonyl)but-3-en-2-yl)carbamate (360 mg, 1.156 mmol, 89 % yield) as a colorless oil.; ^1H NMR (500 MHz, MeOH-d_4) δ 7.88 (d, $J = 7.34$ Hz, 2H), 7.68 (t, $J = 7.34$ Hz, 1H), 7.60 (t, $J = 7.58$ Hz, 2H), 6.90 (dd, $J = 3.42, 15.20$ Hz, 1H), 6.54 (d, $J = 15.16$ Hz, 1H), 4.23 - 4.43 (m, 1H), 1.40 (br. s, 9H), 1.23 (d, $J = 7.34$ Hz, 3H)

(S,E)-4-(Phenylsulfonyl)but-3-en-2-amine, HCl

Tert-butyl (S,E)-(4-(phenylsulfonyl)but-3-en-2-yl)carbamate (360 mg, 1.156 mmol) was dissolved in 4N HCl in dioxane (~3mL) and stirred at rt for 1h. Solvent was removed in vacuo to afford (S,E)-4-(phenylsulfonyl)but-3-en-2-amine, HCl (286 mg, 1.154 mmol, 100 % yield). Product was used without further purification.; ^1H NMR (500 MHz, MeOH-d_4) δ 7.93 (d, $J = 7.34$ Hz, 2H), 7.73 (t, $J = 7.34$ Hz, 1H), 7.65 (t, $J = 7.34$ Hz, 2H), 6.96 (br. d, $J = 2.00$ Hz, 2H), 4.16 (q, $J = 6.52$ Hz, 1H), 1.45 (d, $J = 6.85$ Hz, 3H)

tert-Butyl ((S)-4-methyl-1-oxo-1-(((S,E)-4-(phenylsulfonyl)but-3-en-2-yl)amino)pentan-2-yl)carbamate

In a dry round bottom flask, (tert-butoxycarbonyl)-L-leucine (187 mg, 0.807 mmol) was dissolved with DMF (1 mL). HATU (460 mg, 1.211 mmol) and DIPEA (0.423 ml, 2.422 mmol) were then added and reaction was allowed to stir for 10-15min. (S,E)-4-(phenylsulfonyl)but-3-en-2-amine, HCl (200 mg, 0.807 mmol) was added and the reaction was left to stir for 6 h. The solution was poured into water and extracted with DCM 3 times. Combined organic layer was washed with sat. NaHCO_3 (aq) and brine, dried over MgSO_4 and concentrated. Crude was purified

on FC (0-100% EtOAc:Hexanes gradient) to afford tert-butyl ((S)-4-methyl-1-oxo-1-(((S,E)-4-(phenylsulfonyl)but-3-en-2-yl)amino)pentan-2-yl)carbamate (201 mg, 0.473 mmol, 58.6 % yield).; ¹H NMR (CDCl₃, 500 MHz) δ 7.78 (d, *J* = 7.34 Hz, 2H), 7.53 (t, *J* = 7.34 Hz, 1H), 7.45 (t, *J* = 7.83 Hz, 2H), 6.85 (dd, *J* = 4.89, 15.16 Hz, 1H), 6.39 (d, *J* = 15.16 Hz, 1H), 5.49 (d, *J* = 7.34 Hz, 1H), 4.59 - 4.74 (m, 1H), 4.09 (d, *J* = 6.85 Hz, 1H), 1.45 - 1.56 (m, 1H), 1.36 - 1.44 (m, 2H), 1.30 (s, 9H), 1.14 (d, *J* = 6.85 Hz, 3H), 0.77 (dd, *J* = 6.85, 19.56 Hz, 6H) ; ¹³C NMR (CDCl₃, 126 MHz) δ 172.4, 155.7, 146.9, 140.0, 133.2, 129.6, 129.1, 127.3, 79.6, 60.2, 52.8, 44.7, 41.0, 28.1, 24.4, 22.6, 21.6, 19.2, 14.0

(S)-2-Amino-4-methyl-N-((S,E)-4-(phenylsulfonyl)but-3-en-2-yl)pentanamide

To a small vial charged with tert-butyl ((S)-4-methyl-1-oxo-1-(((S,E)-4-(phenylsulfonyl)but-3-en-2-yl)amino)pentan-2-yl)carbamate (100 mg, 0.236 mmol) was added 4N HCl in Dioxane (1 ml). Reaction was left to stir under nitrogen for 1h, at which time HPLC indicated reaction was complete. Solvent was removed *in vacuo* and product was used directly in next step without further purification.; ¹H NMR (CDCl₃, 500 MHz) δ 7.88 (d, *J* = 7.83 Hz, 2H), 7.70 (t, *J* = 7.34 Hz, 1H), 7.62 (t, *J* = 7.83 Hz, 2H), 6.93 (dd, *J* = 5.87, 15.16 Hz, 1H), 6.62 (d, *J* = 15.16 Hz, 1H), 4.70 (quin, *J* = 6.24 Hz, 1H), 3.88 (t, *J* = 6.85 Hz, 1H), 3.65 (s, 3H), 1.56 - 1.74 (m, 3H), 1.34 (d, *J* = 6.85 Hz, 3H), 0.96 (d, *J* = 6.36 Hz, 3H), 0.93 (d, *J* = 5.87 Hz, 3H)

(S)-2-(3-(5,5-Difluoro-7,9-dimethyl-5H-5l4,6l4-dipyrrolo[1,2-c:2',1'-f][1,3,2]diazaborinin-3-yl)propanamido)-4-methyl-N-((S,E)-4-(phenylsulfonyl)but-3-en-2-yl)pentanamide (263252)

In a dry round bottom flask, 3-(5,5-difluoro-7,9-dimethyl-5H-5l4,6l4-dipyrrolo[1,2-c:2',1'-f][1,3,2]diazaborinin-3-yl)propanoic acid (24 mg, 0.082 mmol) was dissolved in DCM (2 mL)

and cooled to -10°C . HATU (34.4 mg, 0.090 mmol) and DIPEA (0.050 ml, 0.288 mmol) were added and reaction was stirred at -10°C for 10-15min. (S)-2-(3-(5,5-difluoro-7,9-dimethyl-5H-514,614-dipyrrolo[1,2-c:2',1'-f][1,3,2]diazaborinin-3-yl)propanamido)-4-methyl-N-((S,E)-4-(phenylsulfonyl)but-3-en-2-yl)pentanamide was then added and reaction was slowly warmed to rt and left to stir overnight. The solution was poured into water and extracted with EtOAc 3 times. Combined organic layer was washed with 1N HCl, sat. NaHCO_3 (aq) and brine, dried over Na_2SO_4 and concentrated. Crude was purified on FC (20-100% EtOAc:Hexanes gradient) to afford (S)-2-(3-(5,5-difluoro-7,9-dimethyl-5H-514,614-dipyrrolo[1,2-c:2',1'-f][1,3,2]diazaborinin-3-yl)propanamido)-4-methyl-N-((S,E)-4-(phenylsulfonyl)but-3-en-2-yl)pentanamide (15 mg, 0.025 mmol, 30.5 % yield).; ^1H NMR (CDCl_3 , 500 MHz) δ 7.86 (d, $J = 7.83$ Hz, 2H), 7.60 (t, $J = 7.34$ Hz, 1H), 7.52 (t, $J = 7.58$ Hz, 2H), 7.10 (s, 1H), 6.87 (d, $J = 3.91$ Hz, 1H), 6.84 (d, $J = 4.40$ Hz, 1H), 6.65 (d, $J = 7.83$ Hz, 1H), 6.40 (dd, $J = 1.47, 15.16$ Hz, 1H), 6.24 (d, $J = 3.91$ Hz, 1H), 6.21 (d, $J = 7.34$ Hz, 1H), 6.12 (s, 1H), 4.67 (d, $J = 6.36$ Hz, 1H), 4.32 (d, $J = 5.87$ Hz, 1H), 3.22 (t, $J = 7.09$ Hz, 2H), 2.60 - 2.72 (m, 2H), 2.54 (s, 3H), 2.25 (s, 3H), 1.50 - 1.61 (m, 1H), 1.35 - 1.47 (m, 2H), 1.19 (d, $J = 7.34$ Hz, 3H), 0.82 (d, $J = 6.36$ Hz, 3H), 0.79 (d, $J = 6.36$ Hz, 3H); ^{13}C NMR (CDCl_3 , 126 MHz) δ 172.3, 171.4, 160.8, 156.3, 146.7, 144.3, 140.1, 135.3, 133.4, 133.2, 130.0, 129.3, 128.2, 127.6, 123.9, 120.6, 117.0, 60.4, 51.9, 45.1, 40.1, 35.3, 24.5, 24.5, 22.8, 21.8, 19.4, 14.9, 14.2, 11.3; HRMS-ESI (m/z): $[\text{M}+\text{Na}]^+$ calcd for, $\text{C}_{30}\text{H}_{37}\text{BF}_4\text{N}_4\text{O}_4\text{S}$; 261.2489; found, 261.2497

***tert*-Butyl (2-((4-chloro-6-((1-(4-fluorophenyl)ethyl)(isopentyl)amino)-1,3,5-triazin-2-yl)amino)ethyl)carbamate**

General procedure B1 from 2,4,6-trichloro-1,3,5-triazine (250 mg, 1.356 mmol), N-(1-(4-fluorophenyl)ethyl)-3-methylbutan-1-amine (284 mg, 1.356 mmol), DIPEA (0.474 ml, 2.71 mmol) and tert-butyl (2-aminoethyl)carbamate (0.215 ml, 1.356 mmol) gave tert-butyl (2-((4-chloro-6-((1-(4-fluorophenyl)ethyl)(isopentyl)amino)-1,3,5-triazin-2-yl)amino)ethyl)carbamate (464 mg, 0.965 mmol, 71.2 % yield).; ¹H NMR (CDCl₃, 500 MHz) δ 7.16 - 7.40 (m, 2H), 6.90 - 7.08 (m, 2H), 4.10 (dd, *J* = 6.60, 13.45 Hz, 1H), 3.51 (br. s., 2H), 3.19 - 3.41 (m, 2H), 2.03 (d, *J* = 12.72 Hz, 2H), 1.55 (dd, *J* = 6.36, 12.23 Hz, 3H), 1.33 - 1.49 (m, 9H), 1.24 (td, *J* = 6.79, 13.33 Hz, 4H), 0.71 - 0.93 (m, 5H)

tert-Butyl (2-((4-cyano-6-((1-(4-fluorophenyl)ethyl)(isopentyl)amino)-1,3,5-triazin-2-yl)amino)ethyl)carbamate

General Procedure B2 from tert-butyl (2-((4-chloro-6-((1-(4-fluorophenyl)ethyl)(isopentyl)amino)-1,3,5-triazin-2-yl)amino)ethyl)carbamate (200 mg, 0.416 mmol), potassium cyanide (29.8 mg, 0.457 mmol), and DABCO (93 mg, 0.832 mmol) gave tert-butyl (2-((4-cyano-6-((1-(4-fluorophenyl)ethyl)(isopentyl)amino)-1,3,5-triazin-2-yl)amino)ethyl)carbamate (174 mg, 0.369 mmol, 89 % yield).; ¹H NMR (CDCl₃, 500 MHz) δ 7.10 - 7.33 (m, 2H), 7.00 (t, *J* = 8.31 Hz, 2H), 6.13 (d, *J* = 6.85 Hz, 1H), 5.12 (br. s., 1H), 3.41 - 3.57 (m, 2H), 3.21 - 3.39 (m, 3H), 3.12 (dd, *J* = 4.16, 12.47 Hz, 1H), 1.49 - 1.61 (m, 3H), 1.32 - 1.47 (m, 11H), 0.73 - 0.84 (m, 6H)

4-((2-Aminoethyl)amino)-6-((1-(4-fluorophenyl)ethyl)(isopentyl)amino)-1,3,5-triazine-2-carbonitrile

In a dry round bottom flask, tert-butyl (2-((4-cyano-6-((1-(4-fluorophenyl)ethyl)(isopentyl)amino)-1,3,5-triazin-2-yl)amino)ethyl)carbamate (174 mg, 0.369 mmol) was dissolved with a 2:1 EtOAc:4N HCl in dioxane solution and allowed to stir for 30 min. Solvent was removed *in vacuo* to afford 4-((2-aminoethyl)amino)-6-((1-(4-fluorophenyl)ethyl)(isopentyl)amino)-1,3,5-triazine-2-carbonitrile (137 mg, 0.369 mmol, 100 % yield). Compound was carried directly to next step. ¹H NMR (CDCl₃, 500 MHz) δ 7.22 (s, 1H), 7.25 (s, 1H), 6.83 - 7.06 (m, 2H), 5.88 - 6.11 (m, 1H), 5.29 (s, 1H), 3.76 (br. s., 2H), 3.14 - 3.44 (m, 2H), 3.09 (br. s., 1H), 1.47 - 1.68 (m, 3H), 1.27 - 1.44 (m, 2H), 1.11 (br. s., 1H), 0.67 - 0.81 (m, 6H)

N-(2-((4-Cyano-6-((1-(4-fluorophenyl)ethyl)(isopentyl)amino)-1,3,5-triazin-2-yl)amino)ethyl)-3-(5,5-difluoro-7,9-dimethyl-5H-5l4,6l4-dipyrrolo[1,2-c:2',1'-f][1,3,2]diazaborinin-3-yl)propanamide (263473)

3-(5,5-difluoro-7,9-dimethyl-5H-5l4,6l4-dipyrrolo[1,2-c:2',1'-f][1,3,2]diazaborinin-3-yl)propanoic acid (35.4 mg, 0.121 mmol) was dissolved into DMF (0.5 mL) and cooled to 0°C. HATU (46.1 mg, 0.121 mmol) and DIPEA (0.042 ml, 0.242 mmol) were then added and reaction was stirred at 0°C for 5 min. 4-((2-aminoethyl)amino)-6-((1-(4-fluorophenyl)ethyl)(isopentyl)amino)-1,3,5-triazine-2-carbonitrile (30 mg, 0.081 mmol) was dissolved into DMF (0.5 mL) and added dropwise to the stirring solution. Reaction was allowed to warm slowly to rt and left to stir over 6 h. Reaction was monitored by HPLC detecting at 502 nM. Reaction was poured into EtOAc and washed with brine, dried over NaSO₄, and concentrated. Crude was purified by FC (1-100% E:H gradient) to afford N-(2-((4-cyano-6-((1-(4-fluorophenyl)ethyl)(isopentyl)amino)-1,3,5-triazin-2-yl)amino)ethyl)-3-(5,5-difluoro-7,9-dimethyl-5H-5l4,6l4-dipyrrolo[1,2-c:2',1'-f][1,3,2]diazaborinin-3-yl)propanamide (18.5 mg,

0.029 mmol, 35.5 % yield); ^1H NMR (CDCl_3 , 500 MHz) δ 7.26 (s, 1H), 7.22 - 7.25 (m, 1H), 7.14 - 7.19 (m, 1H), 7.00 (t, $J = 8.56$ Hz, 2H), 6.87 - 6.92 (m, 1H), 3.42 (br. s., 1H), 3.30 - 3.40 (m, 3H), 3.17 - 3.30 (m, 4H), 3.05 (dt, $J = 4.89, 12.47$ Hz, 1H), 2.67 (q, $J = 7.34$ Hz, 2H), 2.52 - 2.62 (m, 3H), 2.27 - 2.33 (m, 2H), 2.24 (d, $J = 15.16$ Hz, 1H), 1.49 - 1.58 (m, 3H), 1.35 - 1.48 (m, 1H), 1.28 - 1.35 (m, 1H), 1.17 - 1.23 (m, 2H), 1.07 - 1.16 (m, 1H), 0.77 - 0.84 (m, 5H), 0.75 (d, $J = 6.85$ Hz, 1H).; HRMS-ESI (m/z): $[\text{M}+\text{Na}]^+$ calcd for, $\text{C}_{33}\text{H}_{39}\text{BF}_3\text{N}_9\text{O}$; 668.3215; found, 668.3220

Bradyzoite Competition Assay:

Mice were infected with *T. gondii* tachyzoites (Prugniaud strain) and left for 5 weeks to allow parasite cysts to form on the brain. Infected brains were then removed from euthanized mice and subsequently homogenized (by syringing) in 1ml of 1x PBS, to liberate cysts. Assuming a cyst diameter between 20-50 μm , samples of homogenized brain extract were passed over a 20 μm filter to separate cysts from brain material. Homogenized brain material passes through the filter, while cysts are retained on top of the filter. To gently remove cysts from the filter, the filter was placed into a non-pyrogenic falcon tube (50ml) with PBS and left to incubate for 1 hour at room temperature on a rotator. A 10 μl aliquot of the PBS (now containing cysts) was placed on a haemocytometer and the number of cysts counted. This information was then used to estimate the number of cysts present in the whole sample. Cysts were aliquoted into the wells of a chamber slide that had been coated with Cel-Tak adhesive (Corning) and allowed to settle on the bottom. Wells were then washed with PBS before adding the inhibitors (LHVS or test compound, e.g. triazine). Cysts were left to incubate at room temperature with 200nM BODIPY LHVS (BO-LHVS) alone, or a 1:1 or 1:10 mixture of BO-LHVS and LHVS. This was

repeated for BODIPY-inhibitor (vinyl sulfone and triazine) versus the respective unlabeled inhibitor. After three washes with 1 x PBS, brain material was fixed with 4% paraformaldehyde and stained with rabbit anti-CPL antibodies at 1:200 dilution followed by Alexa 594- conjugated goat anti-rabbit antibodies. Slides were mounted with mowiol and images were captured with a Zeiss Axiovert Observer Z1 inverted fluorescence microscope and an AxioCAM MRm camera and processed using Zeiss Axiovision 4.3 software. If the un-tagged (normal) inhibitor binds to the target, the BODIPY version will not be able to bind as much, and thus BODIPY signal will be lower compared to the signal produced by the BODIPY inhibitor in the absence of a competitor.

Bradyzoite Viability Assay:

Split HFF cells and seed them into the wells of 6-well plates. Leave at 37°C until HFF cells are confluent. Meanwhile, once parasite stocks have egressed from the host cell culture in a T25 flask, pass a large number of drops (e.g. 10 drops) of parasites into a new T25 flask containing confluent HFF cells. Leave for two days at 37°C. After two days, check cells are full of intracellular parasites. Proceed to harvest parasites as follows: 1) Pour off the D10 media and replace with 10 ml fresh D10 media. 2) Using a sterile cell scraper, lift the cells from the surface of the T25 flask by mechanically scraping them off. 3) Transfer the media containing scraped cells to a sterile conical tube. 4) Using a 20G syringe needle, syringe up and down to break open the cells release the parasites. Repeat three times with a 20G syringe needle, then once with a 23G needle. 5) Pass the syringed media through a sterile 0.22µm filter (into a new sterile conical tube).; Place 10 µl of the harvested parasites onto a haemocytometer and count the number of parasites within a 5x5 grid. This count determines the number of parasites in 0.1 µl. Multiply this

by 10 to determine the number of tachyzoites per ul of media. Resuspend the harvested tachyzoites so that there is 1000 tachyzoites per 2 ml of D10 media. Next, place 2 ml of media containing these parasites onto the well of the 6-well plate (that contains the confluent HFF cells, see the first step above). I.e. place 1000 tachyzoites into the well of a 6-well plate that already contains a confluent HFF cells monolayer. Leave the plate at 37°C overnight. The next day, check the HFF cells in the 6-well plate contain intracellular tachyzoites. Aspirate the D10 media from the wells and replace with 2 ml conversion media per well. Place the plate at 37°C in an incubator that contains 0% CO₂. Allow one week for conversion of parasites from tachyzoite to bradyzoite life stage. During this period, replace the conversion media every 24 hours for fresh conversion media. Following the conversion phase, replace the conversion media for conversion media containing the inhibitor/compound-of-interest (e.g. LHVS). Continue to treat for the required amount of time (e.g. one week), replacing the conversion media containing the inhibitor every 24 hours (replacing with fresh conversion media containing fresh inhibitor). Towards the end of the treatment phase, split HFF cells into 6-well plates. Prepare three wells of HFF cells per treatment sample (i.e. for every well in the treatment phase, prepare three wells for the plaquing phase, to allow for three technical replicates).; After the treatment phase, harvest the parasites from the 6-well plate and set up the plaquing phase as follows: 1) Aspirate the media and replace with 1 ml HBSS. 2) Use a cell scraper to mechanically lift the cells containing the bradyzoites from the bottom of the well. 3) Using a 20G syringe needle, syringe up and down to break open the cells and release the parasites. Repeat three times with a 20G syringe needle, then once with a 25G needle. 4) Transfer the syringed media containing the released parasites to a sterile conical tube. 5) To maximize bradyzoite yield, rinse the scraped well with 1 ml HBSS and add this to the conical tube that already contains 1 ml of the syringed parasites (in HBSS). 6)

Add 2 ml of 2X pepsin solution and mix. (Note, pepsin treatment is to kill any tachyzoites). 7) Incubate samples in a water bath at 37°C for 30 min. 8) Stop the reaction by adding 4 ml of 2X neutralization buffer. 9) Centrifuge the samples for 10 minutes at room temperature at 1800g. 10) Very carefully discard the supernatant from the samples, ensuring the pellet remains in the conical tube. 11) Suspend the pellet in 1 ml D10 media. 12) Count the number of parasites using a haemocytometer (as described above). 13) Infect the wells of the 6-well plate with 1000 bradyzoites in 2.5 ml D10 media (seed triplicate wells with 1000 bradyzoites each, for each sample). Important: keep a record of the volume of parasites added to 2.5 ml of media. 14) Leave the plates at 37°C for 12 days without moving them and without any media change. 15) After 10 days stain, pour off the media and stain wells with crystal violet. It is advisable to count the number of plaques under a microscope prior to crystal violet staining (in the event that plaques aren't large enough to be identified following crystal violet staining). At step 11 (above) where parasites were resuspended in 1 ml D10 media, remove 500 ul of the resuspended parasites and transfer to a sterile microcentrifuge tube. Centrifuge samples for 10 min at room temperature at 1000g. Carefully remove the supernatant and store the pellet at -80C until required. Extract genomic DNA using the Qiagen DNA extraction kit (following manufacturer protocol). Elute in 100 ul sterile, nuclease-free distilled water. Determine the number of genomes in the sample by qPCR. Use genomic DNA standards in the qPCR assay to generate a standard curve. Use the TUB2 forward (5'-GCGTCTTCTTGGATTTGGAG-3') and reverse (5'-TGGAGACCAGTGCAGTTGTC-3') primers. The software will generate a "Cq" value for each of the standards and use this to plot a standard curve. A Cq value will also be determined for each sample from the viability assay too. Based on the number of genomes stated for each of the standards, the software will then determine the number of genomes present in each qPCR

reaction. Since 10 ul of the extracted genomic DNA is used in the qPCR reaction, multiply the number of genomes by 10 to determine the number of genomes present in the entire genomic DNA extract (since genomic DNA was eulted into 100 ul of sterile, nuclease-free distilled water). Next, multiply the number of genomes by 2 to determine how many genomes were present in the pellet that was resuspended in 1 ml D10 media (since half of the sample was taken for genomic DNA extraction). Next, divide the number of genomes by 1000 to determine the number of genomes per 1 ul of media. Then, based on the volume of parasites added at step 13 above, we can determine the precise number of genomes added into the well for the plaquing stage. After counting the number of plaques that form, then calculate the number of plaques per 1000 genomes.

Chapter 5 Future Directions

Overview of Objectives

Over the course of this project, several inhibitors of *Tg*CPL have been developed that achieve both potent inhibition and CNS penetrance (**Figure 38**). While these represent significant advancement towards a viable probe with which to validate *Tg*CPL as a clinically relevant target for the treatment of toxoplasmosis, there is still a large body of work remaining to progress toward *in vivo* proof of concept.

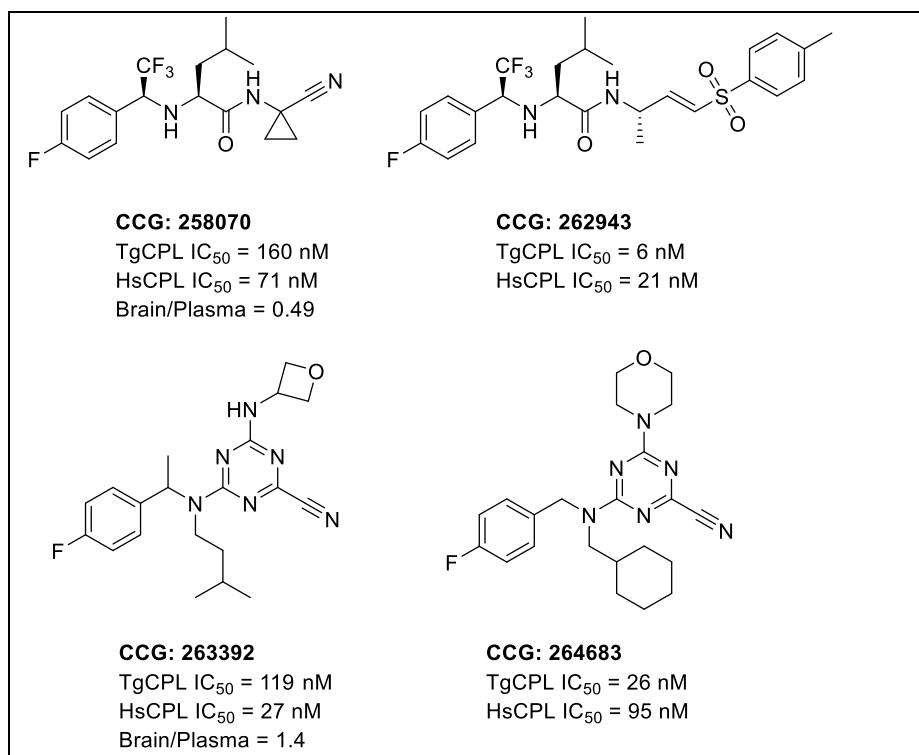


Figure 38. Select developed inhibitors of *Toxoplasma gondii* cathepsin L

One of the key remaining objectives is to achieve robust selectivity (>10-fold) for *TgCPL* over the human isoform. This has been a consistently difficult challenge to overcome, primarily due to the minimal differences in the active site binding pockets between human and parasite cathepsins. To date, analog **264683** has exhibited one of the better inhibitory and metabolic profiles (**Figure 38**), while also displaying the physicochemical properties that are predictive of CNS penetrance. However, several features of this compound preclude advancement toward *in vivo* studies. While the metabolic stability was acceptable (MLM $t_{1/2}$ = 15 min), the solubility was too poor for further PK studies. Similar solubility issues were previously overcome by replacing the P1 morpholine with an oxetane, as seen in compound **263392**. This change not only improved compound solubility, but also improved the exposure levels and BBB permeability in our PK studies (1:1 brain:plasma @ 2h). Additionally, it seems that there is potential for this scaffold to switch binding modes by rotation around the triazine-P2/3 pendant nitrogen bond (**Figure 39**), which may be a reason we see very little change in selectivity in favor of *TgCPL* over the human isoform. Furthermore, the triazine nitrile is known to react with the active site cysteine rapidly, which may obscure any selective effects due to the weakly bound P2-P3 pendants. The modification of the core, conformationally restricting the P2-P3 exchange and improving solubility are all paramount in achieving a refined selectivity profile.

Conformational Restriction

-Variable Binding Modes and Conformational Restriction

The scaffold hop to the triazine nitriles, significantly reduces the number of rotatable bonds versus the dipeptide nitriles. This serves to, further increase the rigidity of the scaffold and has resulted in improved binding, selectivity, and CNS penetrance. However, the triazine nitrile

scaffold may still require further conformational restriction to improve selectivity and its CNS profile. Shown below in **Figure 39**, one of the docking poses suggests the possibility that the P2-P3 vectors may flip, placing the intended P3 4-fluorobenzyl pendant in the S2 pocket.

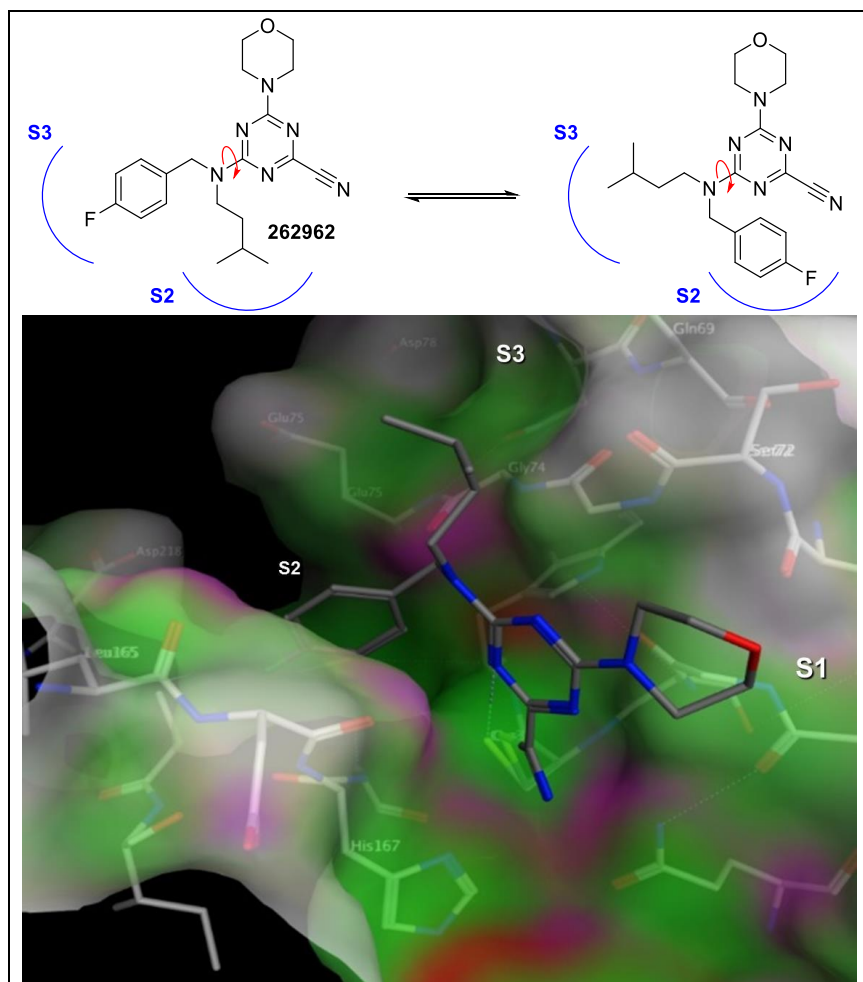


Figure 39. Potential flip of binding mode

Alternative docking pose (right) of **262962** (gray) indicating a possible flip of P2/P3 binding poses. Derived from PDB: 3F75

It is known that human cathepsin L favors a phenylalanine (mimicked closely by the 4-fluorobenzyl) in S2 and is amenable to nearly any lipophilic amino acid. *TgCPL* prefers leucine as the P2 substrate, and given the slightly small pocket size, is somewhat less accepting of larger sidechains such as the 4-fluorobenzyl. This binding mode exchange would result in a

significantly less variable P2 SAR for *HsCPL*. Restricting the scaffold, e.g. by preventing rotation about the triazine-nitrogen bond, would force the P2 and P3 vectors to bind in their respective pockets, enabling a more reliable selectivity differentiation between parasite and human isoforms. **Figure 40** shows proposed changes to the scaffold that could reduce or eliminate the rotational freedom and variable binding modes.

-Example Conformationally Restricted Analogs:

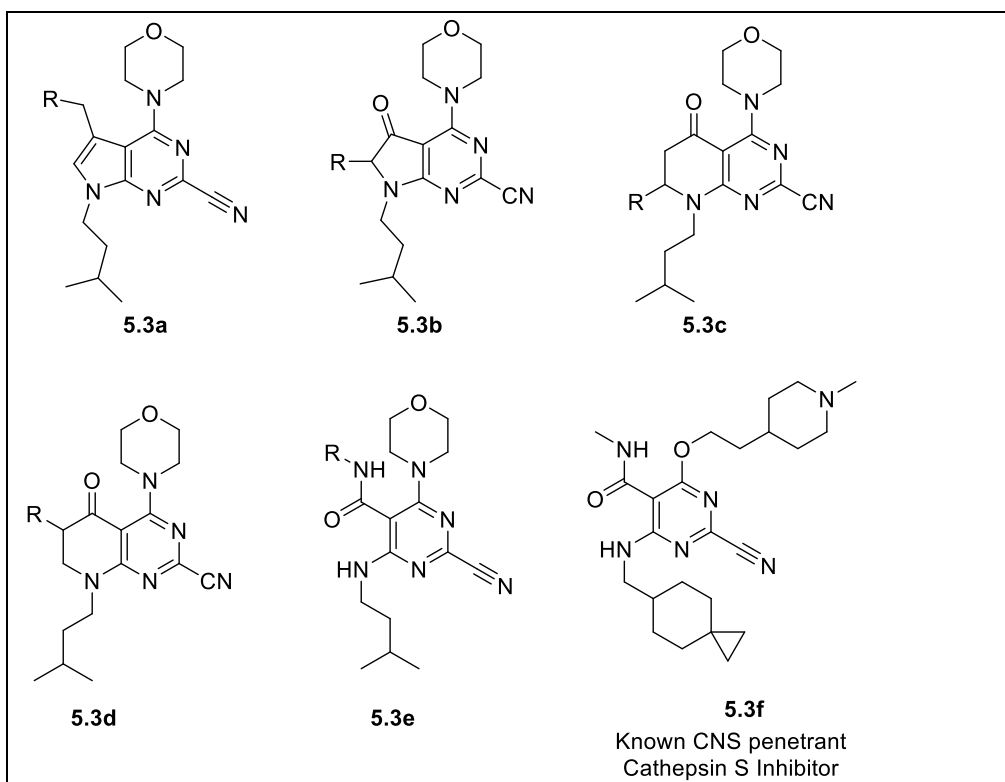


Figure 40. Possible conformational restrictions to keep the desired binding orientation of TgCPL inhibitors

Proposed scaffolds **5.3a-d** exemplify fused ring systems that are predicted to retain the P2-P3 binding motifs. While **5.3b-d** increase overall TPSA, the reduction in rotational freedom would be beneficial for BBB permeability. Compound **5.3e** does not restrict overall rotational

freedom, however it does orient the P2 and P3 vectors in a non-interchangeable manner. While this modification pushed the physiochemical properties toward the limit of CNS penetrance, there is literature precedent (compound **5.3f**) demonstrating this chemotype can still access the CNS.

-Benzylic modification for improved solubility and restriction of binding mode

The docking model of **263251** shows this compound bound with the expected P2/P3 orientation (**Figure 41**). The α -methyl of the P3 pendant docks near the backbone carbonyl of Leu165, with only a 3.95 Å distance between the features. The binding variability could potentially be reduced through either hydrogen bonding or steric interactions at this position.

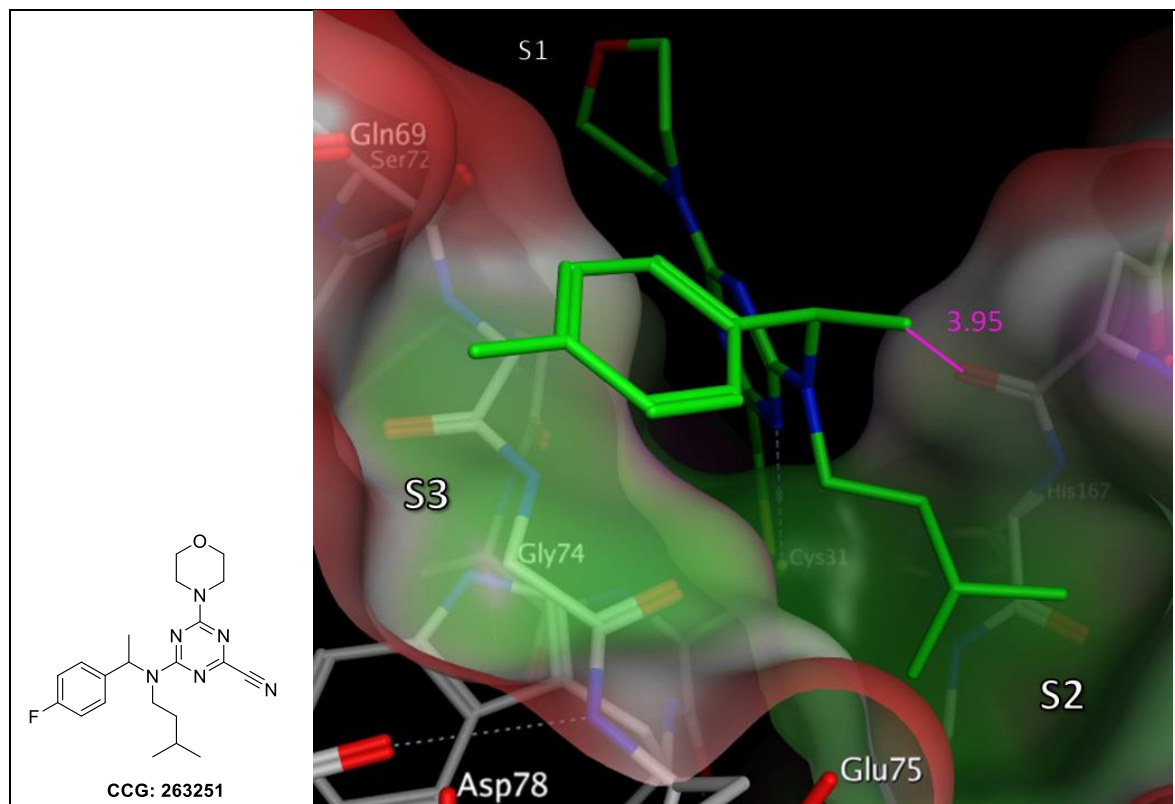


Figure 41. Docking of 263251 in TgCPL
Docking shows a 3.95 Å distance between the α -methyl and amide carbonyl of Leu165. Derived from PDB: 3F75

The formation of a meaningful hydrogen bond between the ligand and backbone residue would serve to improve binding as well as better orient the P3 vector. This idea could be explored through the incorporation of a hydroxyl, or other hydrogen bond donors as shown in **Figure 42 (5.5a)**. As an added benefit, the additional steric bulk of a branched benzylic position would be unfavorable for binding in the S2 pocket further ensuring the desired binding mode pictured in **Figure 41**. If the addition of a hydrogen bond donor proves to be unsuitable for binding, or compromises BBB permeability, perhaps simple substitution of the benzylic methyl with a slightly larger lipophilic group, such as the cyclopropyl (**5.5b**), may be enough to orient the P3 vector in the desired pocket. This would maintain the low TPSA and H-bond donors required for CNS penetration.

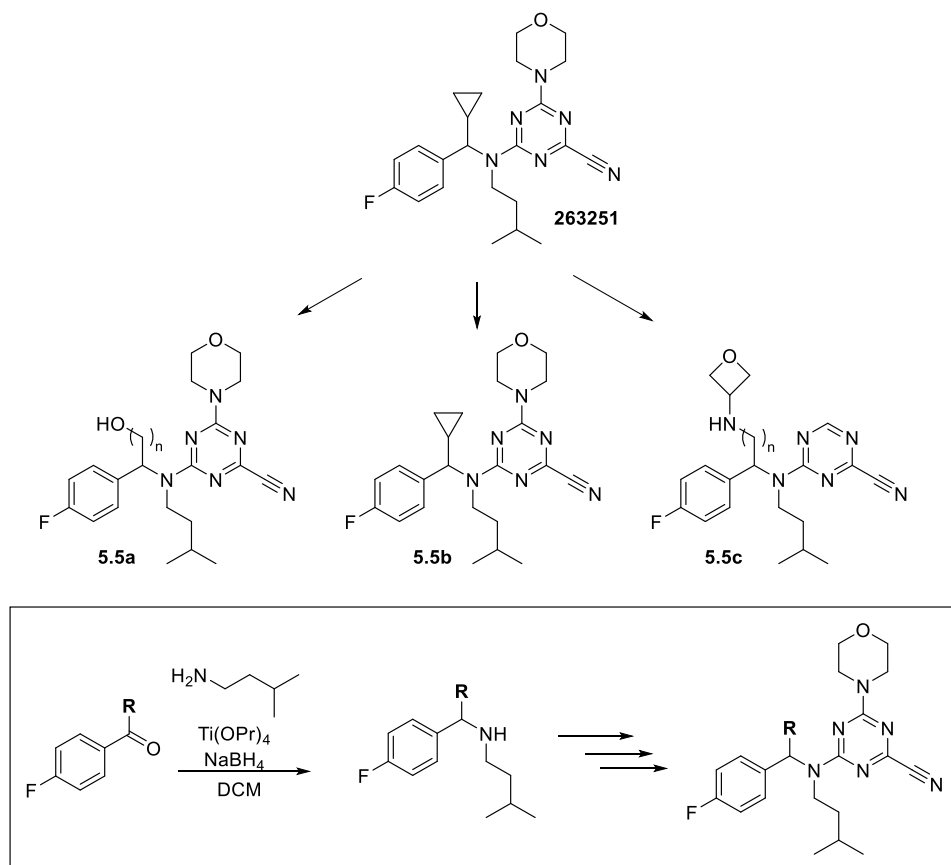


Figure 42. Modifications of benzylic position to impede rotation and improve solubility

Modification in this benzylic position has additional potential to modulate solubility. With the analogs synthesized thus far, solubility is primarily imparted by the P1 morpholine group. As was demonstrated previously in analog **263392**, this can be exchanged with an amino oxetane for improved solubility and still retain CNS penetrance. Given the proximity of this position to the Leu165 carbonyl, the migration of the solubilizing group to this position (**5.5c**) may simultaneously provide the necessary solubility, while restricting rotation via hydrogen bonding with the Leu165 backbone. Given that this location is mostly solvent exposed, much like the P1 morpholine position, we anticipate this will be a tolerated change.

P3 Heterocyclic and Basic Vectors

Work done previously in the Carruthers lab determined the peptide substrate preference for *TgCPL* and *TgCPB*.¹²¹ The proteolysis of small tripeptides was used to elucidate the P2/P3 preferential residues in terms of catalytic turnover.¹⁶⁴ In P2 they found that smaller lipophilic sidechains were preferred, namely Leucine, Valine, and Tryptophan. This data is in agreement with the SAR we have found for our *TgCPL* inhibitors. In P3, the preferential substrates tended to be polar and even charged. Examples include Aspartate, Glutamate, Arginine, Glutamine. A heterocyclic SAR campaign and a fluorine scan of P3 in *HsCPL* revealed significant variability in the inhibitor binding based on the ring system electronics.^{158, 160} Presumably, this is due to a heteroarene π -stack with the amide backbone of Gly64 in the S3 pocket. A similar backbone structure is seen in *TgCPL* and given that the optimal S3 vector we have found is a 4-fluorophenyl, it is reasonable to believe that *TgCPL* will also exhibit a varying preference for certain heteroaromatic vectors that modulate this interaction. Once the appropriate

conformational restriction is found, the synthesis of new analogs can be approached through several potential routes analogous to those of the triazine nitriles shown in Chapter 4.

5.3 Modified Heteroaryl Cores and Intramolecular Stabilization of Iminium Transition

State

It has been incredibly difficult to find anything that is selective for *TgCPL* over *HsCPL*. This could be due to several possibilities. While very similar in topology, *HsCPL* has slightly larger S2 and S3 pockets. This feature seems to impart a higher tolerance for the P2/P3 residues, as compared to the parasite isoform. Additionally, the triazine nitrile warhead is one of the more reactive and potent of the known aryl-nitriles. The triazine nitrile warhead may be too reactive to reliably illuminate the motifs necessary to achieve selectivity in favor of *TgCPL*. Highly reactive nitriles are less dependent on the proximity effects and are able to react with the cysteine even if the P2,P3 vectors are not tightly bound. A slightly less-reactive nitrile would require an initial pre-binding event in order to properly orient the warhead in close proximity to the catalytic cysteine. The greater dependence on the free energy contribution of the initial non-covalent binding event results in a reduced dependence on the high reactivity of the nitrile warhead, and therefore serves to better differentiate the SAR due to P2/P3 binding. Furthermore, the potential off-target effects of a highly reactive nitrile could lead to unwanted off-target effects in later development. Nevertheless, the electrophilic warhead is necessary for *TgCPL* inhibition, as its removal results in a drastic loss of potency. As an alternative, we may need to replace the strongly electron withdrawing triazine with some less reactive, heterocyclic cores. To date, we have only tested a small number of these (**Figure 43**) and found that despite the identical P2-P3 vectors, the electronics of the warhead and core significantly impact potency.

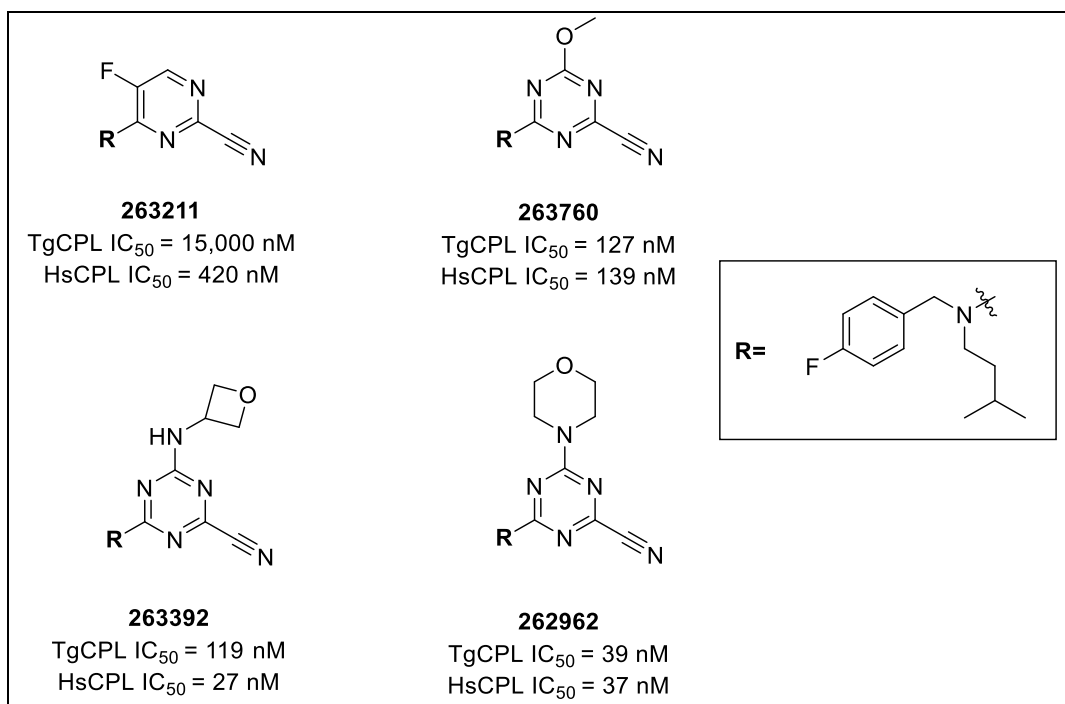
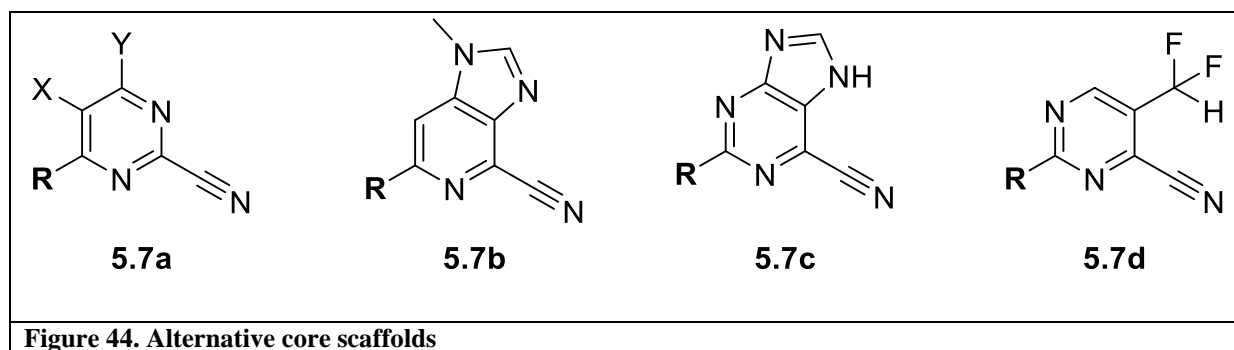


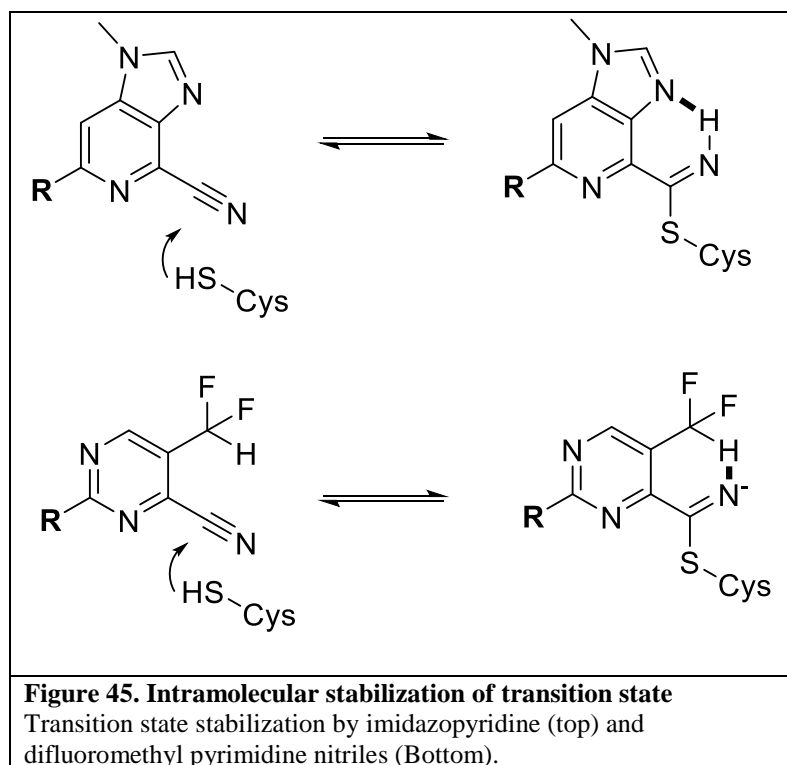
Figure 43. Synthesized alternative cores and TgCPL inhibition

These modifications slightly reduce potency (e.g. **263392** and **263760**) as compared to the lead **262962**. The modulated reactivity may enable the development of a more sensitive SAR model for achieving selectivity between isoforms, as explained above. In the case of **263211**, the values for potency are likely convoluted due to the very poor solubility of the compound when the morpholine group was removed. If the conformational restriction mentioned above enables the rearrangement of the solubilizing group to the benzylic position, the more lipophilic core can be revisited to more accurately assess the electronic effects on potency and selectivity.

Throughout the literature, several similar cores have been employed. **Figure 44** below shows a few proposed examples of heterocyclic-nitrile cores, derived from known human and related parasitic cathepsin inhibitors in literature, that may improve our selectivity profile and PK properties.



Several variations of the pyrimidine nitrile cores (**5.7a**) have been assessed versus HsCPL and rhodesain, revealing significant variation in potency and selectivity. Replacement of the X groups with either Br, Cl, F, and CF₃ can tune the electron withdrawing characteristics of the ring system. Electron donating groups (NH-R or O-R) in the Y-position, similarly modulate the warhead reactivity and provide improvements to solubility. The imizadopyridine nitrile (**5.7b**) and the purine nitrile (**5.7c**) cores have been preceded in literature as potent and selective inhibitors of various human cathepsins, *T. brucei* Cathepsin B, and *P. falciparum* rhodesain.^{159, 165-166} It is postulated that while the electronics of these heterocycles will reduce the initial reactivity of the nitrile warhead when compared to the triazine nitrile, the transition state is stabilized via an intramolecular hydrogen bond between the heterocyclic N(3) and the thioimide NH, leading to improved potency and selectivity (**Figure 45**).¹⁶⁷



While the imidazopyridine and purine cores could improve potency and selectivity, this comes at the cost of increased TPSA, molecular weight and hydrogen bonding. These features make them less desirable for a CNS therapeutic. The (difluoromethyl)pyrimidine nitrile core **5.7d** is a proposed unique core that could preemptively avoid these concerns. There is precedent in literature that the di-fluoro methyl can serve as a ‘masked’ hydrogen bond donor.¹⁶⁸⁻¹⁶⁹ This and related fluorine-induced hydrogen bond donating motifs have been successfully employed in the development of several clinical candidates. This strategy would provide reduced molecular volume and TPSA, while ‘masking’ the hydrogen bond donor, thus favoring CNS penetrance. Importantly, the difluoromethyl is still capable of forming the intramolecular hydrogen bond with the thioimidate transition state, which may provide the same type of selectivity and potency imparted by the imidazopyridines, without compromising our CNS profile.

5.4 Crystallography

One of the greatest challenges in the development of a *TgCPL* inhibitor has been obtaining a *TgCPL* crystal structure with a small molecule bound. To date, the only crystal structure resolved is of mature *TgCPL* with its cleaved propeptide bound in the active site. To date, all our structure-based design has been done generating a model via the superposition of *TgCPL* with *HsCPL* crystal structures bound to various inhibitors. The homology between isoform active site is high and provides a reasonable model to begin the development of small molecule inhibitors; however a true co-crystal of *TgCPL* with inhibitor is paramount in understanding the subtle differences that could lead to isoform selectivity. Given the shallow nature of the enzyme active site and conformational flexibility of the surface residues, it is unclear if our current model is providing an accurate representation. Acquiring a co-crystal of a small molecule inhibitor bound in the enzyme active site would significantly aid further structure-based design. Additionally, the presence of the propeptide tail in the enzymatic assay may influence the inhibitory activity of our compounds. It is unclear what level of effect this might have on the physiological relevance of the biochemical results.

5.4.1 Advances Toward *TgCPL* Co-Crystal

A significant number of approaches have been tried to obtain a crystal structure of *TgCPL* with a small molecule inhibitor bound, but several factors have impeded this goal. Primarily, the obstruction of the catalytic site by the enzyme's pro-peptide tail has been the greatest obstacle. *TgCPL* is an auto-maturase that catalyzes the cleavage of its pro-peptide tail in order to become catalytically active. Once cleaved, the pro-peptide tail is able to re-associate

with the enzyme via strong hydrophobic interactions. This complex of mature enzyme and peptide tail tends to undergo crystallization (e.g. PDB: 3F75) more favorably than that of any enzyme inhibitor complex. Any attempts to form enzyme-ligand co-crystals, even with high affinity irreversible inhibitor LHVS, to date have failed due to the presence of the pro-peptide. Several attempts to optimize conditions for the maturation and inhibition of *TgCPL*, followed by the removal of the pro-peptide tail have been undertaken. While some significant advances were made, overall the attempts have to date been unsuccessful for a variety of reasons detailed below.

TgCPL undergoes auto-maturation when introduced to an acidic environment (pH ~5.5). However, if the maturation is done at higher protein concentration (i.e. >1 mg/mL) the activated enzyme appears to digest itself. We found this can be avoided by maturing the enzyme in more dilute conditions (**Figure 46**) at 37°C for 1-3 h, followed by inhibition of the matured protein with a small molecule inhibitor such as LHVS. Once matured and inhibited, various strategies to separate the cleaved pro-peptide tail from the enzyme were attempted. Ion exchange chromatography, Ni columns, size exclusion, gel filtration, pH adjustment, buffer exchange, dialysis, chaotropic agents (urea), lipophilicity chromatography, and attempts to digest the pro-peptide *in situ* with pepsin have all been unsuccessful in removing the tail completely. The pro-peptide appears to have such a high affinity for the mature cathepsin that overcoming the interactions by conventional separation methods is inadequate.

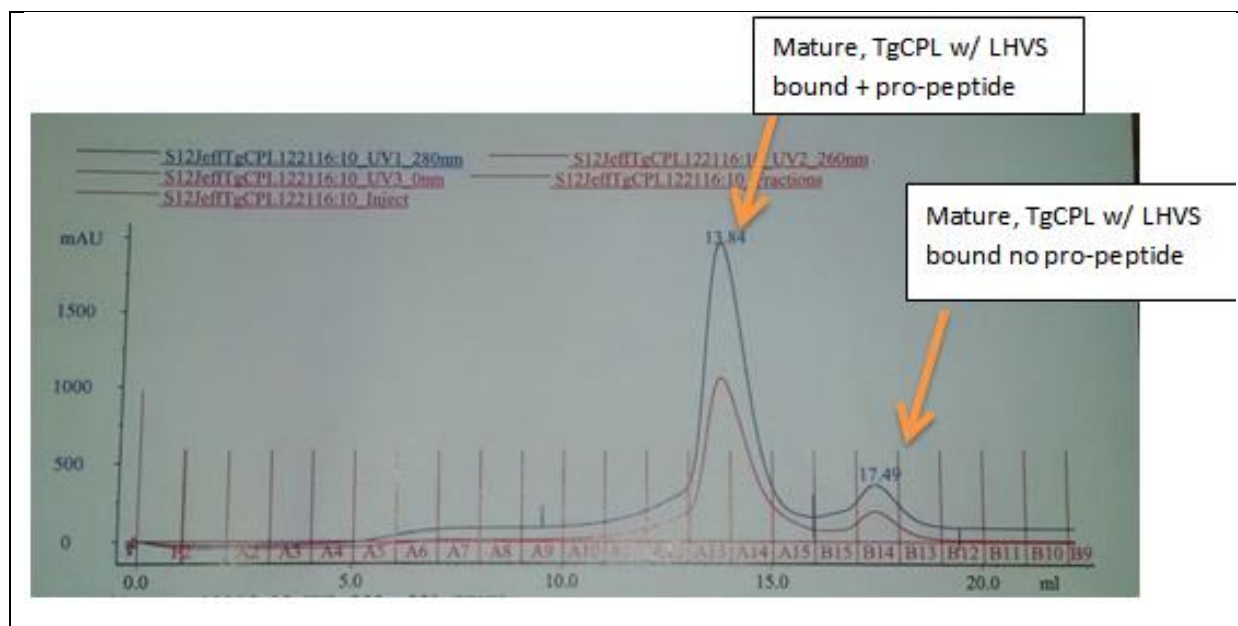


Figure 46. Example purification of mature *TgCPL*

10 mg of apo-*TgCPL* was diluted in activation buffer to 0.1mg/mL and incubated for 2-3h at 37°C. Protein was treated with 5 eq LHVS and incubated overnight. The protein was subjected to a Ni column, followed by purification via FPLC S-12 column. Activation Buffer: pH=5.5; NaAc= 60mM; NaCl= 900mM; DTT= 5mM; EDTA= 2.0mM; *TgCPL* = 0.1mg/mL

In the most successful attempt to date, only a fraction of the sample was successfully purified away from the pro-peptide. Conditions were optimized to fully mature the enzyme in a manner that minimizes auto-digestion. Beginning with 10 mg of mature *TgCPL*, we obtained only 200 μ L at a final concentration of \sim 0.5 mg/mL of the mature *TgCPL* which is inadequate for any crystallization attempts. This sample was the only attempt that provided purified *TgCPL* free of its propeptide tail. Through efforts by the Center for Structural Biology at the University of Michigan, we are now able to produce the apo-*TgCPL* with good yields (>100 mg/L culture versus original prep yields of \sim 1 mg/mL culture). We hoped that we could simply upscale the preparation and do several FPLC purifications to afford enough for crystallization. Unfortunately, this procedure did not translate to scale.

5.5.2 Current Efforts in the Crystallization of *TgCPL*

So far, we have optimized the expression and maturation of apo-*TgCPL*. To avoid auto-proteolysis, *TgCPL* was inhibited with LHVS. This is enabling current studies toward the removal of the pro-peptide tail. Efforts are being made using combinations of buffer exchange, denaturation and refolding, and lipophilicity columns to disrupt this tight binding interaction. If these prove unsuccessful, we envision mutagenesis of a few residues in the pro-peptide tail (primarily those that interface with the lipophilic pocket seen in the crystal structure PDB-3F75) may reduce the enzyme-tail affinity. This disruption of the lipophilic interaction could allow for further separation via size exclusion or ion exchange chromatography. Once a separation method is optimized, LHVS (irreversibly covalent) can be replaced with S-Methyl methanethiosulfonate (MMTS) as the inhibitor to block auto-proteolysis. This will allow for facile reductive re-activation of the catalytic cysteine post-purification in the presence of reversible inhibitors such as the dipeptide and triazine nitriles under crystallization conditions.

5.7 Conclusions

Throughout this project, significant advances have been made in developing small molecule inhibitors of *TgCPL*. We have elucidated key SAR for the inhibition of *TgCPL*, developed potent and CNS penetrant inhibitors across three chemotypes, and demonstrated efficacy against bradyzoite cysts *in vitro*. More work needs to be done to optimize selectivity for the *T. gondii* isoform and to improve upon the PK profile to advance to *in vivo* proof-of-concept

studies. Given the rotational flexibility of the triazine nitrile scaffold, we envision conformational restriction, either through ring closure or steric restriction, will improve our ability to exploit key divergent features between the parasite and human isoforms. We may be able to also use the necessary solubilizing group toward this end, enabling further modification of the triazine core. The triazine nitrile warhead may be too electrophilic (cysteine reactive), overwhelming subtle differences in on-rate between the isoforms that might be necessary for selectivity and increasing the potential for off-target reactivity. Modifications of this core to tune the electronics of the nitrile warhead could be used to achieve parasite cathepsin selectivity. Additionally, potency and CNS profile could be enhanced via the intramolecular stabilization of the thioimidate transition state. Finally, in order to fully enable a structure-based approach, efforts are being made to obtain a *TgCPL* co-crystal structure with a small molecule inhibitor. Success in these aims will provide improved selectivity, potency, and pharmacokinetic profile for these *TgCPL* inhibitors. These second-generation inhibitors can be advanced toward *in vivo* studies, providing proof-of-concept that *TgCPL* inhibition is a viable approach for treating the latent phase of toxoplasmosis.

Bibliography

1. Seeber, F.; Steinfelder, S., Recent advances in understanding apicomplexan parasites. *F1000Res* **2016**, *5*.
2. Ferguson, D. J., Toxoplasma gondii: 1908-2008, homage to Nicolle, Manceaux and Splendore. *Mem Inst Oswaldo Cruz* **2009**, *104* (2), 133-48.
3. Morrissette, N. S.; Ajioka, J. W., The early years of Toxoplasma research: What's past is prologue. *Int J Parasitol* **2009**, *39* (8), 865-9.
4. Innes, E. A., A brief history and overview of Toxoplasma gondii. *Zoonoses Public Health* **2010**, *57* (1), 1-7.
5. Binazzi, M., Historical aspects of cutaneous toxoplasmosis. *Int J Dermatol* **1986**, *25* (6), 401-4.
6. Cox, F. E., History of human parasitology. *Clin Microbiol Rev* **2002**, *15* (4), 595-612.
7. Darling, S. T., Experimental Sarcosporidiosis in the Guinea-Pig and Its Relation to a Case of Sarcosporidiosis in Man. *J Exp Med* **1910**, *12* (1), 19-28.
8. Chaves-Carballo, E., Samuel T. Darling and human sarcosporidiosis or toxoplasmosis in Panama. *JAMA* **1970**, *211* (10), 1687-9.
9. Nye, E. R., Alphonse Laveran (1845-1922): discoverer of the malarial parasite and Nobel laureate, 1907. *J Med Biogr* **2002**, *10* (2), 81-7.
10. Dubey, J. P., History of the discovery of the life cycle of Toxoplasma gondii. *Int J Parasitol* **2009**, *39* (8), 877-82.
11. Dubey, J. P., The history of Toxoplasma gondii--the first 100 years. *J Eukaryot Microbiol* **2008**, *55* (6), 467-75.
12. Weiss, L. M.; Dubey, J. P., Toxoplasmosis: A history of clinical observations. *Int J Parasitol* **2009**, *39* (8), 895-901.
13. Dubey, J. P.; Miller, N. L.; Frenkel, J. K., Toxoplasma gondii life cycle in cats. *J Am Vet Med Assoc* **1970**, *157* (11), 1767-70.
14. Frenkel, J. K.; Dubey, J. P.; Miller, N. L., Toxoplasma gondii in cats: fecal stages identified as coccidian oocysts. *Science* **1970**, *167* (3919), 893-6.
15. Hutchison, W. M.; Dunachie, J. F.; Siim, J. C.; Work, K., Life cycle of toxoplasma gondii. *Br Med J* **1969**, *4* (5686), 806.
16. Hutchison, W. M.; Dunachie, J. F.; Work, K.; Siim, J. C., The life cycle of the coccidian parasite, Toxoplasma gondii, in the domestic cat. *Trans R Soc Trop Med Hyg* **1971**, *65* (3), 380-99.
17. Bennett, J. E.; Dolin, R.; Blaser, M. J., *Mandell, Douglas, and Bennett's infectious disease essentials*. Elsevier: Philadelphia, PA, 2017; p pages cm.
18. McLeod, R.; Mack, D.; Brown, C., Toxoplasma gondii--new advances in cellular and molecular biology. *Exp Parasitol* **1991**, *72* (1), 109-21.
19. Beck, H. P.; Blake, D.; Darde, M. L.; Felger, I.; Pedraza-Diaz, S.; Regidor-Cerrillo, J.; Gomez-Bautista, M.; Ortega-Mora, L. M.; Putignani, L.; Shiels, B.; Tait, A.; Weir, W., Molecular

- approaches to diversity of populations of apicomplexan parasites. *Int J Parasitol* **2009**, *39* (2), 175-89.
20. Duszynski, D. W.; Couch, L., Biology and Identification of the Coccidia (Apicomplexa) of Rabbits of the World. *Biology and Identification of the Coccidia (Apicomplexa) of Rabbits of the World* **2013**, 1-340.
 21. Bogyo, M.; Ward, G., Toxoplasma gondii Chemical Biology. *Toxoplasma Gondii: The Model Apicomplexan - Perspectives and Methods, 2nd Edition* **2014**, 707-730.
 22. Weiss, L. M.; Kim, K., Toxoplasma gondii The Model Apicomplexan - Perspectives and Methods Preface to the Second Edition. *Toxoplasma Gondii: The Model Apicomplexan - Perspectives and Methods, 2nd Edition* **2014**, Xvii-Xvii.
 23. Hunter, C. A.; Sibley, L. D., Modulation of innate immunity by Toxoplasma gondii virulence effectors. *Nat Rev Microbiol* **2012**, *10* (11), 766-78.
 24. Dubey, J. P.; Miller, N. L.; Frenkel, J. K., The Toxoplasma gondii oocyst from cat feces. *J Exp Med* **1970**, *132* (4), 636-62.
 25. Ferguson, D. J.; Hutchison, W. M.; Siim, J. C., The ultrastructural development of the macrogamete and formation of the oocyst wall of Toxoplasma gondii. *Acta Pathol Microbiol Scand B* **1975**, *83* (5), 491-505.
 26. Lelu, M.; Villena, I.; Darde, M. L.; Aubert, D.; Geers, R.; Dupuis, E.; Marnef, F.; Poulle, M. L.; Gotteland, C.; Dumetre, A.; Gilot-Fromont, E., Quantitative estimation of the viability of Toxoplasma gondii oocysts in soil. *Appl Environ Microbiol* **2012**, *78* (15), 5127-32.
 27. Dubey, J. P.; Ferreira, L. R.; Martins, J.; Jones, J. L., Sporulation and survival of Toxoplasma gondii oocysts in different types of commercial cat litter. *J Parasitol* **2011**, *97* (5), 751-4.
 28. Di Cristina, M.; Marocco, D.; Galizi, R.; Proietti, C.; Spaccapelo, R.; Crisanti, A., Temporal and spatial distribution of Toxoplasma gondii differentiation into Bradyzoites and tissue cyst formation in vivo. *Infect Immun* **2008**, *76* (8), 3491-501.
 29. Dubey, J. P.; Lindsay, D. S.; Speer, C. A., Structures of Toxoplasma gondii tachyzoites, bradyzoites, and sporozoites and biology and development of tissue cysts. *Clin Microbiol Rev* **1998**, *11* (2), 267-99.
 30. Markell, E. K.; John, D. T.; Krotoski, W. A., *Markell and Voge's medical parasitology*. 8th ed.; Saunders: Philadelphia, 1999; p viii, 501 p.
 31. Robert-Gangneux, F.; Darde, M. L., Epidemiology of and diagnostic strategies for toxoplasmosis. *Clin Microbiol Rev* **2012**, *25* (2), 264-96.
 32. Jones, J. L.; Kruszon-Moran, D.; Elder, S.; Rivera, H. N.; Press, C.; Montoya, J. G.; McQuillan, G. M., Toxoplasma gondii Infection in the United States, 2011-2014. *Am J Trop Med Hyg* **2018**, *98* (2), 551-557.
 33. Dubey, J. P.; Jones, J. L., Toxoplasma gondii infection in humans and animals in the United States. *Int J Parasitol* **2008**, *38* (11), 1257-78.
 34. Flegr, J.; Prandota, J.; Sovickova, M.; Israili, Z. H., Toxoplasmosis - A Global Threat. Correlation of Latent Toxoplasmosis with Specific Disease Burden in a Set of 88 Countries. *Plos One* **2014**, *9* (3).
 35. Hoffmann, S.; Batz, M. B.; Morris, J. G., Jr., Annual cost of illness and quality-adjusted life year losses in the United States due to 14 foodborne pathogens. *J Food Prot* **2012**, *75* (7), 1292-302.
 36. Scallan, E.; Griffin, P. M.; Angulo, F. J.; Tauxe, R. V.; Hoekstra, R. M., Foodborne illness acquired in the United States--unspecified agents. *Emerg Infect Dis* **2011**, *17* (1), 16-22.

37. Basavaraju, A., Toxoplasmosis in HIV infection: An overview. *Trop Parasitol* **2016**, *6* (2), 129-135.
38. Montoya, J. G.; Remington, J. S., Toxoplasmic chorioretinitis in the setting of acute acquired toxoplasmosis. *Clin Infect Dis* **1996**, *23* (2), 277-82.
39. Jones, J. L.; Kruszon-Moran, D.; Rivera, H. N.; Price, C.; Wilkins, P. P., Toxoplasma gondii seroprevalence in the United States 2009-2010 and comparison with the past two decades. *Am J Trop Med Hyg* **2014**, *90* (6), 1135-9.
40. Innes, E. A.; Bartley, P. M.; Maley, S.; Katzer, F.; Buxton, D., Veterinary vaccines against Toxoplasma gondii. *Mem Inst Oswaldo Cruz* **2009**, *104* (2), 246-51.
41. Pappas, G.; Roussos, N.; Falagas, M. E., Toxoplasmosis snapshots: global status of Toxoplasma gondii seroprevalence and implications for pregnancy and congenital toxoplasmosis. *Int J Parasitol* **2009**, *39* (12), 1385-94.
42. Glasner, P. D.; Silveira, C.; Kruszon-Moran, D.; Martins, M. C.; Burnier Junior, M.; Silveira, S.; Camargo, M. E.; Nussenblatt, R. B.; Kaslow, R. A.; Belfort Junior, R., An unusually high prevalence of ocular toxoplasmosis in southern Brazil. *Am J Ophthalmol* **1992**, *114* (2), 136-44.
43. Mortensen, P. B.; Norgaard-Pedersen, B.; Waltoft, B. L.; Sorensen, T. L.; Hougaard, D.; Yolken, R. H., Early infections of Toxoplasma gondii and the later development of schizophrenia. *Schizophrenia Bull* **2007**, *33* (3), 741-744.
44. Suvisaari, J.; Torniainen-Holm, M.; Lindgren, M.; Harkanen, T.; Yolken, R. H., Toxoplasma gondii infection and common mental disorders in the Finnish general population. *J Affect Disorders* **2017**, *223*, 20-25.
45. Flegr, J., Effects of Toxoplasma on human behavior. *Schizophrenia Bull* **2007**, *33* (3), 757-760.
46. Del Grande, C.; Galli, L.; Schiavi, E.; Dell'Osso, L.; Bruschi, F., Is Toxoplasma gondii a Trigger of Bipolar Disorder? *Pathogens* **2017**, *6* (1).
47. Afonso, C.; Paixao, V. B.; Costa, R. M., Chronic Toxoplasma infection modifies the structure and the risk of host behavior. *PLoS One* **2012**, *7* (3), e32489.
48. Dass, S. A.; Vasudevan, A.; Dutta, D.; Soh, L. J.; Sapolsky, R. M.; Vyas, A., Protozoan parasite Toxoplasma gondii manipulates mate choice in rats by enhancing attractiveness of males. *PLoS One* **2011**, *6* (11), e27229.
49. Pearce, B. D.; Kruszon-Moran, D.; Jones, J. L., The Relationship Between Toxoplasma Gondii Infection and Mood Disorders in the Third National Health and Nutrition Survey. *Biol Psychiat* **2012**, *72* (4), 290-295.
50. Nascimento, F. S.; Dantas, C. D.; Netto, M. P.; Mella, L. F. B.; Suzuki, L. A.; Banzato, C. E. M.; Rossi, C. L., Prevalence of antibodies to Toxoplasma gondii in patients with schizophrenia and mood disorders. *Schizophrenia Research* **2012**, *142* (1-3), 244-245.
51. Fuglewicz, A. J.; Piotrowski, P.; Stodolak, A., Relationship between toxoplasmosis and schizophrenia: A review. *Adv Clin Exp Med* **2017**, *26* (6), 1031-1036.
52. Holub, D.; Flegr, J.; Dragomirecka, E.; Rodriguez, M.; Preiss, M.; Novak, T.; Cermak, J.; Horacek, J.; Kodym, P.; Libiger, J.; Hoschl, C.; Motlova, L. B., Differences in onset of disease and severity of psychopathology between toxoplasmosis-related and toxoplasmosis-unrelated schizophrenia. *Acta Psychiatr Scand* **2013**, *127* (3), 227-38.
53. Celik, T.; Gokcen, C.; Aytas, O.; Ozcelik, A.; Celik, M.; Coban, N., The prevalence of anti-Toxoplasma gondii antibodies in stutterers is higher than in the control group. *Folia Parasit* **2015**, *62*.

54. Torrey, E. F.; Bartko, J. J.; Lun, Z. R.; Yolken, R. H., Antibodies to *Toxoplasma gondii* in patients with schizophrenia: A meta-analysis. *Schizophrenia Bull* **2007**, *33* (3), 729-736.
55. Bo Mortensen, P.; Norgaard-Pedersen, B.; Waltoft, B. L.; Sorensen, T. L.; Hougaard, D.; Torrey, E. F.; Yolken, R. H., *Toxoplasma gondii* as a risk factor for early-onset schizophrenia: Analysis of filter paper blood samples obtained at birth. *Biol Psychiat* **2007**, *61* (5), 688-693.
56. de Boer, J.; Wulffraat, N.; Rothova, A., Visual loss in uveitis of childhood. *Brit J Ophthalmol* **2003**, *87* (7), 879-884.
57. Carme, B.; Bissuel, F.; Ajzenberg, D.; Bouyne, R.; Aznar, C.; Demar, M.; Bichat, S.; Louvel, D.; Bourbigot, A. M.; Peneau, C.; Neron, P.; Darde, M. L., Severe acquired toxoplasmosis in immunocompetent adult patients in French Guiana. *Journal of Clinical Microbiology* **2002**, *40* (11), 4037-4044.
58. Xiao, J.; Yolken, R. H., Strain hypothesis of *Toxoplasma gondii* infection on the outcome of human diseases. *Acta Physiol* **2015**, *213* (4), 828-845.
59. Ramachandran, R.; Radhan, P.; Anand, R.; Subramanian, I.; Santosham, R.; Sai, V., CNS toxoplasmosis in an immunocompetent individual. *Radiol Case Rep* **2014**, *9* (1), e00031.
60. Gontijo da Silva, M.; Clare Vinaud, M.; de Castro, A. M., Prevalence of toxoplasmosis in pregnant women and vertical transmission of *Toxoplasma gondii* in patients from basic units of health from Gurupi, Tocantins, Brazil, from 2012 to 2014. *PLoS One* **2015**, *10* (11), e0141700.
61. Hampton, M. M., Congenital Toxoplasmosis: A Review. *Neonatal Netw* **2015**, *34* (5), 274-8.
62. Buxton, D., Ovine toxoplasmosis: a review. *J R Soc Med* **1990**, *83* (8), 509-11.
63. Porter, S. B.; Sande, M. A., Toxoplasmosis of the central nervous system in the acquired immunodeficiency syndrome. *N Engl J Med* **1992**, *327* (23), 1643-8.
64. Vidal, J. E.; Hernandez, A. V.; De Oliveira, A. C. P.; Dauar, R. F.; Barbosa, S. P.; Focaccia, R., Cerebral toxoplasmosis in HIV-positive patients in Brazil: Clinical features and predictors of treatment response in the HAART era. *Aids Patient Care St* **2005**, *19* (10), 626-634.
65. Antinori, A.; Ammassari, A.; DeLuca, A.; Cingolani, A.; Murri, R.; Scoppettuolo, G.; Fortini, M.; Tartaglione, T.; Larooca, L. M.; Zannoni, G.; Cattani, P.; Grillo, R.; Roselli, R.; Iacoangeli, M.; Scerrati, M.; Ortona, L., Diagnosis of AIDS-related focal brain lesions: A decision-making analysis based on clinical and neuroradiologic characteristics combined with polymerase chain reaction assays in CSF. *Neurology* **1997**, *48* (3), 687-694.
66. Cingolani, A.; DeLuca, A.; Ammassari, A.; Murri, R.; Linzalone, A.; Grillo, R.; Antinori, A., PCR detection of *Toxoplasma gondii* DNA in CSF for the differential diagnosis of AIDS-related focal brain lesions. *Journal of Medical Microbiology* **1996**, *45* (6), 472-476.
67. Antinori, A.; Larussa, D.; Cingolani, A.; Lorenzini, P.; Bossolasco, S.; Finazzi, M. G.; Bongiovanni, M.; Guaraldi, G.; Grisetti, S.; Vigo, B.; Gigli, B.; Mariano, A.; Dalle Nogare, E. R.; De Marco, M.; Moretti, F.; Corsi, P.; Abrescia, N.; Rellecati, P.; Castagna, A.; Mussini, C.; Ammassari, A.; Cinque, P.; Monforte, A. D.; Ne, I. R. I., Prevalence, associated factors, and prognostic determinants of AIDS-related toxoplasmic encephalitis in the era of advanced highly active antiretroviral therapy. *Clinical Infectious Diseases* **2004**, *39* (11), 1681-1691.
68. Derouin, F.; Pelloux, H.; Parasitology, E. S. G. o. C., Prevention of toxoplasmosis in transplant patients. *Clin Microbiol Infect* **2008**, *14* (12), 1089-101.

69. Villard, O.; Cimon, B.; L'Ollivier, C.; Fricker-Hidalgo, H.; Godineau, N.; Houze, S.; Paris, L.; Pelloux, H.; Villena, I.; Candolfi, E., Serological diagnosis of *Toxoplasma gondii* infection: Recommendations from the French National Reference Center for Toxoplasmosis. *Diagn Microbiol Infect Dis* **2016**, *84* (1), 22-33.
70. Rostami, A.; Karanis, P.; Fallahi, S., Advances in serological, imaging techniques and molecular diagnosis of *Toxoplasma gondii* infection. *Infection* **2018**, *46* (3), 303-315.
71. Hill, D.; Dubey, J. P., *Toxoplasma gondii*: transmission, diagnosis and prevention. *Clin Microbiol Infect* **2002**, *8* (10), 634-40.
72. Press, C.; Montoya, J. G.; Remington, J. S., Use of a single serum sample for diagnosis of acute toxoplasmosis in pregnant women and other adults. *Journal of Clinical Microbiology* **2005**, *43* (7), 3481-3483.
73. Dediccoat, M.; Livesley, N., Management of toxoplasmic encephalitis in HIV-infected adults--a review. *S Afr Med J* **2008**, *98* (1), 31-2.
74. Tsai, H. C.; Lee, S. S.; Lin, H. H.; Lin, W. R.; Chen, Y. S.; Huang, C. K.; Liu, Y. C.; Chen, E. R., Treatment of *Toxoplasma* brain abscess with clindamycin and sulfadiazine in an AIDS patient with concurrent atypical *Pneumocystis carinii* pneumonia. *J Formos Med Assoc* **2002**, *101* (9), 646-9.
75. Greene, C. E.; Cook, J. R., Jr.; Mahaffey, E. A., Clindamycin for treatment of *Toxoplasma* polymyositis in a dog. *J Am Vet Med Assoc* **1985**, *187* (6), 631-4.
76. Role of clindamycin in the treatment of toxoplasmosis and pneumocystosis in patients with AIDS. *Eur J Clin Microbiol Infect Dis* **1991**, *10* (3), 175-213.
77. Goldsmid, J. M., Toxoplasmosis and clindamycin. *S Afr Med J* **1980**, *57* (2), 37.
78. Levine, E. M., Risk factors for *Toxoplasma gondii* infection in mothers of infants with congenital toxoplasmosis: implications for prenatal management and screening. *Am J Obstet Gynecol* **2006**, *194* (2), 589; author reply 590.
79. Alves, C. F.; Vitor, R. W., Efficacy of atovaquone and sulfadiazine in the treatment of mice infected with *Toxoplasma gondii* strains isolated in Brazil. *Parasite* **2005**, *12* (2), 171-7.
80. Djurkovic-Djakovic, O.; Nikolic, A.; Bobic, B.; Klun, I.; Aleksic, A., Stage conversion of *Toxoplasma gondii* RH parasites in mice by treatment with atovaquone and pyrrolidine dithiocarbamate. *Microbes Infect* **2005**, *7* (1), 49-54.
81. Pearson, P. A.; Piracha, A. R.; Sen, H. A.; Jaffe, G. J., Atovaquone for the treatment of toxoplasma retinochoroiditis in immunocompetent patients. *Ophthalmology* **1999**, *106* (1), 148-53.
82. Ferguson, D. J.; Huskinson-Mark, J.; Araujo, F. G.; Remington, J. S., An ultrastructural study of the effect of treatment with atovaquone in brains of mice chronically infected with the ME49 strain of *Toxoplasma gondii*. *Int J Exp Pathol* **1994**, *75* (2), 111-6.
83. Gormley, P. D.; Pavesio, C. E.; Minnasian, D.; Lightman, S., Effects of drug therapy on *Toxoplasma* cysts in an animal model of acute and chronic disease. *Invest Ophthalmol Vis Sci* **1998**, *39* (7), 1171-5.
84. Gratzl, R.; Sodeck, G.; Platzer, P.; Jager, W.; Graf, J.; Pollak, A.; Thalhammer, T., Treatment of toxoplasmosis in pregnancy: concentrations of spiramycin and neospiramycin in maternal serum and amniotic fluid. *Eur J Clin Microbiol Infect Dis* **2002**, *21* (1), 12-6.
85. Valentini, P.; Buonsenso, D.; Barone, G.; Serranti, D.; Calzedda, R.; Ceccarelli, M.; Speziale, D.; Ricci, R.; Masini, L., Spiramycin/cotrimoxazole versus

pyrimethamine/sulfonamide and spiramycin alone for the treatment of toxoplasmosis in pregnancy. *J Perinatol* **2015**, *35* (2), 90-4.

86. Merzlova, N. B.; Serova, I. A.; Yagodina, A. Y., [Relevant Principles in the Diagnosis, Treatment, and Prevention of Toxoplasmosis during Pregnancy]. *Med Parazitol (Mosk)* **2015**, (3), 13-7.

87. Doggett, J. S.; Nilsen, A.; Forquer, I.; Wegmann, K. W.; Jones-Brando, L.; Yolken, R. H.; Bordon, C.; Charman, S. A.; Katneni, K.; Schultz, T.; Burrows, J. N.; Hinrichs, D. J.; Meunier, B.; Carruthers, V. B.; Riscoe, M. K., Endochin-like quinolones are highly efficacious against acute and latent experimental toxoplasmosis. *Proc Natl Acad Sci U S A* **2012**, *109* (39), 15936-41.

88. Carruthers, V. B.; Suzuki, Y., Effects of *Toxoplasma gondii* infection on the brain. *Schizophr Bull* **2007**, *33* (3), 745-51.

89. Schultz, T. L.; Hencken, C. P.; Woodard, L. E.; Posner, G. H.; Yolken, R. H.; Jones-Brando, L.; Carruthers, V. B., A thiazole derivative of artemisinin moderately reduces *Toxoplasma gondii* cyst burden in infected mice. *J Parasitol* **2014**, *100* (4), 516-21.

90. Lunghi, M.; Galizi, R.; Magini, A.; Carruthers, V. B.; Di Cristina, M., Expression of the glycolytic enzymes enolase and lactate dehydrogenase during the early phase of *Toxoplasma* differentiation is regulated by an intron retention mechanism. *Mol Microbiol* **2015**, *96* (6), 1159-75.

91. Tomasik, J.; Schultz, T. L.; Kluge, W.; Yolken, R. H.; Bahn, S.; Carruthers, V. B., Shared Immune and Repair Markers During Experimental *Toxoplasma* Chronic Brain Infection and Schizophrenia. *Schizophr Bull* **2016**, *42* (2), 386-95.

92. Fox, B. A.; Falla, A.; Rommereim, L. M.; Tomita, T.; Gigley, J. P.; Mercier, C.; Cesbron-Delauw, M. F.; Weiss, L. M.; Bzik, D. J., Type II *Toxoplasma gondii* KU80 knockout strains enable functional analysis of genes required for cyst development and latent infection. *Eukaryot Cell* **2011**, *10* (9), 1193-206.

93. Miranda, K.; Pace, D. A.; Cintron, R.; Rodrigues, J. C.; Fang, J.; Smith, A.; Rohloff, P.; Coelho, E.; de Haas, F.; de Souza, W.; Coppens, I.; Sibley, L. D.; Moreno, S. N., Characterization of a novel organelle in *Toxoplasma gondii* with similar composition and function to the plant vacuole. *Mol Microbiol* **2010**, *76* (6), 1358-75.

94. Dou, Z.; McGovern, O. L.; Di Cristina, M.; Carruthers, V. B., *Toxoplasma gondii* ingests and digests host cytosolic proteins. *MBio* **2014**, *5* (4), e01188-14.

95. Coppens, I., *Toxoplasma*, or the discovery of a heterophage. *Trends Parasitol* **2014**, *30* (10), 467-9.

96. Di Cristina, M.; Dou, Z.; Lunghi, M.; Kannan, G.; Huynh, M. H.; McGovern, O. L.; Schultz, T. L.; Schultz, A. J.; Miller, A. J.; Hayes, B. M.; van der Linden, W.; Emiliani, C.; Bogyo, M.; Besteiro, S.; Coppens, I.; Carruthers, V. B., *Toxoplasma* depends on lysosomal consumption of autophagosomes for persistent infection. *Nat Microbiol* **2017**, *2*, 17096.

97. Dou, Z.; Coppens, I.; Carruthers, V. B., Non-canonical maturation of two papain-family proteases in *Toxoplasma gondii*. *J Biol Chem* **2013**, *288* (5), 3523-34.

98. Que, X.; Engel, J. C.; Ferguson, D.; Wunderlich, A.; Tomavo, S.; Reed, S. L., Cathepsin Cs are key for the intracellular survival of the protozoan parasite, *Toxoplasma gondii*. *J Biol Chem* **2007**, *282* (7), 4994-5003.

99. Pittman, K. J.; Aliota, M. T.; Knoll, L. J., Dual transcriptional profiling of mice and *Toxoplasma gondii* during acute and chronic infection. *BMC Genomics* **2014**, *15*, 806.

100. Rawlings, N. D.; Barrett, A. J., Evolutionary families of peptidases. *Biochem J* **1993**, *290* (Pt 1), 205-18.
101. Kappelhoff, R.; Puente, X. S.; Wilson, C. H.; Seth, A.; Lopez-Otin, C.; Overall, C. M., Overview of transcriptomic analysis of all human proteases, non-proteolytic homologs and inhibitors: Organ, tissue and ovarian cancer cell line expression profiling of the human protease degradome by the CLIP-CHIP (TM) DNA microarray. *Bba-Mol Cell Res* **2017**, *1864* (11), 2210-2219.
102. Sajid, M.; McKerrow, J. H., Cysteine proteases of parasitic organisms. *Mol Biochem Parasitol* **2002**, *120* (1), 1-21.
103. Erez, E.; Fass, D.; Bibi, E., How intramembrane proteases bury hydrolytic reactions in the membrane. *Nature* **2009**, *459* (7245), 371-378.
104. Hedstrom, L., Serine protease mechanism and specificity. *Chem Rev* **2002**, *102* (12), 4501-24.
105. Hedstrom, L., Serine protease mechanism and specificity. *Chemical Reviews* **2002**, *102* (12), 4501-4523.
106. Rao, C. N.; Reddy, P.; Liu, Y. Y.; OToole, E.; Reeder, D.; Foster, D. C.; Kisiel, W.; Woodley, D. T., Extracellular matrix-associated serine protease inhibitors (M(r) 33,000, 31,000, and 27,000) are single-gene products with differential glycosylation: cDNA cloning of the 33-kDa inhibitor reveals its identity to tissue factor pathway inhibitor-2. *Arch Biochem Biophys* **1996**, *335* (1), 82-92.
107. Quattrocchi, C. C.; Wannenes, F.; Persico, A. M.; Ciafre, S. A.; D'Arcangelo, G.; Farace, M. G.; Keller, F., Reelin is a serine protease of the extracellular matrix (vol 277, pg 303, 2002). *Journal of Biological Chemistry* **2002**, *277* (13), 11616-11616.
108. Cawston, T. E.; Young, D. A., Proteinases involved in matrix turnover during cartilage and bone breakdown. *Cell and Tissue Research* **2010**, *339* (1), 221-235.
109. Rawlings, N. D.; Barrett, A. J., Evolutionary families of metallopeptidases. *Methods Enzymol* **1995**, *248*, 183-228.
110. Rawlings, N. D.; Barrett, A. J.; Bateman, A., MEROPS: the peptidase database. *Nucleic Acids Res* **2010**, *38* (Database issue), D227-33.
111. Bonnans, C.; Chou, J.; Werb, Z., Remodelling the extracellular matrix in development and disease. *Nat Rev Mol Cell Biol* **2014**, *15* (12), 786-801.
112. Vizovisek, M.; Fonovic, M.; Turk, B., Cysteine cathepsins in extracellular matrix remodeling: Extracellular matrix degradation and beyond. *Matrix Biol* **2018**.
113. Ang, K. K. H.; Ratnam, J.; Gut, J.; Legac, J.; Hansell, E.; Mackey, Z. B.; Skrzypczynska, K. M.; Debnath, A.; Engel, J. C.; Rosenthal, P. J.; McKerrow, J. H.; Arkin, M. R.; Renslo, A. R., Mining a Cathepsin Inhibitor Library for New Antiparasitic Drug Leads. *Plos Neglect Trop D* **2011**, *5* (5).
114. Ndao, M.; Beaulieu, C.; Black, W. C.; Isabel, E.; Vasquez-Camargo, F.; Nath-Chowdhury, M.; Masse, F.; Mellon, C.; Methot, N.; Nicoll-Griffith, D. A., Reversible Cysteine Protease Inhibitors Show Promise for a Chagas Disease Cure. *Antimicrob Agents Ch* **2014**, *58* (2), 1167-1178.
115. Deu, E., Proteases as antimalarial targets: strategies for genetic, chemical, and therapeutic validation. *Febs J* **2017**, *284* (16), 2604-2628.
116. Dou, Z.; Carruthers, V. B., Cathepsin proteases in *Toxoplasma gondii*. *Adv Exp Med Biol* **2011**, *712*, 49-61.

117. Zhao, G.; Zhou, A.; Lv, G.; Meng, M.; Sun, M.; Bai, Y.; Han, Y.; Wang, L.; Zhou, H.; Cong, H.; Zhao, Q.; Zhu, X. Q.; He, S., Toxoplasma gondii cathepsin proteases are undeveloped prominent vaccine antigens against toxoplasmosis. *BMC Infect Dis* **2013**, *13*, 207.
118. Sajid, M.; Robertson, S. A.; Brinen, L. S.; McKerrow, J. H., CRUZAIN The Path from Target Validation to the Clinic. *Cysteine Proteases of Pathogenic Organisms* **2011**, *712*, 100-115.
119. Lv, Z. T.; Chu, Y.; Wang, Y., HIV protease inhibitors: a review of molecular selectivity and toxicity. *Hiv Aids-Res Palliat* **2015**, *7*, 95-104.
120. Andrews, K. T.; Fisher, G.; Skinner-Adams, T. S., Drug repurposing and human parasitic protozoan diseases. *Int J Parasitol Drugs Drug Resist* **2014**, *4* (2), 95-111.
121. Larson, E. T.; Parussini, F.; Huynh, M. H.; Giebel, J. D.; Kelley, A. M.; Zhang, L.; Bogoyo, M.; Merritt, E. A.; Carruthers, V. B., Toxoplasma gondii Cathepsin L Is the Primary Target of the Invasion-inhibitory Compound Morpholinurea-leucyl-homophenyl-vinyl Sulfone Phenyl. *Journal of Biological Chemistry* **2009**, *284* (39), 26839-26850.
122. Roth, W.; Deussing, J.; Botchkarev, V. A.; Pauly-Evers, M.; Saftig, P.; Hafner, A.; Schmidt, P.; Schmahl, W.; Scherer, J.; Anton-Lamprecht, I.; Von Figura, K.; Paus, R.; Peters, C., Cathepsin L deficiency as molecular defect of furless: hyperproliferation of keratinocytes and perturbation of hair follicle cycling. *Faseb J* **2000**, *14* (13), 2075-2086.
123. Schirmeister, T.; Kaeppler, U., Non-peptidic inhibitors of cysteine proteases. *Mini Rev Med Chem* **2003**, *3* (4), 361-73.
124. Turk, V.; Stoka, V.; Vasiljeva, O.; Renko, M.; Sun, T.; Turk, B.; Turk, D., Cysteine cathepsins: from structure, function and regulation to new frontiers. *Biochim Biophys Acta* **2012**, *1824* (1), 68-88.
125. Grzonka, Z.; Jankowska, E.; Kasprzykowski, F.; Kasprzykowska, R.; Lamkiewicz, L.; Wiczak, W.; Wieczerek, E.; Ciarkowski, J.; Drabik, P.; Janowski, R.; Kozak, M.; Jaskolski, M.; Grubb, A., Structural studies of cysteine proteases and their inhibitors. *Acta Biochim Pol* **2001**, *48* (1), 1-20.
126. Stoka, V.; Turk, B.; Turk, V., Lysosomal cysteine proteases: Structural features and their role in apoptosis. *Iubmb Life* **2005**, *57* (4-5), 347-353.
127. Lankelma, J. M.; Voorend, D. M.; Barwari, T.; Koetsveld, J.; Van der Spek, A. H.; De Porto, A. P.; Van Rooijen, G.; Van Noorden, C. J., Cathepsin L, target in cancer treatment? *Life Sci* **2010**, *86* (7-8), 225-33.
128. McGrath, M. E., The lysosomal cysteine proteases. *Annu Rev Biophys Biomol Struct* **1999**, *28*, 181-204.
129. Tsuge, H.; Nishimura, T.; Tada, Y.; Asao, T.; Turk, D.; Turk, V.; Katunuma, N., Inhibition mechanism of cathepsin L-specific inhibitors based on the crystal structure of papain-CLIK148 complex. *Biochem Biophys Res Commun* **1999**, *266* (2), 411-6.
130. Siklos, M.; BenAissa, M.; Thatcher, G. R., Cysteine proteases as therapeutic targets: does selectivity matter? A systematic review of calpain and cathepsin inhibitors. *Acta Pharm Sin B* **2015**, *5* (6), 506-19.
131. Inc., C. C. G. *Molecular Operating Environment (MOE)*, 2013.08 2015.
132. Asaad, N.; Bethel, P. A.; Coulson, M. D.; Dawson, J. E.; Ford, S. J.; Gerhardt, S.; Grist, M.; Hamlin, G. A.; James, M. J.; Jones, E. V.; Karoutchi, G. I.; Kenny, P. W.; Morley, A. D.; Oldham, K.; Rankine, N.; Ryan, D.; Wells, S. L.; Wood, L.; Augustin, M.; Krapp, S.; Simader, H.; Steinbacher, S., Dipeptidyl nitrile inhibitors of Cathepsin L. *Bioorganic & Medicinal Chemistry Letters* **2009**, *19* (15), 4280-3.

133. Frizler, M.; Stirnberg, M.; Sisay, M. T.; Gutschow, M., Development of nitrile-based peptidic inhibitors of cysteine cathepsins. *Curr Top Med Chem* **2010**, *10* (3), 294-322.
134. Schmitz, J.; Furtmann, N.; Ponert, M.; Frizler, M.; Loser, R.; Bartz, U.; Bajorath, J.; Gutschow, M., Active Site Mapping of Human Cathepsin F with Dipeptide Nitrile Inhibitors. *ChemMedChem* **2015**, *10* (8), 1365-77.
135. Frizler, M.; Lohr, F.; Furtmann, N.; Klas, J.; Gutschow, M., Structural optimization of azadipeptide nitriles strongly increases association rates and allows the development of selective cathepsin inhibitors. *J Med Chem* **2011**, *54* (1), 396-400.
136. Powers, J. C.; Asgian, J. L.; Ekici, O. D.; James, K. E., Irreversible inhibitors of serine, cysteine, and threonine proteases. *Chem Rev* **2002**, *102* (12), 4639-750.
137. Vicik, R.; Busemann, M.; Baumann, K.; Schirmeister, T., Inhibitors of cysteine proteases. *Curr Top Med Chem* **2006**, *6* (4), 331-53.
138. Borisek, J.; Vizovisek, M.; Sosnowski, P.; Turk, B.; Turk, D.; Mohar, B.; Novic, M., Development of N-(Functionalized benzoyl)-homocycloleucyl-glycinonitriles as Potent Cathepsin K Inhibitors. *Journal of Medicinal Chemistry* **2015**, *58* (17), 6928-6937.
139. Hardegger, L. A.; Kuhn, B.; Spinnler, B.; Anselm, L.; Ecabert, R.; Stihle, M.; Gsell, B.; Thoma, R.; Diez, J.; Benz, J.; Plancher, J. M.; Hartmann, G.; Banner, D. W.; Haap, W.; Diederich, F., Systematic investigation of halogen bonding in protein-ligand interactions. *Angew Chem Int Ed Engl* **2011**, *50* (1), 314-8.
140. McGrath, M. E.; Klaus, J. L.; Barnes, M. G.; Bromme, D., Crystal structure of human cathepsin K complexed with a potent inhibitor. *Nat Struct Biol* **1997**, *4* (2), 105-9.
141. Greenspan, P. D.; Clark, K. L.; Tommasi, R. A.; Cowen, S. D.; McQuire, L. W.; Farley, D. L.; van Duzer, J. H.; Goldberg, R. L.; Zhou, H. H.; Du, Z. M.; Fitt, J. J.; Coppa, D. E.; Fang, Z.; Macchia, W.; Zhu, L. J.; Capparelli, M. P.; Goldstein, R.; Wigg, A. M.; Doughty, J. R.; Bohacek, R. S.; Knap, A. K., Identification of dipeptidyl nitriles as potent and selective inhibitors of cathepsin B through structure-based drug design. *Journal of Medicinal Chemistry* **2001**, *44* (26), 4524-4534.
142. Bromme, D.; Bonneau, P.; Lachance, P.; Storer, A. C., Engineering the S2 Subsite Specificity of Human Cathepsin-S to a Cathepsin-L-Like and Cathepsin-B-Like Specificity. *J Cell Biochem* **1994**, 152-152.
143. Black, W. C.; Bayly, C. I.; Davis, D. E.; Desmarais, S.; Falgueyret, J. P.; Leger, S.; Li, C. S.; Masse, F.; McKay, D. J.; Palmer, J. T.; Percival, M. D.; Robichaud, J.; Tsou, N.; Zamboni, R., Trifluoroethylamines as amide isosteres in inhibitors of cathepsin K. *Bioorganic & Medicinal Chemistry Letters* **2005**, *15* (21), 4741-4744.
144. Gauthier, J. Y.; Chauret, N.; Cromlish, W.; Desmarais, S.; Duong, L. T.; Falgueyret, J. P.; Kimmel, D. B.; Lamontagne, S.; Leger, S.; LeRiche, T.; Li, C. S.; Masse, F.; Mckay, D. J.; Nicoll-Griffith, D. A.; Oballa, R. A.; Palmer, J. T.; Percival, M. D.; Riendeau, D.; Robichaud, J.; Rodan, G. A.; Rodan, S. B.; Seto, C.; Therien, M.; Truong, V. L.; Venuti, M. C.; Wesolowski, G.; Young, R. N.; Zamboni, R.; Black, W. C., The discovery of odanacatib (MK-0822), a selective inhibitor of cathepsin K. *Bioorganic & Medicinal Chemistry Letters* **2008**, *18* (3), 923-928.
145. O'Shea, P. D.; Chen, C. Y.; Gauvreau, D.; Gosselin, F.; Hughes, G.; Nadeau, C.; Volante, R. P., A Practical Enantioselective Synthesis of Odanacatib, a Potent Cathepsin K Inhibitor, via Triflate Displacement of an alpha-Trifluoromethylbenzyl Triflate. *J Org Chem* **2009**, *74* (4), 1605-1610.
146. Truong, V. L.; Gauthier, J. Y.; Boyd, M.; Roy, B.; Scheigetz, J., Practical and efficient route to (S)-gamma-fluoroleucine. *Synlett* **2005**, (8), 1279-1280.

147. Humphrey, G.; Chung, C. K.; Rivera, N. R.; Belyk, K. M., Asymmetric synthesis for preparing fluoroleucine alkyl esters. Google Patents: 2013.
148. Fanelli, R.; Martinez, J.; Cavelier, F., Expedient Synthesis of Fmoc-(S)--Fluoroleucine and Late-Stage Fluorination of Peptides. *Synlett* **2016**, 27 (9), 1403-1407.
149. Smith, H. J.; Simons, C., *Proteinase and peptidase inhibition : recent potential targets for drug development*. Taylor & Francis: London ; New York, 2002; p xvi, 412 p.
150. Bryant, C. M.; Bunin, B. A.; Kraynack, E. A.; Patterson, J. W., N-cyanomethyl amides as protease inhibitors. 2001.
151. Sani, M.; Sinisi, R.; Molteni, M.; Jagodzinska, M.; Huguenot, F.; Bruche, L.; Zanda, M., The trifluoroethylamine function as peptide bond replacement. *Chim Oggi* **2006**, 24 (3), 42-43.
152. Gauthier, J. Y.; Black, W. C.; Courchesne, I.; Cromlish, W.; Desmarais, S.; Houle, R.; Lamotagne, S.; Li, C. S.; Masse, F.; McKay, D. J.; Ouellet, M.; Robichaud, J.; Truchon, J. F.; Truong, V. L.; Wang, Q.; Percival, M. D., The identification of potent, selective, and bioavailable cathepsin S inhibitors. *Bioorganic & Medicinal Chemistry Letters* **2007**, 17 (17), 4929-4933.
153. Rydberg, P.; Gloriam, D. E.; Olsen, L., The SMARTCyp cytochrome P450 metabolism prediction server. *Bioinformatics* **2010**, 26 (23), 2988-2989.
154. Braun, M. G.; Castanedo, G.; Qin, L.; Salvo, P.; Zard, S. Z., Introduction of Trifluoroethylamine as Amide Isostere by C-H Functionalization of Heteroarenes. *Org Lett* **2017**, 19 (15), 4090-4093.
155. Schmitz, J.; Li, T. W.; Bartz, U.; Gutschow, M., Cathepsin B Inhibitors: Combining Dipeptide Nitriles with an Occluding Loop Recognition Element by Click Chemistry. *Acs Med Chem Lett* **2016**, 7 (3), 211-216.
156. Altmann, E.; Aichholz, R.; Betschart, C.; Buhl, T.; Green, J.; Lattmann, R.; Missbach, M., Dipeptide nitrile inhibitors of cathepsin K. *Bioorganic & Medicinal Chemistry Letters* **2006**, 16 (9), 2549-2554.
157. Di, L.; Rong, H.; Feng, B., Demystifying brain penetration in central nervous system drug discovery. Miniperspective. *J Med Chem* **2013**, 56 (1), 2-12.
158. Giroud, M.; Ivkovic, J.; Martignoni, M.; Fleuti, M.; Trapp, N.; Haap, W.; Kuglstatter, A.; Benz, J.; Kuhn, B.; Schirmeister, T.; Diederich, F., Inhibition of the Cysteine Protease Human Cathepsin L by Triazine Nitriles: AmideHeteroarene pi-Stacking Interactions and Chalcogen Bonding in the S3 Pocket. *ChemMedChem* **2017**, 12 (3), 257-270.
159. Ehmke, V.; Winkler, E.; Banner, D. W.; Haap, W.; Schweizer, B.; Rottmann, M.; Kaiser, M.; Freymond, C.; Schirmeister, T.; Diederich, F., Optimization of Triazine Nitriles as Rhodesain Inhibitors: StructureActivity Relationships, Bioisosteric Imidazopyridine Nitriles, and X-ray Crystal Structure Analysis with Human CathepsinL. *Chemmedchem* **2013**, 8 (6), 967-975.
160. Giroud, M.; Harder, M.; Kuhn, B.; Haap, W.; Trapp, N.; Schweizer, W. B.; Schirmeister, T.; Diederich, F., Fluorine Scan of Inhibitors of the Cysteine Protease Human Cathepsin L: Dipolar and Quadrupolar Effects in the pi-Stacking of Fluorinated Phenyl Rings on Peptide Amide Bonds. *Chemmedchem* **2016**, 11 (10), 1042-1047.
161. Vasishta, A.; Baker, P. R.; Preece, P. E.; Wood, R. A.; Cuschieri, A., Inhibition of proteinase-like peptidase activities in serum and tissue from breast cancer patients. *Anticancer Res* **1988**, 8 (4), 785-9.

162. Gauthier, J. Y.; Chauret, N.; Cromlish, W.; Desmarais, S.; Duong, L. T.; Falguyret, J. P.; Kimmel, D. B.; Lamontagne, S.; Leger, S.; LeRiche, T.; Li, C. S.; Masse, F.; McKay, D. J.; Nicoll-Griffith, D. A.; Oballa, R. M.; Palmer, J. T.; Percival, M. D.; Riendeau, D.; Robichaud, J.; Rodan, G. A.; Rodan, S. B.; Seto, C.; Therien, M.; Truong, V. L.; Venuti, M. C.; Wesolowski, G.; Young, R. N.; Zamboni, R.; Black, W. C., The discovery of odanacatib (MK-0822), a selective inhibitor of cathepsin K. *Bioorg Med Chem Lett* **2008**, *18* (3), 923-8.
163. Giessler, K.; Griesser, H.; Gohringer, D.; Sabirov, T.; Richert, C., Synthesis of 3'-BODIPY-Labeled Active Esters of Nucleotides and a Chemical Primer Extension Assay on Beads. *Eur J Org Chem* **2010**, (19), 3611-3620.
164. Parussini, F.; Coppens, I.; Shah, P. P.; Diamond, S. L.; Carruthers, V. B., Cathepsin L occupies a vacuolar compartment and is a protein maturase within the endo/exocytic system of *Toxoplasma gondii*. *Mol Microbiol* **2010**, *76* (6), 1340-57.
165. Altmann, E.; Cowan-Jacob, S. W.; Missbach, M., Novel purine nitrile derived inhibitors of the cysteine protease cathepsin K. *J Med Chem* **2004**, *47* (24), 5833-6.
166. Cai, J. Q.; Bennett, D. J.; Rankovic, Z.; Dempster, M.; Fradera, X.; Gillespie, J.; Cumming, I.; Finlay, W.; Baugh, M.; Boucharens, S.; Bruin, J.; Cameron, K. S.; Hamilton, W.; Kerr, J.; Kinghorn, E.; McGarry, G.; Robinson, J.; Scullion, P.; Uitdehaag, J. C. M.; van Zeeland, M.; Potin, D.; Saniere, L.; Fouquet, A.; Chevallier, F.; Deronzier, H.; Dorleans, C.; Nicolai, E., 2-Phenyl-9H-purine-6-carbonitrile derivatives as selective cathepsin S inhibitors. *Bioorganic & Medicinal Chemistry Letters* **2010**, *20* (15), 4447-4450.
167. Cai, J. Q.; Fradera, X.; van Zeeland, M.; Dempster, M.; Cameron, K. S.; Bennett, D. J.; Robinson, J.; Popplestone, L.; Baugh, M.; Westwood, P.; Bruin, J.; Hamilton, W.; Kinghorn, E.; Long, C.; Uitdehaag, J. C. M., 4-(3-Trifluoromethylphenyl)-pyrimidine-2-carbonitrile as cathepsin S inhibitors: N3, not N1 is critically important. *Bioorganic & Medicinal Chemistry Letters* **2010**, *20* (15), 4507-4510.
168. Zafrani, Y.; Yeffet, D.; Sod-Moriah, G.; Berliner, A.; Amir, D.; Marciano, D.; Gershonov, E.; Saphier, S., Difluoromethyl Bioisostere: Examining the "Lipophilic Hydrogen Bond Donor" Concept. *J Med Chem* **2017**, *60* (2), 797-804.
169. Erickson, J. A.; Mcloughlin, J. I., Hydrogen-Bond Donor Properties of the Difluoromethyl Group. *J Org Chem* **1995**, *60* (6), 1626-1631.